INFORMATION TO USERS

This dissertation was produced from a microfilm copy of the original document. While the most advanced technological means to photograph and reproduce this document have been used, the quality is heavily dependent upon the quality of the original submitted.

The following explanation of techniques is provided to help you understand markings or patterns which may appear on this reproduction.

1. The sign or "target" for pages apparently lacking from the document photographed is "Missing Page(s)". If it was possible to obtain the missing page(s) or section, they are spliced into the film along with adjacent pages. This may have necessitated cutting thru an image and duplicating adjacent pages to insure you complete continuity.

2. When an image on the film is obliterated with a large round black mark, it is an indication that the photographer suspected that the copy may have moved during exposure and thus cause a blurred image. You will find a good image of the page in the adjacent frame.

3. When a map, drawing or chart, etc., was part of the material being photographed the photographer followed a definite method in "sectioning" the material. It is customary to begin photoing at the upper left hand corner of a large sheet and to continue photoing from left to right in equal sections with a small overlap. If necessary, sectioning is continued again — beginning below the first row and continuing on until complete.

4. The majority of users indicate that the textual content is of greatest value, however, a somewhat higher quality reproduction could be made from "photographs" if essential to the understanding of the dissertation. Silver prints of "photographs" may be ordered at additional charge by writing the Order Department, giving the catalog number, title, author and specific pages you wish reproduced.

University Microfilms

300 North Zeeb Road
Ann Arbor, Michigan 48106

A Xerox Education Company

THE UNIVERSITY OF OKLAHOMA

GRADUATE COLLEGE

INFRARED CORRELATION SPECTROSCOPY WITH APPLICATION TO CO_2 UNDER ATMOSPHERIC CONDITIONS

A DISSERTATION

SUBMITTED TO THE GRADUATE FACULTY

in partial fulfillment of the requirements for the

degree of

DOCTOR OF PHILOSOPHY

By

DAVID JOHN LYSOBEY

Norman, Oklahoma

1972

INFRARED CORRELATION SPECTROSCOPY WITH APPLICATION

TO CO_2 UNDER ATMOSPHERIC CONDITIONS

A THESIS

APPROVED FOR THE DEPARTMENT OF PHYSICS

By

[signatures]

I gratefully acknowledge Dr. Sybrand Broersma, my major advisor. His support and understanding and his technical advice were an essential element in the completion of this dissertation. I am pleased to acknowledge Dr. John Canfield, who introduced me to the experiment and who guided me over some of the rough spots. I also wish to acknowledge the initial contribution and technical advice of Dr. Richard A. Day. I would like to express my gratitude to Dr. Fritz Krause who supported the contract and who provided many valuable suggestions during the course of the work. Special thanks are due Carl T. Bush for writing a very comprehensive computer program to handle the data analysis.

Abstract

An experiment has been performed to investigate the fluctuations in the infrared absorption for CO_2 under conditions which are typical of the lower atmosphere. The 4.3 micron vibration-rotation bands of CO_2 were found to be a suitable absorption process. We are primarily interested in determining spectroscopic correlation signatures of the gaseous medium rather than in determining the total radiation or heat transferred through the medium.

It was shown that the relationship between the fluctuations in the optical variables and the thermodynamic variables can be described by a Taylor series expansion of the absorption coefficient. A spectral inversion was then shown to be possible by going to the fluctuating absorption coefficient spectrum. One of the important results of the experiment is that we have been able to isolate the dependence of the fluctuating absorption coefficient on the CO_2 concentration at a particular wavelength position in the 4.3 micron bands. Thus a single measurement of the fluctuating absorption coefficient can be used to find the CO_2 concentration. A second measurement at a different wavelength position can similarly be used to find the temperature; and a third measurement can be used to find the total pressure.

The atmospheric conditions were shown to be suitable for measuring fluctuation structure of the gaseous medium. This is accomplished by measuring the power spectral density function for the fluctuating intensity. The introduction of the time series or the

or the fluctuations is an extension of the conventional means (the use of steady state conditions) of obtaining spectroscopic information.

The characteristics of the various possible spectra are discussed and related. The absorption coefficient derivatives were calculated and plotted; the dependence of these derivatives on the total pressure, the absorber concentration and the temperature was determined. The temperature results are of particular significance because the influence of temperature on the absorption is generally neglected in the literature; most investigators have used the total absorption (where the T dependence is small and often neglected) rather than the spectral absorption. We have used spectral absorption coefficients.

The results of the experiment are discussed in terms of Band Model predictions; some high resolution data is also presented.

This fluctuation approach is related to a Crossed Beam Correlation Technique; this is a remote sensing technique which is being applied to atmospheric pollution analyses and water resources control. The results presented here can be used to calibrate the crossed beam system for atmospheric work and are an aid in disentangling the resultant space-time correlations.

TABLE OF CONTENTS

LIST OF FIGURES

INFRARED CORRELATION SPECTROSCOPY WITH APPLICATION TO CO_2 UNDER ATMOSPHERIC CONDITIONS

CHAPTER I.

INTRODUCTION

This Dissertation is concerned with a method of spectroscopic analysis which utilizes the fluctuation in the optical and thermodynamic variables. This method measures the mean transmitted intensity and the fluctuations about this mean intensity which occur as a result of the fluctuations of the thermodynamic variables which characterize the given gas. The gas serves as an extinction or an absorption medium; the resultant fluctuations of the absorption coefficient are calculated and related to the thermodynamic variables via a Taylor series expansion about the mean values. The thermodynamic variables can then be determined and the fluctuation structure of the gas can also be found.

This introduction of the time variable or the fluctuation, is an extension of the conventional means of obtaining spectroscopic information. The fluctuations also allow the resultant spectra to be measured as correlations in terms of the optical and thermodynamic variables.

The results are used in conjunction with a Crossed Beam Correlation Technique.[10] This is a remote sensing technique which is being applied to atmospheric pollution analysis and water resources control.

Conventional spectroscopy generally assumes that the absorption takes place under steady state conditions for the gas, where therefore the absorption does not change with time. In this experiment we have

perturbed these steady state conditions by introducing known fluctuations into the gas and have measured the resultant fluctuations in the intensity. The fluctuations are generated by acoustic excitation of the gas. This method has potentially more information than the steady state method in the form of statistical and deterministic information concerning the time series which is associated with the fluctuations. For example, one can attempt to determine the response of the absorption process to various amplitude and frequency harmonic acoustic excitation signals or to a band limited white noise acoustic excitation signal. In particular, the phase relationship between the optical and the thermodynamic fluctuations is of interest. The fluctuation structure can be determined by fourier transforming the time series. Thus the fluctuations or the introduction of the time variable represents a further means of analyzing the basic absorption process, over and above the steady state method. It allows for the introduction of the δK (absorption coefficient fluctuation) spectrum which can then be used in conjunction with the K (mean absorption coefficient) spectrum as a means of analyzing the absorption process.

These fluctuations are typical of the real world; the earth's atmosphere for example contains such fluctuations in the form of turbulence and simple pressure and temperature variations with time.

We are primarily interested in determining spectroscopic correlation signatures of the gas, rather than in determining the total heat transferred through the gas. These signatures contain information about the relationship between the optical and thermodynamic variables and therefore information about the medium through which the light

travelled. This information is basically concerned with the dependence of the mean spectra on 1. the number of absorbers, 2. the population of the states, 3. the line broadening effects resulting from pressure broadening, 4. the spectral position, and 5. the spectral bandpass, as well as the dependence of the fluctuation spectra on numbers one (1.) through five (5.) and the fluctuations of the quantities involved in numbers one through three.

When such relationships are established, one can in principle, invert the spectra to obtain the thermodynamic variables such as temperature, partial pressure of the absorbing gas, and total pressure which characterize the gas. One can also determine the fluctuations in the temperature and the pressure which are in addition related to the turbulence or fluctuation structure of the gas.

Theoretical analyses have not been very successful in producing accurate spectral inversions mainly because of uniqueness problems; the radiative transfer equations are quite difficult to solve in the general case. Furthermore it has not been possible to predict precisely, in a theoretical manner, the dependence of the absorption process on the thermodynamic variables such as temperature, for bands of overlapping spectral lines. Thus it becomes necessary to perform carefully controlled experiments which will enable one to empirically determine such relationships. The resultant inversion will be strictly valid only for the range of conditions specified in the experiment; however, if the conditions are typical of the atmosphere then naturally the results will be applicable to the atmosphere. This is the case in our experiment.

Our experiments were performed on an Optical Absorption Cell built specifically to measure mean value absorption coefficients and fluctuations about these mean values for a gaseous medium. The 4.3 micron vibration-rotation bands of CO_2 were chosen as a suitable extinction process. CO_2 was chosen because it exists in the atmosphere in well mixed trace quantities, and its 4.3 micron spectrum is not overlapped by the spectra of other atmospheric constituents such as H_2O. CO_2 is also a large factor in establishing the heat balance in the earth's atmosphere; the quantity of CO_2 is therefore of utmost importance for ecological reasons. This quantity can vary significantly as a result of the combustion process of fossil fuels and must therefore be monitored.

The acoustic excitation is limited to small fluctuations, which are typical of the atmosphere, and therefore we assume that one can neglect the higher order terms in the Taylor series expansion, above the linear terms. We do not consider pressure fluctuations greater than about one half of one percent of the total static pressure.

The spectral absorptions rather than the total absorption for a band are of interest to us here, even though such spectral absorptions are dependent on the bandpass. The basic reason is that spectral absorptions contain more available information about the absorption medium than does the total absorption. A total absorption is given by a single number for the entire vibration-rotation band of interest; whereas the spectral absorption is a function of the position of the slit in the spectrum or band. One therefore retains the information (in a useable form) concerning the vibration-rotation band contour

even though the rotational fine structure has been averaged out. The averaging intervals or slit widths are large enough so that Band Model results can be utilized; thus we deal primarily with low resolution spectra.

High resolution mean value spectra can also be measured to determine the spectroscopic constants such as the rotational constants, line spacings and halfwidths, although suchinformation is available for the more common molecules. High resolution fluctuation spectra require a much larger compression ratio than is used in this experiment, and therefore they cannot be measured in our case.

The wavelength range that we covered was sufficient to include all the rotational lines that were active in the absorption process for our set of conditions. The static absorber path is homogeneous and has a length equal to the expected correlation length in the atmosphere, as measured with the Crossed Beam System.

The absorber concentration has a minimum in the atmosphere of about .03% by volume; therefore, we used this value as our minimum absorber concentration and included values up to about four times as large. This we felt covered the nominal increases in CO_2, due to pollution, near the surface of the earth. The total pressures and the temperature ranges were centered about one atmosphere and room temperature. The acoustic excitation was limited to approximately harmonic signals with low frequency and amplitude; this was felt to be necessary only because it was easier to establish the feasibility of the whole experimental approach if narrow band signals were employed initially. The next step is to use broad band signals.

The output of the absorption cell can be given as an instantaneous intensity, $I' = I + \delta I$. I is the mean value and δI is the fluctuation about the mean. I and δI are measured separately and a mean value absorption coefficient K and a fluctuation about the mean δK are then calculated. These values are measured as correlations for all possible combinations of the thermodynamic variables and the wavelength. Various test were also performed to check the dependence on the fluctuation δP and the bandpass $\Delta\lambda$.

The purpose of the experiment was first to see if such an approach would work under typical atmospheric conditions. The sensitivity of the absorption fluctuations to the thermodynamic variable fluctuations had to be determined. Since the fluctuations are very small, it had to be determined empirically whether or not sufficient signal existed to allow for accurate measurement. Thus the magnitudes of the signals had to be determined. It was also of interest to determine what new information was available using this type of approach, as compared to the conventional approach.

It had to be established that the theoretical formulation used was a valid description of the fluctuating absorption process. The transformation between the optical and thermodynamic variables is in the form of a Taylor series expansion which contains the three linear terms, each of which is made up of a partial derivative and a fluctuating thermodynamic variable. Also one must determine whether or not an inversion of the spectrum can be made with such a formulation.

To make the inversion simpler it was decided to search the spectrum for possible regions or points where the dependence of the

absorption was dominated by one or two of the thermodynamic variables. This might allow one to eliminate one or two of the terms in the Taylor series expansion. A point can be predicted for CO_2 where the absorption coefficient is independent of the temperature and therefore the derivatives with respect to temperature vanishes; this is plausible and therefore it was checked empirically. There is no substantial reason to believe that such a point might also exist for the total pressure.

These predictions are in terms of the mean value absorption coefficient; similar predictions for the fluctuating absorption coefficient (for example, is there a point where δK is independent of T) are not easily made. These points or crossovers had to be established empirically.

Furthermore, such dependencies are a function of the spectral bandpass as well as the spectral position; these functional dependencies are not accurately established theoretically, especially in band model results, and therefore require an experimental approach.

And, of course, it is of interest to determine exactly how the correlation spectra do vary with changes in the thermodynamic variables. Depending on the results of this experiment, the whole approach may find application to various atmospheric remote sensing programs now being considered.

As a further important purpose, the experiment is to be used to calibrate a Crossed Beam Correlation Experiment[10] which is being operated under atmospheric conditions. As explained in section IIB, this technique utilizes the statistical information in a turbulent atmosphere to determine local temperatures, local concentrations, and local

pressures in a region obtained by triangulation using two or more crossed beams. The complete integration along the line of sight from the source to the detector is no longer as restrictive in this approach; local information can be determined inside this source-detector common volume. This technique also supresses spectroscopic interference by other atmospheric constituents (self filter), and detector noise.

The results of this technique are in the form of space-time covariance functions; these functions are most easily disentangled by resorting to the use of calibration reference spectra from single beam measurements. Our experiments produce the needed reference spectra. The required format of the data is shown in Section IIB, to be that of partial derivatives of the absorption coefficients and cross correlations between the fluctuating optical and thermodynamic variables.

As already indicated, one of the most important potential applications of such an approach is in the area of pollution. This spectroscopic approach offers a solution to the problem of detecting the quantity of various infrared active pollutant gases that might exist in, for example, the earth's atmosphere (or any synthetic or nonearth atmosphere). One can also measure the pressure and temperature of these gases in the same way. This is done remotely; this is a very important attribute of the method since it is often not possible to gain access to various regions of interest. For example, one might wish to monitor the pollutants being emitted from a smokestack without actually having to insert a probe at the outlet of the stack.

Another region of interest is that of water resources control.

Using H_2O instead of CO_2 as the tracer gas allows one to map evaporation and transpiration rates over areas that have critical water supply problems. This technique should allow one to measure cloud top temperatures; such information is necessary when attempting to control the amount of precipitation in a given area.

These techniques also have general application in the monitoring of stable inversion layers which can be quite hazardous in metropolitan areas, due to health endangering air pollution levels. These pollution levels tend to build up because vertical mixing is generally prohibited when this condition prevails.

CHAPTER II

THEORY

The theory will be divided into three main sections. The first will discuss infrared spectral lines in terms of isolated lines as well as bands of lines. The second section deals with atmospheric radiative transfer, with special emphasis on the Crossed Beam Correlation Technique. The third section deals with the thermodynamic variable dependence of the Absorption Process. We shall try to indicate, in the theory sections, the basis for the subsequent analysis as well as the connections between the various disciplines used in the analysis, and the extent to which it is necessary to draw from the results of each of them. The analysis is confined to that which is applicable to the carbon dioxide molecule under atmospheric conditions.

A. Infrared Spectral Line Analysis

A spectral line is the result of a radiative transition between an upper and a lower state in an absorption or emission process. The resultant distribution of radiation over the complete wavelength range is characterized by: (1) the wavelength position which is determined by the energy difference between the upper and the lower states; (2) the intensity which is determined by the probability of the transition occurring and the population of the states; (3) the line shape and width

which depend on line broadening processes such as collision and Doppler processes, as well as the natural line broadening process.

The specification of this spectral line can be given in terms of the single isolated line absorption coefficient, $K(\nu - \nu_s)$, where

$$K(\nu - \nu_s) = Sf(\nu - \nu_s). \qquad (1)$$

ν is the frequency, ν_s the position of the unperturbed line, S the integrated absorption, and $f(\nu - \nu_s)$ is the line shape factor which is dependent on the line halfwidth. The integral of $f(\nu - \nu_s)$ over all ν is equal to unity and therefore the integral of $K(\nu - \nu_s)$ over all ν is equal to S.

We shall now consider the line shape and width, the line intensity, and the line position separately.

1. Line Shape and Width. All individual spectral lines are polychromatic due to the effects of natural line broadening; however this broadening is usually dominated in a given physical situation by collision and/or Doppler effects. The combination of these effects is represented by the Voight profile. Doppler effects are dominant at low pressures or high altitudes in the atmosphere (above 50 km) and collision effects are dominant where Local Thermal Equilibrium exists, that is, below 50km. We will concern ourselves only with line shapes which are described by collision effects. In particular we will consider only adiabatic collisions where the collision induced transition is not allowed.

The most familiar result is the basic Lorentz line shape given by

$$f(\nu - \nu_s) = 2/\pi \frac{\Delta\omega_{\frac{1}{2}}}{(\nu-\nu_s)^2 + (\Delta\omega_{\frac{1}{2}})^2} \quad . \qquad (2)$$

$\Delta\omega_{\frac{1}{2}}$ is the halfwidth of the line and represents the frequency range over which the intensity of the line is $\geq$ half its maximum value. This is a classical result based on the Impact Theory of Collisions; the line shape as given above is specifically for the case of strong encounters. Lorentz[21] derived this result in 1906 by assuming the radiation is instantaneously cut off or "interrupted" at each collision. The same result was derived by Weisskopf[34] who avoided the complete interruption hypothesis; he assumed that when the phase change was approximately unity, a collision occurred and the subsequent wave train was completely incoherent relative to the previous one, without being broken off.

The more sophisticated Impact Theories such as that of Foley[11] consider the phase change in greater detail. For typical atmospheric conditions, the theory of Foley predicts an absorption coefficient given by

$$K(\nu-\nu_s) = S/\pi \; \frac{\Delta\omega_{\frac{1}{2}}}{(\nu-\nu_s+.725\Delta\omega_{\frac{1}{2}})^2+(\Delta\omega_{\frac{1}{2}})^2} \qquad (3)$$

The positive constant, .725, indicates a line shift slightly toward lower frequencies. There is no line asymmetry predicted by this formula. The Lorentz type of line shape is best for high temperature and for wavelengths near the core of the line, since the collision frequency is reduced and therefore the coherence time is increased.

The other basic collision broadening theory is the Statistical Theory.[23] This theory considers the probability function for the occurence of the possible perturber configurations relative to the absorber. For a nonpolar, symmetric molecule, the resultant intensity distribution is given by (for p = 6 Van der Waals forces)

$$I(\omega-\omega_s) = 0 , \quad \text{for } \omega-\omega_s > 0 \quad \text{(blue)} \tag{4}$$

$$I(\omega-\omega_s) = (2\pi/3)(\Delta\gamma)^{\frac{1}{2}} n(\omega-\omega_s)^{-3/2} \exp-\left[4\pi^3/9\left(\frac{|\Delta\gamma|n^2}{\omega_s-\omega}\right)\right], \text{ for } \omega-\omega_s<0 \text{(red)} \tag{5}$$

where $\omega = 2\pi\nu$. $\Delta\gamma$ is the energy difference between the initial and final states and n is the perturber number volume density. This is of course an asymmetric line shape. A halfwidth can be defined; it is given by $\Delta\omega_{\frac{1}{2}} = .822\pi^3\Delta\gamma\, n^2$. For large $|\omega - \omega_s|$, $I(\omega - \omega_s) = \text{const.}$ $(\omega_s-\omega)^{-3/2}$. These results are best for high densities of perturbers and wavelengths that are in the wings of the line.

Lindholm[20] developed a more general theory of collision broadening which gives the Statistical and Impact Theories as limiting cases. The Lindholm results can be given, for sufficiently large distances from the unperturbed line center (far wings) by

$$K(\nu-\nu_s) = .933M^2S\Delta\omega_{\frac{1}{2}}\pi^{-1}[(\nu_s-\nu)M]^{-3/2} \quad \text{(red)} \tag{6a}$$

$$K(\nu-\nu_s) = .638M^2S\Delta\omega_{\frac{1}{2}}\pi^{-1}[(\nu-\nu_s)M]^{-7/3} \quad \text{(blue)} \tag{6b}$$

where $M = 27.8(c/\bar{v})^{6/5}\,(\Delta\gamma)^{1/5}$. $\bar{v}$ is the mean relative velocity of molecules. There is therefore a faster fall off in intensity predicted for the violet wing than for the red wing.

The regions of the spectral lines beyond a few cm^{-1} from the line centers, typically absorb less and have a smaller absorption coefficient than that predicted by a Lorentz line shape with the same halfwidth. The Lorentz line shape can however be corrected by a multiplicative function of frequency $\chi(\nu - \nu_s)$ to yield an empirical line shape given by

$$f(\nu-\nu_s) = f_L(\nu-\nu_s)\chi(\nu-\nu_s) . \tag{7}$$

χ has a value of approximately unity near the line center and falls off away from the line center, to values on the order of 10^{-3} for very large values of $(\nu - \nu_s)$. Winters, Silverman and Benedict[35] have concluded that for the line wings beyond the bandhead of the 4.3 Micron bands of CO_2, χ is given approximately by $\exp - a(|\nu - \nu_s| - \nu_{min})^b$ for $\nu \geq \nu_{min}$ and $\nu_{min} \approx 5$ cm^{-1}. a and b are empirical constants.

The functional dependence of the halfwidth on the thermodynamic variables, for the special case of binary gas mixtures is given by

$$\Delta\omega_{\frac{1}{2}} = (1/2c)(2/kT)^{\frac{1}{2}} C_{a,b}[P+(B-1)P_a] \qquad (8)$$

P is the total pressure equal to the sum of the partial pressure of the absorber, P_a, and the partial pressure of the broadener P_b; $C_{a,b}$ is a function of the collision crosssection for the absorber and broadener and their reduced mass. B is the self broadening coefficient of the absorbing gas relative to the broadening gas; for CO_2 broadened by N_2, B is approximately equal to 1.30. The quantity in brackets in (8) is the equivalent pressure, P_e. For our experiment, $P_a << P$ and therefore P_e reduces to P.

Burch et al[4] have given the ratios of the normalized halfwidths due to foreign gas broadening over that due to selfbroadening of CO_2 as .83 for N_2, 1.17 for H_2, .68 for O_2, .65 for Ar and .49 for H_e. The dependence of the halfwidths on the rotational quantum numbers is not significant, especially for nonpolar molecules; we shall assume, as do most Band Models*, that $\Delta\omega_{\frac{1}{2}}$ is independent of J.

2. Line Intensity. The transition probability from the state

---

*See Chapter II, section 4..

k to the state j can be analyzed from the standpoint of the time dependent Schrodinger Equation and from the phenomenological standpoint of Einstein, where the Einstein coefficients are introduced. Upon comparing the resultant expressions for the k → j transition probabilities, one finds that

$$B_{kj} = (2\pi/3\hbar^2)|R_{kj}|^2 \ , \tag{9}$$

where B_{kj} is the integral Einstein Coefficient for absorption and R_{kj} is the electric dipole matrix element.

These concepts can be related to macroscopic quantities by first specifying an expression for the net rate of energy transfer between radiation and matter. This can be given by

$$\frac{d\rho(\nu_{kj})}{dt} = h\nu_{kj}[A_{kj}n_j - B_{kj}\rho(\nu_{kj})(n_k - g_k/g_j\, n_j)] \tag{10}$$

where ρ is the radiation energy density, ν_{kj} is the frequency of the k - j transition, n_k is the number of molecules in the $k^{\underline{th}}$ state, g_k is the statistical degeneracy for the $k^{\underline{th}}$ state, and A_{jk} is the integral Einstein coefficient for spontaneous emission.

Now on a macroscopic level

$$dE = I_\nu \cos(\hat{x},\hat{n})\, d\omega_{\hat{x}} d\sigma_{\hat{n}} d\nu dt \ , \tag{11}$$

where I_ν is the spectral intensity, $\hat{x}$ a unit vector in the direction of propagation, $\hat{n}$ a unit normal vector to the area element $d\sigma$ and dE is the energy transport. Furthermore the radiation energy density can be given by

$$d\rho = \frac{1}{c} I_\nu d\omega_{\hat{x}} \ . \tag{12}$$

In terms of the absorption process only, equation (10) can therefore be rewritten as

$$\left.\frac{dI_\nu}{ds}\right|_{\text{absorption}} = -h\nu_{kj}B_{kj}n_k \frac{1}{c} I_\nu\left(1 - \exp - \frac{h\nu_{kj}}{kT}\right) , \qquad (13)$$

where ds = cdt, and we have assumed equilibrium and used the Boltzmann distribution for the population of the states. A mass absorption coefficient $K'(\nu)$ can be defined by invoking Lambert's Law; this is given by

$$dI_\nu = -K'(\nu)I_\nu \rho' ds_{\hat{x}} \qquad (14)$$

where ρ' is the mass density and $ds_{\hat{x}}$ is the line element corresponding to the path of radiation in the medium. Redefining a volume absorption coefficient $K(\nu)$ (cm^{-1}), and assuming that $B_{kj}(\nu) = B_{kj} f(\nu - \nu_{kj})$ where $f(\nu - \nu_{kj})$ is the line shape factor, equation (13) is rewritten as

$$\rho' K'(\nu-\nu_{kj}) = K(\nu-\nu_{kj}) = +h\nu_{kj}n_k B_{kj} f(\nu-\nu_{kj})\frac{1}{c}\left(1 - \exp \frac{h\nu_{kj}}{kT}\right) . \qquad (15)$$

Integrating over all frequency space yields the integrated absorption S, given by

$$S = h\nu_{kj}B_{kj}\frac{1}{c}n_k\left(1 - \exp - \frac{h\nu_{kj}}{kT}\right) . \qquad (16)$$

In terms of a partition function and the electric dipole matrix element, S can also be written as

$$S = \frac{4\pi^2}{3ch}\nu_{kj}|R_{kj}|^2 n g_k \frac{1}{Q}\exp - E(k)/kT \left(1 - \exp - \frac{h\nu_{kj}}{kT}\right). \qquad (17)$$

Q is the partition function of the molecule , exp - E(k)/ kT is the Boltzmann distribution and n is the total number (density) of molecules in all states.

These concepts can now be applied to molecules. We shall consider only the linear symmetric ($D_{\infty h}$) triatomic molecule, CO_2, for which we shall be concerned only with the vibrational and rotational tran-

sitions. Let us define $j = v'J'l'$ and $k = v\ J\ l$ for $k \rightarrow j$ where J is the rotational quantum number, $v = v_1, v_2, v_3$ are the vibration quantum numbers for the three normal modes of vibrati on, and l is the vibrational angular momentum quantum number, and also let $g_k = g_J\, g_l\, g_v$ for the lower state, where $g_l = (2 - \delta_{10})$, $g_j = (2J + 1)$, g_v = unity, and $Q_K = Q_V Q_R$ where Q_V and Q_R are the vibrational and rotational partition functions for the molecule. Furthermore we define $\left|R_{v\ J\ l}^{v'J'l'}\right|^2$ in terms of a pure rotational electric dipole matrix element $\left|\alpha_{J\ l}^{J'l'}\right|^2$ which includes the statistical weight factors, a pure vibration non-rotating oscillator electric dipole matrix element $\left|\beta_{v\ l}^{v'l'}\right|^2$, and $\left|\gamma_{v\ J\ l}^{v'J'l'}\right|^2$ which is a correction factor for the interaction of vibration and rotation. Equation (17) can then be rewritten as

$$S_{v\ J\ l}^{v'J'l'} = \frac{4\pi^2}{3ch}\,\nu_{v\ J\ l}^{v'J'l'}\,\frac{n}{Q_V Q_R}\,\exp -\left[\frac{E_V(v_1 v_2 v_3 l) + E_R(J)}{kT}\right] \left|\alpha_{J\ l}^{J'l'}\right|^2 \left|\beta_{v\ l}^{v'l'}\right|^2 \left|\gamma_{v\ J\ l}^{v'J'l'}\right|^2 (1 - \exp -h\nu_{v\ J\ l}^{v'J'l'}/kT)\ . \tag{18}$$

The 4.3 micron region of CO_2 is predominantly composed of parallel bands for which $\Delta l = 0$. If $l = 0$, then the transitions are $\Sigma - \Sigma$ transitions, if $l = 1$ then $\pi - \pi$ transitions, and so forth. The ν_3 vibrational fundamentals of CO_2 are represented by $|\beta|^2 \propto (v_3 + 1)$ and $\Delta v_3 = 1$, Δv_2 = zero. The corresponding rotational line strengths are given in terms of $|\alpha|^2$ for the P,Q, and R branches, as $J\,\delta_{J-1,\,J''}$, $0\,\delta_{J,J''}$, and $(J + 1)\,\delta_{J+1,\,J''}$. The expression for the parallel band ground state fundamental of CO_2(4.3microns) is found from (18) by setting l, v_1, v_2, v_3 = zero, and using $\Delta l, \Delta v_1, \Delta v_2$ = zero, $\Delta v_3 = 1$, $\Delta J = \pm 1$.

It is possible to define an integrated band absorption by summing

(18) over J and J'. This leads to the concept of a total integrated band absorption, which is obtained by summing the integrated band absorption over all possible vibrational transitions in the given region. Thus, to rigorously calculate a spectrum it is necessary to calculate much more than just the ground state fundamental if one expects to get reasonable agreement with experiment. One must also include the overtones and combination bands. The total integrated band absorption for the 4.3 micron region of CO_2 is 2700 atm^{-1} cm^{-2}, at 300°K (note: 1 Atm.= 760 mmHg).

3. Energy Levels and Line Positions. The anharmonic Schrodinger equation does not break up into a number of independent equations as it does when only the harmonic quadratic terms are considered in the potential. However, higher order terms can be considered by using time independent perturbation theory. The resultant energy expression, to second order, for a linear symmetric triatomic molecule such as CO_2 can be given by

$$E/hc = \sum_{i=1}^{3} \omega_i (v_i + \tfrac{1}{2}d_i) + \sum_{i=1}^{3} \sum_{j\ i} x_{ij}(v_i + \tfrac{1}{2}d_i)(v_j + \tfrac{1}{2}d_j) + g_{22}l^2 \quad . \tag{19}$$

This contains terms which are linear and also quadratic in the vibrational quantum numbers, and crossterms containing quantum numbers from two different vibrational modes. d_i is the degeneracy index for the $i^{\underline{th}}$ vibrational mode; the ω_i are potential constants and the x_{ij} are anharmonic constants. In the special cases where $g_{22}l^2$ is replaced by $x_{11}(l^2 - 1)$, these constants are given by[8]

$\omega_1 = 1351.2$	$x_{22} = -1.3$	$x_{23} = -11.0$
$\omega_2 = 672.2$	$x_{33} = -12.5$	$x_{11} = 1.7$
$\omega_3 = 2396.4$	$x_{12} = 5.7$	
$x_{11} = -0.3$	$x_{13} = -21.9$	

Using these values one can determine the frequency of the fundamentals of the parallel ν_3 bands of CO_2 from the expression given by

$$\omega(v_1v_2v_3l \rightarrow v_1v_2v_3+1) = \omega_3 2x_{33}(1+v_3) + x_{13}(v_1+\tfrac{1}{2}) + x_{23}(v_2+1) \quad . \tag{20}$$

The ground state fundamental is therefore given by $\omega(0000 \rightarrow 00010) = \omega_3 + 2x_{33} + \frac{1}{2}x_{13} + x_{23} = 2349.4\ cm^{-1}$.

Overtones and combinations are determined in exactly the same way. The vibrational anharmonic states of a linear triatomic molecule which is symmetric have also been calculated to third order in the v^S by Stull, Wyatt, and Plass[31]. The third order constants are very small.

It is now necessary to include the effects of rotation; this is done by calculating the vibration-rotation energy levels. The resultant energy expression (including vibration (harmonic plus anharmonic), rotation, and vibration-rotation) for the rotating vibrating linear symmetric triatomic molecule is given by equation (19) plus terms of the form

$$B_v[\ J(J+1) - l^2] \tag{21}$$

where B_v is given by

$$B_v = B_e[1 - \sum_{i=1}^{3}(v_i + \tfrac{1}{2}d_i)\alpha_i] \quad . \tag{22}$$

The α_i are referred to as convergence factors; they have been determined with the aid of experiment, for CO_2. The best averages of these

factors are given by[8]

$$B_e \alpha_1 = +0.00058$$

$$B_e \alpha_2 = -0.00045$$

$$B_e \alpha_3 = +0.00307$$

B_e is given by $h/8\pi^2$ Ac and is referred to as the equilibrium rotational constant; A is the equilibrium moment of inertia. B_e has been determined by Courtoy[7] to be 0.3916 for $C^{12}O_2^{16}$. The rotational constants B_{0000} and B_{0010} are given by Courtoy as 0.39021 and 0.38712 respectively (using $B_{v_1v_2v_3l}$).

An additional contribution to the vibration-rotation interaction results from the influence of nonrigidity or centrifugal stretching. This means that an additional term has to be added to (19) and (21) in the form of

$$D_v[J(J+1) - l^2]^2 \quad . \tag{23}$$

If one allows for the approximation $D_v \approx D_{v'}$, then $D_v \approx 4B_e^3/\omega_1^2$. Stull, Wyatt and Plass[30] have shown that the value of D_v is less than 5×10^{-7} B_v for CO_2.

The rotational term value can therefore be given by

$$F_v = B_v[J(J+1)-l^2] - D_v[J(J+1)-l^2]^2 \tag{24}$$

To determine the frequency of the vibrational rotational transitions in wave numbers as a function of J, one subtracts the term value of the lower state from that of the upper state. For $\Sigma - \Sigma$ bands, the formulas for the fine structure in the P and R branches (there is no Q branch) are given by

$$\nu_P = \nu_0 - (B_{v''}+B_{v'})J - (B_{v''}-B_{v'})J^2 + 2(D_{v''}+D_{v'})J^3 \tag{25a}$$

$$\nu_R = \nu_o + 2B_{v'} + (3B_{v'}-B_{v''})J - (B_{v''}-B_{v'})J^2 - 2(D_{v''}+D_{v'})(J+1)^3 \quad . \quad (25b)$$

The line spacing, d, can be obtained from $\nu(J+1) - \nu(J)$. Gray[14] has used the approximation

$$\tfrac{1}{2}d_m = (B_{v''}+B_{v'}) - 2(B_{v''}-B_{v'})m - 6(D_{v''}+D_{v'})m^2 \qquad (26)$$

for Σ-Σ transitions in calculations for the 4.3 micron parallel bands of CO_2 (M = - J for P branch and J + 1 for R branch).

The rotational constant in the lower vibrational state is greater than the rotational constant in the upper vibrational state; in other words $B_{v''} > B_{v'}$. Therefore the J^2 term in (25) results in a slight convergence of the lines in the R branch(toward the band center), and a slight divergence of the lines in the P branch , with increasing J. The D term leads to a convergence of the rotational lines with increasing J in both branches and therefore to a general contraction or shrinkage of the entire band. Since the J^2 term increases faster than the J term, a Band Head is formed in the R branch. For the parallel band ground state fundamental of CO_2 this is established at $J_{B.H.}$ = R 122 at 2397.1 cm^{-1}.

The odd J" transitions are missing in CO_2 due to the zero spins of the oxygen nuclei. This missing line phenomena can be detected by noticing that the P branch line series is π out of phase with the R series.

The fine structure for Σ-π bands is determined in exactly the same way. These bands are perpendicular bands with a P,Q, and R branch. An example of this band type is the ν_2 ground state fundamental

for CO_2 at 15 microns.

$\pi - \pi$ bands must be considered; these are parallel bands with a P,Q, and R branch ($l = \pm 1$, $\Delta l = 0$, $\Delta J = 0, \pm 1$). There are no fundamentals of this type. The difference bands generally belong to a sequence which is initiated with a $\Sigma - \Sigma$ band and therefore the $\pi - \pi$ spectra usually overlap the $\Sigma - \Sigma$ spectra. an example of this type of band for CO_2 is given by $(0101), \pi u) \rightarrow (0111, \pi g)$ at 2336 cm^{-1}; this is a combination difference band. The fine structure can again be found from the rotational term value by using $l^2 = 1$ in both states.

4. Band Models. Since isolated spectral lines exist only as exceptions, we must now consider the concept of a Band Model. We are interested in formulating a model to describe the band structure resulting from N "interacting" spectral lines. This includes making estimates of the position, shape and width, and intensity of the spectral lines for the molecular spectra and conditions of interest, and then averaging the results over a given frequency interval. The most difficult aspect of determining the model is that the intensity versus wavelength distribution is a fast oscillating typically irregular distribution; this is due to the sharp vibration-rotation spectral lines which are the basic elements of the spectrum. The two main aspects of determining a model are:

1. estimate a spectral distribution function for the single line and the N "interacting" lines.
2. determine the pertinent spectral interval over which to average the line distribution predicted in number 1.

The difficulty in number one is that the oscillations are hard to define;

only those distributions functions which are integrable are of any use. If we restrict the analysis to pressure broadening effects, then the Lorentz line shape can be used for each line. The distribution function for the N spectral lines is the main subject of Band Models. This function is generally divided into two classes: 1. deterministic functions and 2. random functions.

In the typical infrared absorption experiment, the upper limit for the averaging interval is that region which does not significantly alter the vibration-rotation band contours, and over which the blackbody spectrum is approximately constant. The lower limit for the averaging interval is that value which no longer smooths out the fast oscillations, or the fine structure, of rotational lines. Typical intervals are on the order of 25 cm^{-1} and contain several rotational lines.

It is customary to assume that the functional form for the average value process is given by the absorption or equivalent width; which is defined by

$$W_{\nu'} = \frac{1}{\Delta\nu} \int_{\nu'}^{\nu'+\Delta\nu} (1 - \exp - \sum_{i=1}^{N} K_i(\nu)u)d\nu \qquad (27)$$

for a homogeneous path. K_i is the absorption coefficient for the $i^{\underline{th}}$ spectral line and ν' is the position of the averaging interval of width $\Delta\nu$ and u is the absorber amount. This leads to the concept of a generalized absorption coefficient which varies much slower with frequency (on the order of the vibration-rotation contour) than the line absorption coefficient which varies as the rotational line structure.

When the spectral interval includes <u>all</u> the spectral lines in a given band, the measured equivalent width is than equal to the true equivalent width. This leads to the relationship given by

$$\int_{\nu_1}^{\nu_2} W(\nu)d\nu = \int W'(\nu)d\nu \quad , \tag{28}$$

which defines the Total Equivalent Width or Total Absorption. The integrand on the r.h.s. defines a true equivalent width as would be defined by an instrument of infinite resolving power; the l.h.s. has an integrand which is a measured or apparent equivalent width as measured with an actual instrument. When $W(\nu)$ is averaged over a complete but finite band from ν_1 to ν_2 containing all the spectral lines in the band then it is equal to the average (over all frequencies) of the true equivalent width, as expressed in (28).

We shall now very briefly consider some of the better known models. The Elsasser Band Model was the first to be investigated; it is applied to cases which have complete order in their spectral line structure. It assumes a periodic pattern for the rotational line positions, equally intense lines and equal halfwidths, with a line shape given by the Lorentz line shape. The equivalent width is therefore given by

$$W_{\nu'} = \frac{1}{\Delta\nu}\int_{\Delta\nu}(1 - \exp - \sum_{n=-\infty}^{+\infty}\frac{S\gamma u}{(\nu-nd)^2 + \gamma^2})d\nu \tag{29}$$

This can be expressed in terms of periodic and hyperbolic functions and solved although the general solution is not straight forward. One therefore generally considers the solutions in terms of limiting approximations. The weak line approximation is characterized by a rotational fine structure (before averaging) which is relatively smooth and by line centers which are shallow and nonblack. This condition exists for large foreign gas pressures and small amounts of absorber; the equivalent width is given by

$$W_{W.L.} = 1 - \exp - Su/d \tag{30}$$

u is the absorber amount and d is the line spacing. The strong line approximation is characterized by extreme fluctuations and black line centers; this occurs for small foreign gas pressures and large absorber amounts. The equivalent width is given, for the Elsasser band, by

$$W_{S.L.} = \frac{2}{\pi} \int_0^z \exp - z'^2 dz' \qquad (31)$$

where $z = (\pi S u \gamma / d^2)^{\frac{1}{2}}$. γ now denotes the line halfwidth; this integral is the error function erf(z).

There is an ill defined region between the weak and strong line regions. In this region the arguments of the exponential and error functions are given in terms of $P^m u^l$.[28] The approximate ranges of the exponents are $0 \lesssim m \lesssim \frac{1}{2}$ and $\frac{1}{2} \lesssim l \lesssim 1$; the m and l exponents therefore change at different rates and in the opposite directions when leaving the strong line region. Thus the exponents vary considerably and in a generally unspecified manner within this region, although m is usually less than 1. The temperature dependence is not as easily determined in this region, although it should vary in a smooth way between the weak and strong line dependencies.

The last approximation is the nonoverlapping line approximation. The only condition for this approximation is negligible overlapping of the lines and therefore and therefore small broadening pressures. The equivalent width is given by

$$W_{N.O.L.} = \beta \psi \exp - [J_o(i\psi) - J_1(i\psi)] \qquad (32)$$

where $\beta = Su/2\pi\gamma$ and $\psi = 2\pi\gamma/d$. The $J^{\underline{s}}$ are zero and first order Bessel functions of the first kind with imaginary arguments. For small values of ψ, this reduces to

$$W_{N.O.L.}\ (\text{linear}) = Su/d, \qquad (33)$$

while for large ψ

$$W_{N.O.L.} \text{ (square root)} = 2(S\gamma/d^2)^{\frac{1}{2}}. \qquad (34)$$

When dealing with highly irregular distributions of spectral lines, the Statistical Model is of some use. The line positions are assumed to be completely random in this model, and the line intensities are assumed to be randomly distributed over the band. The Lorentz line shape is generally used and the halfwidth is assumed constant. For an infinite number of lines and a Dirac delta function distribution for the line intensities, the equivalent width is given by

$$\bar{W}_{\delta} = 1 - \exp - [\beta\bar{\psi} \exp -\beta\bar{\psi}(J_o(i\bar{\psi}) - iJ_1(i\bar{\psi}))] \quad . \qquad (35)$$

Goody[12] also derived a similar result in terms of the exponential distribution of the line intensities. The weak line approximation to (35) is identical to equation (29). The strong line approximation is given by

$$\bar{W}_{S.L.,\delta} = 1 - \exp - (\tfrac{2}{\pi}\beta^2\bar{\psi})^{\frac{1}{2}} \quad . \qquad (36)$$

The nonoverlapping line approximation is given by expression (32).

Due to the different functional dependence of the two models, it can be shown that the Elsasser Model saturates faster than the Statistical Model; this fact is generally used to determine the best model to use for a given set of data.

These are the two basic models; they are limiting cases in the sense that one uses a completely deterministic line structure and the other a random line structure. The Random-Elsasser Model is an obvious generalization of these two models; it uses a random superposition of a number of Elsasser bands which can have different line intensity, spacing, and position. This model describes fairly well, the physical

situation of a strong regularly spaced ground state fundamental which is overlapped by several also regularly spaced overtones and combinations. This situation describes the 4.3micron region of CO_2; twelve separate overlapping bands have been measured in this region and at least thirty are predicted. It is somewhat startling that the Random-Elsasser results significantly depart from the Elsasser results and move toward the Statistical results for very small values of n, where n is the number of Elsasser bands considered. For n = 2 and $S_1 = 10S_2$, the absorption predicted by this model is about halfway between the Elsasser and Statistical results.[26]

The Quasi-Random Model is characterized by the fact that it closely represents the actual spacing of the lines by dividing the interval into a number of subintervals within which the lines are localized and assumed randomly distributed. This model allows for a more accurate simulation of the actual intensity distribution than the above models and takes into consideration the wing contribution from lines outside the interval. What this model gains in accuracy, it loses in simplicity and computational time; also apriori knowledge of the rotational fine structure is required.

The last model that we shall consider is the Modulated Band Model. King proposed to modulate the infinite line array model, such as the Elsasser Model and the Statistical Model, with an exponential envelope before the total band frequency integration is performed. The exponential decay type envelope is used to describe the fact that in a typical vibration-rotation band, the intensities of the lines near the center of the band are stronger than those near the wings of the band. The re-

sults of this model can be given in terms of a "strong" and a "weak" approximation. We shall give these approximations in terms of some experimental results of Howard, Burch and Williams[15] for CO_2, even though these results were not considered in terms of this model at that time. For small absorption and the "weak" approximation, they found that

$$\int W(\nu)d\nu = cu^{\frac{1}{2}} (P + p)^k \qquad (37)$$

fit their data quite well. For large absorption and the "strong" approximation, they found that

$$\int W(\nu)d\nu = C + D\log u + K\log (P + p) \qquad (38)$$

fit their data quite well. Howard, Burch and Williams found that for their parameters, all the 4.3 micron CO_2 data fit the "strong" approximation quite well. They found that the constants, C = 27.5, D = 34 and K = 31.5 fit their data if P and p are in mmHg, u in atm-cm, and the log is in the base 10. Remember, this is for total absorption not the spectral absorption.

In somewhat similar fashion Burch, Gryvnak, and Williams[5] have determined that the total absorption for CO_2 has a form given by

$$\int W(\nu)d\nu = a(uP_e^{\,b})^c \quad . \qquad (39)$$

For the 4.3 micron region, a = 15.0, b = .75 and c = .54 with P_e in mmHg and $\int W d\nu$ in cm^{-1}. Thus the dependence on u is stronger than the dependence on P_e. This result is similar to that expected in the ill defined region.

B. The Radiative Transfer Process

We will now briefly consider the fundamentals of the radiative transfer process applied to the atmosphere; this will be used as a ba-

sis from which to explain the crossed beam correlation technique. The analysis is on a macroscopic level.

1. Fundamentals. When radiation comes into contact with a given medium, the radiant energy can be modified due to the interaction of the radiation and the matter. We will now describe such interactions by assuming the existence of extinction and emission processes, which both include scattering.

The various processes that define the extinction and emission processes can be combined to define an equation of radiative transfer which is given for plane parallel geometry by

$$(1/\rho \sec(\hat{x},\hat{n}))\frac{\partial I_\lambda}{\partial z} = -\xi_\lambda I_\lambda + j_\lambda \quad , \tag{40}$$

where

$$j_\lambda = \frac{1}{4\pi}\int P(\hat{x},\hat{x}')S_\lambda I_\lambda d\omega_{\hat{x}} + j_\lambda^{(t.e.)} \quad , \tag{40a}$$

$$\xi_\lambda = K_\lambda + S_\lambda \quad . \tag{40b}$$

ρ is the mass density, $\hat{x}$ is a unit vector in the direction of radiation, $\hat{n}$ is a unit normal to a surface element, z is an axis in the vertical direction, ξ_λ is the extinction coefficient and j_λ is the emission coefficient. j_λ is made up of a contribution due to scattering where S_λ is a scattering coefficient and $P(\hat{x}, \hat{x}')$ is an angular distribution function, and a contribution $j_\lambda^{(t.e.)}$ due to true emission. ξ_λ is made up of a true absorption coefficient K_λ and the scattering coefficient S_λ.

Using the geometry in Figure 1, the solution of this equation can easily be found, with the use of an integrating factor, to be

$$I_\lambda(0) = I_\lambda(z)\exp - \int_0^z \rho\sec(\hat{x},\hat{n})\,\xi_\lambda dz'' + \int_0^z j_\lambda \rho \sec(\hat{x},\hat{n})\left[\exp - \int_0^{z'} \rho \sec(\hat{x},\hat{n})\xi_\lambda dz''\right]dz' \quad . \tag{41}$$

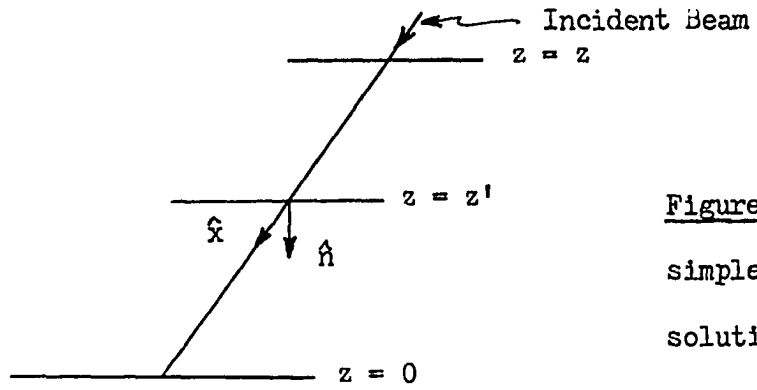

Figure 1. Geometry for simple emission-absorption solution.

This is the formal solution of the radiative transfer equation, z" is a dummy variable of integration between z = zero and z = z'. The first term in (41) represents the intensity of the original incident beam at the position z = z attenuated by the intervening matter in its path from z = z to z = 0. The second term is the intensity due to emission at all interior points along the path reduced by the matter between each element at z' and the position z = zero.

It is convenient to define a source function, τ_λ, which relates the emission and extinction coefficients; it is given by

$$\tau_\lambda = j_\lambda / \varepsilon_\lambda . \tag{42}$$

In Local Thermal Equilibrium, the source function is given by the blackbody intensity $B_\lambda(T_Z)$ and the solution (41) reduces accordingly, where $j_\lambda \rightarrow j_\lambda^{(t.e.)}$ and $\varepsilon_\lambda \rightarrow K_\lambda$. The radiative transfer equation now contains the two variables B_λ and I_λ and therefore requires an additional constraint equation for uniqueness. This auxiliary equation is given by the corresponding flux density equation. These equations are very general in nature and can often be reduced considerably when applied to a specific situation. The exact solution of these general equations is, as a

rule not possible, and one is forced to resort to such approximations as the Differential Approximation, and the Thick and Thin Limits where mean value absorption coefficients such as the Rosseland and Planck mean absorption coefficients are defined.

But these mean value absorption coefficients are no longer valid in a strongly nongray condition as is found for our experimental conditions, and in fact such as approach can lead to highly inaccurate results. Instead, one resorts to a Band Energy Approximation[2] which breaks the complete spectrum into N bands each of which can be treated separately. Approximations are made, over this limiting or basic interval, for the wavelength distributions. This leads directly to the Band Model approach discussed in section II.A.4 .

One generally considers the radiative transfer problem only in the sense of treating the medium as a black box containing a model of the mechanism for the interaction of light and matter, with a given input and a resultant output. In many instances, however, one is interested primarily not in the radiation that is transferred through a given medium as in heat transfer problems, but rather in the characteristics of the medium through which the light passes. The light or radiation, after passing through the medium, acts as a "signature" which can be used to describe certain properties of the medium. We are interested in determining these signatures.

The radiative transfer equation, as we have described it above, consists of an integral(s) over the light path from the source to the detector. Therefore one determines with their use, spatially averaged properties of the medium. On the other hand Hot Wire Probes can be used

to measure certain properties of the medium in the form of point measurements. The usage of one type of measurement over the other depends on the application, although a spatial resolution somewhere between these two limits is generally needed. Actually, some spatial averaging may be beneficial because it allows one to achieve statistical regularity in the measurements.

Thus it is of interest to consider whether one can use the radiative transfer approach discussed above, and still measure local information about the medium inside the volume along the optical path from the source to the detector. It has been found that the retrieval of local information is made possible by taking advantage of one or more of the remaining independent variables in the radiative transfer formulation. These variables can be the wavelength, the remaining space variables, or the time. The solution requires in a basic sense, repeating the measurement over a range of the chosen remaining variables. We shall consider only the time variable which leads to the Crossed Beam Correlation Method.

2. Crossed Beam Correlation Technique.[10] Let us now consider the case where the radiative transfer system consists of two (or more) crossed beams. The point of intersection of the two beams is assumed to be variable in the medium; it is determined by the source/detector configuration. After selecting the region of interest by triangulation of the two beams, the resultant intensities from each beam are shifted in time, multiplied together and averaged over time.

The instantaneous signal at each detector represents the sum total of all fluctuations occurring along the path at a particular time. Those fluctuations which occur sufficiently far from the beam intersec-

tion point are not correlated and average to zero; the resultant measurement is a space time correlation function. This function has a contribution only from those fluctuations which occur within a correlation area centered about the beam intersection point; therefore: local information and remote sensing applications. The remote sensing application is a valuable attribute of the crossed beam system since point probes or any probe that must be inserted at the actual point being measured will always perturb the field. It also allows one to monitor regions hitherto inaccessible to mechanical probes.

This approach represents a significant departure from most classic radiative transfer approaches (which are usually under steady state conditions in time) in that it takes advantage of the statistical information given in the form of the fluctuations about the mean values.

Consider the geometry of the crossed beam system in Figure 2. This allows for a variable beam intersection point and integration from the source to the detector, and a spatial separation of the two beams in the x direction given by ξ. The medium can be inhomogeneous and can be assumed to be a turbulent flow field moving in the + x direction. The two solutions to the corresponding radiative transfer equation can be given by

$$I_\lambda^{(1)}(x,y,z+\zeta_d) = I_\lambda^{(1)}(x,y,z-\zeta_s)\exp -\int_{-\zeta_s}^{+\zeta_d} \varepsilon_\lambda(x,y,z+\zeta'')d\zeta'' + \int_{-\zeta_s}^{+\zeta_d} j_\lambda(x,y,z+\zeta')\exp -\int_{\zeta'}^{+\zeta_d} \varepsilon_\lambda(x,y,z+\zeta'')d\zeta''d\zeta' \quad , \tag{43a}$$

and

$$I_\lambda^{(2)}(x,y+\eta_d,z) = I_\lambda^{(2)}(x,y-\eta_s,z)\exp -\int_{-\eta_s}^{+\eta_d} \varepsilon_\lambda(x,y+\eta'',z)d\eta'' + \int_{-\eta_s}^{+\eta_d} j_\lambda(x,y+\eta',z)\exp -\int_{\eta'}^{+\eta_d} \varepsilon_\lambda(x,y+\eta'',z)d\eta''d\eta' \quad . \tag{43b}$$

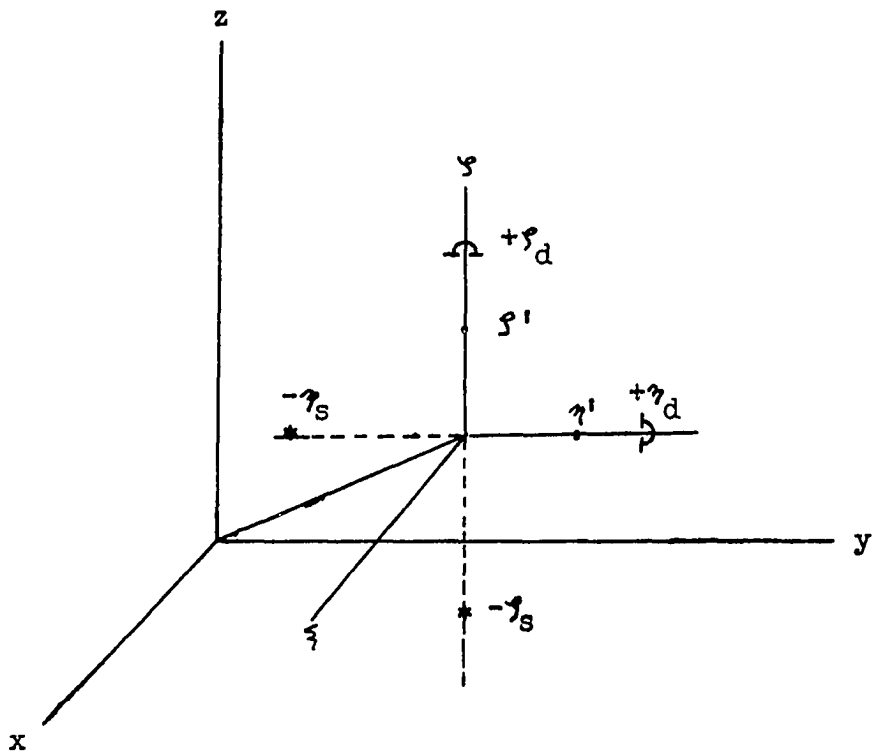

Figure 2. Geometry for Crossed Beam System. * = source, ζ = detector.

These solutions represent instantaneous values and therefore j_λ, I_λ and ε_λ are function of time. Separating these instantaneous values into time averaged mean values and fluctuations about the mean leads to

$$I_\lambda(\vec{x},\vec{\xi},t) = \langle I_\lambda(\vec{x},\vec{\xi},t)\rangle_t + i_\lambda(\vec{x},\vec{\xi},t) \quad , \qquad (44a)$$

$$\varepsilon_\lambda(\vec{x},\vec{\xi},t) = \langle \varepsilon_\lambda(\vec{x},\vec{\xi},t)\rangle_t + e_\lambda(\vec{x},\vec{\xi},t) \quad , \qquad (44b)$$

$$j_\lambda(\vec{x},\vec{\xi},t) = \langle j_\lambda(\vec{x},\vec{\xi},t)\rangle_t + \jmath_\lambda(\vec{x},\vec{\xi},t) \quad . \qquad (44c)$$

We are basically interested in the fluctuations about the mean; in particular, we are interested in that fluctuation component which is due to the fluctuations in the thermodynamic state variables of the medium.

In the general case, the total fluctuating intensity for either of the two beams can be found from equation (43), however the expression is long and becomes somewhat unwieldy. Therefore we go to the

special case where the extinction process dominates the emission process. This occurs when we restrict the problem to short wave radiation transfer. In this case equation (43a) reduces (with the use of 44a and 44b) to

$$\langle I_\lambda^{(1)}(x,y,z+\tau_d,t)\rangle + i_\lambda^{(1)}(x,y,z+\tau_d,t) = \tag{45}$$
$$= I_\lambda^{(1)}(x,y,z-\tau_s)\exp - \int_{-\tau_s}^{+\tau_d} \langle \varepsilon_\lambda(x,y,z+\tau'',t)\rangle d\tau'' \exp - \int_{-\tau_s}^{+\tau_d} e_\lambda(x,y,z+\tau'',t)d\tau''.$$

Now, the extinction process can be arranged so that the integral

$$\int_{-\tau_s}^{+\tau_d} e_\lambda(x,y,z+\tau'',t)d\tau'' \tag{46}$$

is sufficiently small to permit linearization. This can always be arranged by adjusting the mean absorption level.[10]

The average intensity is given by

$$\langle I_\lambda^{(1)}(x,y,z+\tau_d,t)\rangle = I_\lambda^{(1)}(x,y,z-\tau_s)\left\langle \exp - \int_{-\tau_s}^{+\tau_d} \varepsilon_\lambda(x,y,z+\tau'',t)d\tau''\right\rangle . \tag{47}$$

The source fluctuations are neglected at this point in the development of the theory since the fluctuations of interest are those due to the medium, not the source.

We now make the approximation that

$$\left\langle \exp - \int_{-\tau_s}^{+\tau_d} \varepsilon_\lambda(x,y,z+\tau'',t)d\tau''\right\rangle = \exp - \int_{-\tau_s}^{+\tau_d} \langle \varepsilon_\lambda(x,y,z+\tau'',t)\rangle\, d\tau'' . \tag{48}$$

The condition for this approximation to be valid can be found by expanding the exponentials on both sides of (48) and substituting $\langle \varepsilon_\lambda \rangle + e_\lambda$ for ε_λ. The equality holds when terms to second order and higher in the fluctuating absorption coefficient given by (for example)

$$\left\langle \left[\int_{-\tau_s}^{+\tau_d} e_\lambda(x,y,z+\tau'',t)d\tau''\right]^2\right\rangle \tag{49}$$

are very small. This condition is again the linearization condition mentioned above. Therefore equation (45) can be given by

$$\langle I_\lambda^{(1)}(x,y,z+\zeta_d,t)\rangle + i_\lambda^{(1)}(x,y,z+\zeta_d,t) =$$
$$= \langle I_\lambda^{(1)}(x,y,z+\zeta_d,t)\rangle\left[1 - \int_{-\zeta_s}^{+\zeta_d} e_\lambda(x,y,z+\zeta'')d\zeta''\right] \quad . \tag{50}$$

The intensity fluctuations at the detectors reduce to

$$i_\lambda^{(1)}(x,y,z+\zeta_d,t) = -\langle I_\lambda^{(1)}(x,y,z+\zeta_d,t)\rangle_t \int_{-\zeta_s}^{+\zeta_d} e_\lambda(x,y,z+\zeta'',t)d\zeta'', \tag{51a}$$

$$i_\lambda^{(2)}(x,y+\eta_d,z,t) = -\langle I_\lambda^{(2)}(x,y+\eta_d,z,t)\rangle_t \int_{-\eta_s}^{+\eta_d} e_\lambda(x,y+\eta'',z,t)d\eta''. \tag{51b}$$

These expressions represent the product of the mean intensity at the detector and the integral of the extinction coefficient fluctuations along the entire path from the source to the detector.

Let us now multiply these two detector signals together and average over time which gives the "two beam product mean value" given by

$$G_\lambda(x,y,z) = \frac{1}{T}\int_0^T i_\lambda^{(1)}(t)i_\lambda^{(2)}(t)dt \quad . \tag{52}$$

Substituting for i_λ leads to

$$G_\lambda(x,y,z) = \langle I_\lambda^{(1)}(x,y,z+\zeta_d,t)\rangle_t \langle I_\lambda^{(2)}(x,y+\eta_d,z,t)\rangle_t$$
$$\int_{-\eta_s}^{+\eta_d}\int_{-\zeta_s}^{+\zeta_d} \overline{e_\lambda(x,y,z+\zeta'',t)e_\lambda(x,y+\eta'',z,t)}d\eta''d\zeta'' \quad . \tag{53}$$

where the overbar represents the time average. This expression is a reduced space time covariance function. Neglecting the spatial integration for a second, we have a time averaged product of the fluctuations at the points $(x,y,z + \zeta'', t)$ and $(x,y + \eta'', z,t)$. If these points are sufficiently spatially separated then the resultant time average for that separation will go to zero (if averaged long enough) on statistical grounds. Only points clustered about the beam intersection point within a prespecified area will yield nonzero contributions to the time

integral. Therefore the limits on the above integrals over η and ξ can be changed to those corresponding to the correlation area of the medium without changing $G(x,y,z)$. Analytic expressions for the correlation area have been derived[9] in terms of the covariance function and the rms intensities.

To find the magnitude of the fluctuations of a given property of the medium, it is necessary to know the size of the correlation area and the magnitude of the fluctuations of the extinction coefficients as well as the relationship between these two properties. Calibration measurements from a single beam experiment can be used to determine the essential properties of the extinction coefficient as a function of the general properties of the medium. Our experiments were designed with this in mind.

The components of the source and the detector noise that are statistically independent will average to zero if averaged long enough, and therefore this technique can be used in situations involving low signal to noise levels.

To demonstrate the power of this technique one must consider the general case where one beam is displaced a distance ξ in the "flow" direction and where a time delay τ is introduced between the two beams; this results in a space time covariance function given in terms of $G(x+\xi, y,z,\tau)$. This leads to measurements of eddy lifetimes, turbulence spectra, flow velocities and so forth.[10]

The application of the crossed beam correlation technique that we are most interested in can be referred to as Crossed Beam Molecular Spectroscopy. The difference between this and conventional spectroscopy

is that we are now dealing with the local fluctuations in the optical variables due to the local fluctuations in the thermodynamic state variables, instead of considering only the steady state values that are averaged over the path length as in conventional spectroscopy.

For simplicity only, we now assume that true absorption dominates the extinction process and therefore we neglect scattering. The instantaneous absorption coefficient is now a function of the instantaneous values of the partial pressure of the absorber, the total pressure and the temperature, which are themselves dependent on position and time. If the fluctuations are small enough, then the instantaneous absorption coefficient can be expanded in a Taylor series expansion about the mean value, and only linear terms kept. This leads to an absorption coefficient fluctuation given by

$$\delta K = \frac{\partial}{\partial p}K(P,T,p)\Big|_{\bar{P},\bar{T},\bar{p}}\delta p + \frac{\partial}{\partial P}K(P,T,p)\Big|_{\bar{P},\bar{T},\bar{p}}\delta P + \frac{\partial}{\partial T}K(P,T,p)\Big|_{\bar{P},\bar{T},\bar{p}}\delta T + \cdots \quad . \tag{54}$$

When this is substituted for an absorption coefficient fluctuation fixed at the minimum beam separation separation point (which is therefore no longer a function of (ξ,η,ζ), the general crossed beam molecular spectroscopy result can be given by

$$\begin{aligned} R(\vec{x},\vec{\xi},\tau) = {} & \frac{\partial\bar{K}}{\partial p}\iint \overline{\delta p(\vec{x},t)\delta K(\vec{x}+\vec{\xi},t+\tau)}\,d\eta\,d\zeta + \\ & + \frac{\partial\bar{K}}{\partial P}\iint \overline{\delta P(\vec{x},t)\delta K(\vec{x}+\vec{\xi},t+\tau)}\,d\eta\,d\zeta + \\ & + \frac{\partial\bar{K}}{\partial T}\iint \overline{\delta T(\vec{x},t)\delta K(\vec{x}+\vec{\xi},t+\tau)}\,d\eta\,d\zeta \quad . \end{aligned} \tag{55}$$

where we have normalized the result to the product of the mean intensities of each beam and where $\bar{K}$ is the absorption coefficient evaluated at the mean value. R is equal to G divided by the two mean intensities.

The area integrals are spatial cross correlations with a temporal cross correlation in the integrand; these factors are responsible for the localization and are referred to as Turbulence Factors. If an optical filter is placed over beam number two, then the turbulence factor (Q_p, Q_p and Q_T) defined by the area integrals in equation (55), are independent of λ. These factors are multiplied by the three mean value derivatives which are functions of λ.

Equation (55) is not sufficient to determine the local thermodynamic properties of a given medium, and therefore calibration measurements must also be performed. A single beam experiment can be used to determine the expected magnitudes of the partial derivatives of the absorption coefficient with respect to the thermodynamic variables, evaluated at their mean values; the temporal crosscorrelations between the fluctuations of the thermodynamic variables and the fluctuations of the absorption coefficients (for the single beam); and the temporal correlation of the fluctuations of the intensities in the special case of equal beams.

These quantities will help disentangle the space-time correlations in equation (55) and can be used to calibrate the crossed beam system. It is not sufficient to use only static or nonfluctuating measurement conditions, even though they could be used to determine the mean value derivatives; it is necessary to establish, experimentally, typical atmospheric fluctuation conditions from which measurements can be made. Our experiment established this.

These measurements can also be used to search for possible positions in the spectrum where one or two of the mean value derivatives

vanish; this greatly simplifies the analysis by reducing (55) to one or two terms. The concept of frozen composition, where $P/p = f$, a constant also simplifies the above relationship; this condition can be assumed to exist in the atmosphere for CO_2 (see cell conditions section).

The next step is to set up an actual crossed beam system in the laboratory which again simulates the atmospheric fluctuation conditions. One can also easily establish a gas flow in a direction perpendicular to the two beams; this can also be done in the single beam experiment although it was not done in our experiment. Finally field tests should be performed.

Let us also mention that one has an option of using an active or a passive system. In a passive system, situated for example in the atmosphere, the fluctuations of the given tracer element may be detected by using scattered and reflected sunlight. This requires the use of two telescopes.

C. Dependence of the Absorption on the Thermodynamic Variables

We shall now consider the dependence of the absorption and the absorption coefficient on the variables P,T,and u, the total gas pressure, the temperature, and the absorber amount. The dependence will be considered in terms of single line expressions and band model results. The variation with the slit width or bandpass is considered.

1. Pressure Dependence. Band models generally assume a Lorentz line shape can be used to accurately describe the individual spectral lines. They further assume that the halfwidth is independent of the rotational quantum number, J; this is not strictly true[4,35] in a

vibration-rotation band, but it is a reasonable assumption[1] which we shall use.

Since the halfwidth is linearly proportional to the total gas pressure, the frequency or wavelength of the radiation and the pressure can be simply correlated through the Lorentz line shape expression. We can assume here that the equivalent pressure $P_e = P + 0.30p$ is approximately equal to the total pressure P and that the total pressure is approximately equal to the foreign gas pressure, since $p \ll P$ in our experiments. Note the equivalent pressure gives an added weight to the absorber partial pressure; this is because the broadening resulting from collisions of like molecules is usually quite efficient relative to foreign gas broadening. Self broadening is an important consideration only when the CO_2 partial pressure is comparable with the total pressure; it is therefore neglected in our experiments.

The Lorentz line shape is given by equation (2) which can be rewritten as

$$f(\nu-\nu_s) = \frac{2}{\pi} \frac{\gamma}{(\nu-\nu_s)^2 + \gamma^2} \qquad (56)$$

where γ = halfwidth of the line. This is for a single isolated line. A graph of this function versus $(\nu - \nu_s)$ indicates that as the halfwidth and therefore the total pressure increases the line center decreases and the wings increase; crossover* regions are indicated for small ranges of P. An integration of $f(\nu - \nu_s)$ over all ν between $-\infty$ and $+\infty$ shows that the total area of the spectral line is hence independent of P. Thus even though large values of P smooth the line structure, an average

*Crossover refers to the point(s) common to the initial and final shapes.

value will be maintained if the total spectral area is included.

A spectral bandpass that covers the entire line will not therefore see a pressure dependence. A narrow bandpass near the core will see a decrease in the height of the line with an increase in pressure and a bandpass out in the wings will see an increase in the line with an increase in pressure. A properly positioned slit at intermediate values of ν will record a pressure independent line over a small reange of P.

We have implicitly assumed in this discussion that the line center was nonblack which is tantamount to a weak line condition in a band model analysis. For black line centers (which is a strong line condition for band models) the Lorentz line shape formula reduces to $2/\pi \ \gamma/(\nu - \nu_s)^2$. This obviously does not equal a constant when integrated over all ν; instead it leads to an increase in area with an increase in P. Thus there is a positive Absorption-pressure dependence or correlation for the entire band or any nonblack portion of it; crossovers cannot exist for this case. The pressure dependence is again a maximum near the core of the line.

But this has all been for a single isolated line; if instead a bandpass is used which may or may not be infinite but does include several of these spectral lines (which are now assumed to exist) which may or may not overlap, one expects that the pressure dependence as discussed above will change. In fact one expects that there will <u>not</u> be a strong pressure dependence for nonoverlapping nonblack lines in this case, since the comparatively wide slit should include a fair portion of the wings as well as the line centers, atleast for lines that are near the center of the slit. For nonoverlapping or black line centers, one expects that

a stronger pressure dependence will occur.

To analyze this situation, we need to integrate over the given line distribution; this leads to a band model approach.

The line distribution relative to the line shape dependence only is given for the Elsasser Model by

$$K = \bar{S} \sum_{n=1}^{N} \frac{\gamma}{(\nu - nd)^2 + \gamma^2} \tag{57}$$

where $\frac{\gamma}{(\nu - nd)^2 + \gamma^2}$ is the distribution function which corresponds to a P - J(n) correlation. The shape and the height of each of these N lines does not change as n changes; only the position of the line changes and therefore the correlation is a constant with respect to the line shape and amplitudes (or pressure mechanism). This leads one to suspect the small P dependence for a larger number of lines with non-black centers.

A band model analysis yields an absorption for the weak line approximation given by

$$W_{W.L.} = 1 - \exp - \beta\psi \tag{58}$$

where $\beta = Su/d$, S is the integrated absorption, u the absorber amount and d is the line spacing. This expression is independent of the band model chosen to represent the given spectrum, and it is independent of the total pressure P. The independence with respect to P is reasonable since the basic band models (Elsasser, Statistical) use an integration over all space. This independence of P is also true in the linear region of the nonoverlapping line approximation where

$$W_{N.O.L.}^{(L.)} = \beta\psi \tag{59}$$

where $\beta\psi = Su/d$. These expressions are for an infinite bandpass, but

we must also consider the case of a finite bandpass. This has been calculated by Plass[6] for the nonoverlapping line approximation. He has shown that for a bandpass $\Delta\nu = D = nd$, the required expression can be given by

$$W^{(L.)}_{N.O.L.,D} = \frac{2}{\pi}\beta\gamma \tan^{-1}(n\pi/\beta) \qquad (60)$$

(This expression reduces to (59) when $n \to \infty$). There is now a pressure dependence since $\beta = 2\pi\gamma(P)/d$ and $= Su/2\pi\gamma(P)$. Therefore an infinite bandpass yields a pressure independent absorption (59) but a finite bandpass leads to one that is dependent on the pressure. Since the linear region of the nonoverlapping line approximaion is a special case of the weak line approximation, we shall assume that a P dependence will occur for narrow slits in this case also (if not is saturation); in fact as a result of the possible and expected overlapping of the lines, the P dependence should be greater for the same size slit than in the nonoverlapping line case.

In the strong line approximation and in the square root region of the nonoverlapping line approximation, there is always a pressure dependence for the entire band if below saturation. For a strong line approximation,

$$W_{S.L.} = \text{erf}\,((2/\pi)\beta^2\gamma)^{\frac{1}{2}} = \text{erf}\,(\pi Su\gamma/d)^{\frac{1}{2}} \quad . \qquad (61)$$

where $\gamma = \gamma(P)$. This is for the Elsasser Model, and a similar expression holds for the Statistical Model. The nonoverlapping line approximation square root region is given by

$$W^{(S.R.)}_{N.O.L.} = ((2/\pi)\beta^2\gamma)^{\frac{1}{2}} \quad . \qquad (62)$$

In both cases, there is a maximum P dependence of $P^{\frac{1}{2}}$. For a finite interval, in the nonoverlapping square root case, using $\Delta\nu = D = nd$, one has

an expression given by[26]

$$W^{(S.R.)}_{N.O.L.,D} = (2\beta^2\gamma/\pi n^2)^{\frac{1}{2}}(1-\mathrm{erf}(z)) + 1 - \exp -z^2 \quad . \qquad (63)$$

There is an increased P dependence for this case over that in (62). Therefore one is again led to narrow bandpass.

The illdefined region should contain information that is between the weak and the strong line approximations; the pressure dependence of the Absorption A is generally given by $P^{m'}$ where $0 < m' \leq \frac{1}{2}$. Therefore one might expect, in some cases, a reasonable pressure independence for the entire band. One can also expect pressure dependencies that are similar to the strong line case. Thus we see that a bandpass that does not include all the lines in the band will generally lead to pressure dependence. The P dependence is strongest in the core regions of the band where the lines are strongest and deepest and most likely to be characterized by the strong line approximation or the square root nonoverlapping approximation. The character of the lines will change toward the linear nonoverlapping line approximation (or weak line approximation) as one approaches the wings of the band, which results in a minimal pressure dependence for the wing regions (most band models do not take this into consideration).

2. Temperature Dependence. Let us first consider the temperature dependence in terms of a single isolated spectral line. The absorption coefficient is given as the product of the integrated absorption S and the line shape factor $f(\nu - \nu_s)$, both of which are temperature dependent. We again use the Lorentz line shape factor; the corresponding halfwidth has a temperature dependence given by

$$\gamma(T) = \gamma'_o(T_o/T)^{\frac{1}{2}} \quad . \qquad (64)$$

When $f(\nu - \nu_s)$ is plotted versus $(\nu - \nu_s)$ with T as a parameter one again sees that the total area of the curve remains constant as T is varied. An increase in T increases the center region and decreases the wing region; a crossover region is expected for a limited range of T as a result of this part of K. When $f(\nu - \nu_s)$ is inserted into the Elsasser Model formalism, a T - J(n) correlation occurs; this is again constant with respect to the shape and amplitude of each line (the correlation between ν and T for a single line is as explained above). A slight dependence of γ on J does usually occur however we neglect it here. Therefore the T dependence in $f(\nu - \nu_s)$ is for a single line.

It has been shown by Drayson[1] that this temperature dependence is secondary relative to that of S, and can usually be neglected. Therefore we shall now consider S as a function of T. Let us remember that S is obtained from K by integrating over all values of ν; therefore S is independent of ν, but it is multiplied by the function $f(\nu - \nu_s)$. Equation (18) can be used to give, to an approximation, the integrated absorption for a single line in a parallel band. It is given by

$$S = \frac{A(2J + 1)}{T} \exp - BJ(J + 1)/T \qquad (65)$$

where A and B are constants. This represents the distribution function for the integrated absorption of a single rotational line as a function of J and T. It is a result of the varying absorber number density and the varying population, as a function of T. It is valid for gases in LTE (Local Thermal Equilibrium) with only small low frequency pressure fluctuations. The distribution over a single line is given in terms of $f(\nu - \nu_s)$.

The J-T dependence or correlation in (65) leads to a change in

the amplitude or height of the lines as a function of J and to a varying temperature dependence from line to line. Figure 3 is a plot of S versus J with T as a parameter; each J value represents the spectral position in the band of the corresponding rotational transition. The area under the curve increases only slightly with increasing temperature and therefore one is led to expect a temperature crossover region for the band of lines, for a small range of T.

As T increases, the core regions of the band decrease and the wings increase (this of course does not happen as such in the pressure case). A negative temperature dependence of S therefore occurs when a narrow slit is placed in the core regions of the band and a positive dependence occurs for a narrow slit placed in the wings of the band. A properly positioned slit should record a negligible temperature for intermediate J values, over a small range of T. A bandpass which includes the entire band of lines should only record a slight dependence on temperature. The bandpass must be large enough to smooth the rotational fine structure. Before analyzing this function in more detail, we shall now consider its relationship to the overall picture.

Unfortunately the expression given by (65) cannot be used in tact in band model formulations since the band models would not remain in closed form[1]. This is a serious limitation of the band models; they do not correctly correlate spectral position with temperature and cannot alone be used to predict the temperature dependence over the total band. When the J-T dependence in (65) is not included, the approximately constant area of the band (S versus J curve) for a small range of T is no longer true and the slight shift in the peaks of the band also do not oc-

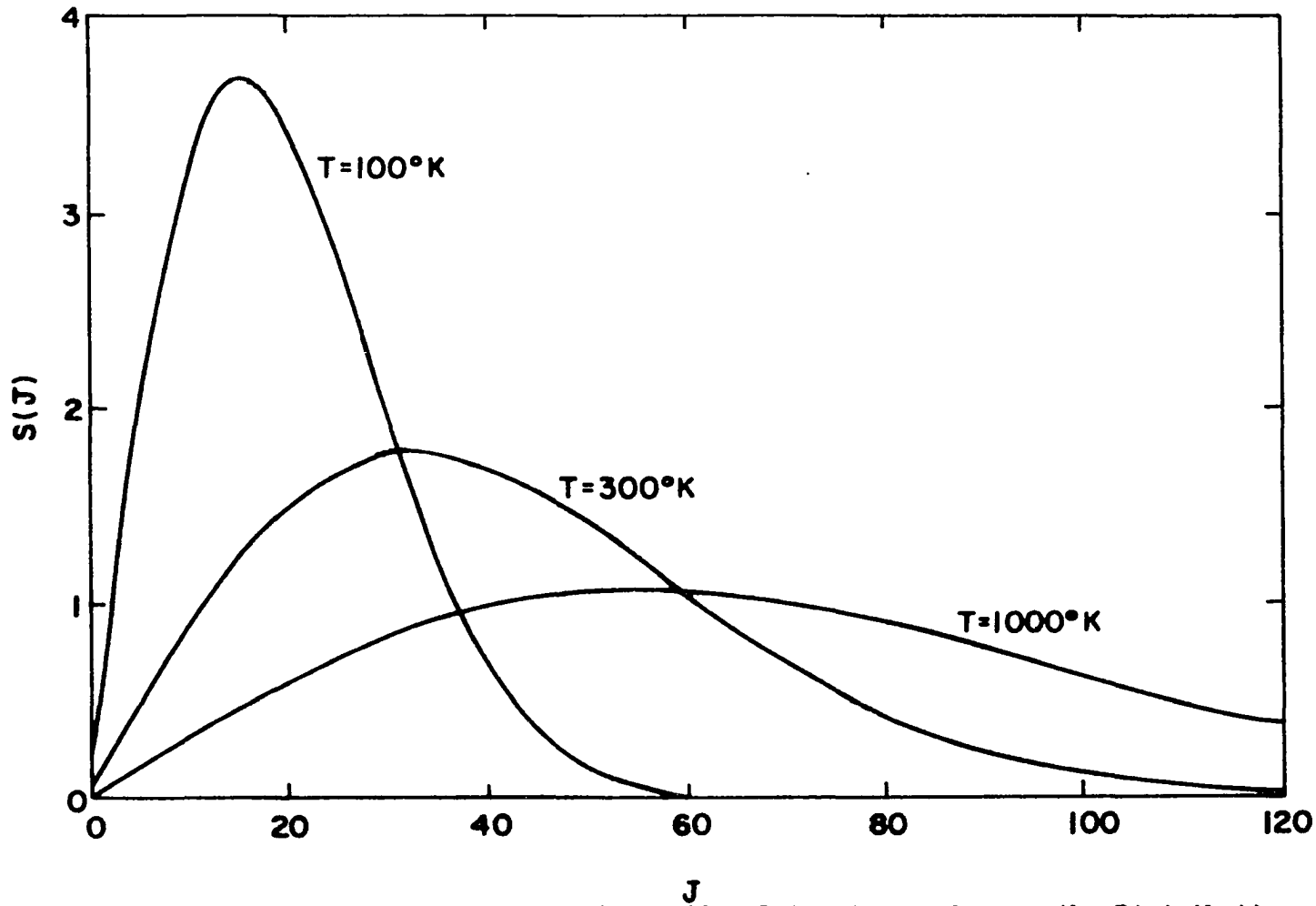

Figure 3 . Effect of Temperature and Rotational Quantum Number on the Distribution of the Integrated Absorption,S, over a Band.

cur.

Band models are forced to make the assumption that S is not an explicit function of position in the spectrum, and therefore S can be removed from the frequency integrations and line summations. They do however use assumed distributions for S relative to some nominal value which is determined empirically. These distributions of S are generally considered to be for a standard temperature and functionally independent of the spectral line positions, although they are used to simulate this dependence. Since an average value of S is found and the J-T correlation is assumed to be lost, the arrangement of the given lines in the interval is no longer critical, which leads to the possibility of various nonphysical but statistically useable distributions for S.

The Elsasser Model assumes that S is a single constant value for all lines in the interval; therefore all S are equal to some nominal value S_o and the intensity profile over the interval is uniform. The Statistical Model uses one of two integrated absorption distributions for each line; either a single Dirac delta function or a single Poisson function is generally used as the probability density function. The same nominal value of S, given by S_o and used in the probability density function, is used for each line. The Statistical Model therefore assumes that the integrated absorptions are similar for each line in the sense that the predicted values are all determined from an identical distribution function. The Modulated Band Model uses an exponential distribution of S which decays from a nominal value of S and represents the change in S from the band center to the wings.

The variable S is then averaged over the assumed distribution

and a single mean value $\overline{S(T_o)}$ is obtained and used in the band models; the Elasser and Statistical Models use an infinite interval or an infinite number of lines. Thus one generally assumes that band models predict the absorption for a band at a constant, standard temperature. The variable T in (65) is then replaced by T_o and the halfwidth reduces to $\gamma = \gamma'_o$.

However, this is not to say that the T dependence in (65) is lost entirely; in fact it can be utilized for band models to an approximation. If the average over the interval includes a significant portion of the entire band, then S is interpreted only in terms of a standard temperature; but if the predicted spectral absorption is for a relatively small portion of the band then one can use the temperature dependence. An integrated absorption $\bar{S}_{J'}$ is found for all possible spectral interval positions, J', in the given band. If the variation of the temperature dependence with J is not significant over the given interval, then the J dependence of S within the interval can be replaced by a constant mean or nominal value which varies in a smooth though undetermined way with J', but which can be removed from the sum over the lines in the interval. The T dependence for the J'.th spectral interval can then be approximated by [25, 19]

$$\bar{S}_{J'}(T) = \frac{Aa(\langle J\rangle_{J'})}{T} \exp -Bb(\langle J\rangle_{J'})/T \quad . * \qquad (66)$$

The average values of the functions of J are different for each interval position J' and depend on the width of the interval. For large J

---

*See page 54 for a further discussion of this expression.

where $J \simeq J + 1$, $b \simeq |a|^2$; the constants might then be reweritten as $|\Delta\omega|$ and $|\Delta\omega|^2$.

If the spectral interval is small enough and the number of spectral interval positions used is large enough, then the cumulative average temperature results should be reasonable. The quantities a and b can be determined by fitting (66) to low resolution data or by using an estimate of the distribution with J' in an average value expression.

Assuming that (66) represents the temperature dependence for the J' interval and using the ω notation, one can find the minimum temperature dependence by taking the derivative of (66) with respect to T and setting the result equal to zero. This results in an expression given by

$$\bar{S}_{J'}(T)(1 - B|\Delta\omega|^2/T) = 0 \quad . \tag{67}$$

Besides the solution where $\bar{S}_{J'}$ is zero, there are two solutions which give the minimum temperature dependence; they are given by

$$|\Delta\omega| = \pm(T/B)^{\frac{1}{2}} \tag{68}$$

and represent regions in the P and in the R branches. Therefore, as expected the temperature crossover regions will increase slightly with increasing temperature. This result can be interpreted in terms of the strong line and the weak line absorption coefficients, although the results are equivalent to (68) except for a factor of 3/2 in the strong line case. One must also realize that the corresponding absorption coefficients are only for a reasonably small J interval centered

at some J'.

Let us now consider the temperature dependence of S in more detail by using a line by line analysis; this yields the expression given by equation (18). We now define an integrated band absorption as

$$S_{B\ v\ l}^{v'l'} = \sum_{J,J'} S_{v\ J\ l}^{v'J'l'} \tag{69}$$

where the sums are over all possible rotational transitions (which is analagous to assuming an infinitely wide bandpass). Equation (69) can be simplified by defining an average value frequency given by $\bar{\nu}_{v\ l}^{v'l'}$ which represents the band center frequency; this is defined using the expression given by

$$\bar{\nu}_{v\ l}^{v'l'}(1 - \exp -h\bar{\nu}_{v\ l}^{v'l'}/kT) \sum_{J,J'} \left|\alpha_{J\ l}^{J'l'}\right|^2 \exp -E_R(J)/kT =$$

$$= \sum_{J,J'} \nu_{v\ J\ l}^{v'J'l'} \left|\alpha_{J\ l}^{J'l'}\right|^2 \left|\gamma_{v\ J\ l}^{v'J'l'}\right|^2 \exp -E_R(J)/kT\ (1 - \exp -h\nu_{v\ J\ l}^{v'J'l'}/kT). \tag{70}$$

Now, using the fact that the $|\alpha|^2$ terms follow the Burger- Dorgelo summation rules, the integrated absorption for a parallel band reduces to

$$S_{B\ \ v\ l}^{(\parallel)\ v'l} = \frac{4\pi^2}{3ch}\bar{\nu}_{v\ l}^{v'l} \frac{ng_l}{Q_V(T)} \left|\beta_{v\ l}^{v'l}\right|^2 \exp -E_V(v_1v_2v_3l)/kT(1 - \exp -h\bar{\nu}_{v\ l}^{v'l}/kT)\ , \tag{71}$$

where $|\beta|^2$ is also temperature dependent.

Now, in a single vibration-rotation band region there are many overlapping bands; if we include only the ν_3 fundamentals where $\Delta v_3 = 1$ (harmonic oscillator approximation), then we can define a Total Integrated Band Absorption, S_{Total} by

$$\begin{aligned} S_{Total} = \sum_{v_3} S_{B\ \ v_1v_2v_3\ l}^{(\parallel)\ v_1v_2v_3+1l} &= \frac{4\pi^2}{3ch}\nu_3 n(1 - \exp -h\nu_3/kT) \\ &\sum_{v_3} \frac{g_l}{Q_V(T)} \exp -E_V(v_1v_2v_3l)/kT \left|\beta_{v_1v_2v_3\ l}^{v_1v_2v_3+1l}\right|^2 . \end{aligned} \tag{72}$$

If we allow for an average value of $|\beta|^2$, and use the fact that $n = p / kT$, then (72) can be rewritten as

$$S_{Total} = \frac{const.}{T} p\overline{|\beta|^2} (1 - \exp -h\nu_3/kT) \qquad (73)$$

Breeze[3] et al have shown that an average value of $|\beta|^2$ can be defined as $(1 - \exp - h\nu_3 / kT)^{-1}$; this cancels with the induced transition term and the resultant temperature dependence is given by const. / T. This is for a region which contains all the rotational transitions of the ν_3 fundamentals. If anharmonic effects are allowed, then the temperature dependence is a more complicated function involving exponential temperature terms.

Let us now consider only a finite portion of the rotational line structure of a parallel band ground state fundamental such as that for CO_2 at 4.3 microns. In this case Δl = zero, Δv_1, Δv_2 = zero, $\Delta v_3 = 1$; l, v_1, v_2, v_3 = zero and therefore (69) reduces to, for low temperatures,

$$S_B = \frac{4\pi^2}{3ch} \frac{\nu_3 p \left|\beta_{00}^{10}\right|^2 g_1}{kTQ_V(T)Q_R(T)} \exp -E_V(0000)/kT \qquad (74)$$
$$\sum_J (2J+1)\exp -BJ(J+1)/kT \quad .$$

If this were summed over all J, then the summation would cancel with Q_R, the rotational partition function, resulting in an expression similar to (71). But instead we shall now assume the $J^{\underline{s}}$ are continuous and integrate (74) over a finite number of lines or more accurately, over a finite bandpass. If we assume $J \approx J + 1$, then the integration yields an expression given by

$$S_B = \frac{4\pi^2 \nu_3 p \left|\beta_{00}^{10}\right|^2 B g_1}{3ch\, Q_V(T)Q_R(T)} \exp -E_V(0000)/kT(1 - \exp -BJ_N^2/kT) \quad . (75)$$

We have assumed the lower limit of integration is the band center. For a large bandpass, where $BJ_N^2 / kT \gg 1$,

$$S_B = \frac{4\pi^2}{3ch} \frac{\nu_3 p \left|\beta_{00}^{10}\right|^2 g_1}{Q_V(T) Q_R(T) B} \exp -E_V(0000)/kT \quad . \tag{76}$$

For small bandpass, $BJ_N^2 / kT \ll 1$,

$$S_B = \frac{4\pi^2}{3ch} \frac{\nu_3 p \left|\beta_{00}^{10}\right|^2 g_1 J_N^2}{Q_V(T) Q_R(T) kT} \exp -E_V(0000)/kT \quad . \tag{77}$$

Therefore the smaller bandpass results in the stronger temperature dependence as expected. One can also express $S_{v\ J\ 1}^{v'J'1}$ in terms of $S_{B\ v\ 1}^{v'1}$ at the same temperature. When this is done, an average value integrated absorption is defined which has a form which is similar to that in equation (66).[27]

These and similar expressions can also be used to define regions of maximum dependence on J and the thermodynamic variables by maximizing the expression with respect to, for example, J and T simultaneously. However these results are of limited accuracy and will not be considered here since they aren't essential to performing the experiment.

The temperature dependence of an actual absorption spectrum is always more complicated than we have assumed it to be, due for example, to overlapping bands of weak lines which have band centers which differ considerably from that of the strong ground state fundamental. Thus one must consider an actual case and work through all the details peculiar to that case to get a valid temperature dependence.

The Quasi-Random Band Model is an exceptional model in that it can be used to determine temperature dependencies. In the limit, one can choose subintervals in the band that are so small that each spectral

line is localized and therefore its spectral position determined precisely; however, this requires apriori high resolution data as an input. Temperature and frequency dependent results are given using this model, by $\bar{S} / \bar{d} = \sum_i S_i / d_i$ or $\overline{S^{\frac{1}{2}}} / \bar{d} = \sum_i S_i^{\frac{1}{2}} / d_i$. Figure 4 shows some results of a calculation by Gray[14] for the 4.3 micron bands of CO_2 using the quasi random band model. The temperatures are roughly within our range; notice that the lower temperature curves are on the inside of the family of curves for the core region and on the outside in the wings. This therefore indicates temperature crossover regions on both sides of the band for a small range of T.

Malkmus[22] has used a semi-rigorous approach to predict the absorption for the 4.3 micron bands of CO_2. Figure 5 reproduces some of his results which indicate the expected temperature crossover regions on either side of the band.

3. Absorber Amount Dependence. The absorber amount dependence of the absorption is the simplest of the three thermodynamic variable dependencies. On a single line basis, the absorber amount dependence is in the integrated absorption expression; it is given in terms of n, the absorber number volume density. Using the ideal gas law, one finds that S is linearly proportional to the partial pressure of the absorber, p. One can define an integrated absorption by the expression

$$S = S_o u \tag{78}$$

where u is the absorber amount given by the absorber mass volume density (which is proportional to p) times the thickness of the gas along the light path, l. S_o is independent of the absorber amount; remembering

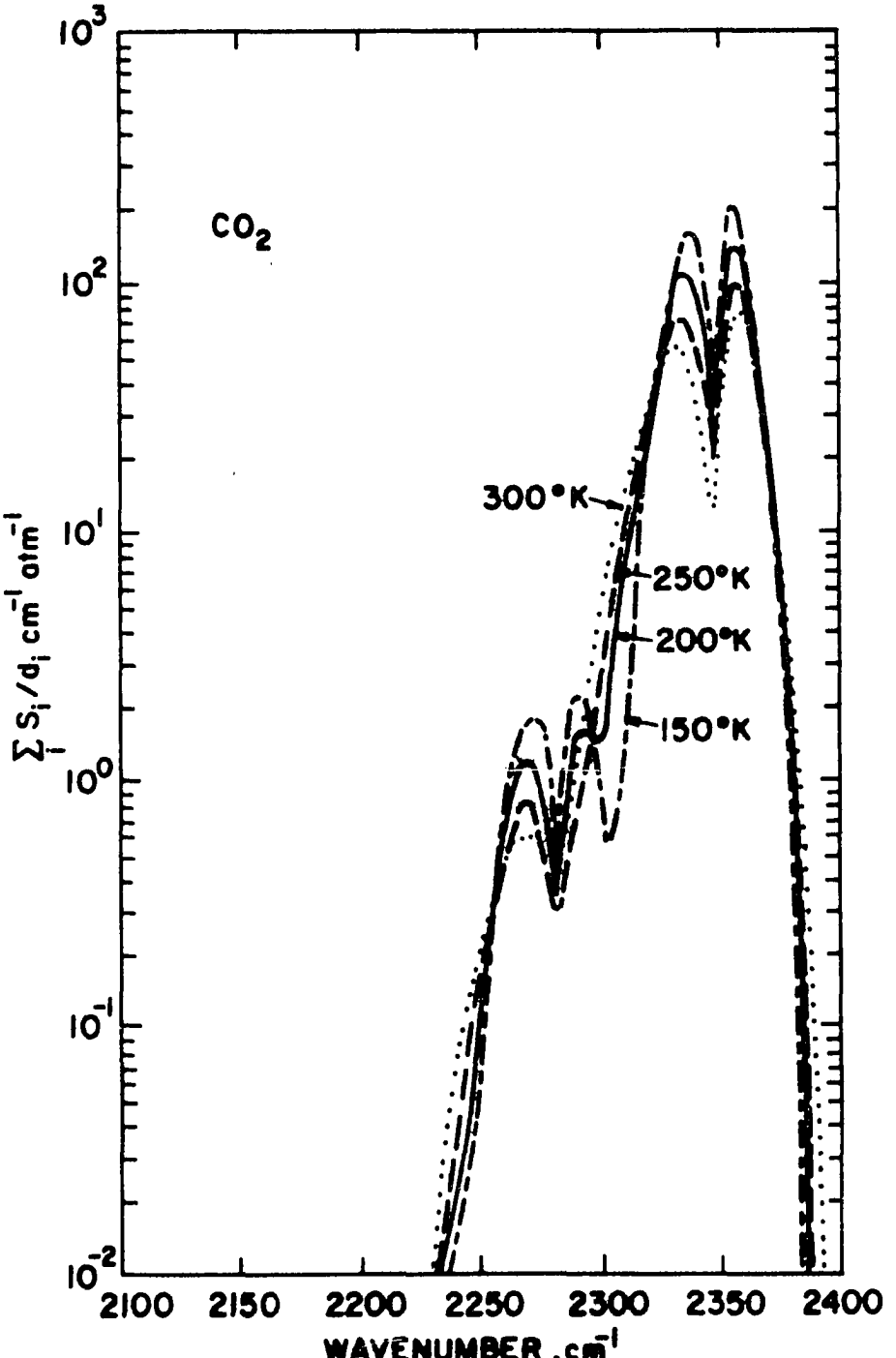

Figure 4 . The Average Value of (S/d) as a Function of Wave number with T as a Parameter (reprinted from reference 14).

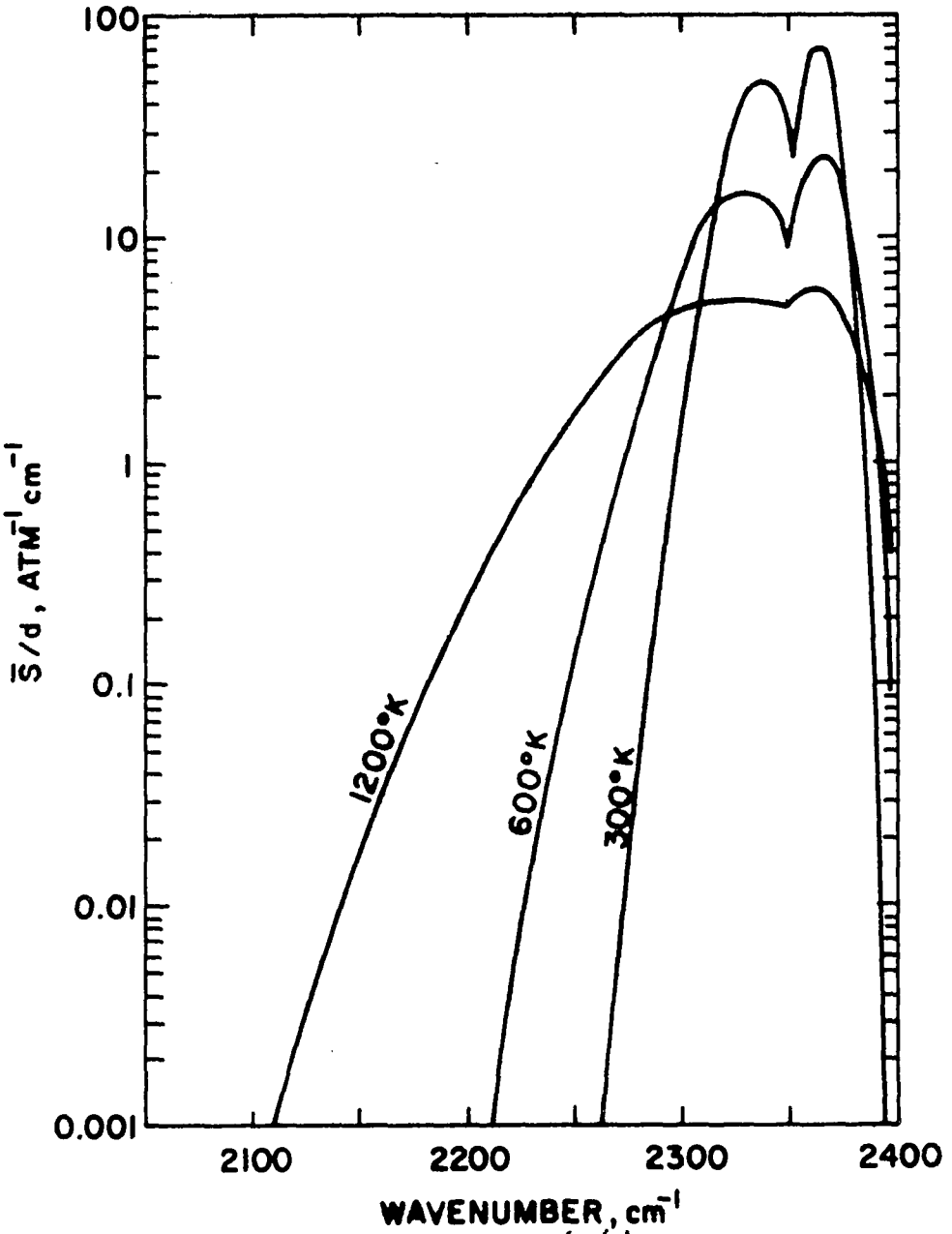

Figure 5 . The Average Value of (S/d) as a Function of Wavenumber with T as a Parameter(reprinted from reference 22).

this definition, we shall now drop the subscript on S_o. The extinction can therefore be given by

$$\epsilon(\nu-\nu_s) = Sf(\nu-\nu_s)u \tag{79}$$

As u increases the absorption increases over the entire line, except for the black line region. One does not therefore get the complicated dependences which lead to crossover regions and positive and negative dependencies over the lines that were obtained in the temperature and foreign gas pressure case.

Selfbroadening effects can be taken into consideration by defining an equivalent pressure; however in the atmospheric situation these effects are usually neglected. Certainly any selfbroadening effects due to CO_2 can be neglected since there is only a .03% concentration of CO_2 in the atmosphere.

One must consider the possibility of a spectral line center becoming black and no longer contributing to the absorption for increases in u. With this in mind and in order to take into consideration the overlap of the neighboring lines, we shall now employ the method of band models.

The weak line approximation is independent of the particular model chosen; it yields a result given by

$$W_{W.L.} = 1 - \exp - \beta\psi \tag{80}$$

where $\beta\psi = Su / d$. Therefore in the weak line approximation the absorption coefficient is linearly proportional to u and therefore linearly proportional to p and to l. The results for the linear region of the nonoverlapping line approximation are given by

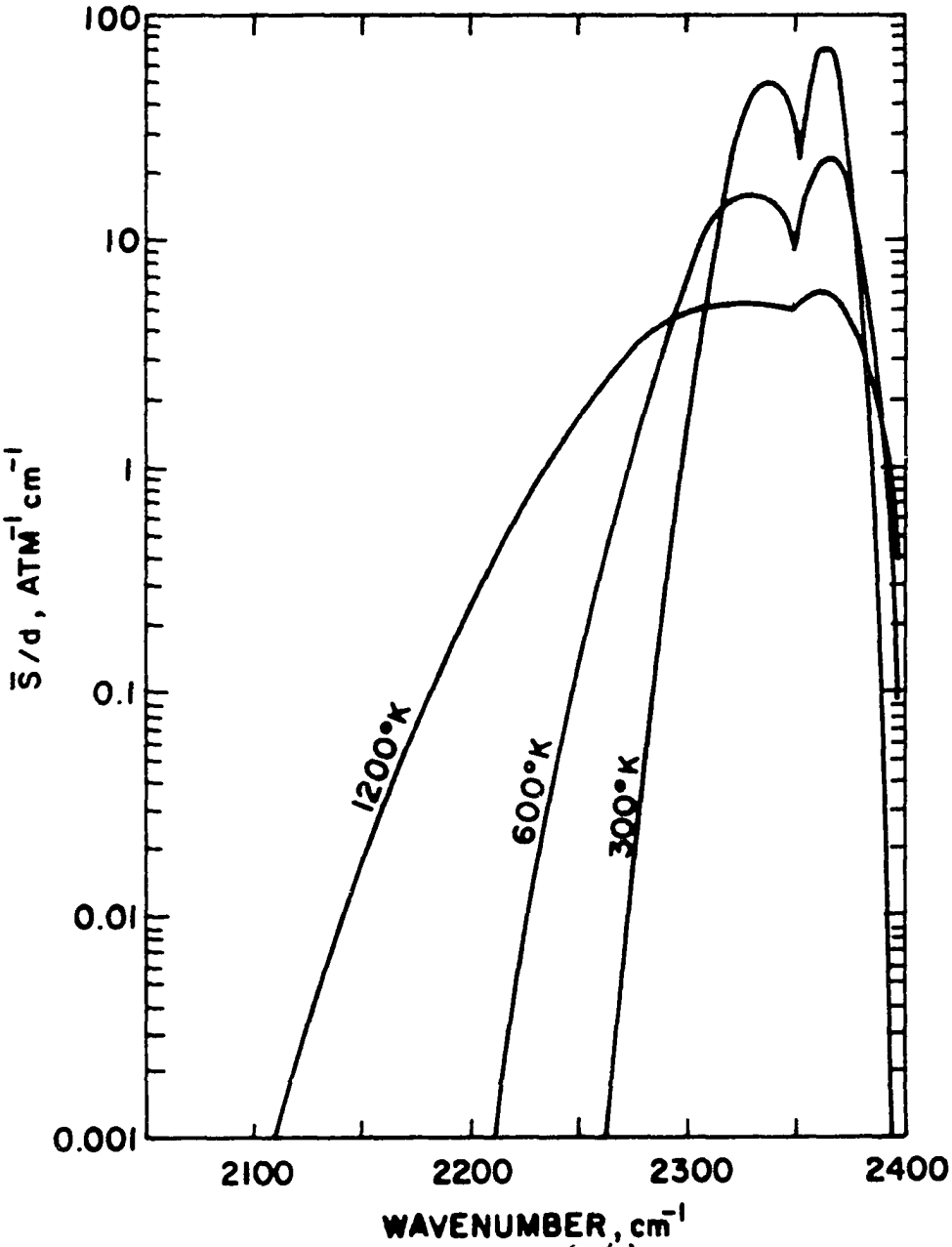

Figure 5 . The Average Value of (S/d) as a Function of Wavenumber with T as a Parameter(reprinted from reference 22).

this definition, we shall now drop the subscript on S_o. The extinction can therefore be given by

$$\epsilon(\nu-\nu_s) = Sf(\nu-\nu_s)u \tag{79}$$

As u increases the absorption increases over the entire line, except for the black line region. One does not therefore get the complicated dependences which lead to crossover regions and positive and negative dependencies over the line[illegible]ined in the temperature and foreign gas pressure c[illegible]

Selfbroaden[illegible] consideration by defining an equival[illegible]tmospheric situation these effects are us[illegible]ny selfbroadening effects due to CO_2 can be neg[illegible]a .03% concentration of CO_2 in the atmosphere.

One must consider the possibility of a spectral line center becoming black and no longer contributing to the absorption for increases in u. With this in mind and in order to take into consideration the overlap of the neighboring lines, we shall now employ the method of band models.

The weak line approximation is independent of the particular model chosen; it yields a result given by

$$W_{W.L.} = 1 - \exp - \beta\psi \tag{80}$$

where $\beta\psi = Su / d$. Therefore in the weak line approximation the absorption coefficient is linearly proportional to u and therefore linearly proportional to p and to l. The results for the linear region of the nonoverlapping line approximation are given by

$$W_{N.O.L.}\ (\text{Linear}) = \beta\psi = Su\ /\ d, \tag{81}$$

and therefore the absorption is linearly proportional to u in this region. Although this expression is for an infinite spectral interval, a finite spectral interval will not change the dependence on u.

In the strong line approximation for say the Statistical Model, the absorption is given by

$$W_{S.L.} = 1 - \exp - (2\ /\pi\ \beta^2\psi)^{\frac{1}{2}} \tag{82}$$

for the equally intense distribution of intensities; $\frac{2}{\pi}\beta^2\psi = 2(S\gamma u/d^2)^{\frac{1}{2}}$. The absorption is therefore characterized by a function of $(Pu)^{\frac{1}{2}}$. This approximation is characterized by black line centers and overlapping lines, where therefore the increase in absorption with u is due primarily to the wings of the lines.

In the square root region of the nonoverlapping line approximation, the absorption is given by

$$W_{N.O.L.}\ (\text{Square Root}) = 2(S\ \gamma u\ /\ d^2)^{\frac{1}{2}}; \tag{83}$$

the absorption is therefore given by a power law dependence for the product of P and u raised to the one half power.

The u dependence of the absorption in the ill defined region can be assumed to be given by $u^{l'}$ where the range of l' is given roughly by $\frac{1}{2} \lesssim l' \leq 1$. The corresponding P dependence is given by $P^{m'}$ where $0 < m' \lesssim \frac{1}{2}$. Thus we see that the dependence on the absorber amount should always be stronger than that for P.

The dependence on u is a maximum for nonoverlapping nonblack lines and becomes less as the lines overlap and grow toward black line centers. The minimal dependence is in the strong line approximation for large values of ψ.

The bandpass and the position of the spectral interval is not critical for the u dependence; a strong u dependence should occur over the entire band, for any portion of it. However, a maximum u dependence will occur in the intermediate regions of the band.

In conclusion, we have found that a maximum u dependence and a minimum P dependence occurs for the weak line approximation region of validity; the opposite is true for the strong line region of validity. In an actual band the core regions typically signify the strong line case and the wing regions the weak line case, although a band model is generally used only to describe the band in terms of one or the other approximation. Also, the T dependence should dominate the P dependence in the wings of the band.

The pressure dependence under the condition of frozen composition should remain approximately linear for all band model approximations since the partial pressure of the absorber must increase with increases in the total gas pressure in a proportional way. Since $p = fP$, the strong line and weak line absorption coefficients for the frozen composition case are given by

$$K_{W.L.} = Sf\ P\ /\ d \tag{84}$$

and

$$K_{S.L.} = 2\left(\frac{S_1 \gamma_o\ f}{T^2\ ld^2}\right)^{\frac{1}{2}} P, \tag{85}$$

and similarly for p. f is the CO_2 concentration.

Thus we are led to another dependency, namely that for f. We see from these expressions that an increase in f will lead to an increase in the absorption coefficient; the power law dependence is from the square root law in the strong line region to the linear relation in the

weak line region. It is sometimes convenient to use f as one of the variables instead of p, as we shall see. As noted previously f is about constant in the stmosphere except near the surface of the earth where, for example, various pollution sources will increase the CO_2 concentration.

CHAPTER III

EXPERIMENT

A. Equipment Description

1. Introduction. We shall now consider a description of the equipment used to perform this experiment. It is referred to as "An Optical Absorption Cell with Variable Path Length and Temperature."[6] This cell was built during the years 1966 to 1969 by IITRI* specifically to measure optical absorption coefficients of gases. It functions basically as an infrared spectrophotometer, (although it was initially built for ultraviolet work) and has considerable operational flexibility. We now present the substance of the cell and the more pertinent details of the equipment. We start at the source and work toward the detector and then consider the electronics.

2. Cell. The incident light intensity is furnished by an infrared globar element--a $\frac{1}{4}$ inch rod of silicon carbide with specially coated ends for good electrical contact. An AC line-load regulator followed by a Perkin Elmer ballast tube type power supply are used to provide the power for the globar. The excessive thermal gradients that always exist near the globar element contacts require the use of a stainless steel water jacket for cooling purposes. Typical operating

---

*Illinois Institute of Technology Research Institute, Chicago, Illinois.

currents are five amperes with a resultant source color temperature of about 1500° K.

The near blackbody spectrum first encounters a mechanical light chopper; this chops the light signal into a square wave of about 340 c/s. The frequency is measured with a Hewlett-Packard digital frequency counter. In addition, a reference signal is obtained from the chopper; a small battery-operated secondary light source is placed about five inches below the globar on one side of the chopper wheel and a photocell with an R-C circuit is placed on the other side to monitor the resultant chopped secondary signal. The secondary or reference signal is then immediately fed into an Adyu preamp and sent to the electronics.

The incident light then passes through a window and enters the cell at the left end. The light is now in a vacuum and remains so until it passes into the center section which contains the cell space. A first surface mirror placed approximately one focal length from the globar reflects the light at a right angle down the cell towards the center section. The left end will accommodate mirror diameters up to two and one half inches. The light passes into a mullite ceramic tube on the end of which a calcium fluoride (CaF_2) or a Harshaw T-12 window is fasted. The mullite tube together with a second symmetrical tube coming from the other end defines the cell space. The inside of the tubes are evacuated and open at the ends away from the center of the cell. The mullite tubes, which were chosen because of their stable characteristics over a wide temperature range, have a 5.08 mm O.D. and 4.13 mm I.D. The lengths of the tubes define the cell length; this

can be varied by changing the tubes from approximately one meter down to a few millimeters without changing the position of the optical components or the optical components themselves or the strength of the incident light intensity. This represents one of the special features of the cell.

The cell region within which the gas is confined therefore has a surface area defined by the two windows at the ends of the mullite tubes, the outside of the tubes themselves and a stainless steel tube (within which the mullite tubes fit) with a 7.0 cm I.D. and a 1.22 meter length. The stainless steel tube is fitted with bellows at the ends to allow for temperature contraction and expansion. The outside of the mullite tubes, which is inside the cell region, contains temperature and pressure fluctuation measuring devices.

Eight Copper-Constantan thermocouples in ceramic sheaths (four on each end) are located at any desired position along the cell length. The thermocouple wires exit through a vacuum seal at the eight radial cylindrical chambers at the ends of the cell; these chambers store extra thermocouple wire and allow for a simple change of the thermocouples. These wires go to two terminal blocks and then to a common temperature reference junction. Liquid nitrogen reference temperatures were used and a bridge was used to measure the thermoelectric emf[S].

A model 701A Kistler pressure transducer is also mounted adjacent to the light path through the cell; it requires a low noise, low capacitance connection to a Kistler charge amplifier (Model 566) located outside the cell. The connection is in the form of a capillary

glass tube inside of which a single wire from the transducer is carried and over which a brass cylinder is placed; this forms the mechanical support as well as the electrical connection. This device measures the fluctuations about the mean pressure in the cell. Besides support brackets for the thermocouples and mounting brackets for the mullite tubes there is nothing else in the cell region; this is of interest from an outgassing standpoint.

The light then goes through the cell space and through the right end window (both windows have 47.5 mm diameters and are 4 mm thick) into the right end. The inside of the right end mullite tube is again evacuated. The light is then reflected at right angles from a second first surface mirror and focussed on the input aperture of a McPherson monochromator.

The uniformity of the light beam was checked photographically at three centimeter intervals along the cell; considering the size of the globar element and the poor quality of the optics, the beam was found to be reasonably well collimated in the cell space.

The light beam then enters the McPherson type monochromator; the light distribution at the entrance slit was very uniform over a 2 mm wide slit. A Kodak long wave pass interference filter with a 2.82 micron cut on point mounted on a sapphire substrate was mounted after the exit slit to counteract stray radiation problems. The transmission of the filter is approximately 87% and uniform over the region of interest in the experiment.

The light passes through the window and is then reflected by a third mirror and focussed onto a diffused junction photovoltaic

indium antimonide detector cooled to liquid nitrogen temperatures.

The monochromator is evacuated through the input aperture and a main vacuum connection at the rear of the monochromator.

The detector housing was not evacuated; it was flushed continuously with a very slight positive pressure of nitrogen gas.

The three signals from the detector, and the reference and the pressure fluctuations, are then used as inputs to the electronics.

Before getting into the electronics, it is necessary to discuss the methods used to achieve temperature and pressure control, as well as the basics of the gas handling apparatus. The cell has separate and easily interchangeable heating and cooling units, although the cooling unit is easily adapted, through the use of heating tapes, for use as a heating unit as well. In this way a liquid bath can be used to increase temperature stability and uniformity. The heating unit consists of a series of heating tapes wrapped about a cell tube which are then covered with insulation. The cooling unit has a double-walled stainless steel construction, the inside of which can be maintained at a vacuum for additional insulation. The coolant bath requires three liters of liquid to cover the cell tube, and nine liters to completely fill the container. The total length of the stainless steel cell tube which is in direct contact with the bath is four feet; this gives a fairly uniform temperature over one meter. The cell has been used from 196° K to slightly more than 400° K, although one expects that the cell will operate at a much higher temperature.

The evacuation of the three sections of the cell is accom-

plished with two rotary pumps and two liquid nitrogen cold traps; each section could be controlled separately. It should be mentioned that the right and left ends as well as the gas handling manifolds are pumped continuously so that outgassing is not a problem in these regions. The gas mixture pressures are fixed by introducing gas from a pressurized size LA contained into an evacuated cell and stopping at the desired pressure. These pressures could be read in the cell by an oil manometer or thermocouple gauge, but mainly they are read with the Alphatron gauge. Calibration curves were determined between McCleod manometer and Alphatron gauges. A Bourdon gauge was available for use at pressures significantly above one atmosphere. Although the cell is designed for pressures below one atmosphere, one can use up to about two atmospheres with a little caution.

The gases were introduced through a system of tubing referred to as the gas manifold; this system can be evacuated. Figure 6 is a line drawing of the manifold showing the various connections and interconnections. This system permits a controlled flushing and pumping of any or all of the three main sections of the cell. It can be used to preheat or cool the incoming gases; the pressure in the manifold is measured with the thermocouple gauge.

The pressure fluctuations can be generated by one of two mechanisms, a piston modulator or a loud speaker plus cavity modulator. The piston modulator was designed to be used at up to 3 Hertz, but was not used in this experiment. The speaker is used as the modulator in this experiment. The speaker is a hi-fi 12 inch reinforced cone speaker rated at about 100 watts; it is mounted on the top

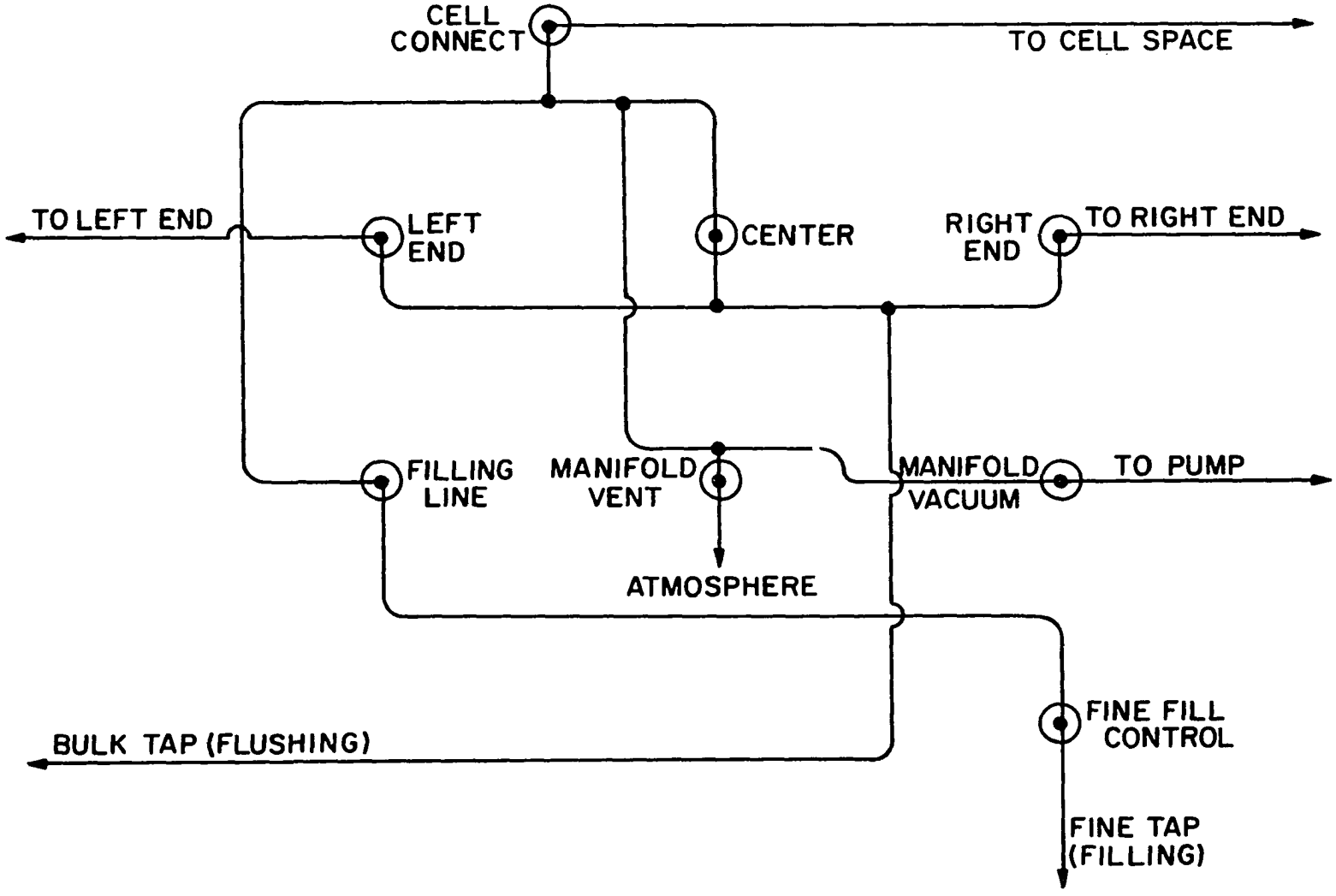

Figure 6 . Diagram of Cell Manifold Used in Gas Handling Operations.

plate of a one foot deep cylindrical tank. A pipe is connected from the cavity to the cell; a valve is also available to interconnect the upper and lower spaces of the speaker when evacuating the cell. The gas is modulated with an approximate sinusoidal pressure fluctuation. A signal generator and a Dynakit 40 watt hi-fi amplifier are used to drive the speaker; a band limited white noise generator can also be used. The amplitude of the pressure fluctuation is controlled at a given frequency by controlling the input voltage to the speaker.

3. Electronics. The measurements are made primarily with a Princeton Applied Research (PAR) Model 220 Lock in Amplifier (LIA). The optical signals are fed into a PAR Model 213 Preamp and then had the option of going into a selective amplifier (PAR Model 210) before entering the LIA. The reference signals are amplified and sent into the reference channel of the LIA. The output of the Lock in Amplifier is recorded with a dual pen, specially made, solid state, strip chart recorder made by Honeywell. The pressure fluctuation is also measured with the LIA.

The second means of recording the data is with an Ampex FR- 100B magnetic tape recorder modified to include ES 100 electronics. Fourteen channels are available in this tape recorder. A set of six Dynamic Model 4550 d.c. amplifiers are used to amplify the signals before going into the FM record modules of the tape recorder. The outputs of the FM reproduce modules are fed into a galvanometer amplifier and then into a Model 1508 Visicorder Oscillograph; this allowed us to have a reasonably permanent visual recording of the

signals that are on the tape. The data processing equipment includes a digitizer and a computer program referred to as MLTCOR. This is a multichannel correlation program developed by Wachowski and Phillips[33] to calculate statistics for aerodynamics and atmospheric turbulence based on the crossed beam technique. A modular Fortran IV based data analysis program was also developed at the University of Oklahoma to perform routine calculations and least square fits. A Slant Tab program was also used to predict the expect CO_2 absorption levels.

B. Modes of Operation

There are two basic modes of peration of the cell; these are (see Figure 7):

1. Static Mode (α)
2. Dynamic mode (β)

The static mode, which will be referred to as "α", is the method of operation which measures mean value intensities. This is the mode of operation used by most infrared spectroscopy researchers. The second mode, which is referred to as "β", measures fluctuations about the mean value intensity.

In our experiments, a static or α trace was recorded at a given set of parameters, and then immediately after the α trace, the β trace was recorded under an identical set of parameters. There is a β trace for each and every α trace that was recorded.

It is interesting to note that the two modes of operation can be run simultaneously. This requires two Lock In Amplifiers when done; the chopper frequency is typically one to two orders of magnitude higher than the pressure fluctuation frequency which then acts as a

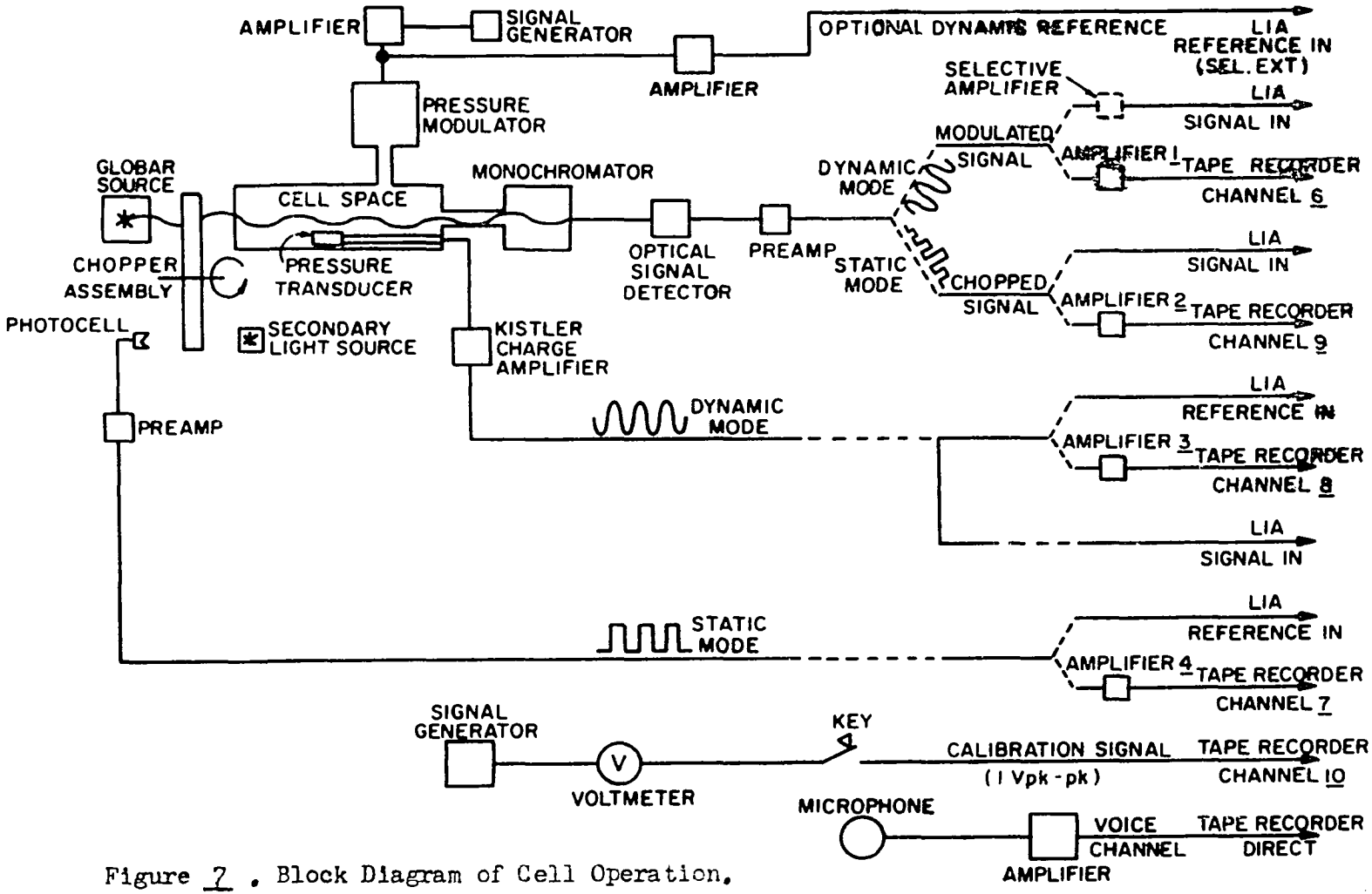

Figure 7 . Block Diagram of Cell Operation.

modulation or band envelope with the chopper frequency as the carrier. The chopper and the pressure modulator are run simultaneously, and the single optical signal which contains the information of both modes is fed into one LIA set to measure the signal at the chopped frequency and another set to measure the signal at the modulator frequency. This approach is not possible if very large fluctuations are used due to possible distortions in the average intensity measurement. A single channel on the tape recorder will replace the two separate channels when operated in this simultaneous manner. Time is utilized to much better advantage in this method of operation, and the α and β traces will be run under exactly identical conditions instead of the nearly identical conditions when the two modes are run separately. We did not have the necessary equipment to do this.

We shall now describe the two modes of operation separately, beginning with the static mode. In this mode, the speaker is turned off and the light chopper is turned on. The globar signal which is under approximate steady state conditions passes through the chopper which turns the light beam on and off periodically. This chopped signal passes into the gaseous absorption medium in the cell where it is partially absorbed and then goes on to the monochromator where the fourier transform of the resultant light distribution is formed. The spectrum is then imaged onto the detector which creates an electrical signal which is proportional to the transmitted intensity of the light incident on the detector. This signal is then fed into the "Signal In" of a LIA or onto magnetic tape, or both.

The necessary reference signal that is synchronous with the

chopped optical signal is obtained from the secondary light source photocell assembly; it is used as the reference input of the LIA or it is recorded on magnetic tape, or both.

The output of the LIA is a d.c. signal which is equal to the rms value of the approximate square wave mean intensity signal. This output was recorded with a strip chart recorder; it can also be recorded by a voltmeter with digital paper tape output.

The tape recorder was used, in some cases, to record the raw optical and reference signals. This data was then digitized and processed by computer.

The data is always recorded as intensity versus wavelength over the 4.3 micron band for all combinations of P, T, f.

An additional scan is made prior to the transmitted intensity (I) scans; it records the incident intensity (I_o) as a function of wave length using the same methods and techniques used to make the transmitted intensity runs, only this time the cell is evacuated of all absorbing gas.

Turning to the dynamic mode, we find that this mode is operated with the speaker turned on and the chopper turned off and positioned so that the blades do not obstruct the light. This mode is run immediately after the α mode and uses the same general parameters that were used for the α mode.

The signal generator is set so that the pressure modulator generates a particular pressure signal, δP (with its corresponding temperature signal, δT). The pressure fluctuation amplitude is monitored and set at the proper value by using the Kistler transducer, the

output of which is monitored with the LIA. This signal is used as the LIA reference signal.

An optional reference signal can be obtained from the input signal of the pressure modulator. The phase of the signal is adjusted and calibrated relative to the Kistler output; the amplitude of the signal is proportional to the Kistler output. In fact, the pressure modulator can be driven by the LIA by using the LIA in the internal mode; this creates an internal reference signal which is synchronous with the signal driving the speaker and therefore the pressure fluctuations. The phase can again be adjusted relative to the Kistler output. It must be realized that the actual pressure modulation signal from the Kistler output must be recorded for each trace regardless of the reference used.

The globar produces a nonchopped signal which enters the cell as a d.c. signal. The temperature and pressure modulations of the gas then modulate the d.c. or mean value intensity signal at the same frequency as the pressure modulations. This modulated optical signal which is riding on the mean value signal, is passed into the monochromator and then on to the detector. The signal then has an option of going through a selective amplifier and then on to the "Signal In" of the LIA, or going straight to the LIA (it can also be recorded on magnetic tape).

The resultant output of the LIA is a d.c signal which is equal to the rms value of the approximately sinusoidal optical fluctuating intensity signal. (It would be convenient to use a LIA whose output was proportional to the product of the amplitudes of the optical signal

and the pressure signal (the reference signal); a simple multiplication circuit can also be used.) The LIA output is recorded on a strip chart recorder; it can also be monitored by a voltmeter with a digital paper tape output.

In some cases, the magnetic tape recorder was used to record the raw optical fluctuation signal and pressure fluctuation signal (Kistler output). This data was then digitized and processed via computer.

The data was recorded as the fluctuation intensity versus wavelength over the 4.3 micron band for all combinations of P, T, f. The pressure fluctuation signal was recorded before and after each run (and monitored continuously) with the LIA, and recorded over the entire band with the tape recorder.

It is suggested that the pressure and temperature fluctuations both be recorded continuously with the tape recorder and a strip chart recorder during all runs. One also prefers to have an I_o trace for each and every transmitted intensity trace, however, this requires a dual beam system or at least a separate detector to monitor the light source at the source.

In general, all traces (both α and β) were made at a constant scan rate through the 4.3 micron region, the traces were therefore continuous in wavelength. However, due to the necessity of using long piecelengths in the data processing methods, the data was also in some instances, recorded on magnetic tape in discrete wavelength steps (see Measurements Section for a further analysis).

In summary, the basic data that was recorded was the mean in-

tensity (I) versus wavelength, the fluctuation intensity (δI) versus wavelength, and the total pressure fluctuation, δP. Additional data such as the thermodynamic conditions, optical and band pass settings, gain settings and calibration factors, ambient conditions, integration times and so forth were also recorded for each and every trace.

From the LIA data one next calculates the mean absorption coefficient K, and the fluctuating absorption coefficient δK. This represents the basic data set.

The data that is recorded on tape is digitized at the proper sampling rates and correlated; both crosscorrelations and autocorrelations, normalized and nonnormalized are obtained for suitable ranges of time lags and for various piecelengths. Accumulative and piecewise correlations are calculated; standard deviations and variances, rms values and mean values, and errors are calculated for τ = zero. Some of these results are then compared to the LIA results.

C. Cell Conditions

The conditions were determined mainly by the fact that they must be compatible with Crossed Beam Correlation studies being performed at NASA-MSFC.* Typical low altitude atmospheric conditions are assumed in general. Further restrictions are imposed by the fact that we are using the 4.3 micron region of the absorption spectrum of CO_2. Other restrictions exist in the form of theory and equipment limitations and, of course, the time limitations.

The first condition that we will consider is that the fluctuations introduced into the cell are assumed adiabatic. Any process

---

*Marshall Space Flight Center, Huntsville Alabama.

that is carried out in such a manner as to exclude the possibility of heat entering or leaving the system is assumed to represent an adiabatic process; for example, a sudden expansion and subsequent compression of a gas can be adiabatic since time might not allow for a flow of heat to and from the system. To show that adiabaticity is a valid approximation for our experiment, we appeal to Fourier's law of heat flow given by[16]

$$\frac{dQ}{d\tau} = \kappa A \nabla T \tag{86}$$

where dQ is the heat conducted in a given direction during time $d\tau$, ∇T is the temperature gradient in a given direction, κ is the thermal conductivity and A is the area. Using the fact that the heat stored in a given differential body is given by $dQ = mc_v(\partial T/\partial \tau)d\tau$, where m is the mass, and c_v is the specific heat at a constant volume,

$$\frac{dT}{d\tau} = \kappa A \nabla T / mc_v \quad . \tag{87}$$

Assuming nitrogen gas, $mc_v \simeq .18$ cal / ^{o}C and $\kappa = 5 \times 10^{-5}$ cal / cm sec ^{o}C. If we allow for $\nabla T = .1$ ^{o}C / cm, then the corresponding time constant given by (87) is on the order of 40 seconds. The fluctuations in our experiment are at approximately 15 c/s which has a period of about .06 seconds. Since this is three orders of magnitude less than the time constant, we assume that the adiabatic approximation is good. The low end of the frequency range can be determined by the frequency response of the electronics; the LIA has a low frequency cutoff of about .1 c/s which is a period of 10 seconds. This is still a valid adiabatic condition. The high frequency range is limited by the fact that maximum power transfer in the atmosphere is close to 1 c/s; we are not, there-

fore, interested in frequencies in the kilocycle range where the adiabatic condition may again brea down due to large temperature gradients (because of the short wavelengths).

The adiabatic condition can be expressed by

$$PV^{\gamma} = \text{constant} \tag{88}$$

where V is the volume and γ is the ratio of the specific heat at constant pressure to that at constant volume. For N_2, this factor is given by $\gamma \approx 4/3$. Using the ideal gas law, equation (88) reduces to

$$\frac{\delta T}{T} = \frac{\gamma - 1}{\gamma} \frac{\delta P}{P} \tag{89}$$

where $\gamma - 1/\gamma = \frac{1}{4}$.

The actual pressure fluctuations that occur in the actual cell region are difficult to define precisely because of the rather complicated geonetry of the cell space and speaker chamber. We do know, however, that a reasonably pure sinusoidal input to the speaker does yield a Kistler output that is periodic and which looks very much like a sinusoid. We also know that there is enough turbulence in the cell when the speaker is turned on to slowly mix the foreign gas with the absorber gas.

One further condition relative to the pressure fluctuation is the wavelength of the longitudinal sound wave must be much larger than the cell length; this will allow for a uniform pressure wave over the length of the cell. However, the speed of sound is dependent on the existing temperature of the gas; it is determined as a function of temperature from the Laplace expression and is given by

$$v = (\gamma kT/m)^{\frac{1}{2}} . \tag{90}$$

γ is the ratio of the specific heats, k is the Boltzman constant, and m is the average mass of a single molecule which can therefore be given by $m = 1.66 \times 10^{-7} M$ kg, where M is the molecular mass.

Assuming a standard air mixture, the speed of sound changes from 312 m/s at 243° K to 397 m/s at 393° K. The corresponding wavelength for a 15.1 c/s sound wave changes from 21 meters at 243° K to approximately 26 meters at 393° K; the wavelength is approximately 23 meters at room temperature. These temperature values represent the maximum values used in this experiment. The length of the cell is less than one half meter. It is, therefore, expected that since $\lambda \gg 1$, the pressure wave will be reasonably uniform over the cell space. Also, the change in wave length with temperature should not significantly change the cell conditions.

The magnitudes of the pressure fluctuations were determined by those values which exist in the atmosphere and which the crossed beam correlation system can measure. The magnitude of the pressure fluctuations used in our experiment were typically on the order of one half of one percent of the static or hydrodynamic pressure. As already mentioned, the frequency of oscillation that was used in this experiment was 15.1 c/s; a value closer to 1 c/s would have been preferred, but equipment limitations (not the electronics) would not allow us to go below 15 c/s. The signal used was, of course, periodic; this enabled us to use a LIA to measure the signals. The LIA results could then be used in a comparison with the results that were obtained by recording the raw data on tape and using a computer analysis. The magnetic tape recording and subsequent data processing allows for the use of

nonperiodic or band limited white noise fluctuations; however, the method and procedures were best proved using periodic signals first.

Another condition that is assumed to exist in the cell is that of frozen composition. This means that the relationship between the partial pressure of the absorber and the foreign gas pressure is assumed to be a constant,[27,19], in other words $p/P = f$ = constant, and therefore df = zero. As already mentioned, $f \approx .033\%$ in the atmosphere for altitudes as high as 75 km; this is referred to as the CO_2 concentration. P or p can be considered to be an intermediate variable; an increase of one necessarily requires an increase in the other. The relationship also holds for the pressure fluctuations, where $dp/dP = f$ = constant.

A further condition on the cell is in the form of a slit width or spectral band pass criterion.

Although a good deal of high resolution data has been recorded in this experiment, we are primarily interested in low resolution data which does not contain the fast oscillations of the individual lines. If one attempts to use high resolution data to obtain signatures of the absorbing gas, one soon finds that the rapid and extreme fluctuations in the intensity of the line absorption coefficient "buries" the dependence on the thermodynamic variables, which is what we are looking for. Furthermore, the position of the slit with frequency or wavelength is much more sensitive and subject to error for the high resolution data than it is for the low resolution data. A shift in the position of a very narrow slit, of .03 cm^{-1} will typically lead one from a line center to a line trough or wing; this leads to

dynamic range problems as well as simple positioning problems. Also, the thermodynamic variable dependence changes from line to line (for example, the temperature) as well as over a single line thus creating further variables that would have to be considered and controlled in a high resolution analysis. The fact that isolated spectral lines are an exception and overlap of the lines must usually be considered is a further problem for a high resolution analysis.

The most severe limitation of a high resolution analysis is a simple signal to noise problem; there is very little power available when one uses small slit widths. The crossed beam correlation technique is designed to handle minimal signal to noise problems; however, when operated under typical atmospheric conditons, it still needs all the signal possible. Thus the power requirement alone restricts one to wide slits and correspondingly low resolution data.

If the band pass contains several rotational lines of a vibration-rotation spectra, then Band Model results can be used. For the 4.3 micron bands of CO_2, this means a band pass on the order of .04 microns[1]. Our experiment used a .08 micron (40 cm^{-1}) triangular spectral band pass which corresponded to input and output slit widths of 2 millimeters.

A .08 micron band pass covers a little less than one third of the CO_2 4.3 micron vibration-rotation bands region; this region has on the order of 50 ground state fundamental rotational lines which are active in the absorption process for our range of parameters. The band pass therefore contains about 15 lines. As a comparison, it can be shown [24] that for the statistical band model, a band pass range

given by 10 d $< \Delta\nu <$ 40 d will yield valid band model results.

A further criterion for the size of the band pass is imposed by the fact that different size intervals lead to varying dependencies of the absorption on the thermodynamic variables; this is discussed in Section IIC.

The contribution of stray radiation was found to be considerable. Although these problems could have been tolerated, we were able to eliminate them quite easily. There were eliminated, as mentioned in the equipment section, by inserting a long wave pass filter at the output of the monochromator. Figure 8 is a plot of the mean value intensity with and without the filter for 100% CO_2 at approximately 1 atmosphere and room temperature. The two traces cannot be compared exactly since the shape of the entire spectrum changes when the filter is inserted; however, the 4.60 micron intensity was set at 66 divisions with the optical filter and at 86 divisions without the filter. The 100% CO_2 concentration was chosen because it absorbed all the light in the core regions of the CO_2 spectrum. Notice that the intensity went to zero as expected, when the filter was used; this eliminated the necessity of subtracting out the stray radiation contribution from each trace. The filter adds to the accuracy of the data since the stray radiation contribution will vary as a function of pressure, temperature and so forth. Consequently, it is not known very accurately.

The shape of the entire spectrum that was within the range of the indium antinomide detector is given in Figure 9. The optical filter with the 2.82 micron cut on and the sapphire substrate, was

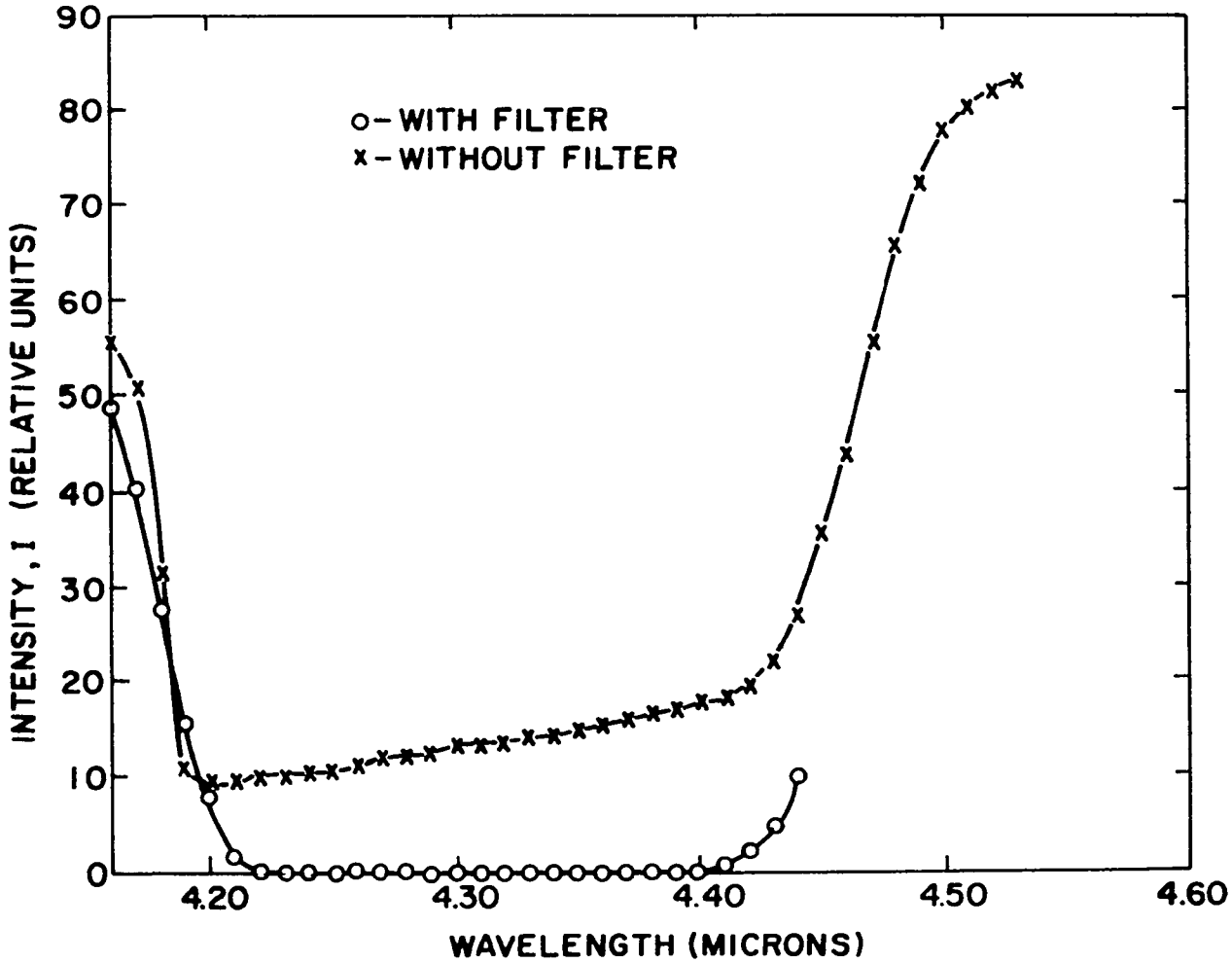

Figure 8 . Intensity versus Wavelength with and without Filter

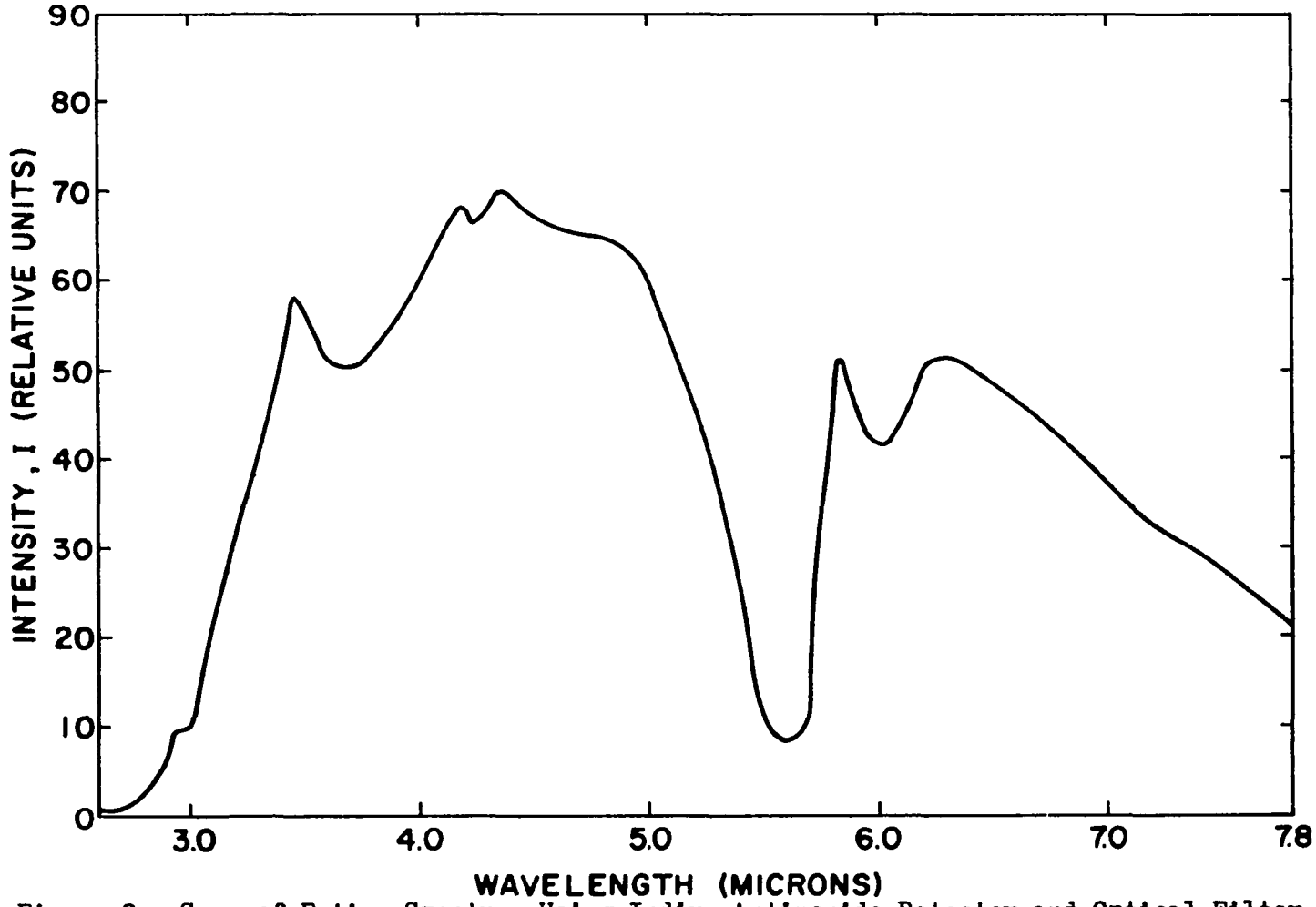

Figure 9 . Scan of Entire Spectrum Using Indium Antimonide Detector and Optical Filter. Note the Position of the 4.3 micron CO_2 Bands. The Gas Mixture was Basically Nitrogen Gas with a Slight Concentration of CO_2.

in the system when this was recorded. Note the CO_2 bands near 4.24 microns and the fact that the intensity is at 66 divisions at 4.60 microns. The gas mixture was basically N_2 gas with a slight CO_2 concentration to indicate the presence of the CO_2 band; it was at one atmosphere and room temperature.

One of the most difficult experimental problems that had to be solved was to determine the optimum gas handling conditions; those conditions which allow us to maintain the needed CO_2-N_2 mixture in the cell. These problems were solved on a procedural basis; a mass spectrometer could have been used to great advantage to determine exactly how much CO_2 was in the cell at any given time, however one was not available for our experiment.

The problems were generally broken down into two main categories:

1. adsorption-desorption phenomena on the cell walls and windows.
2. slow diffusion of the absorbing gas with the broadening gas.

Although these problems can't be eliminated entirely (especially number 1.), they can be controlled by careful experimentation and technique. The key words to this technique in our case were flushing, pumping, premixed gas, and complete cell time history. Since these problems took considerable time and effort to solve, we will be somewhat detailed in our analysis.

Since our experiments were to simulate atmospheric conditions, we initially filled the cell with lab air and recorded the absorption spectrum for CO_2. The absorption was as predicted, however we had no control over the CO_2-N_2 mixture.

Therefore we initially mixed pure N_2 and pure CO_2 in the cell in the required proportions to simulate the atmospheric conditions. The required partial pressure of the CO_2 was on the order of 200 microns at one atmosphere total pressure and thus the measurements of p were critical. Our initial attempts at creating a valid CO_2-N_2 mixture were in error by as much as 500 percent.

The most critical problem is the slow diffusion of the CO_2 with the N_2. We found that "pockets" of CO_2 were formed in the cell when the N_2 broadening gas was introduced (before or after the CO_2). This is simply solved by mixing the gas in the cell with a fan or in our case the turbulence generated by the speaker. A fan is to be preferred because of the relatively long times that are required for the speaker to uniformly mix the two gases. We found that the mixing times could be reduced by adding a fraction of the broadening gas, N_2, before the absorber gas and then adding the balance of N_2. The mixing problem was essentially eliminated in our case by premixing the gas before it is inserted into the cell. However the mixing did not solve the adsorption-desorption problem that is sometimes loosely referred to as outgassing problems.

It has been shown[29] that a gas will always be contaminated by the container which it is in; however conditions can be established to minimize this dependence.

The adsorption of the absorber gas on the cell walls was essentially complete within minutes after the gas was introduced into the cell; this was evidenced by the fact that the recorded absorption was never seen to be less than that at the initial fill

time (if well mixed). The fact that it was adsorbed on the walls was determined by filling the cell with a CO_2-N_2 mixture which then "contaminated" the cell walls with CO_2 by adsorption; this mixture was then pumped out and a vacuum of about one micron was created in the cell for an hour or so. The cell was then immediately filled with pure N_2 at about one atmosphere to negate any possibility of leaks in the cell. An absorption trace was made within minutes after the fill with N_2 and then another trace was recorded several hours later. A significant increase in absorption occurs after several hours; this can only be due to desorption of the CO_2 that was adsorbed to the cell walls. The desorption rate reached a maximum in a typical situation after about one day. This indicated to us that all the recording for a particular series of runs should be complete within approximately a half of a day.

Thus it became necessary to control the amount of CO_2 adsorbed on the cell walls. This was done by keeping the cell on a strict schedule; limits on 1. the amount and type of gases used in the cell, 2. the length of time the gases were kept in the cell, 3. the temperature and pressure ranges and methods of attaining equilibrium, and so forth, were imposed. It was important that cumulative adsorption effects be kept to minimum from one series of measurements to the next.

These cumulative or residual effects were controlled and reduced mainly by the rigorous flushing and pumping procedures. The flushing was done primarily with N_2 but CO_2-N_2 mixtures were also necessary. The pumping times were critical; it was found that

an optimum pumping time occurred for which the I_o trace showed minimal adsorption. We found that it was best to keep a very slight residual amount of N_2 (on the order of a few microns) in the cell just prior to filling with the required mixture; this seemed to allow for a protective coating of N_2 on the cell walls and windows which kept the CO_2 adsorption to a minimum. It reminded one of a saturation point for the cells walls, beyond which the gases would not adsorb as readily.

The gas handling manifold system was kept under strict operating conditions; similar pumping and flushing procedures were used here also. When introducing gas into the cell a slight positive pressure was maintained in the manifold at all times to keep any gases already in the cell from coming back out. Also, a minimal velocity of flow of the gases into the cell during the filling operation was considered essential (large flow velocities were found to create uncertainties in the amount and purity of the gas in the cell). See the measurement conditions and procedures section for a further analysis of the gas handling techniques.

These procedures allowed us to achieve results which were repeatible to one percent. The accuracy was determined by operating the cell under conditions which were compatible with conditions used by other groups, and comparing the results; the agreement was very good.

We would like to make some suggestions which should help in controlling these gas handling problems in any experiment:

1. avoid corners and sharp angles in the cell space.

2. install a gas mixing device, such as a fan, in the cell.
3. use a vacuum pump and flushing system that is versatile but not elaborate; it should not add to the problems in number one (1) above. The pumps should be capable of creating a good vacuum in a reasonably short time; the speed of the pumping should be controllable.
4. establish (by trial and error) optimum gas handling procedures and use them, always.
5. keep an accurate log of the conditions the cell is under, for all times.

A further parameter that had to be established was the length of the cell or the thickness of the gaseous medium through which the light passed. This was established directly by the expected correlation area of the crossed beam measurements. A correlation length on the order of one meter was assumed to be typical for the atmospheric case. Our experiment was set at a constant cell length of 375 mm for all runs.

We assume that pressure broadening is dominant over Doppler broadening; therefore we use Lorentz line shapes to describe the lines.

It is necessary to establish the correct equilibrium conditions for our experiment; does radiative equilibrium (R.E.) or thermal equilibrium (T.E.) exist or perhaps local thermal equilibrium (L.T.E.) ?

In complete thermal equilibrium, a body must gain an amount of energy equal to its loss; if this equilibrium is not maintained then the associated radiation is referred to as nonequilibrium radiation. "Thermal equilibrium radiation" is referred to as blackbody radiation; it possesses some general properties that characterize it.

The intensity of this radiation is independent of the nature of the associated matter and it is isotropic; the functional form of the intensity in terms of wavelength is given by Planck's Law. Kirchoff's Law which is obtained from an energy balance expression, holds under complete thermal equilibrium. When this law holds, the matter is in thermal equilibrium and the absorption and emission processes are defined using the equilibrium distribution for the populations of the molecular states.

Unfortunately, complete thermal equilibrium simply does not exist in the atmosphere or in our cell; to avoid rather severe complications, an alternative concept was used and referred to as Local thermal equilibrium. In this case the matter can be divided into "patches" over which a local definite temperature can be defined, and for which one can associate equilibrium thermal radiation. The total thermal radiation of the matter can then be determined if we know the distribution of the temperature as a function of position in the body. Therefore a gas with a temperature gradient can be in local thermal equilibrium but not in complete thermal equilibrium. For L.T.E., the change in intensity with position, in the radiative transfer equation, no longer goes to zero as it does for Kirchoff's Law and T.E. (see equation 40).

Before considering the mechanism for L.T.E. let us consider radiative equilibrium. In this case the effects of the radiative process are the defining properties for the system equilibrium. When radiation is the predominant or only mode of energy transfer, then the system is in radiative equilibrium. The amount of energy

emitted by each element of matter in the path of the radiation must equal the amount absorbed; in other words there is no net energy exchange between the radiation and the matter and there are no sources or sinks of energy.

Now, the extent to which a given gaseous medium under the influence of incoming thermal radiation can be characterized by T.E. or L.T.E. depends strongly upon the collision frequency of the molecules. A collision is defined as a nonradiative interaction between neighboring molecules of a gas during which energy may be exchanged between the internal energy modes (including translation). A molecule which is excited due to "true infrared absorption", for example, may suffer a subsequent energy loss due to intermolecular collisions or it may lose it due to a radiative process. If the collision frequency is sufficiently high then the medium will assume a state of L.T.E.; if the rate of collisions is not high enough the radiation mode is the predominant factor and the system assumes a state of radiative equilibrium. If the density of the gas is too low, resulting in an insufficient collision rate, the population distribution of the energy levels will not be according to Boltzmann, when the gas is subjected to incident radiation. The temperature is no longer well defined.

More specifically, L.T.E. is the result of the interchange of translational, vibrational, rotational and electronic energy between molecules in a collision (we shall ignore the electronic excitation since this is an infrared analysis). Translational energy is essentially unquantized and is exchanged freely; it is usually used to define the kinetic temperature. Translational energies adhere to

a Maxwell-Boltzmann distribution. But the vibrational and rotational levels need not be populated according to this distribution even though the translational mode is. The internal modes have different (collisional) relaxation times and therefore adjust to equilibrium at different rates. The translational mode adjusts more rapidly than the other modes. If the rotational and vibrational states are not in equilibrium with the translational state (if there is a lag), then L.T.E. is not valid. In general, the rotational states reach equilibrium faster than the vibrational states unless the spectrum is a vibration-rotation band in which case the rotational lifetime will be the same as the vibrational lifetime.

So, if the (collisional) vibrational relaxation time, η , (which is inversely proportional to the collision time and also the total pressure) is much less than the natural lifetimes, φ , of the vibrational excited states, then the collisional processes will dominate the radiative processes and L.T.E. will be established. We assume that the induced emissions due to the external source of radiation are not significant, which is a good assumption in our experiment.

The equilibrium condition is therefore determined by the magnitude of η / φ for the vibrational mode.

The (collisional) vibrational relaxation time for CO_2 at $T = 300^{\circ}K$ and one atmosphere is $\eta = 2.53 \times 10^{-6}$ seconds as found experimentally. Typical collisional rotational relaxation times for gases are very small being on the order of 10^{-9} seconds. The (natural) radiative vibrational lifetimes for the fundamental 4.3 micron band of

CO_2 is given by 2.4×10^{-3} seconds. Therefore η/φ is approximately 10^{-3} and the CO_2 absorber gas is most certainly in L.T.E..

The transition from L.T.E. to R.E. takes place in the atmosphere at about 50 km[17]. Above this height radiative equilibrium is assumed. (Also CO_2 is dissociated above around 75 km.)

Thus we see that the relatively long lifetimes of molecular vibration-rotation transitions allow us to use L.T.E. and Boltzmann distributions for the populations of the states. This is no longer true for extremely low densities or pressures corresponding to values on the order of one millibar or 3/4 mm Hg or less.

The additional effect of acoustic excitation of the gas does not disturb this condition since the frequencies are low and the amplitudes are small.

CO_2 will condense for low temperatures; this limits the quantity of CO_2 that can be used. For typical atmospheric concentrations, this does not occur until about 130-140° K and lower, and is therefore not a problem in our experiments. The sublimation temperature of CO_2 is 194.7° K.

D. Measurement Conditions

There are two basic measurements: a mean value intensity measurement and a fluctuating intensity measurement with a corresponding pressure fluctuation measurement. All the procedures were established so that best accuracy and repeatibility possible would be obtained. It was also necessary that the data be recorded under conditions that allow for a comparison of any one part of the data

with any other part.

It is necessary to have good equilibrium conditions in the equipment room; varying air currents and temperatures for example cause about a 2% error in the measurements. This was in part due to the globar, but was also a malfunction of the electronics, especially the chart recorder. The experiment was commenced only when the cell and the electronics appeared to be in approximate thermal equilibrium.

The gas handling conditions and procedures were the most difficult to establish. The main concern was to maintain a constant amount of CO_2 in the cell over the various ranges of temperature, pressure and CO_2 concentration during the time required to make the given series of measurements. We shall now briefly describe this procedure; the reader is referred to the cell conditions section for further details.

The cell was baked prior to each new gas concentration (using the lowest concentrations first) at a temperature slightly more than 400°K; this temperature was greater than the temperature of any of our runs. We then set the cell at equilibrium for the highest temperature and ran through a series of pressure runs starting with the lowest pressure are used. A single temperature series with the pressure changes was completed without interruption in about 14 hours. The cell was then flushed and pumped using a 22 hour procedure that was established by trial and error for our equipment and which was adhered to always for each and every run. After this was accomplished, the cell was again considered to be ready for immediate operation. The next lower temperature series was performed in a

manner entirely identical to the previous series, and so forth. This was repeated for all temperatures for that particular CO_2 concentration, and then the cell was baked again at four hundred plus degeees Kelvin. The next higher CO_2 concentration series was then performed.

Let us now assume that a stable condition has been reached in the cell at a particular temperature and that the cell has been evacuated and is at about one micron. It is now necessary to record an I_o trace ($I = I_o$ exp-kl). This is a record of the incident intensity since there is assumed to be no absorbing gas in the cell. Actually there is typicaly a very small residual absorption measured during this I_o trace, as in most experiments; this is due to various slight anomalies in the equipment, it will not significantly affect the results if the effects are not large. Immediately after this a transmitted intensity trace or I trace was recorded. The parameters and conditions for the two traces were maintained at the same values except that after the I_o trace was completed, the cell was filled with a CO_2-N_2 gas mixture.

For these α traces, the entrance and exit slits of the monochromator were both set at 2mm which corresponds to a .08 micron or 40 cm^{-1} bandpass including the convolution.* In order to make all the data comparable, it was necessary to use the same bandpass for all traces; this is what we did. It was also necessary to calibrate the incident; this of course was a relative calibration. This was done by setting the monochromator at a point outside of the 4.3 micron CO_2 band and adjusting the globar power input until a nominal value intensity was recorded with

---

*When the fine structure traces were recorded, we used a .09 cm^{-1} bandpass which compares to about a .07 cm^{-1} mean rotational line half-width for CO_2.

the LIA. The wavelength setting used was 4.60 microns; the amplitude was recorded at 66 divisions on the chart recorder for two to three minutes at a given LIA integration integration time (τ = 300 milliseconds), sensitivity, and gain for the LIA and optical signal amplifiers. This magnitude was the maximum useable globar intensity; it was considered necessary that this value be stable. In addition, a zero intensity trace was recorded for a short time interval; this was done by inserting an opaque piece of material between the globar and the chopper. These two intensity calibrations were done before and after each and every trace that was recorded in this experiment. If these conditions were not met, the entire system had to be recalibrated.

Another condition that was maintained at a constant value for all I_o traces and all I traces, was the speed of the chopper; it was set at 340 c/s and monitored intermittently with a digital frequency counter. A change in chopper frequency will alter the signal to noise level in the output.

It was found that small drifts and instabilities in the output of the globar were generally unavoidable. The drifts were linearly detrended for all runs before the data was considered to be raw data. If the drifts were greater than 2% than the run was repeated. The instabilities were usually averaged out.

The phase difference between the chopped optical signal and the corresponding reference signal was adjusted externally to give a zero phase difference between the two signals. This was done by mechanically positioning the secondary source-photocell assembly so that the optical signal and the reference or secondary signal turn on and off simultaneously.

The monochromator scan speed for the I_o and the I traces was set at 160 $\mathring{A}$ / minute, although a higher scan speed could be used, and the LIA integration time was set at 300 milliseconds. The wavelength interval used was 4.16 microns to 4.40 microns; this was sufficient to record all the spectral lines that significantly participated in the absorption process for these conditions. The reference signal amplitude was not critical although it had to be maintained above a minimum value. Ambient conditions were recorded on a separate α data sheet for each run.

Thus an I_o trace and an I trace were recorded by the LIA on the strip chart recorder. In some cases, the raw optical and reference signals were also passed through amplifiers #2 and #4 and recorded over the complete wavelength interval on channels #7 and #9 of the magnetic tape, for both I and I_o. O-grams were recorded as the signals were being put on tape. Timing marks and a 1.0V pk-pk amplitude calibration were also recorded on channel # 10. A voice channel can be used to record the pertinent identification details of the run. The traces that were recorded on tape were then sent to NASA-MSFC for data processing. The data was sampled with a 0.0008 second sample interval, although 0.0004 seconds is more desireable. The piecelengths were chosen to be 3.5 seconds; 5 second piecelengths can be used when the α and β data are interrelated. Two minute piecelengths or accumulative lengths are used for the discrete wavelength segment tapes. Time lags out to about five times the fundamental period were tabulated for the piecewise correlations. τ = zero data was also tabulated.

Referring back to the completion of the I_o trace, the cell was then immediately filled with the desired CO_2-N_2 gas mixture at the lowest

pressure value. This was allowed to reach equilibrium and an I trace was recorded under conditions nearly identical to those used to record the I_0 trace. The ambient conditions were maintained the same as were the intensity calibrations, bandpass, integration time , scan speed and interval, and so forth.

The α trace was completed in about 20 minutes and then the β trace was immediately begun, so that it too could be recorded under nearly identical conditions to those used to record the α traces.

The β trace required that the pressure fluctuation be set at a prespecified value which was a constant for all β runs.* The Kistler output was set for 40 divisions on the chart with a LIA integration time of 10 seconds at given sensitivity and gain settings. These parameters are equivalent to those used to measure the intensity fluctuation signal and therefore the two measurements are compatible. The Kistler output was set and recorded before each β trace for two to three minutes; it was also checked and recorded for two to three minutes after each trace to make sure it was stable and at the correct values (it was also recorded on magnetic tape).

This is the δP measurement; it was set at 5.68 mmHg pk-pk at 15.1 c/s for every constant δP, β trace. The transducer was calibrated at our request, by the factory, at 15.1 c/s.

The required gain settings for the optical fluctuations of the β traces (δI) were on the order of 10^{-3} times those used to record the optical signal of the α traces. If the selective amplifier was used, it

---

*Except those for which $P \propto \delta P$ and for which δP increases linearly for a constant P,T,f. See Chapter VI. section G.

had to be calibrated for every trace to make certain that the gain was unity. Whether or not it was used was determined by the expected S/N. It was tuned at 15.1 c/s in the resonance mode with a Q of 10. The selective amplifier was not used in the magnetic tape circuit.

The phase of the pressure signal was assumed to be 180° out of phase with the optical signal; this was checked and found to be true within $\pm 5^{\circ}$. This amount of error leads to a negligible change in the output. A zero fluctuating intensity level was determined before and after each trace, in addition to the mean value intensity calibrations. This was recorded again at 4.60 microns and used as our zero fluctuating intensity level. The zero δI^{-} level was independent of the gas in the cell; Argon, Nitrogen and CO_2-N_2 mixtures gave the same zero level. This tended to be one or two divisions negative for most traces. The LIA integration time for the optical β signal was set at 10 seconds as already mentioned and the scan speed of the monochromator was reduced to 80 $\mathring{A}$/minute because of the lower signal to noise levels. The slit widths were the same as these used in the α data, but the wavelength range was increased .02 microns on either end of the band; this was mainly for better accuracy in the data point at the beginning and at the end of each recorded trace. The remaining conditions were recorded on a separate β data sheet for each run.

The raw δI signal and δP signal were in some cases, also passed through amplifiers #1 and #3 and recorded over the complete wavelength interval on channels #6 and #8 of the magnetic tape. Timing marks and a 2V pk-pk amplitude calibration were again recorded on channel #10. Oscillograms were made at the time of recording; a voice channel can also

be used. The β data that was recorded on magnetic tape was digitized at .004 seconds, although .003 second intervals may be more useful. The piecelengths were chosen to be 10 seconds; larger piecelengths are not advisable for continuous traces due to the changing mean. Three minute piecelengths or accumulative lengths are used on the discrete wavelength tapes. Time lags up to about five times the fundamental period were tabulated for the piecewise correlations, for the continuous data. τ = zero data was also tabulated.

A β trace was recorded, including set up time, in about 50 minutes.

As mentioned in the modes of operation section, the data was also recorded on tape in discrete wavelength segments. The monochromator was set at a particular wavelength and the data recorded for two to three minutes; the monchromator was then set to a different wavelength and again the data was recorded for two or three minutes, and so on. Twenty six equally spaced wavelength points were chosen; this resulted in a "staircase" type of record for δI(or I). The segments were separated by an exceptionally large signal before and after each discrete segment; a computer program is easily written to detect these spikes and therefore the information can easily be located on the tape. The timing marks on channel # 10 can also be used to locate the information. It is also possible to "step" the monochromator automatically.

The calibration factors needed because of the different waveshapes and the various gains, and so forth, are included in the data sections.

The same monochromator grating was used to form all the spectra;

it was a 150 l/mm grating with a 212.8 Å/mm dispersion.

The pressure measurements were recorded before and after each run with the Alphatron gauge. This was factory calibrated and also checked against an oil manometer and a McCleod gauge. The accuracy of the Alphatron guage on the x100 mmHg scale was about $\pm$ 2 - 5 mmHg.

The temperature measurements were monitored intermittently throughout the scan; they were found to be accurate within $\pm$ 2°K.

The CO_2 amount was determined by using various CO_2 concentrations gases with a balance of N_2, measuring the total pressure, and then multiplying by the constant, f. The path length was known. The gas mixtures used were certified standard mixtures that had been checked by analysis.

One source of error arose from the fact that the ratio I/I_o was approximately unity in the far wings of the bands; this leads to the possibility of ratios that were just slightly greater than unity becausc of various inaccuracies in the measurements. The worst error was about $\frac{1}{2}$ %. The data was not corrected for this error even though such a condition is forbidden theoretically; rather it was left as is. This served as an indication of the accuracy with which the data was recorded.

The temperature fluctuation had a poor signal to noise ratio and couldn't be measured with the LIA. The copper-constantan thermocouples are expected to have a response time that will just allow us to measure these fluctuations. The amplitude of this δT fluctuation should be down by a factor of four from the corresponding δP fluctuations according to the adiabatic relation. It is expected that the 15.1 c/s δT signal can be extracted from the noise by recording the data on tape and processing it with extremely long piecelengths, by computer.

Care must also be exercised in maintaining a proper and constant level of liquid nitrogen in the detector dewar; improper levels (in particular overfilling the dewar) can lead to 1% errors in the data.

The data was processed for equal wavelength intervals, which unfortunately did not always fall at extrema. The regions of the δI and I versus λ traces (that were recorded with the LIA) that had the largest slopes were probably the most inaccurately tabulated, although we were very much aware that this condition often occurs in data that is reduced by hand.

The speaker was never operated under static total pressure conditions of less than 250 Torr, in connection with the possibility of speaker damage. Figure 10 represents the amplitude of the pressure fluctuations in the absorption cell at one atmosphere (as measured with the Kistler transducer) as a function of frequency of oscillation with speaker power as a parameter. The peak at about 15 c/s is due to a resonance effect in the speaker cavity.

The nominal signal to noise ratio that existed during α measurements was much greater than unity. The signal to noise levels for the β data were not, and were not expected to be, as good. Figure 11 is an indication of the expected signal to noise levels in the dynamic mode. The absorption spectrum of a .121% CO_2 concentration gas at about one atmosphere and room temperature, with a nominal pressure fluctuation was recorded under identical conditions, first with the LIA and then with an a.c. voltmeter (the LIA used in the a.c. voltmeter mode). Although the a.c. voltmeter was not expected to measure very low voltages, it did zero for a near zero amplitude signal at about three divisions on

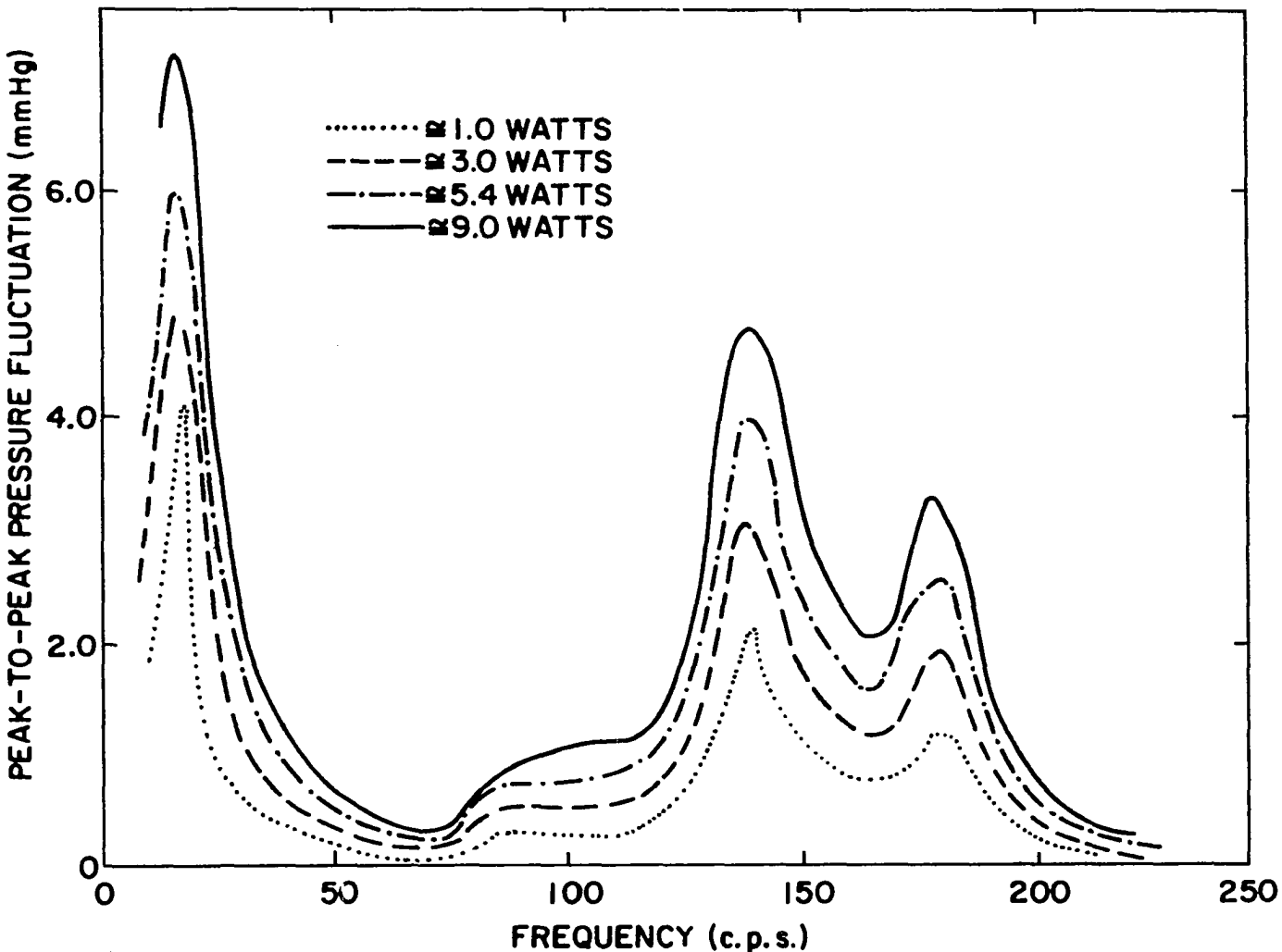

Figure 10. Pressure Fluctation in the Absorption Cell as a Function of the Input Frequency with Speaker Power as a Parameter.

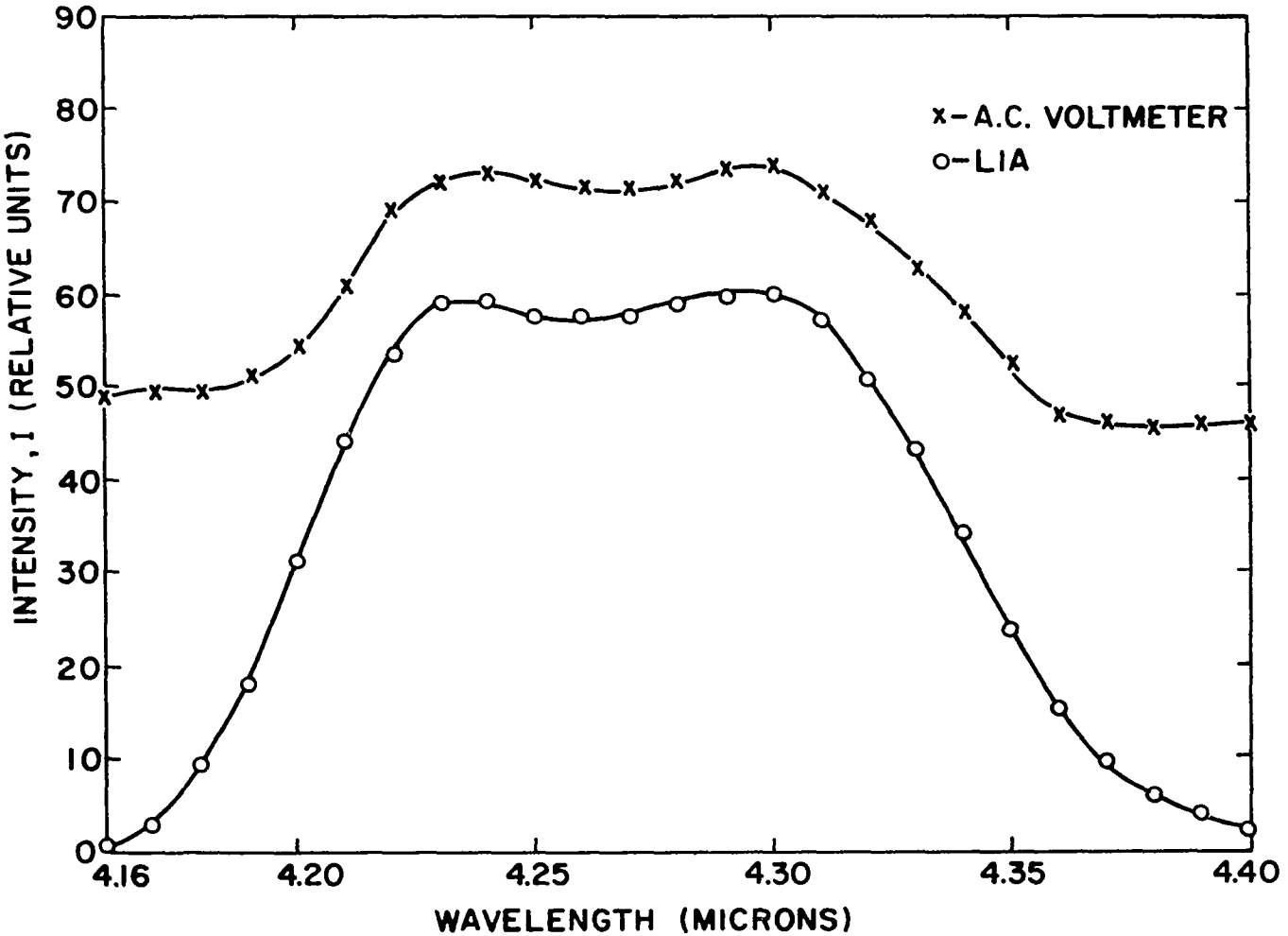

Figure 11 . Indication of Expected Signal to Noise Levels in the Dynamic Mode Measurements. The Crosses Correspond to a Measurement of a Given Detector Output with an A.C. Voltmeter; the Circles Represent the Identical Output Measured with a LIA.

the relative units scale. One can assume that the LIA measurement was basically a measurement of the signal whereas the a.c. voltmeter represented a measurement of the signal plus the mean noise. This represents one of our best S/N conditions for the dynamic mode; most β traces were recorded under worse S/N levels, a few were better. If a selective amplifier tuned at 15.1 c/s in the resonance mode with a Q of 10 is inserted into the a.c. voltmeter circuit, the noise level in the wings reduces to about 7 divisions on the relative units scale.

The corresponding α trace measured in the same way was about 3% higher overall for the a.c. voltmeter result compared to the corresponding LIA result.

The relationship between the mean intensity and the fluctuating intensity is given in Figure 12. It shows that the fluctuating intensity is strongest in the core regions where the interaction between the light and the gas is strongest. The time axis is used to display the approximately harmonic waveform of δI, as used in this experiment. I is basically a steady state measurement; δI is the fluctuation about this mean value. Therefore the instantaneous intensity is given by $I' = I + \delta I$ where $\delta I = A \cos 2 \pi f_{\delta P} t$. A is the maximum amplitude of the fluctuation and $f_{\delta P}$ is the frequency of the oscillation. When the measurement is made at $f_{\delta P}$, the quantity δI is measured. If the measurement is made at $2 f_{\delta P}$, then the first harmonic is measured. This coresponds to the second order terms in the Taylor series approximations since these terms contain cosine squared terms. These terms should start to contribute for very large fluctuations; they will include interactions between the thermodynamic variables and also the

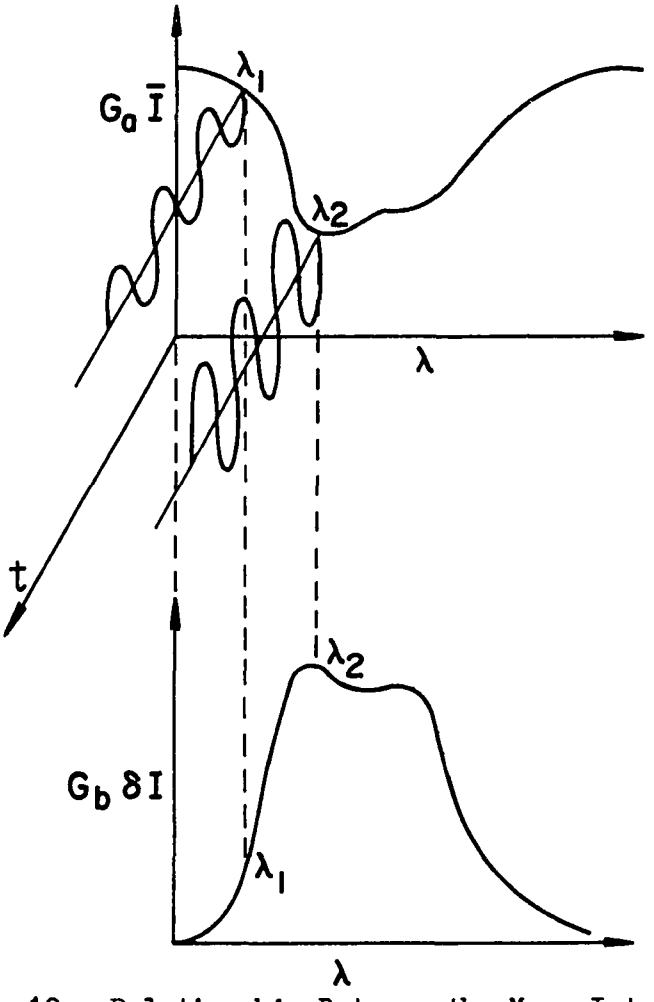

Figure 12 . Relationship Between the Mean Intensity and the Fluctuating Intensity. t represents the acoustic excitation time axis; the $G_{\underline{=}}^{S}$ represent the fact that different amplifier gains are necessary to measure the two signals ($G_a \ll G_b$). We have assumed that the core region of the mean value trace has values of I which are greater than the maximum possible fluctuation, δI, for the given conditions. A black core region will lead to a zero δI in that region.

derivatives. All the fluctuations were small in this experiment. If a measurement is made at the chopper frequency then I is measured. The fact that the mean intensity is in the form of a square wave is an artificiality, introduced only to increase the signal to noise level of the measurement.

The LIA or phase sensitive detector is an "average responding rms calibrated" instrument. The output of the instrument can be considered to be a single point narrow band normalized crosscovariance between the optical input signal and the reference signal; it is normalized by the rms value of the fluctuating reference signal and can be set for any phase difference between the two signals, over a range of 370°. The LIA will not measure a d.c. signal. The LIA output can therefore be given in the case of the β data, by

$$\text{LIA OUTPUT} = \frac{\overline{\delta I \cdot \delta P}\,\big|_{\phi = \phi'}}{\delta P_{rms}} \tag{91}$$

where $\delta I \equiv (I' - I)$ and $\delta P \equiv (P' - P)$. ϕ is a particular phase (or time lag) usually set to measure the maximum amplitude of the fundamental. When the data is recorded on magnetic tape the instantaneous values are recorded, and therefore one must remove the means before comparing the β data with the LIA data. In terms of the LIA, the α measurements (and also therefore the β measurements) are tabulated as pk-pk values because we want the total d.c. level for I; remember the chopped signal is a square wave resulting from the fact that the light is completely turned off and then completely turned on.

The tape recorder was calibrated in terms of the expected signal parameters with a TC - 10 Ampex Tape Recorder Calibration unit.

CHAPTER IV

BASIS FOR ANALYSIS OF RESULTS

Let us first consider the static results. The basic quantities that are measured are the transmitted and the incident intensities, given by I and I_o. The transmission can immediately be defined as I divided by I_o and therefore the absorption can be given by

$$A = 1 - I / I_o \ .* \qquad (92)$$

We have not as yet made any assumptions about the form or content of the results. Such absorptions can be analyzed by plotting them as a function of wavelength and the thermodynamic variables for a given bandpass. The resultant spectra (A versus λ) can be integrated with the use of a planimeter for example, to obtain the total absorption for a given band or bands of lines.

It is convenient to go a step further and use the results of Band Model calculations. Of course these introduce assumptions about the content of the data in the form of position and intensity distributions of the included lines. This allows one to introduce the concept of a generalized absorption coefficient which is a slowly varying

---

*This expression defines spectral quantities; however, the λ subscripts on I, I_o and A are dropped for convenience.

function of wavelength as compared to a line absorption coefficient. This generalized absorption coefficient is also assumed to be averaged over the light path from the entrance of the cell space to the exit; it is therefore, in this sense, an average value absorption coefficient. One finds that the various band models use different assumptions about the line distributions, however, these differences are not overly restrictive in the sense that the resultant expressions for the absorption do not vary significantly from one model to the next. In particular, the absorption expressions resulting from the two basic and quite divergent models, the Elsasser and Statistical Models are both given by $1 - \exp -K_{W.L.} l$ in the weak line limit and can be given by erf $(k_{S.L.} l)$ and $1 - \exp - k_{S.L.} l$ in the strong line limit. It can be shown that the error function and one minus the exponential function are almost identical except that the Elsasser Model saturates a little faster than the Statistical Model. (that is, the Absorption approaches a limiting value near unity faster for the Elsasser Model than for the Statistical Model). As a result, we therefore assumed that the absorption can be given by

$$A = 1 - \exp - Kl. \tag{93}$$

This has the same form as the well known Beer-Lambert expression which assumes that the change in intensity is proportional to the incident intensity and the amount of absorbing matter in the light path; this is given by

$$I = I_o \exp - Kl, \tag{94}$$

for the static measurements.

In our experiments, the length of the cell, given by l, is a

constant. We have chosen to define a volume absorption coefficient by removing an 1 from the extinction function. Whether or not this is strictly justified in terms of the various approximations that we shall use does not concern us here; 1 is a constant of unit length so the quantity represented by K must therefore have the units of Length^{-1}.

The dynamic or fluctuation measurements are in terms of δI, the fluctuation of the intensity about the mean value intensity. This quantity is related to the fluctuating absorption coefficient, using equation 94, by

$$\delta K = -\delta I/lI \quad . \tag{95}$$

The symbol represents the fluctuation operator; this denotes the change or fluctuation in the variables due to the acoustic excitation process. The right hand side of (95) is measured and therefore known. The left hand side can be expanded in a Taylor series expansion about the mean values, and is given by

$$\begin{aligned} \delta K = {} & \frac{\partial K}{\partial \bar{P}}\Big|_{\bar{P},\bar{T},\bar{p}} \delta P + \frac{\partial K}{\partial \bar{T}}\Big|_{\bar{T},\bar{p},\bar{P}} \delta T + \frac{\partial K}{\partial \bar{p}}\Big|_{\bar{p},\bar{P},\bar{T}} \delta p + \\ & + \tfrac{1}{2}\frac{\partial^2 K}{\partial \bar{P}^2}\Big|_{\bar{P},\bar{T},\bar{p}} (\delta P)^2 + \tfrac{1}{2}\frac{\partial^2 K}{\partial \bar{T}^2}\Big|_{\bar{T},\bar{p},\bar{P}} (\delta T)^2 + \tfrac{1}{2}\frac{\partial^2 K}{\partial \bar{p}^2}\Big|_{\bar{p},\bar{T},\bar{P}} (\delta p)^2 + \\ & + \frac{\partial^2 K}{\partial \bar{P}\partial \bar{T}}\Big|_{\bar{P},\bar{T},\bar{p}} \delta P \delta T + \frac{\partial^2 K}{\partial \bar{P}\partial \bar{p}}\Big|_{\bar{P},\bar{p},\bar{T}} \delta P \delta p + \frac{\partial^2 K}{\partial \bar{p}\partial \bar{T}}\Big|_{\bar{p},\bar{T},\bar{P}} \delta p \delta T + \cdots \quad . \end{aligned} \tag{96}$$

Note the form of the interactions between P,T,p in the second order terms.

We will use fluctuations that have a maximum amplitude which is sufficiently small so that only the linear terms in equation (96) have to be retained. Therefore equation (96) reduces to

$$\delta K = \frac{\partial K}{\partial \bar{P}}\Big|_{\bar{P},\bar{T},\bar{p}} \delta P + \frac{\partial K}{\partial \bar{T}}\Big|_{\bar{T},\bar{p},\bar{P}} \delta T + \frac{\partial K}{\partial \bar{p}}\Big|_{\bar{p},\bar{P},\bar{T}} \delta p \quad . \tag{97}$$

The validity of this needs to be determined experimentally.

Our experiments were performed under the condition of frozen composition. This is given by

$$p / P = f = \text{constant} \tag{98}$$

Therefore an increase in P necessarily means an increase in p in any given run. Assuming this condition, it is possible to expand δK using as a basis, the quantities P, T,f. Since df = zero, equation (97) reduces to two terms given by

$$\delta K = \frac{\partial K}{\partial P}\Big|_{\bar{P},\bar{T},\bar{f}} \delta P + \frac{\partial K}{\partial T}\Big|_{\bar{T},\bar{f},\bar{P}} \delta T \quad . \tag{99}$$

The first partial derivatives in (97) are related to those in (99) by a set of transformation equations which are easily derived. It must be remembered that the variable P in equation (99) is associated with an "intermediate variable" p. An increase in P therefore represents an increase in the number of absorbers and in increase in the pressure broadening effects.

A further condition on the data can be given in terms of the adiabatic condition; this is given by

$$\frac{\delta T}{T} = \frac{\gamma - 1}{\gamma} \frac{\delta P}{P} \quad ; \tag{100}$$

and represents another important coupling relation. If desired, equation (99) can be further reduced using (100) to give

$$\delta K = \left[\frac{\partial K}{\partial P}\Big|_{\bar{P},\bar{T},\bar{f}} + \frac{\partial K}{\partial T}\Big|_{\bar{T},\bar{f},\bar{P}} \frac{\gamma - 1}{\gamma} \frac{T}{P}\right] \delta P \quad . \tag{101}$$

It is necessary to realize that each of the partial derivative expressions is a definite function of all the thermodynamic variables. Therefore the expressions for δK are quite complex.

The absorption coefficients can be expressed in terms of the weak and strong line approximations. The resultant expressions are given

by

$$K_{W.L.} = S(T)p/d = S(T)fP/d \quad , \tag{102}$$

$$K_{S.L.} = 2\left(\frac{S(T)\gamma_o Pp}{d^2 lT^{\frac{3}{2}}}\right)^{\frac{1}{2}} = 2\left(\frac{S(T)\gamma_o f}{d^2 lT^{\frac{3}{2}}}\right)^{\frac{1}{2}} P \quad . \tag{103}$$

S is an integrated absorption, γ_o is the line halfwidth evaluated at S.T.P, d is the line spacing. S can roughly be given by

$$\bar{S}(T)_{\lambda'} = (Aa_{\lambda'}/T)\exp Bb_{\lambda'}/T \tag{104}$$

for reasonably small spectral intervals positioned at λ'. This expression can of course be substituted into (102) and (103). The partial derivatives of these expressions are straight forward.

Unfortunately expressions (102) and (103) are not sufficient to describe the absorption over the complete range of thermodynamic variables. A considerable amount of the data that is recorded in this experiment can be adequately described only by the ill defined region formulation of the absorption coefficient dependence on the thermodynamic variables. In this region, the weak and strong line limits converge to a single expression given

$$K_{I.D.R.} \propto p^l P^m \quad . \tag{105}$$

The temperature dependence is not as simply determined. We have therefore used either the strong line or the weak line temperature expression in this region, depending upon which expression best fits the data.

The coefficients l and m can be expected to vary roughly between $\frac{1}{2}$ and 1, and $\frac{1}{2}$ and 0 respectively. When the two coefficients equal $\frac{1}{2}$ then the strong line approximation holds; when l = 1 and m = 0, the weak line approximation holds. The variation of the exponents as a function of p and P is not strictly defined, but can be determined experimentally by fitting the data to expressions such as (105).

In terms of absorber concentration, equation (105) is given by

$$K_{I.D.R.} \propto f^{l} p^{m+1} \quad . \tag{106}$$

The sum of l and m can vary between $\frac{1}{2}$ and 3/2, although one expects the maximum to be closer to 1 than to 3/2. The dependence of K on f can be found from this expression by keeping P constant; the exponent again varies between $\frac{1}{2}$ and 1. The dependence of K on P with f held constant is determined from (106).

Plass[26] has stated that over a limited range of β and ψ, the absorption data itself should follow a power law of the form

$$A \propto p^{l'} p^{m'} \quad . \tag{107}$$

This formulation for the absorption has been used by Burch, Gryvnak and Williams[5] for CO_2. This form should hold very well in the nonoverlapping line approximation[28]; however, for data that is in the ill defined region and closer to the saturation region than to the transparent gas region, one expects that the values of l' and m' will be somewhat smaller than l and m due to the fact that the absorption is beginning to "bend" into saturation. This effect must be absorbed into the l' and m', whereas, in the absorption coefficient formulation, the l and m can remain the same (due to the one minus the exponential expression) as the data approaches this region. One therefore expects l and m to be valid over a much wider range than that for l' and m'.

The dependence of δK on the thermodynamic variables can be simplified by controlling the variables experimentally and recording the resultant δI / -1I. For example, if δP is varied proportional to P, then T will remain constant for a given temperature and the effect of P on δI is more easily determined. The effect of p on δI for frozen

composition is found by keeping P constant and varying f. T is kept constant to minimize other effects.

CHAPTER V

DATA AND DATA PROCESSING PROCEDURES

The most basic data set, as recorded with the LIA, consists of three sets of low resolution measurements: I_o, I, and δI versus wavelength, over the complete and continuous wavelength range from 4.16 to 4.40 microns. The traces were recorded for all possible combinations of temperature, total pressure and CO_2 concentration. The temperatures used were 243, 275, 297, 353, and 393° K; the total pressures were 422, 528, 632, 738, 841, 948, and 1053 mm Hg; and the CO_2 percentage concentrations were .030%, .065%, .093, and .121%. The corresponding range of the CO_2 partial pressure is .1266 mm Hg to 1.2741 mm Hg in 28 steps.

It was decided to sample this data at .01 micron intervals from 4.16 to 4.40 micronas. This sampling interval gave a reasonable spectral resolution and limited the number of data points per trace to 25; a larger number of points might be preferred but the increased computational time is restrictive. With these conditons, the total number of data points for just the most basic data set is already at 7500 pieces.

Additional data was also recorded in the form of both α and β traces for variable δP at constant P,T,f, λ; variable $\Delta\lambda$ for constant P,T,f, δP; and $\delta P \propto P$ for constant T,f, $\Delta\lambda$. This brings the total number

of basic data points up to about 10,000, not including any calculations or the magnetic tape data. This data was selected out of a considerably larger volume of data which includes in some cases, a wider range of variables.

The intensity data (δI and I) was tabulated as the magnitude of the signal at the chart recorder or LIA output. However, it was considered necessary to reduce these intensity values to that which existed at the output at the optical detector. This eliminated signal modification (not noise modification) due to various instrument factors and allowed for a direct comparison between the α and β data, and also the LIA data and the magnetic tape data which was also reduced to those values which exist at the detector output.

This meant going through a series of calibration factors that are introduced between the input and the output of the electronics. The measurements are given in terms of peak to peak values for reasons specified in the measurement section. The waveforms of the signals must be taken into consideration since the LIA is an rms measuring instrument. For the LIA data, this meant multiplying the I and I_o values of the chart recorder (as tabulated in the raw data dump) by the constant $a^{(I)} = 1.00 \times 10^{-1}$. This factor includes only the preamp gain, the LIA sensitivity, and a factor of two which transforms the rms value of the approximate square wave to a peak to peak value. The δI values were multiplied by a $^{(\delta I)}$ which was calculated to be 1.41×10^{-4} or 2.83×10^{-4} for this most basic data set. This factor includes only the preamp gain, the LIA sensitivity and a constant equal to 2.83 to go from an rms measurement to a peak to peak measurement.

The δP measurements had to be converted from the values recorded on the strip chart with the LIA to values which were compatible with the P measurements. This was done by again going back through the electronics to the output of the Kistler transducer. Using the factory calibration factor (see Section III.D) for this particular transducer (given as the charge sensitivity and equal to 5.25 pcb / psi), the constant $a^{(\delta P)}$ was calculated at 1.42×10^{-1} mm Hg / div. This leads to $\delta P = 5.68$ mm Hg pk - pk for the constant δP traces. This factor includes only the preamp gain, the LIA sensitivity, the Kistler Amplifier gain, the constant equal to 2.83 for the waveform, and the calibration factor 5.25.

The same procedure was necessary for the magnetic tape data. The various channels on the tape were set to utilize the dynamic range in the optimum way.

The first calculations (on the LIA data) made were of the transmission (I / I_o) and the absorption ($1 - I / I_o$). These were calculated for all combinations of P,T,f, . The absorptions were also plotted versus wavelength.

The LIA data was also processed (using the calibration factors) to yield mean value absorption coefficients and fluctuations of the mean absorption coefficients. These were both tabulated for the same ranges of P,T,f, and λ as given above. The tables of I_o, I, δI, A, T, K, and δK, represent the basic data set for the LIA portion of the experiment and the starting point for all subsequent analysis.

A considerable amount of high resolution data was also recorded in this experiment although the cell conditions were not optimized so

as to record the best possible high resolution information. This data was recorded to give us a better understanding of the nature of the actual absorption process as it occurs in this experiment with these conditions. The data covered various total pressures and CO_2 concentrations; it was recorded using identical recording parameters for each trace, so that the resultant traces could be compared. We used a slit width of .09 cm^{-1} which was the smallest setting for which a reasonable S/N level could be determined.

The magnetic tape data was digitized and processed in a manner described in the measurements section. Both continuous and segmented wavelength procedures were used to record the data on tape. Only a few typical series were taped in these experiments, although enough data was recorded and processed to establish the best procedures to be used when recording the data in this manner. We did not feel that the magnetic tape approach to data taking was warranted in the initial stages of the experiment due to the very long data processing "turn around times"; we did not have the necessary digitization and computer processing facilities to do the processing ourselves.

The data was processed with MLTCOR. The multichannel correlation program MLTCOR was developed by Wachowski and Phillips[33] to calculate statistics for atmospheric and aerodynamic turbulence based on the Crossed Beam Technique. The purpose of the program is to statistically analyze simultaneously recorded time histories of meteorological data by calculating an average of mean values, rms values, and correlation and covariance functions which approximate the mathematical model of stationarity and infinitely long time histories to the largest practical

amount.

The program is written in Fortran IV using modular techniques and dynamic storage allocation. The piecewise concept was used in writing this program. A long time series is logically broken up into a series of smaller pieces. Correlations, mean values, rms values, and variances are then calculated for each piece along with their standard statistical errors. Modified correlations can then also be formed; such operations as normalizing, detrending, or subtracting the product of the means to form the covariance can also be performed. Any of these operations can be performed individually or in combinations. The calculations for each piece are then accumulated over separate periods of the data with provisions for deleting individual data pieces within the accumulative period. Periodic printouts can be used to monitor peecewise statistics and errors.

This program was used to process the instantaneous intensity time histories of α and β signals; the δI and δP signals of the β data were of prime concern.

Returning to the LIA data, a modular Fortran IV based data analysis program was developed to handle the graphing and least square fitting procedures, and various other calculations that followed from this LIA data. This program consists of a set of subroutines which perform the specific operations on the basic data set and which communicate with each other through a common data pool. The desired sequence of analysis is directed and controlled by a user supplied main program. The modularity of the construction allows one to add new capabilities to the analysis operations without modifications of the existing routines.

The main type of analysis considered by this program is described

by the least square curve fitting regression equation of the form

$$Y = A_1 + A_2 X' + \cdots + A_N X^{N-1}. \qquad (108)$$

The first step in such a calculation is the accumulation of the sums over the data points which comprise the coefficients of the normal equations. Next, the set of normal equations are reduced to a triangular form by the Gauss method of elimination. The fitting parameters are determined through the process of back substitution. When fitting equations with nonlinear parameters, special care must be taken to apply appropriate weighting factors to the data points. Failure to do this will cause the desired statistical basis of the fit to be in error due to the effect of the transformations used for the reparameterization of the fitting equations. In general if the transformation $f(y_i)$ is applied to each data point y_i, then its corresponding weight $w_i = 1/\sigma_i^2$ must be equal to $w_i = 1/\sigma_i'^2$ where the new $\sigma_i' = \frac{d}{dy} f(y_i)\sigma_i$ (σ_i is the variance). In this program, routine TRSFRM is used to perform the proper coordinate transform and to direct PLF to retransform the desired parameters. Routine PLF is the basic curve fitting routine. It performs the least squares regression analysis on data contained in various x-y arrays. Routine PLF also calculates, for each curve fit, a summary report which gives a table of x, y measured, and y calculated, the difference and percentage difference between the measured and calculated values of y.

The program was also used to perform plotting operations; these were performed by routine DSPLAY in conjunction with routine IMAGE. Some 6000 curves were obtained from the automatic scaling and plotting of about 64,000 points.

The LIA data set was recorded on magnetic tape for convenience

and to facilitate the data processing operations.

A complete description of the program is given in the Master's thesis of C.T.Bush (University of Oklahoma, Physics Department, 1971).

The program was used to calculate K and δK from I, δI, and 1. It was then used to plot the basic data as families of curves of I and δI, and K and δK versus wavelength with P,T,f as parameters. This enabled us to obtain an intuitive feeling for the data and served as a monitoring device (the δI, I curves) to detect errors made in the digitizing and keypunching operations. The data was also plotted as K and δK versus P,T.f with λ as a parameter. This served as a guide for the curve fitting and most important it allowed us to establish a general view of the basic trends in the data. The next step was to fit the mean absorption coefficients to equations which are found in Chapter IV and used to predict the expected thermodynamic variable dependence. The resultant smoothed data is then differentiated to obtain the mean value absorption coefficient derivatives with respect to P,T,and f. Various other related calculations are also made including a comparison of the calculated and measured fluctuating absorption coefficients.

Data was also recorded using extreme values of the CO_2 partial pressure or the absorber amount.

CHAPTER VI

ANALYSIS OF RESULTS

A. Introduction

This section is concerned with an analysis of the data taken in this experiment. We are primarily concerned with the low resolution data although a section is devoted to the high resolution spectra. This high resolution analysis will give the reader some insight into the form of the data before it is smoothed by the wide bandpass.

The low resolution data is first analyzed on the basis of an Absorption spectrum analysis as is generally done in the literature. Of course, this applies only to the static data. We then analyze the fluctuating intensity and the mean intensity spectra in terms of their dependencies on P,T and f and their general form. These are then related to the fluctuating absorption coefficient spectrum and an explanation is given for why such a spectrum is formed. The use of the δK spectrum as the basis for a spectral inversion is discussed.

The mean value absorption coefficients are then considered and related to the weak line and strong line approximations; the derivatives are calculated and displayed. The functional dependence of the K spectrum is stressed. We have also attempted to stress the similarities and differences between the various possible spectra.

The relationship between the magnetic tape results and the LIA results is then considered and the fluctuation structure of the gas is determined for our single beam case.

B. High Resolution Data

Considerable effort was expended in this experiment in attempting to understand the basic physical mechanisms involved in the infrared absorption process. It was felt that a thorough understanding was attainable only through an analysis of the behavior of the individual rotational lines in a group of N interacting lines. Such an analysis really requires that the experiment be performed under high resolution since the line interactions in a given situation can only roughly be described theoretically. Thus even though this relatively high spatio-spectral frequency information is eventually averaged out or smoothed in this experiment its understanding is essential, both mathematically and experimentally. We shall now take a qualitative look at some typical intensity versus wavelength (I vs. λ) traces before any smoothing was performed.

Figure 13 is a sample of six traces recorded under identical recording conditions but different thermodynamic conditions. These represent the 4.3 micron vibration-rotation absorption bands of CO_2 at room temperature. The individual rotational lines are clearly visible as is the vibration-rotation contour of the bands. The traces are lined up so that equal rotational quantum numbers (J) or wavelengths fall on the same vertical lines. The top of the figure contains the fairly shallow rotational lines curve. Each of the six traces is recorded

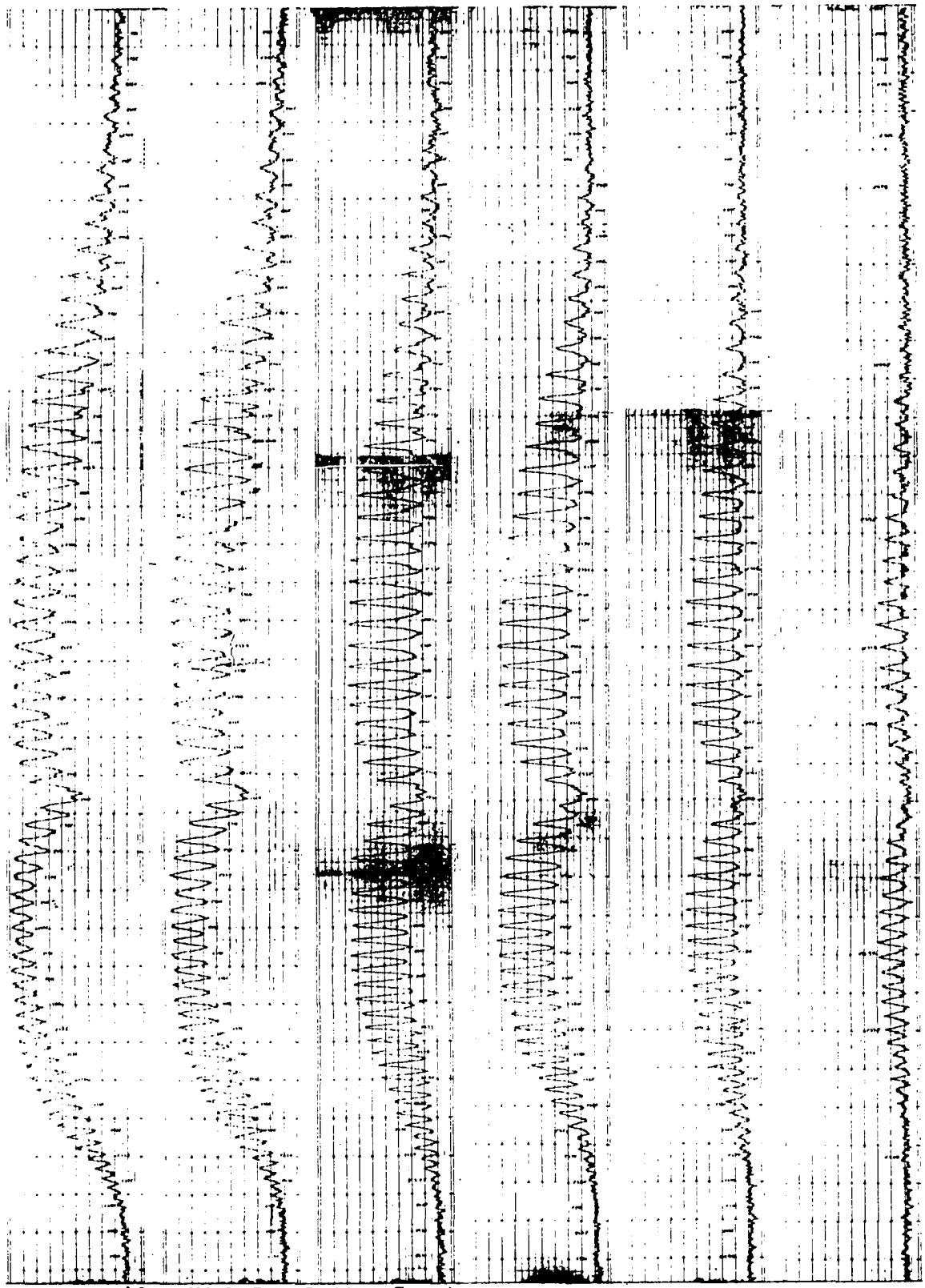

Figure 13 . High Resolution Spectra

on the same scale of 0 - 100 divisions on the chart recorder paper which forms the background of each trace. Zero represents complete absorption or zero transmitted intensity. The right hand side of each trace is at about 4.16 microns; the left hand side is at about 4.40 microns. The various trends between the six traces are comparable.

One notices that the rotational lines fall into two groups; the group on the low wavelength side (right hand side) forms the R branch and the group on the high wavelength side forms the P branch. There is no distinct Q branch for these bands, since the predominant ground state fundamental is a Σ-Σ transition. The absence of the Q branch is detected by the broad peak or zero gap near the center right of the traces at approximately 4.26 microns. The rotational lines are labeled starting with J = 0 in the R branch and J = 1 in the P branch; the alternate J lines are missing due to the zero spins of the oxygen nuclei. The fact that the alternate lines are missing is evidenced by the π phase shift when going from the P branch line sequence to the R branch line sequence. One notes further that the line spacing is contracting in the R branch and expanding in the P branch; this is due to a vibration-rotation interaction term of the form J^2 in the rotational term value. The band head in the R branch is not visible under these conditions.

Another very important point that this figure shows is that the R branch is much "cleaner" than the P branch; in other words the effect of overlapping overtones and combinations (such as a π-π transition) is more predominant in the P branch. Note that the regions between the intermediate to high J lines in the P branch show the presence of weak

rotational lines (which are consistent from one trace to the next) probably from a π-π species transition. Such lines are also seen in the region between the P and the R branches.

As an example, the (0101,π) - (0111,π) transition for CO_2 has an integrated intensity which is only slightly more than an order of magnitude smaller than the ground state fundamental given by (0000,Σ) - (0010,Σ). This therefore overlaps the 4.3 micron ground state fundamental; it has a weak Q branch and a band origin near 2336 cm^{-1} which is in the P branch of the ground state fundamental.

The effect is as expected. If higher temperatures were used, these lines would make an even more significant contribution. The presence of these weak lines is the main factor which prohibits the smoothed data from ever reaching a firm strong line limit.

If the reader will count the rotational lines, there is an average of about 50 active lines in each trace. The strength of the lines in each band roughly follows that of the equilibrium distribution for the population of the states.

One of the limitations of these traces is that the band width of the recording instrument was about .09 cm^{-1} whereas the expected average halfwidth for these lines is about .07 cm^{-1}. Therefore the lines were not resolved too well.

Let's now consider the effects of the variables f and P. The first or uppermost trace was recorded at a total pressure of approximately 841 mmHg and a percentage CO_2 concentration of roughly .006%.. The lines are very shallow in this case and there is a minimal amount of overlap. If we assumed that the lines were well resolved

then this would represent a weak line approximation and possibly a linear nonoverlapping line approximation.

Unfortunately the depth of the rotational lines is probably closer to a black line center condition (zero divisions) than the trace indicates. The less well resolved the line is, the less the apparent depth of the line. Furthermore, an increase in total pressure signifies an increase in line width and therefore in a better resolved line. This can result in an increase in the apparent depth of the line with an increase in the foreign gas pressure although the increased broadening decreases the true depth of the line. However, this type of pressure effect is not too severe in these illustrations.

The CO_2 percentage concentrations and the total pressures of the next five traces below the top one (1) are: (2) .030%,422 mmHg; (3) .030% CO_2, 1053 mmHg; (4) .121%, 422 mmHg; (5) .121%, 841 mmHg; (6) .121%, 1053 mmHg.

Traces two and three represent an increase in total pressure at constant f; the number of absorbers and the line broadening increases from two to three. The .03% represents the lowest CO_2 concentration used consistently in these experiments. Trace three is starting to show considerable line overlap. Both traces are assumed to be in the ill defined region; trace two being closer to the weak line limit than three. Traces four, five and six again show an increase in total pressure for constant f; this is the largest concentration used in the basic data set. One can see from this series that the core region of the R branch is starting to approach a complete black condition, which signifies saturation. These traces are also in the ill defined region; the last two

traces being obviously nearer the strong line condition than the weak line. There is an extreme overlap in the core regions of trace six. If trace six were recorded at the lower temperatures, then the blackness condition would be even more pronounced.

Curves two and four show an increase in f for the lowest total pressure. This represents a change in only the number of absorbers. The same situation exists in traces three and six only this time the highest total pressure is used. Notice that the higher the CO_2 partial pressure, the larger the number of lines that are active in the absorption process.

C. Conventional Analysis in Terms of Absorption.

The generally accepted method of analyzing absorption spectra[26,5] has been to plot the data as Absorption in the strong line, weak line and nonoverlapping line approximations. Only static or nonfluctuating data has been analyzed this way and the temperature dependence is generally not considered. Although it is not our intent to use this method as our basis for analysis, we shall now give a sample of the type of results to be expected when using this approach. It is necessary to understand that we are not primarily interested in establishing the validity of the weak or strong line approximations, and therefore we restricted our measurements to a range which encompassed our atmospheric-crossed beam conditions only.

Figures 14-22. are a sample of the spectral absorption plotted (using the computer) as a function of wavelength for various parameters. There are three sets of families of curves; three sets of curves with

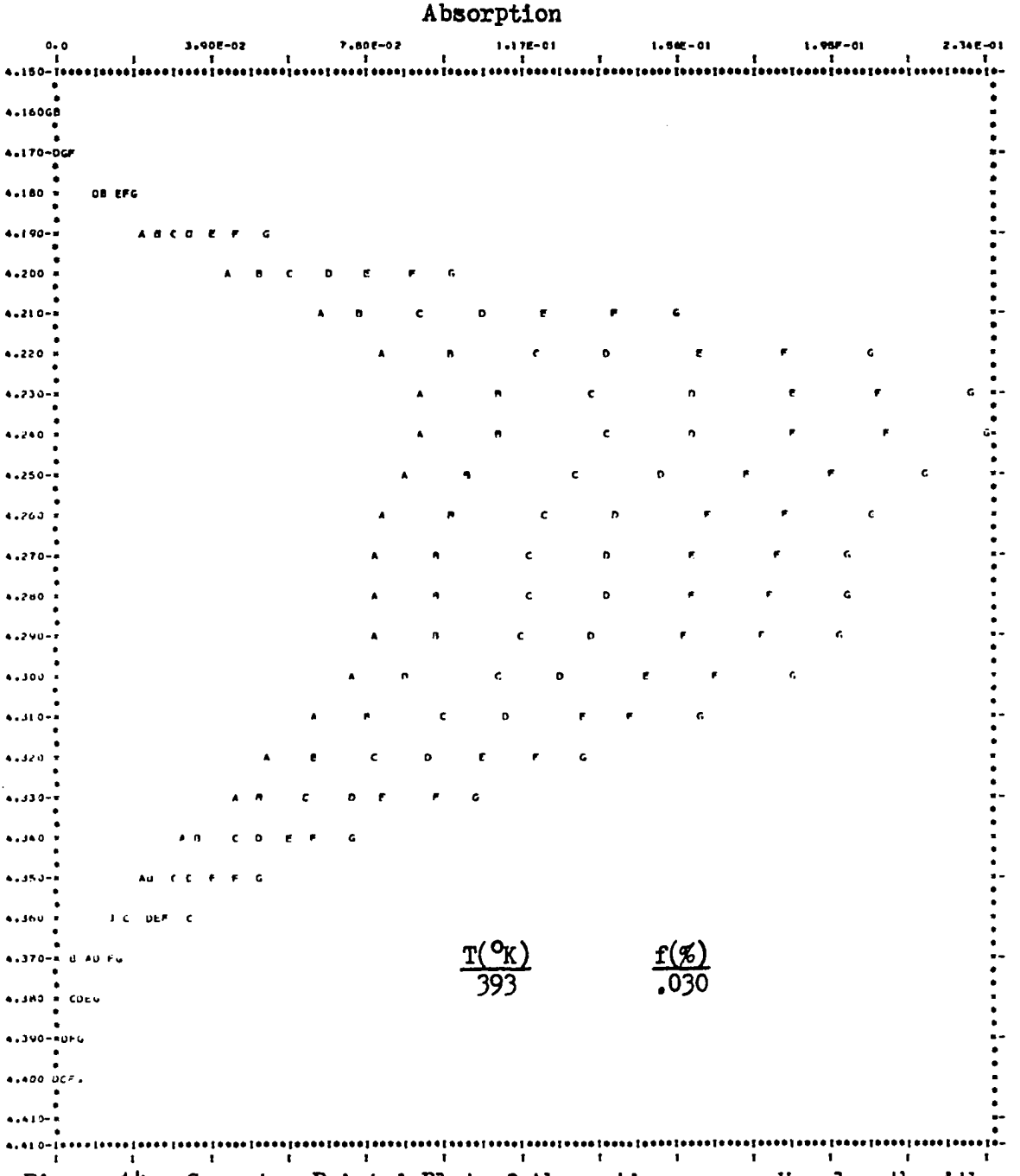

Figure 14 . Computer Printed Plot of Absorption versus Wavelength with P as a Parameter. Plot Symbols Represent Pressure P from 422 mmHg to 1053 mmHg in Alphabetical Order.

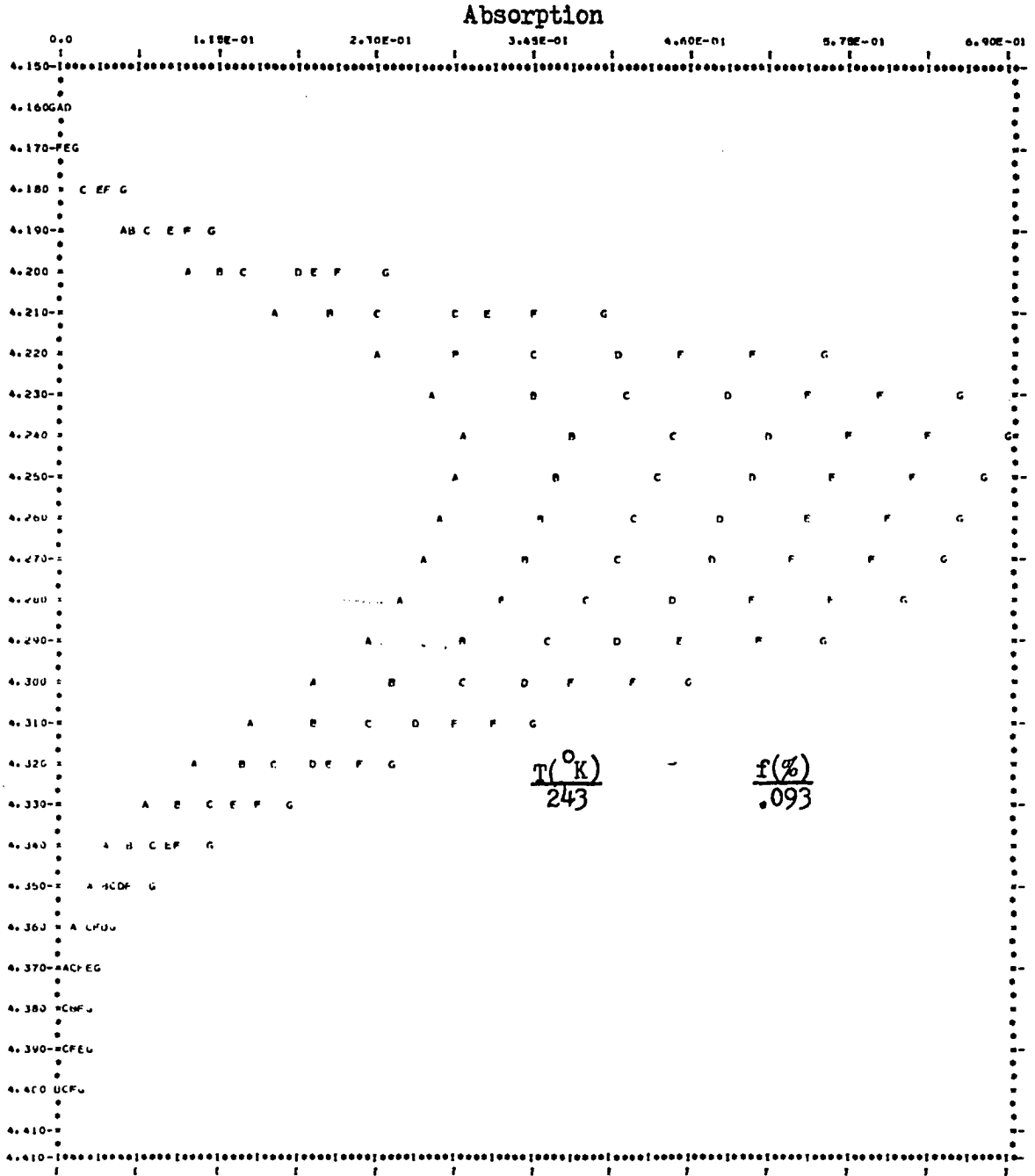

Figure 15. Computer Printed Plot of Absorption versus Wavelength with P as a Parameter. Plot Symbols Represent Pressure P from 422 mmHg to 1053 in Alphabetical Order.

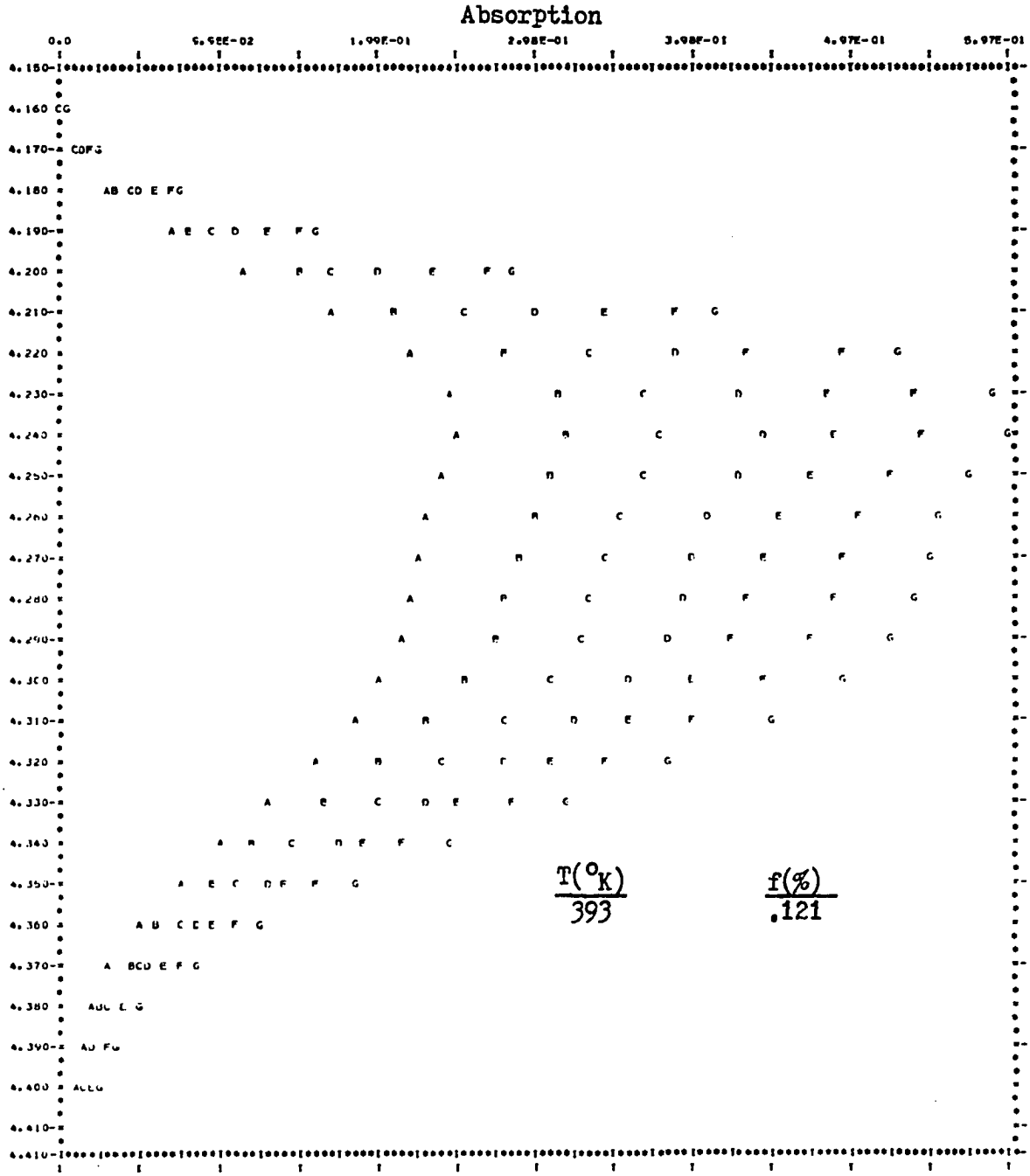

Figure 16. Computer Printed Plot of Absorption versus Wavelength with P as a Parameter. Plot Symbols Represent Pressure P from 422 mmHg to 1053 mmHg in Alphabetical Order.

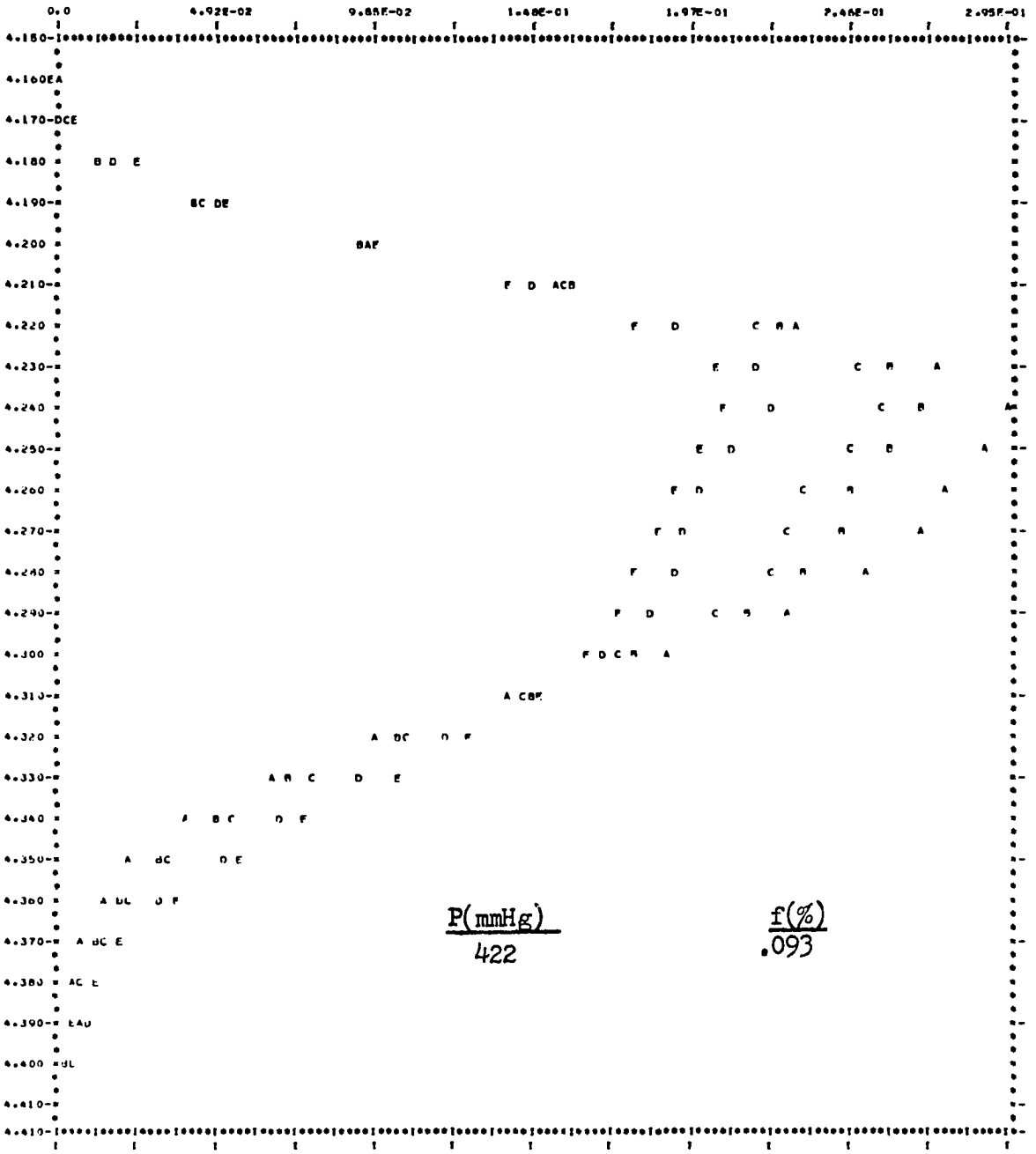

Figure 17. Computer Printed Plot of Absorption versus Wavelength with T as a Parameter. Plot Symbols Represent Temperature T from 243°K to 393° in Alphabetical Order.

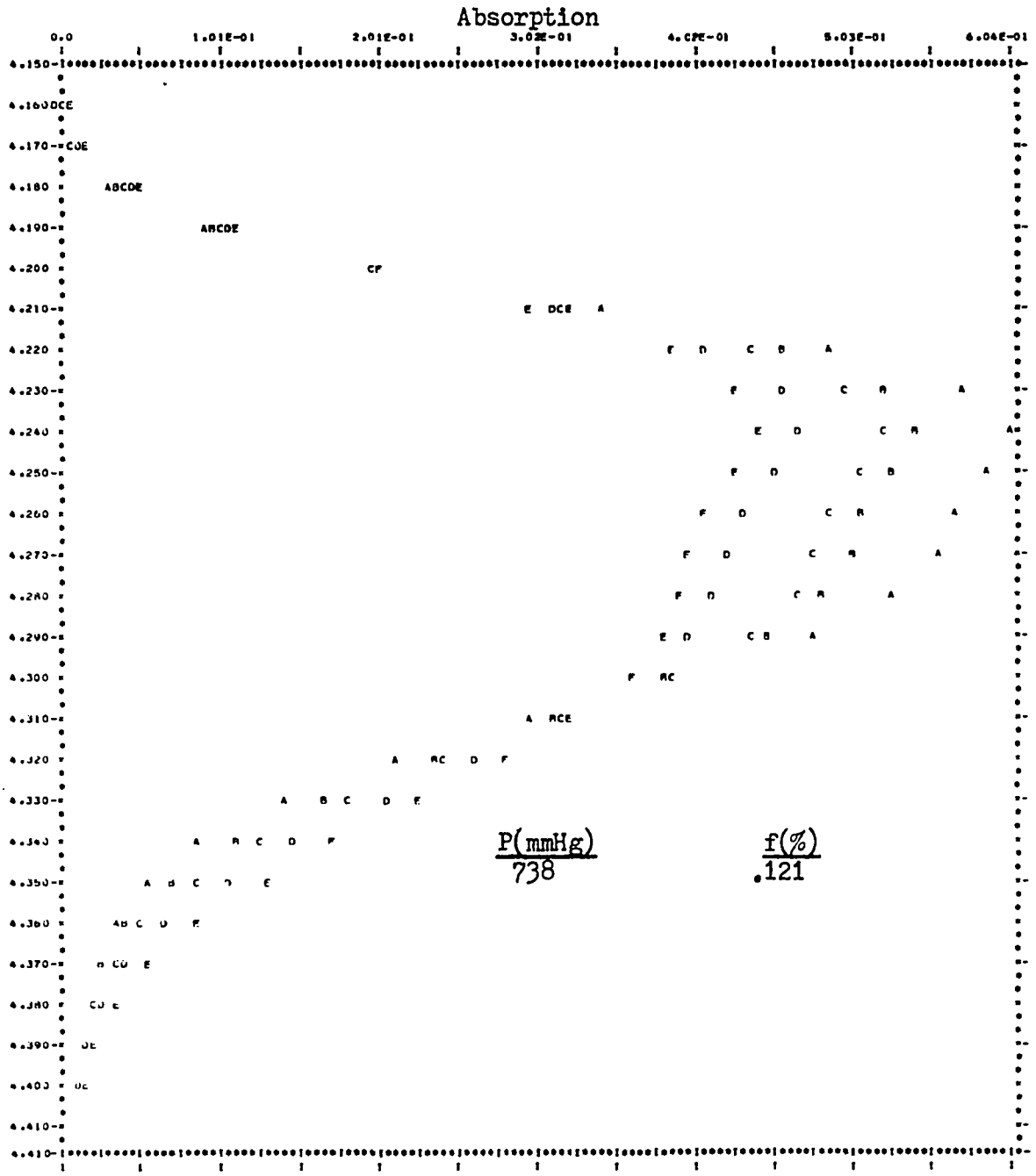

Figure 18. Computer Printed Plot of Absorption versus Wavelength with T as a Parameter. Plot Symbols Represent Temperature T from 243°K to 393°K in Alphabetical Order.

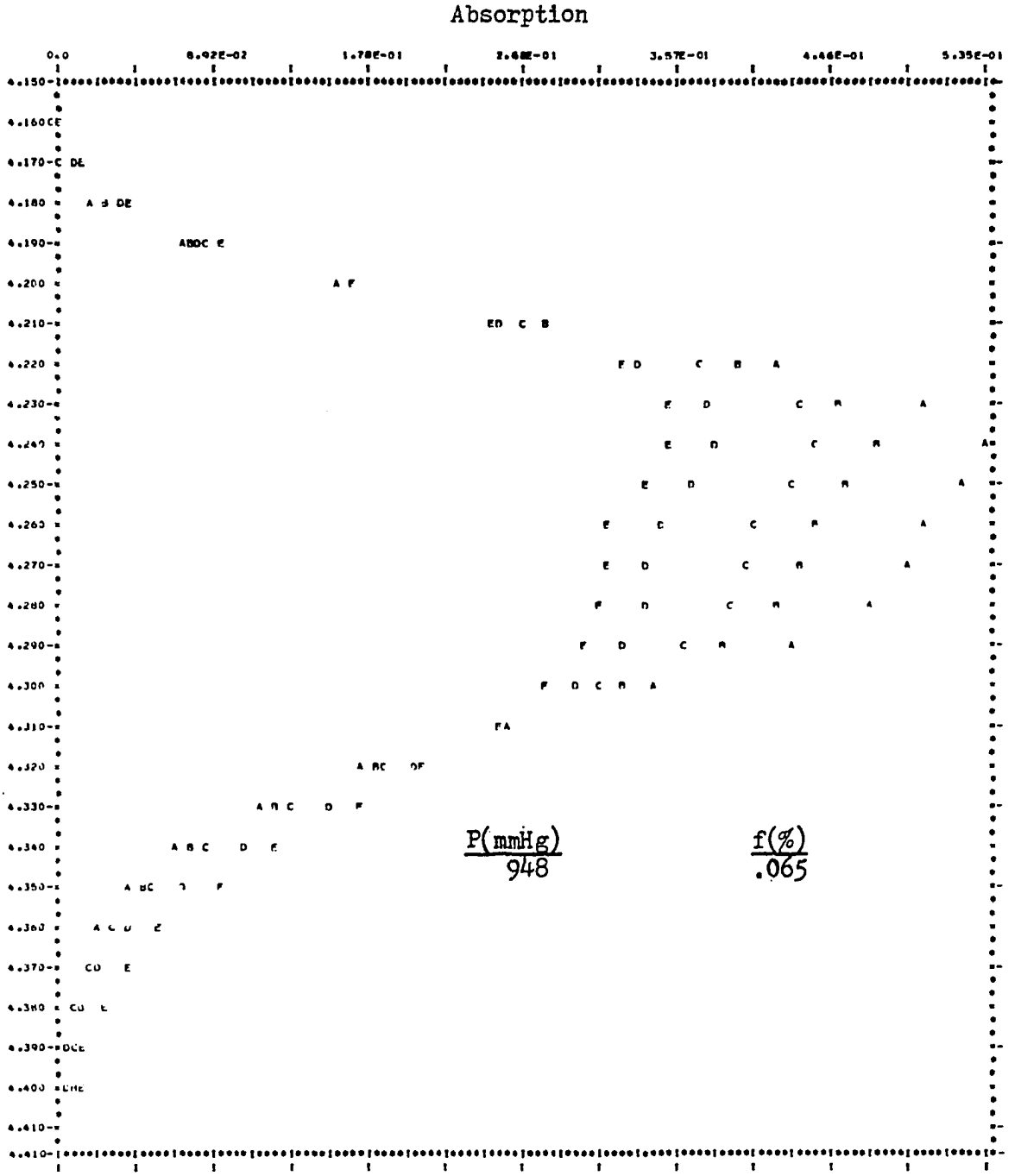

Figure 19. Computer Printed Plot of Absorption versus Wavelength with T as a Parameter. Plot Symbols Represent Temperature T from 243°K to 393°K in Alphabetical Order.

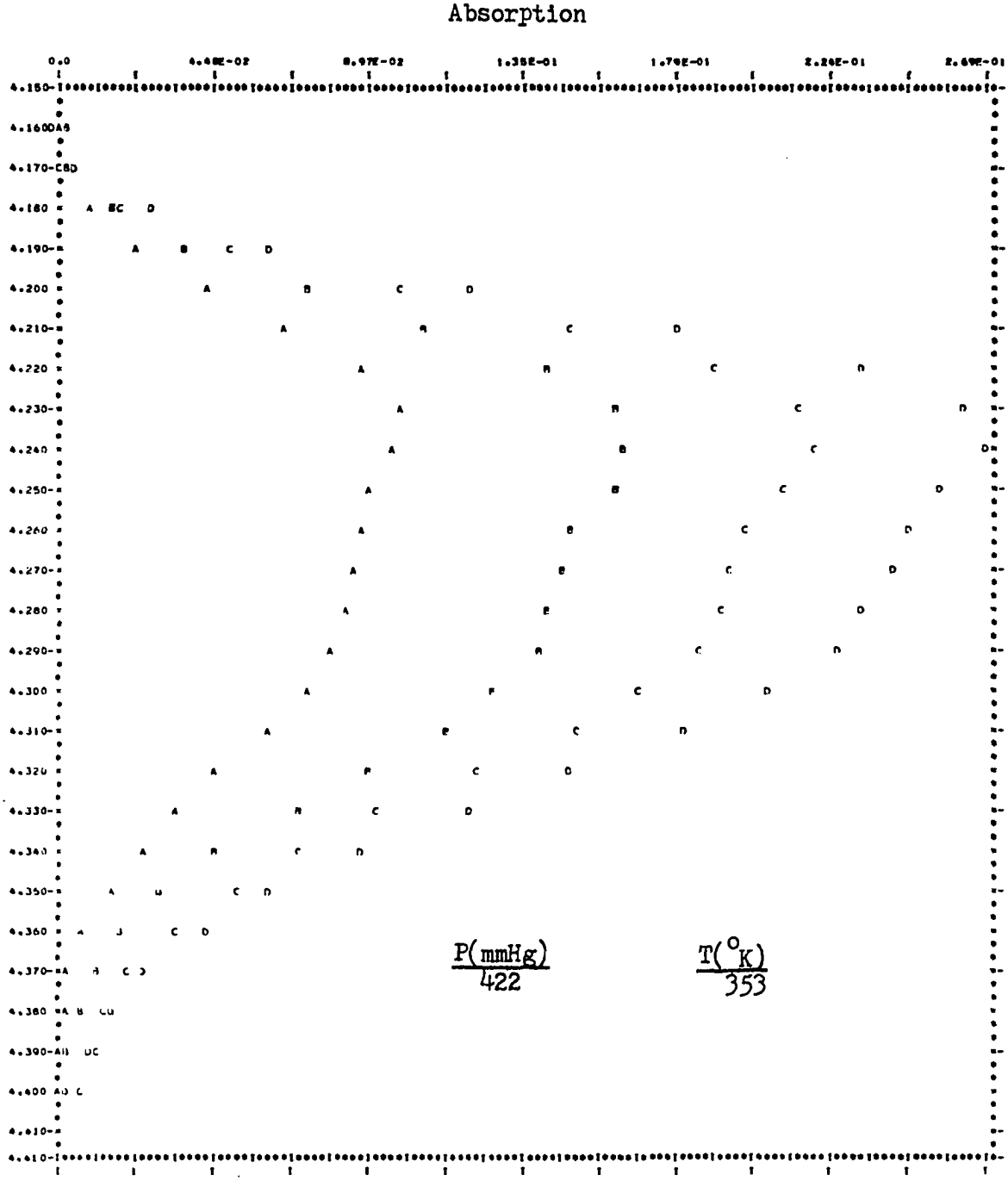

Figure 20. Computer Printed Plot of Absorption versus Wavelength with f as a Parameter. Plot Symbols Represent CO_2 Concentration f from .030% to .121% in Alphabetical Order.

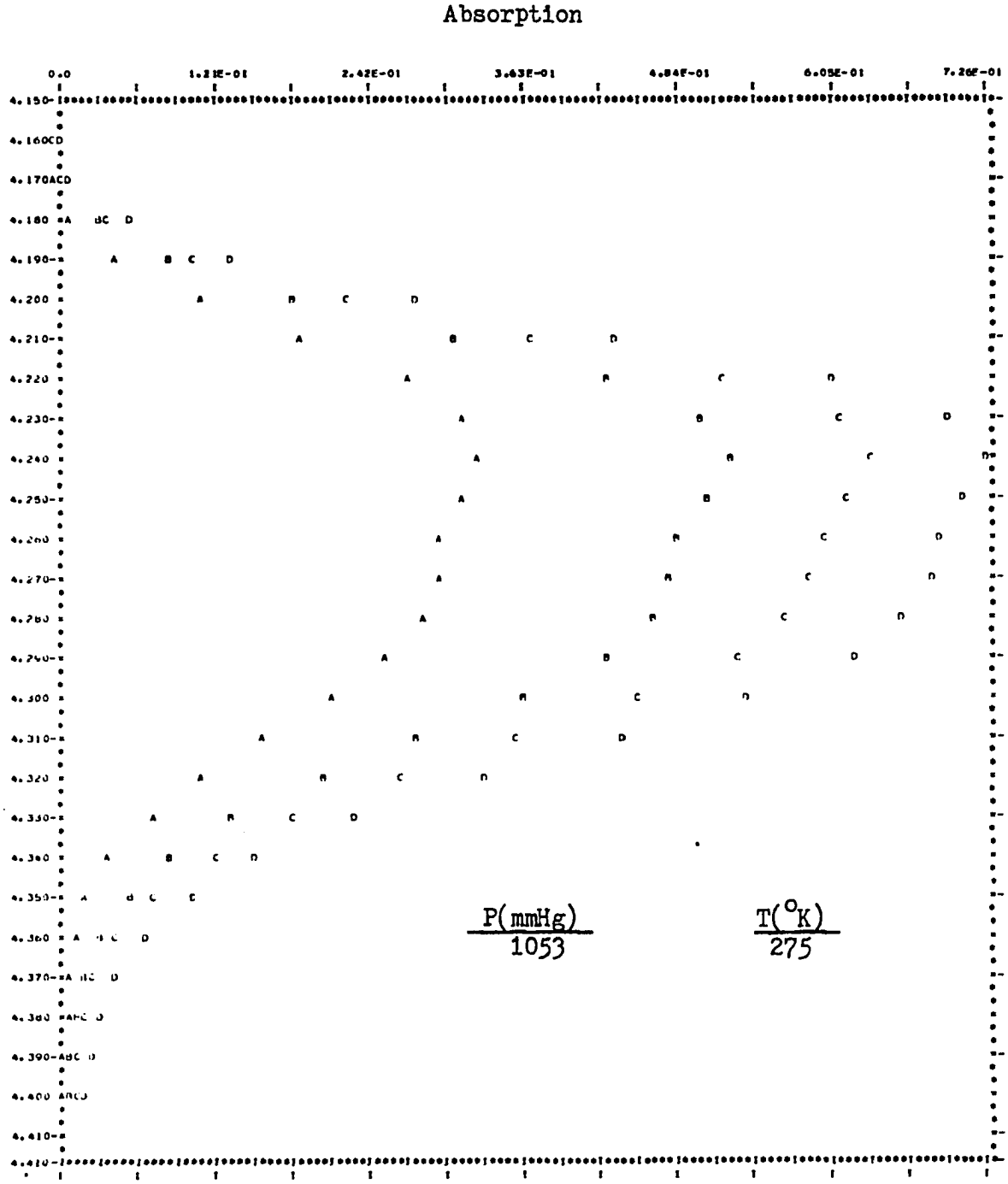

Figure 21. Computer Printed Plot of Absorption versus Wavelength with f as a Parameter. Plot Symbols Represent CO_2 Concentration f from .030% to .121% in Alphabetical Order.

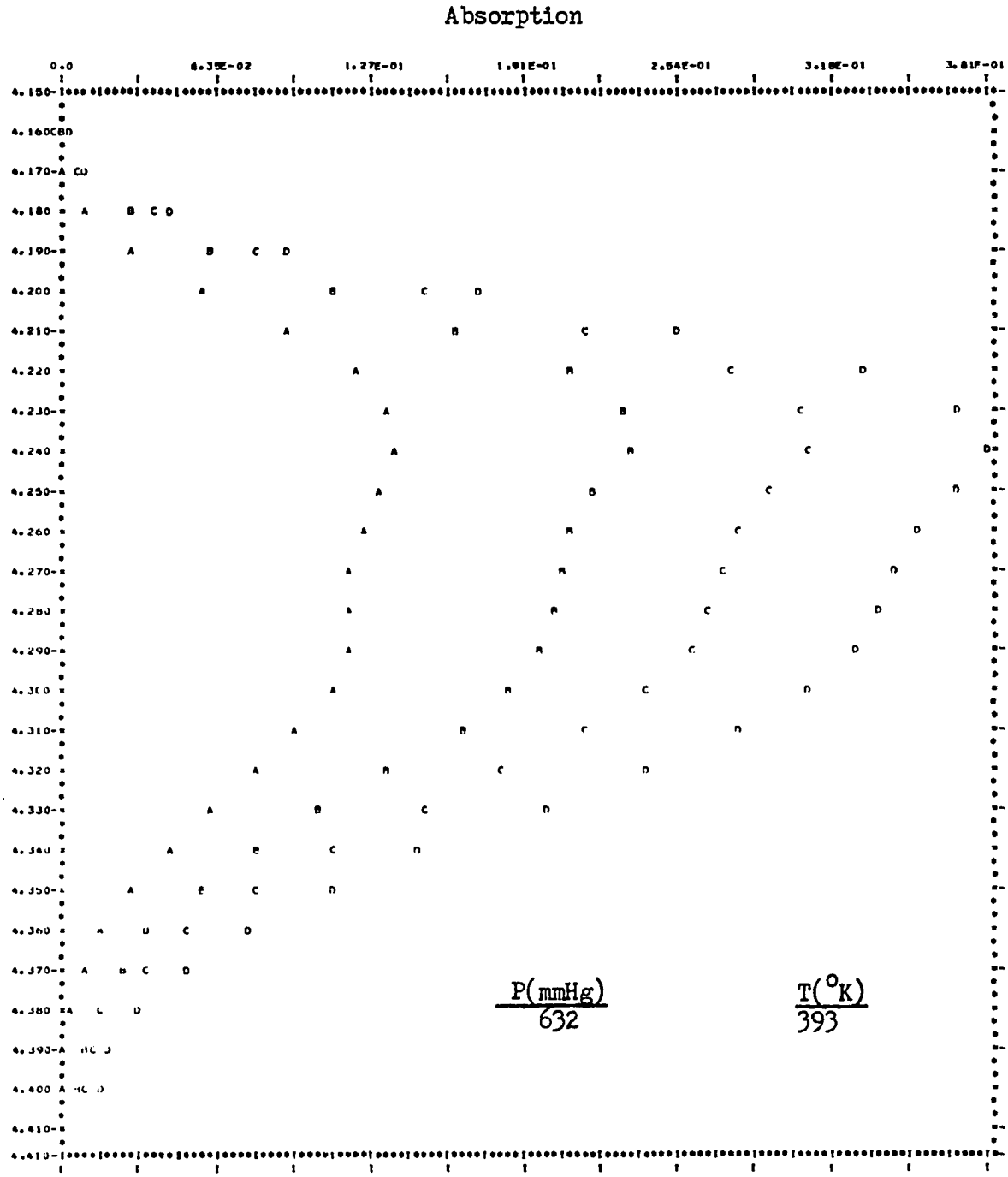

Figure 22. Computer Printed Plot of Absorption versus Wavelength with f as a Parameter. Plot Symbols Represent CO_2 Concentration f from .030% to .121% in Alphabetical Order.

P as a parameter, three with T as a parameter and three with f as a parameter. Note the change in the size of the band for changes in P,T and f. These graphs establish the general trends and are representative of the quality of the data.

Figure 23. is an example of the spectral absorption plotted in the strong line approximation format as A versus pP ($=P^2f$). The condition of frozen composition is valid. Three separate wavelengths were chosen; $\lambda = 4.20$ is in the intermediate region on the low wavelength side, $\lambda = 4.24$ microns is in the core of the band, and $\lambda = 4.35$ is in the intermediate-wing on the high wavelength side of the band. The zero gap remember, is at about 4.26 microns. The pressure and concentration values for this figure (as well as Figure 24) include all the values used in the basic data set. As indicated in the figure, the curves in each of the three sets closer together as the spectral lines go toward blacker line centers from 4.35 to 4.24 microns. However the lines are obviously not coincident even in the 4.24 micron set and therefore none of the sets are valid strong line approximations. This is as expected due to the presence of the weaker lines in the region. The $\lambda = 4.35$ micron set is expected to be furthest away from the strong line approximation.

It is possible to get a rough measurement of the exponents in the power law of A versus pP from these graphs. Noting equation (101), the exponents for $\lambda = 4.24$ are given by $m' + 1' \approx .97$, $1' \approx .68$; for $\lambda = 4.20$, $m' + 1' \approx .95$, $1' \approx .67$; and for $\lambda = 4.35$, $m' + 1' \approx .91$, $1' \approx .91$. The P dependence for constant f remains about constant and the f dependence increases when going from the strong line approximation.

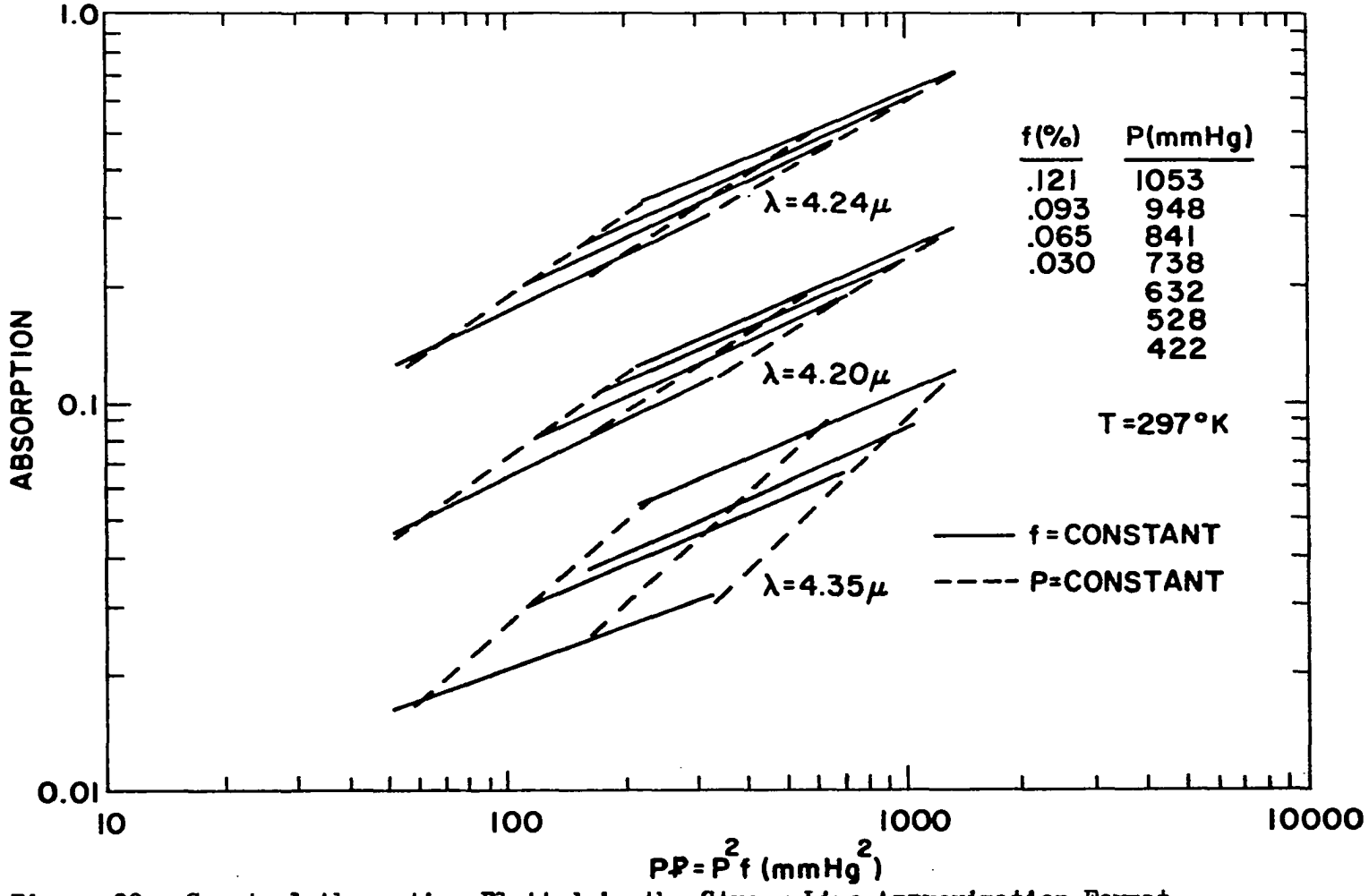

Figure 23 . Spectral Absorption Plotted in the Strong Line Approximation Format.

The P dependence for constant p is small ($m' < .5$) and becomes extremely small in the 4.35 micron case. This suggests a weak line approximation for this set.

Figure 24 is an example of the spectral absorption plotted in the weak line approximation format as A versus p(= Pf). Frozen composition remains as a valid condition. This is the same absorption data that was plotted in Figure 23, only now we are testing for the weak line approximation. The curves in the λ = 4.24 micron set are widely separate now compared to the λ = 4.35 micron set; the curves in this set (4.35) are now approximately coincident. In fact it was not possible to accurately draw more than one P = constant curve for this set. The conclusion is that the λ = 4.35 micron data can be described by the weak line approximation for that set of parameters, mainly for that temperature. This is an indication that the line centers are non-black for this case (see Figure 13). Note the wide divergence of the same curves when plotted in the strong line format. The exponents obtained from the plot should be approximately those obtained in the strong line plot. They are given here as: $m' + 1' \approx .98$, $1' \approx .65$ for λ = 4/24 microns; $m' + 1' \approx .93$ $1' \approx .64$ for $\lambda = 4.20$; $m' + 1' \approx .91$, $1' \approx .91$ for λ = 4.35 microns. Note that in both figures, $m' + 1'$ remains in the range $.5 \lesssim m' + 1' \lesssim 1$; $1'$ remains in the range $.5 \lesssim 1' \lesssim 1$; and m' remains in the range $0 < m' \leq .5$. This is to be expected for all the Absorption data.

As a result of this sample analysis, we must conclude that most of the data is in the ill defined region, except for the wing regions which can probably be described by the weak line approximation. Also

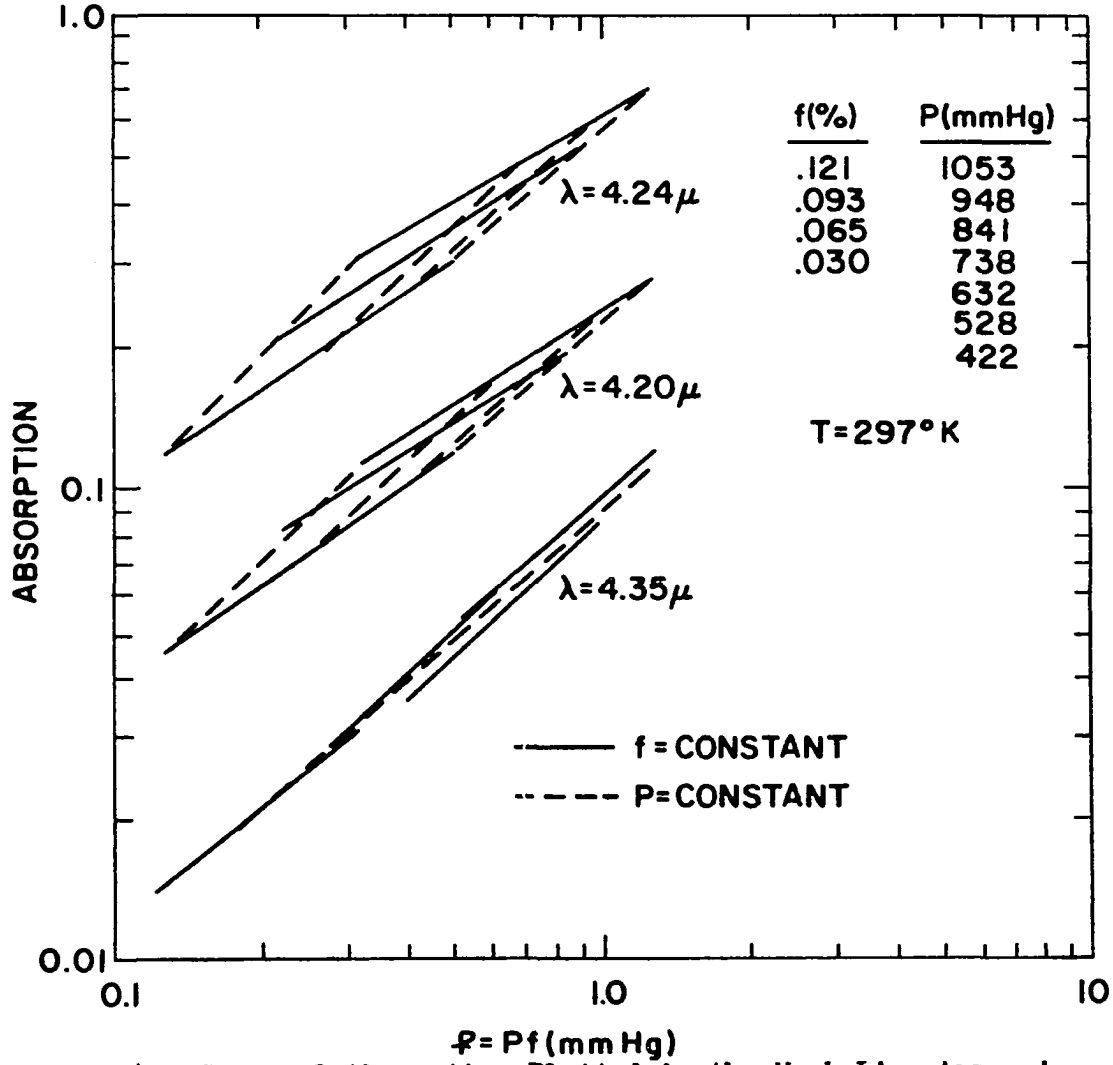

Figure 24 . Spectral Absorption Plotted in the Weak Line Approximation Format.

the dependence o f at constant P is less than the dependence on P at constant f, although the dependence on p at constant P is greater than that on P at constant p.

The range of pressures and concentrations used for Figures 23 and 24 covered the entire range used in this experiment; however only the room temperature data was used.

We shall not analyze the data as to its temperature dependence by using this method; rather we shall wait and use the absorption coefficient method instead. However it is of interest to display the temperature dependence of the Absorption graphically. These linear graphs will give an indication of the quality of the temperature dependence data and will establish the general trends to be expected. Figures 25, 26, and 27 show the Absorption versus temperature with P and f as parameters. The highest, the lowest and an intermediate P, and the four concentrations are used. The same three wavelength values are used here as were used in Figures 23 and 24, Figure 25 at $\lambda = 4.24$ microns shows a general decrease in the absorption with increasing temperature. Figure 26 at $\lambda = 4.20$ microns shows that the Absorption is to a very good approximation, independent of the temperature. Figure 27 at $\lambda = 4.35$ shows a reversal of the trend in Figure 25; the absorption at 4.35 increases with increasing temperature. In fact, although the mean absorption level is less at $\lambda = 4.35$ than at $\lambda = 4.24$, the temperature dependence is stronger at 4.35 than at 4.24. That is, the temperature dependence is stronger in the intermediate wing regions than it is in the core, and it is in the opposite direction. There is a point between these two regions at which the temperature dependence should be negli-

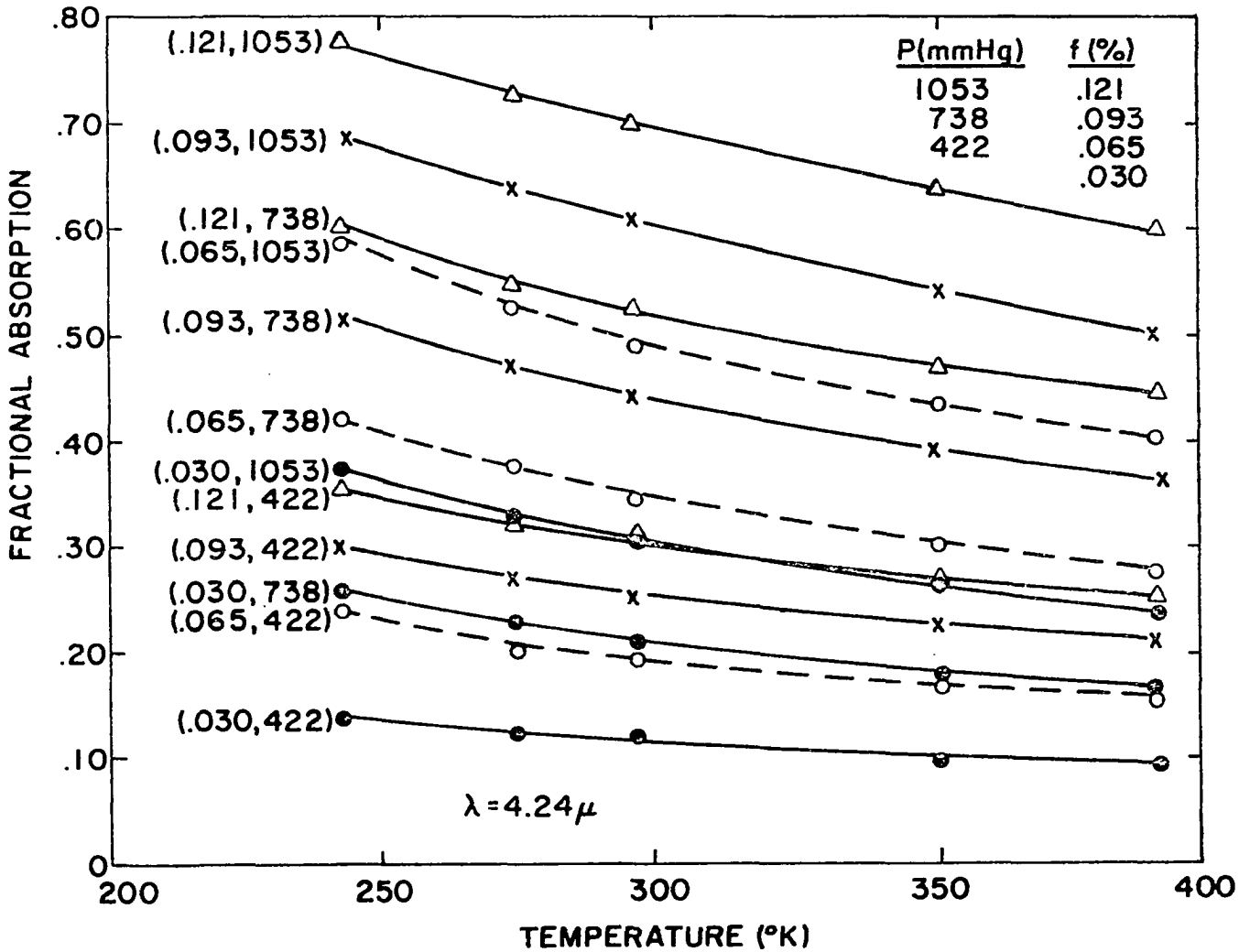

Figure 25 . Absorption versus Temperature at 4.24 microns.

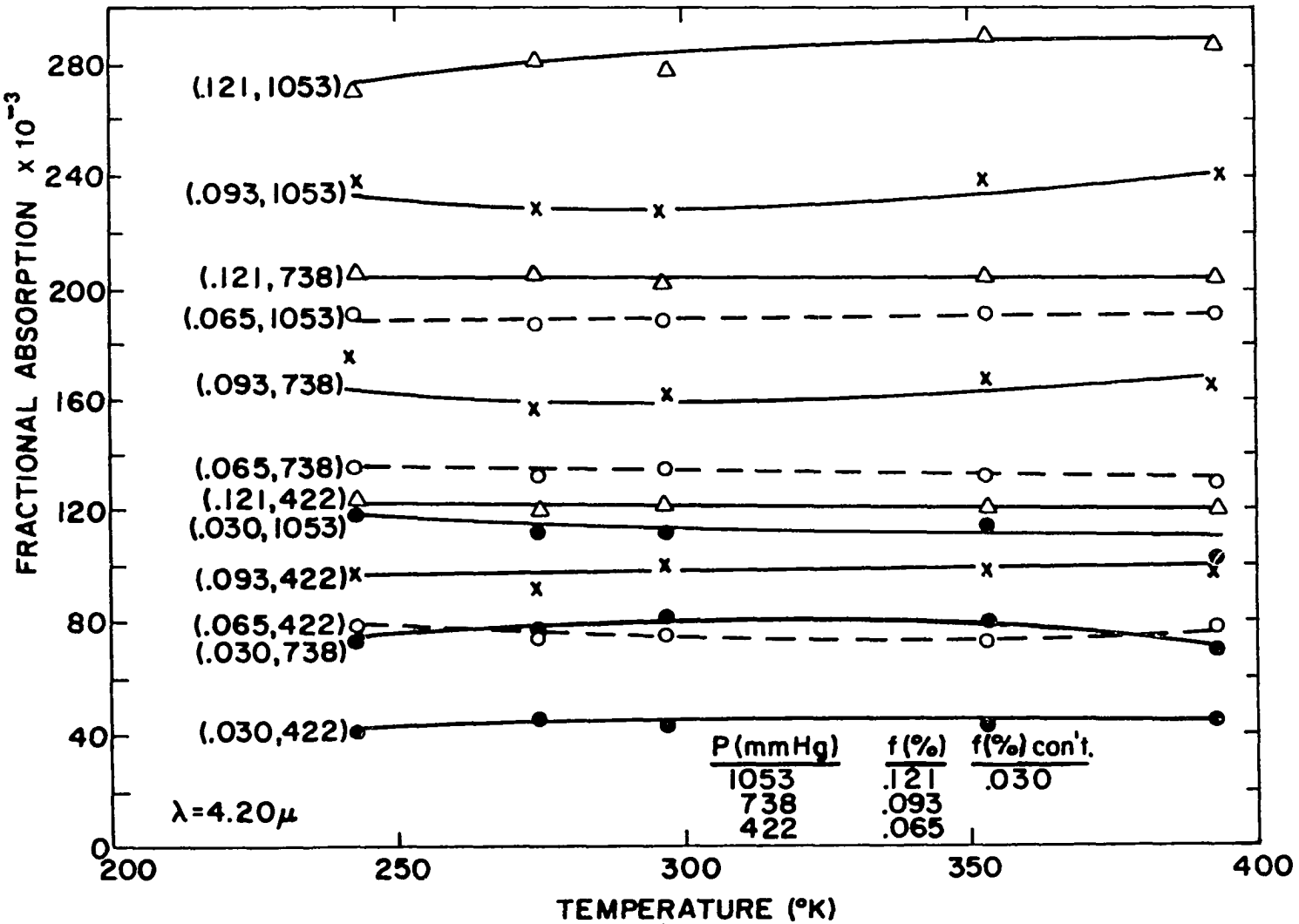

Figure 26 . Absorption versus Temperature at 4.20 microns.

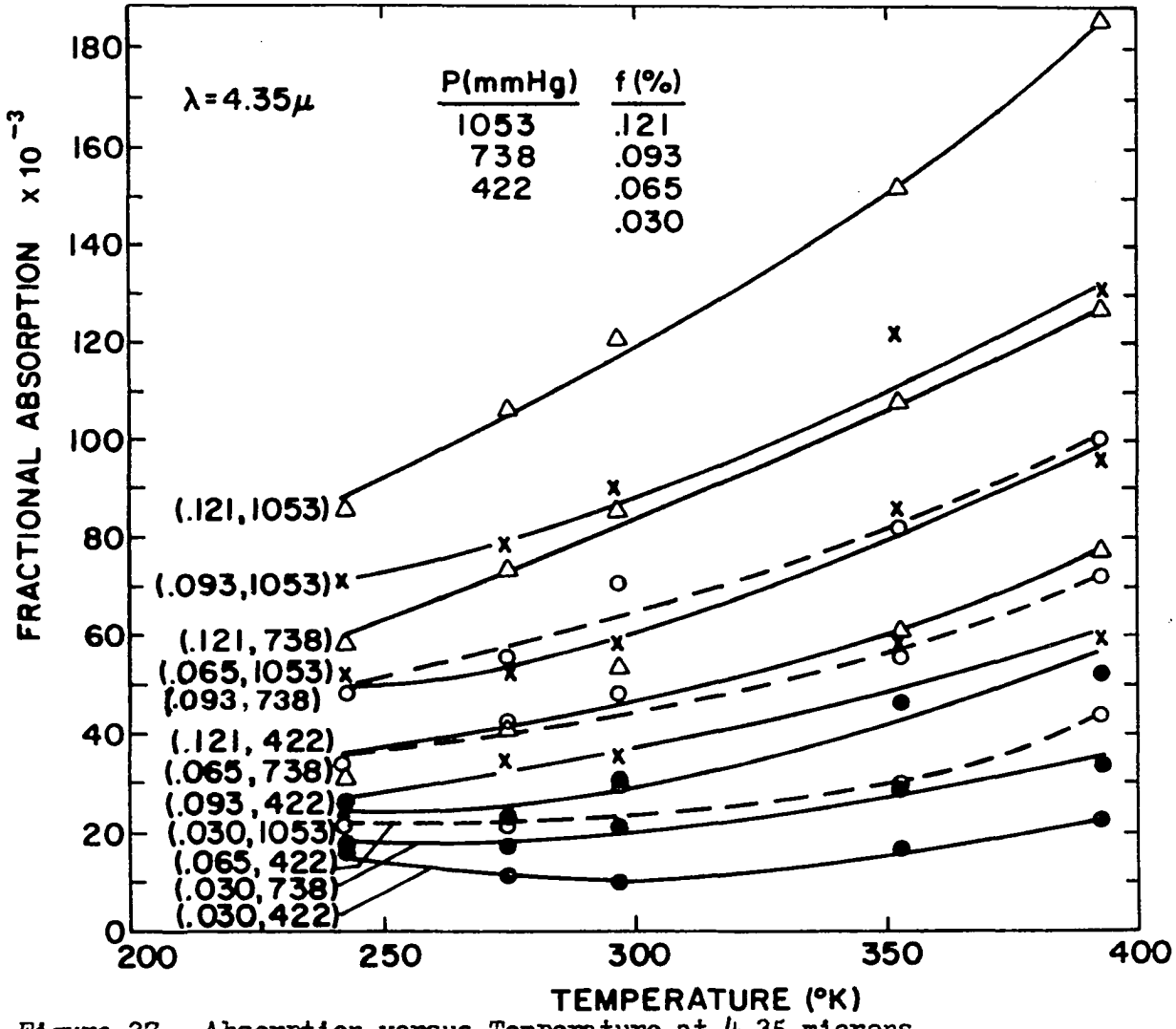

Figure 27 . Absorption versus Temperature at 4.35 microns.

gible over a small range of T as predicted. No such cross overs exist in this format for the pressure.

It is also possible to plot this data in the strong line format of Howard, Burch and Williams[15] (see equation 38). However such an approach basically assumes a total absorption (see Modulated Band Model) and is not particularly pertinent to our analysis. Therefore this semi-log type of analysis is not done here although such an approach could easily be made.

D. Intensity Spectra.

This section should give the reader an indication of the form of the data as it exists for our conditions, at the output of the LIA. It can also be used to show the extent of the smoothing performed by the .08 micron bandpass (compare with Figure 13). By plotting the data as a family of curves one can also get an idea of the amount of change in the intensities I and δI for a given change in a particular thermodynamic variable. This will serve as an indication of the accuracy necessary to properly record the signals as well as a means of establishing the correct trends in the fluctuating absorption coefficient, since $\delta K = -\delta I/II$. Each curve in the families of curves represents one particular scan through the 4.3 micron region for a particular P,T.f for one value of $\Delta\lambda$ and one value of δP (where applicable).

Figures 28, 29, and 30 are a sample of the intensity, I, plotted against the wavelength, λ, with P,T, and then f as parameters. These results are straight forward. The P - I dependence (for constant f) is negative over the entire band; that is, an increase in P (for constant f)

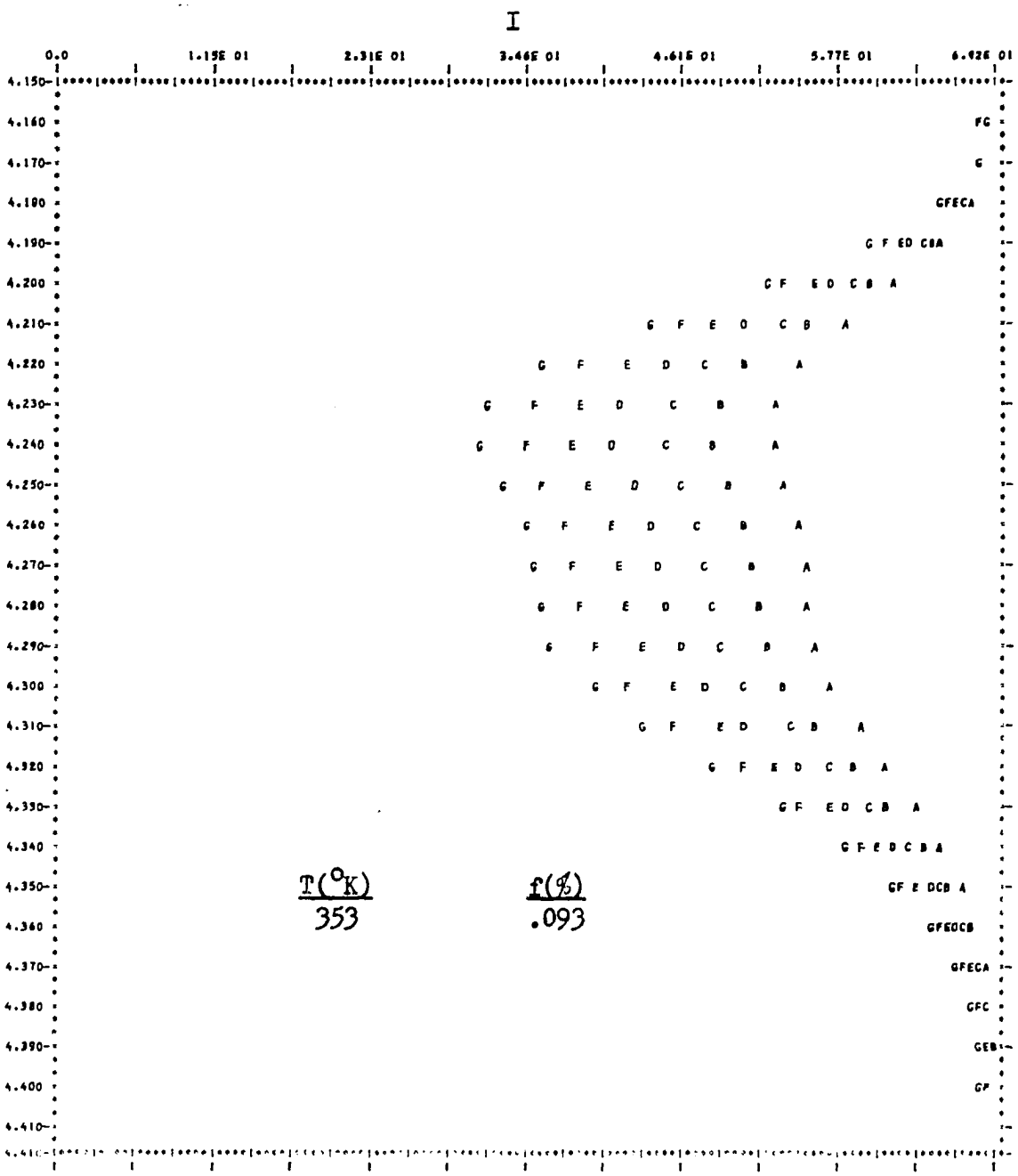

Figure 28 . Computer Printed Plot of the Intensity I versus Wavelength with P as a Parameter. Plot Symbols Represent Pressure P from 422 mmHg to 1053 mmHg in Alphabetical Order.

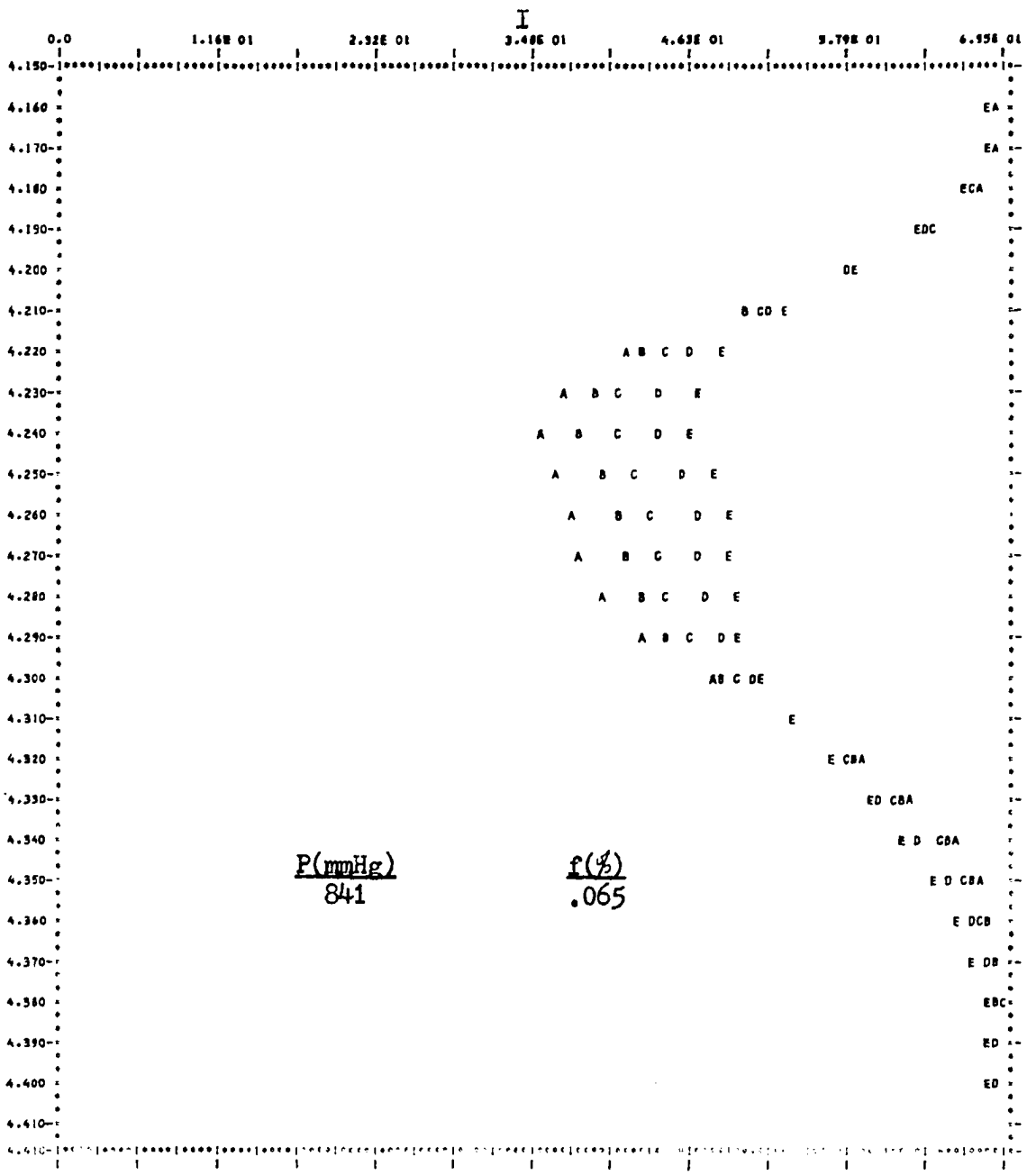

Figure 29 . Computer Printed Plot of the Intensity I versus Wavelength with T as a Parameter. Plot Symbols Represent Temperature T from 243°K to 393°K in Alphabetical Order..

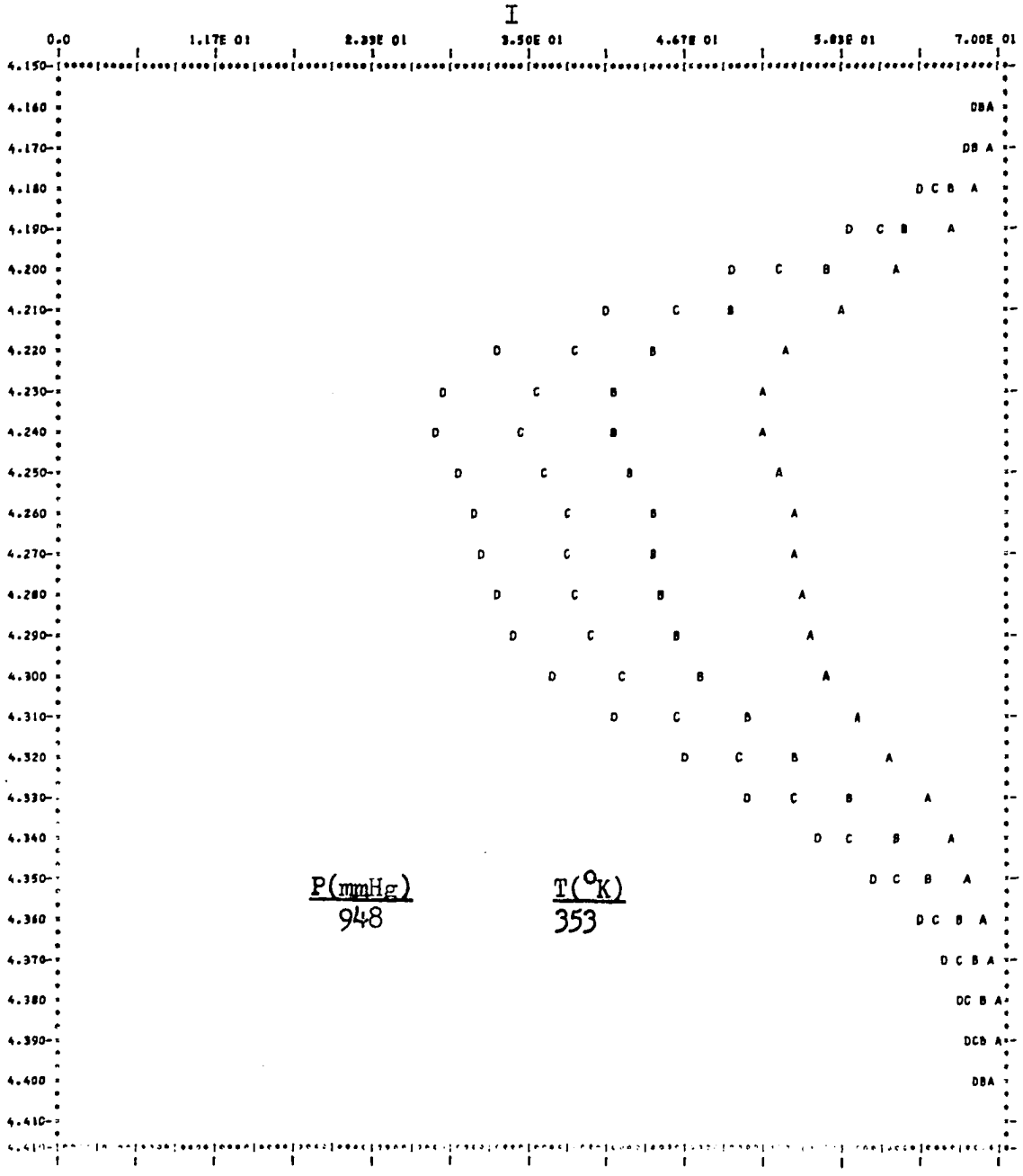

Figure 30 . Computer Printed Plot of the Intensity I versus Wavelength with f as a Parameter. Plot Symbols Represent CO_2 Concentration f from .030% to .121% in Alphabetical Order.

produces a decrease in I (or an increase in absorption). The P dependence is stronger in the core regions of the band and weaker in the wings. This P (constant f) dependence is reasonably independent of whether the absorption is in the weak or strong line condition. The T dependence of I is positive in the core regions and negative in the intermediate and wing regions of the band. The crossover points are at about $\lambda = 4.20$ and $\lambda = 4.31$ microns. The T - I dependence is stronger on the high wavelength side of the band compared to that on the low wavelength side. The f-I dependence (for constant P) is negative and strong over the entire band; the dependence is strongest in the core regions. These thermodynamic variable dependencies of I are as predicted. Due to the fact that the temperature dependence goes from positive to negative, one expects that a narrow slit will record a stronger temperature dependence than a wide slit.

The dependence of δI on P,T, and f is given in Figures 31 thru 36. There is a good deal of information contained in these δI spectra that is easier to get at here than in any other data form.

Figures 31 and 32 show δI versus λ with P as a parameter for constant f. Figure 31 represents an expected near strong line case (low T, high f) and Figure 32 represents an expected weak line case (high T, low f). The dependence on P (with constant f) is minimal in the weak line region over the entire band; no definite trend is discernible in Figure 32, possibly due to the lack of accuracy of the recording. The corresponding P dependence in the near strong line case is considerable especially in the core regions of the band. These two cases represent opposite extremes for the δI - P dependence.

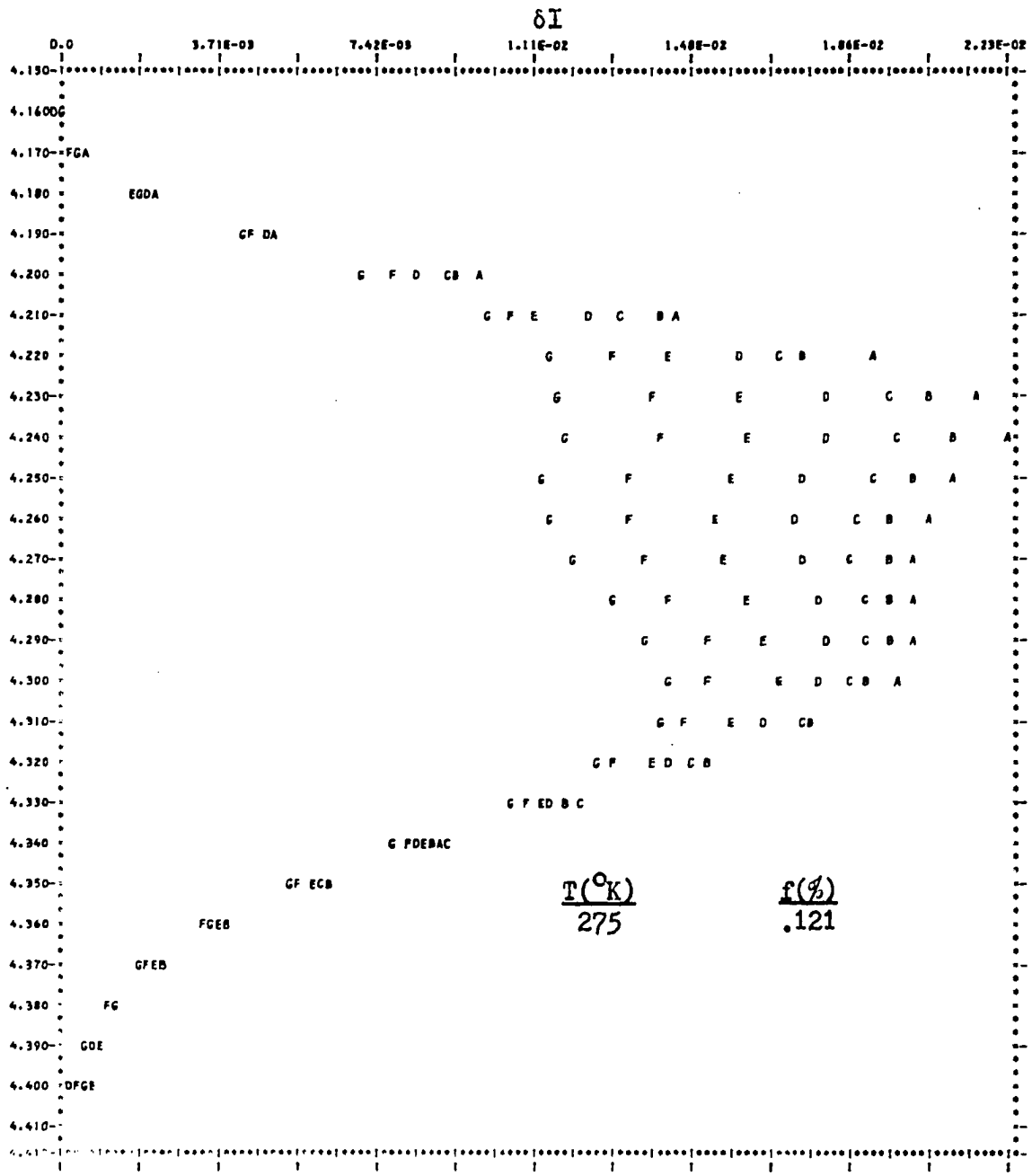

Figure 31 . Computer Printed Plot of the Fluctuating Intensity δI versus Wavelength with P as a Parameter. Plot Symbols Represent Pressure P from 422 mmHg to 1053 mmHg in Alphabetical Order.

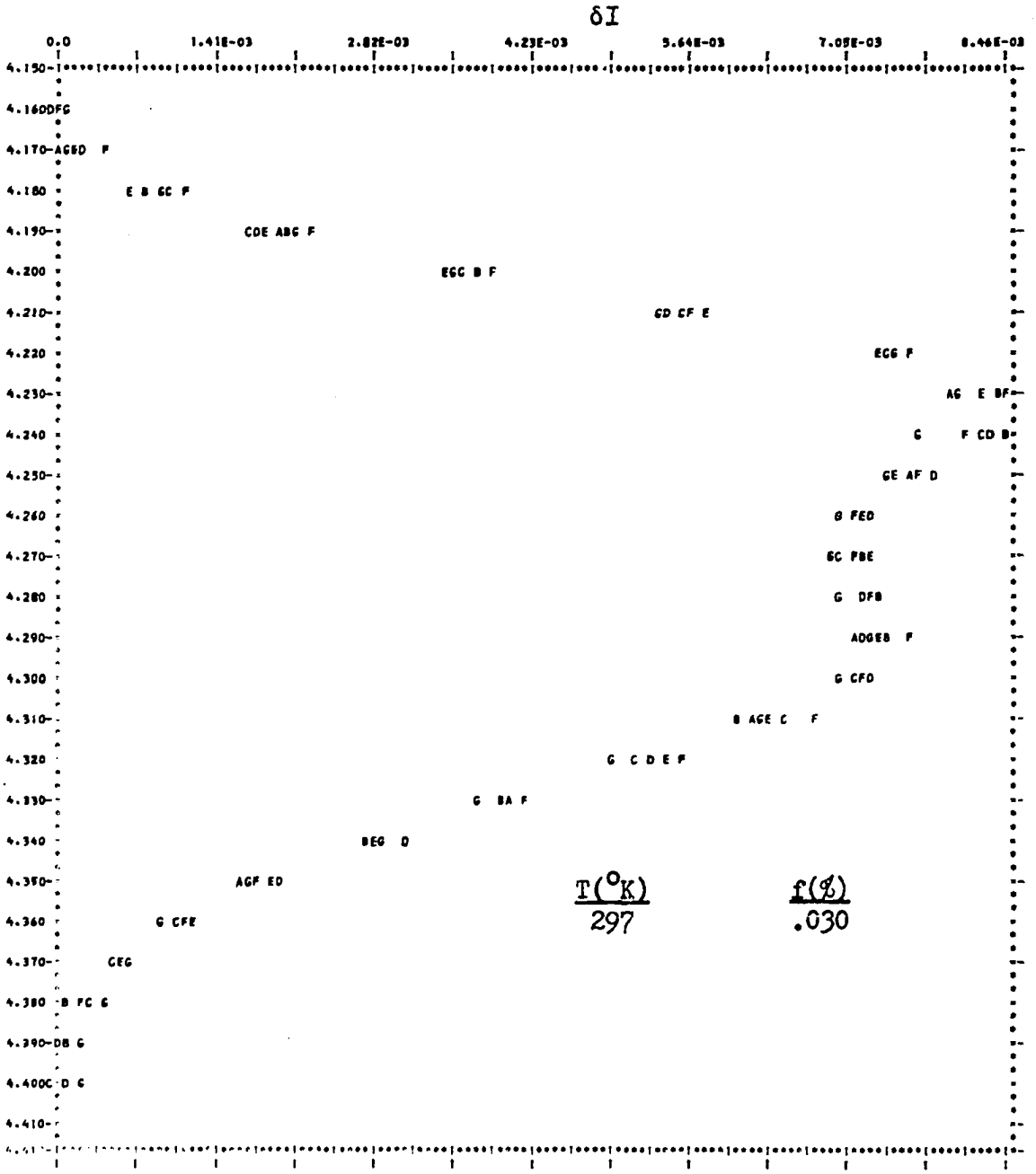

Figure 32 . Computer Printed Plot of the Fluctuating Intensity δI versus Wavelength with P as a Parameter. Plot Symbols Represent Pressure P from 422 mmHg to 1053 mmHg in Alphabetical Order.

As one moves away from the weak line case a stronger P-δI dependence starts to occur over the entire band. A reasonably strong negative P dependence occurs at λ = 4.31, 4.32, and 4.20 as well as over the core regions. A slight negative P dependence occurs at λ = 4.35 microns. These wavelength points have been noted because they are of particular importance in an analysis which will be considered in section G.

Thus in general the δI-P dependence (constant f) is strongest in the core of the band and is negative over the entire band. When this is compared with the I-P dependence (constant f), one finds that the ratio of δI and I produces a smaller resultant P dependence than either the δI or the I-P dependence alone. This is because the P dependence is in the same direction for the δI and I spectra; namely negative. For a strong P dependence one should therefore go to the I spectra and use a narrow bandpass positioned near the core. The resultant (δI/I)-P dependence is positive, but not very strong.

Figure 33 is an example of the usual T-δI dependence. The T-δI dependence is negative in the core and positive in the intermediate to the wing regions. The T dependence crosses over at approximately λ = 4.20 and 4.32 microns. The positive T dependence which occurs on the low wavelength side of the band is not as strong as that on the high wavelength side. The strongest T dependence does occur in the wing regions of the band, although the dependence is not always measureable due to the small signals in these regions. Note the T dependence in the wing regions of Figure 33. The strongest measureable T dependence for our experimental conditions occurs in the region from λ = 4.35 microns. One is

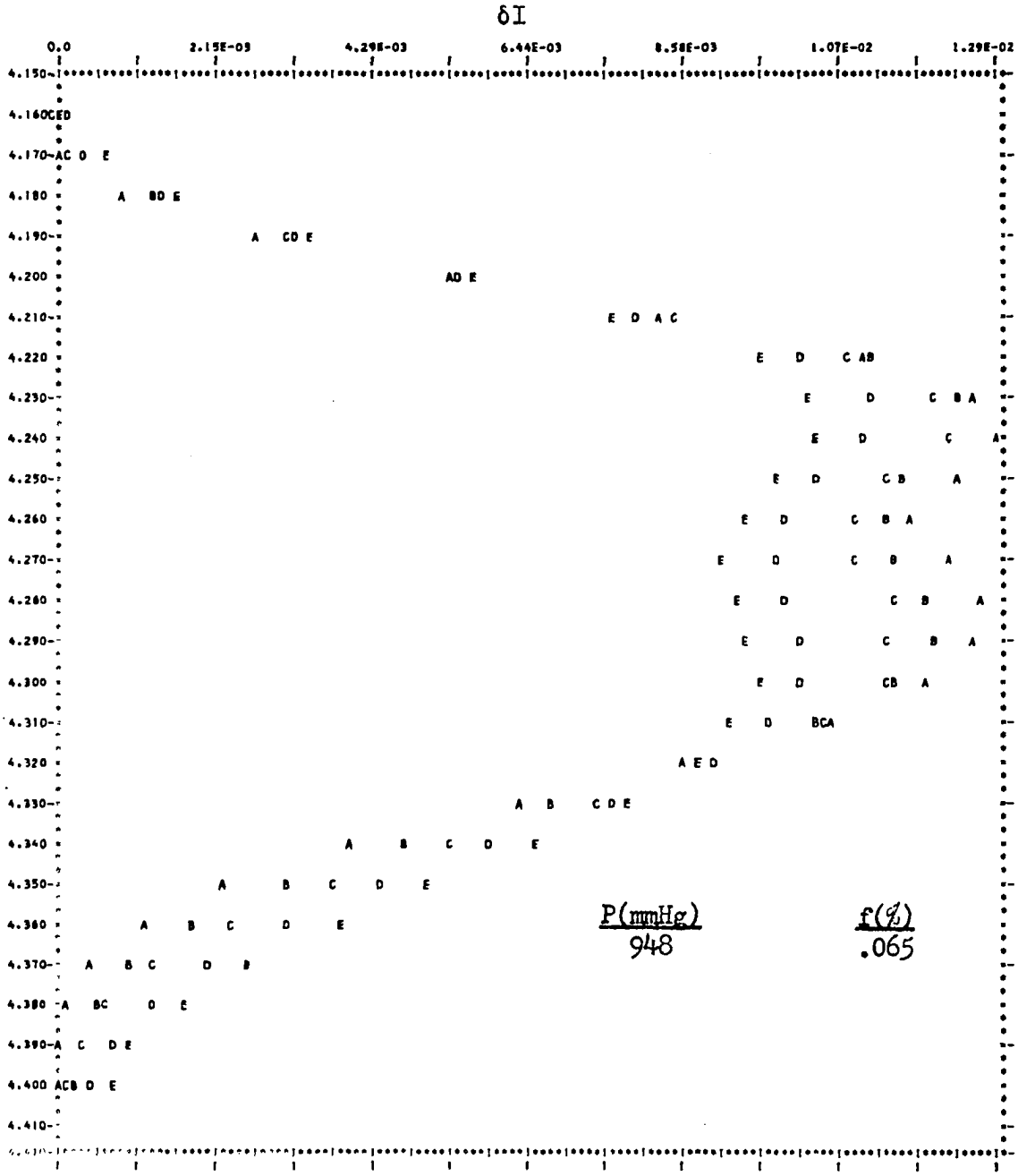

Figure 33 . Computer Printed Plot of the Fluctuating Intensity δI versus Wavelength with T as a Parameter. Plot Symbols Represent Temperature T from 243°K to 393°K in Alphabetical Order.

again led to a narrow slit width for the strongest temperature dependence. The temperature dependence of δI in the core is strongest for near weak line conditions and is therefore dependent on pressure and concentration.

When these experimental results are compared to the I - T dependence, one finds that the δI - T dependence is generally in the opposite direction (relative to I - T) over the entire band, although the 4.20 micron crossover is the same and the high wavelength crossover is nearly the same. When the ratio of δI and I is taken, the resultant $(\delta I/I)$ - T dependence should be stronger than that of the δI and I spectra alone and the T crossovers should remain about the same. The direction of the $(\delta I/I)$ - T dependence is that of δI - T.

Figure 34 is a sample of the usual δI - f dependence. This dependence is positive over the entire band and represents the overall strongest of the three thermodynamic variable dependencies for δI, especially in the core, The δI - f and I - f dependencies are in the opposite directions; the ratio of the two spectra should therefore produce an even stronger dependence on f which is in the direction of the δI - f dependence.

Thus we must consider the possibility of defining new spectra which are composed of say the product or the ratio of the basic δI and I spectra. The purpose in forming the new spectra would be to enhance or suppress certain effects, or the thermodynamic variable dependencies, which exist in the δI and/or I spectra. Before considering this point further let us first discuss an effect we refer to as the Reversal Effect.

A very interesting and rather dramatic effect occurs in the

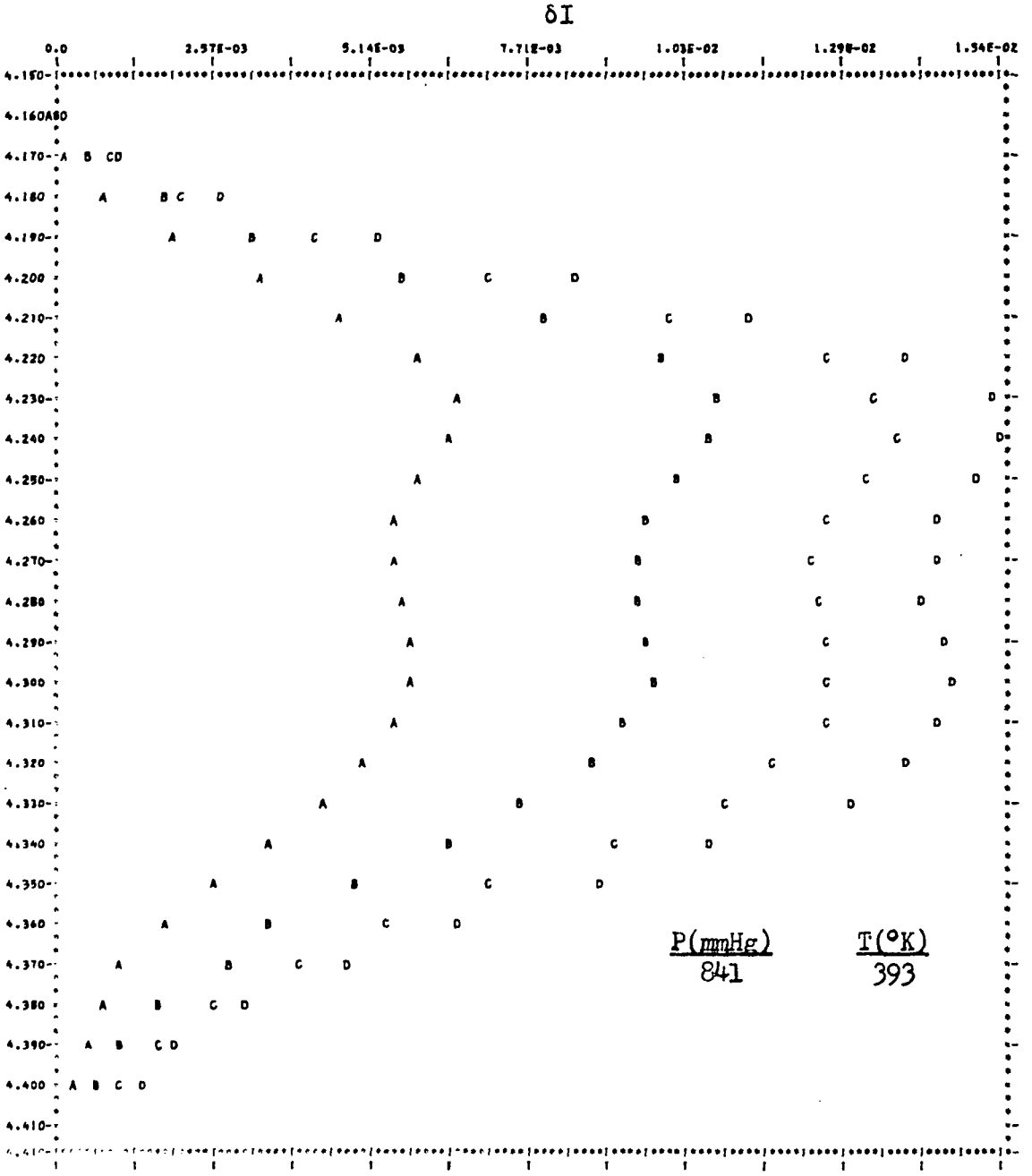

Figure 34 . Computer Printed Plot of the Fluctuating Intensity δI versus Wavelength with f as a Parameter. Plot Symbols Represent CO_2 Concentration f from .030% to .121% in Alphabetical Order.

δI data which can readily be seen in plots of δI vs. λ with T or with f as a parameter, and can be seen slightly when P (constant f) is a parameter. This effect is manifest as a "reversal" in the deeper core regions of the usual δI dependence. If the parameters are such that a substantial near strong line limit is produced, then the regions that have the black line centers will reverse their dependence on the thermodynamic variables T and f. For the 4.3 micron CO_2 region, the R branch is normally stronger than the P branch and should therefore reverse sooner. Figure 35 is an example of this phenomenon given in terms of the T dependence.

Upon comparing this figure with Figure 33, one notices that here, the R branch maximum is lower than the P branch maximum and that the T dependence has started to reverse in the R branch core regions. The lowest temperature curve, which is expected to have the blackest line centers, has reversed the most. An increase in T now leads to an increase in δI in this region. The higher temperature curves do not have as strong a black line center region and have not therefore reversed yet. This is a very substantial effect when the data is in this spectral format; it could be used as a test for the blackness of the rotational line centers (strong line limit).

The black line centers naturally also have an effect on the I spectrum. As predicted with the band model approach, the dependence of A and therefore I on the thermodynamic variables does change (independent of δI) when going from the weak line to the strong line case. The interesting thing is that the dependence of I on the thermodynamic variables is sufficient to keep the reversal effects from appearing in the

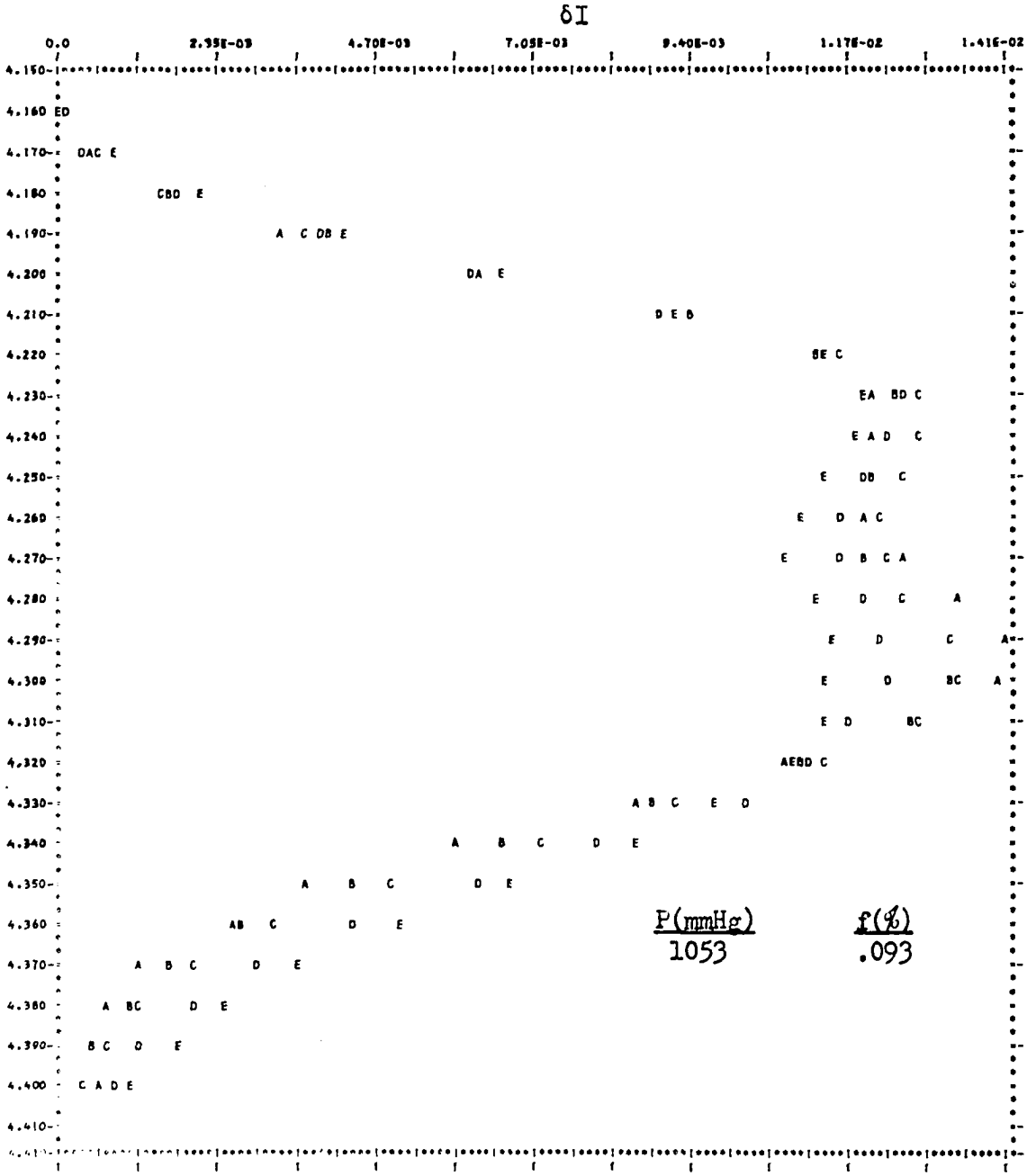

Figure 35 . Computer Printed Plot of the Fluctuating Intensity δI versus Wavelength with T as a Parameter. Plot Symbols Represent Temperature T from 243°K to393°K in Alphabetical Order.

fluctuating absorption coefficient spectrum (see Figure 47). In other words, when the ratio $\delta I/I$ is formed the reversal resulting from the δI data is removed by the large changes in I. This is an important result; the shifts in the P and R branch maxima no longer occur and the R branch maximum is always larger than the P branch maximum. The reversal of the thermodynamic variable dependence is no longer evident.

The same type of analysis applies to the δI - f and I - f data. Figure 36 is an example of the reversal effect in terms of the δI - f dependence (compare this figure with Figure 34). All but the low concentration data exhibits this reversal. It has the effect of changing from a positive δI - f dependence to a negative one when going into the black line center case. The reversal is again absent in the corresponding δk spectrum (see Figure 49) due to the negative dependence of I on f.

Figure 31 exhibits this effect for a δI - P dependence; it is displayed only as a shift in the relative heights of the R and P branch maxima. The lower P (constant f) curves show a larger P branch maxima than an R branch maxima. One suspects that the increased pressure broadening is enough to smooth the lines and keep then from having dominant black line center regions, even though the number of absorbers also increases.

The basis for such a reversal can be seen most easily by resorting to the electronics analogy of a carrier wave which is modulated by some signal. If the amplitude of the carrier wave (in our case I) becomes less than the possible maximum modulation amplitude (in our case δI) then the carrier amplitude limits the modulation amplitude.

The instantaneous optical signal at some particular wavelength

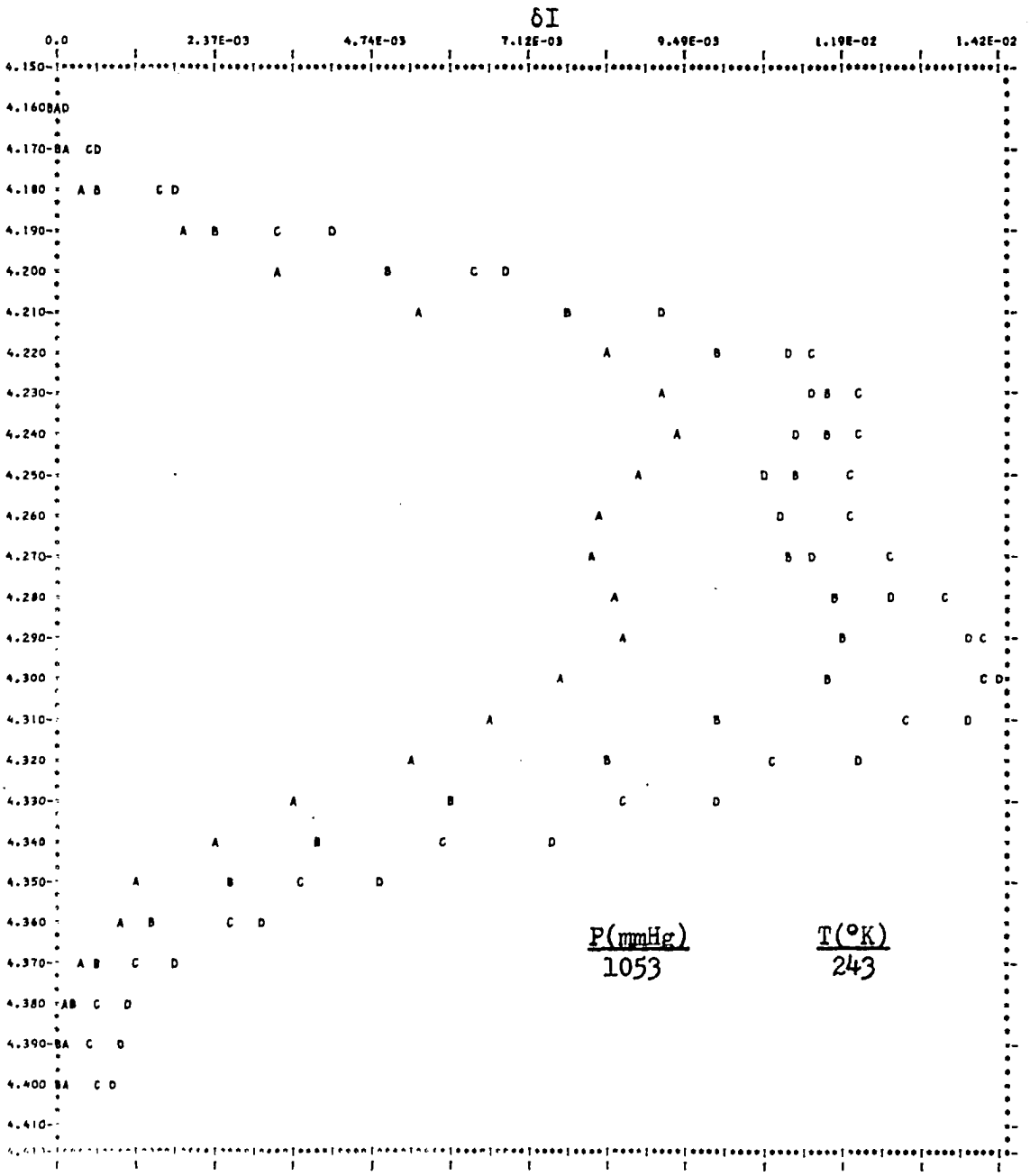

Figure 36 . Computer Printed Plot of the Fluctuating Intensity δI versus Wavelength with f as a Parameter. Plot Symbols Represent CO_2 Concentration f from .030% to .121% in Alphabetical Order.

can be described as $|A + B\cos 2\pi ft|$ since the pressure fluctuation in this experiment is harmonic. The modulus is necessary since on can't have a negative light intensity or a negative pressure for that matter. When $B > A$, where B represents the fluctuation intensity of an individual line and A is the individual line mean value intensity, the harmonic optical waveform will start to "flip over" at the minimum amplitude points as if a π phase shift had been introduced over that region. The minimum will start to move toward a maximum as B increases; frequency doubling is possible.

This reversal can be used as an indicator for the absorption level of the data. For example, when the δI spectrum starts to show a reversal, the data set can be limited to that which exists below or above the reversal point.

For the range of parameters chosen in this experiment the reversal effect was not yet well established. Even so, this effect, which we see can greatly effect the δI spectrum, is not apparent in the δK spectrum anyway. Also, as I gets very samll, so does δI; this leads to the possibility of a greater range of measureability for the δK spectrum as compared to δI spectrum. Furthermore, if the thermodynamic variable dependence of I and δI on P for example, is identical in particular region(s) of the band, than the δK spectrum will be independent of that particular variable in that given region even though δI and I may not be. We have already seen that the P(constant f) dependence is positive over the band for both δI and I. Thus one should possibly achieve a pressure independent region in the δK spectrum without needing pressure crossover points in either I or δI or both.

The usual T and f dependence is in the opposite direction for

I-T and δI-T, and I-f and δI-f. This leads to an expected enhancement of these dependencies when the δK spectrum is formed in addition to the expected suppression of the P(constant f) dependence. This is a desireable state of affairs when attempting to invert a spectrum to obtain the thermodynamic vatiables.

In addition, it is more convenient and more accurate (for a wide range of data) to use the absorption coefficients (both mean and fluctuating) rather than the absorption or the intensities themselves, when attempting to determine the thermodynamic variable dependence. Also the turbulence or fluctuation structure can be obtained from the δK spectra as well as the δI spectra. Thus we conclude that it will be beneficial to form the δK spectrum. The characteristics and properties of this spectrum can best be seen by plotting it; this is considered in section G of this chapter.

E. Dependence on Spectral Bandpass

Now that we have determined the importance of the δK spectrum, we can go back and establish the dependence of this spectrum on the spectral bandpass, $\Delta\lambda$. It is also of interest to note the dependence of the intensity spectra on the spectral bandpass.

Figure 37 is a plot of the Intensity, I versus Wavelength, λ with bandpass, $\Delta\lambda$, as a parameter. Semilog paper was used for convenience. Note the fact that the intensity decreases quite rapidly with decreasing $\Delta\lambda$. Also, the zero gap and the P and R branch maxima become more pronounced as the resolution increases. The fine structure in the P branch is just visible at the lowest value of $\Delta\lambda$; this represents a

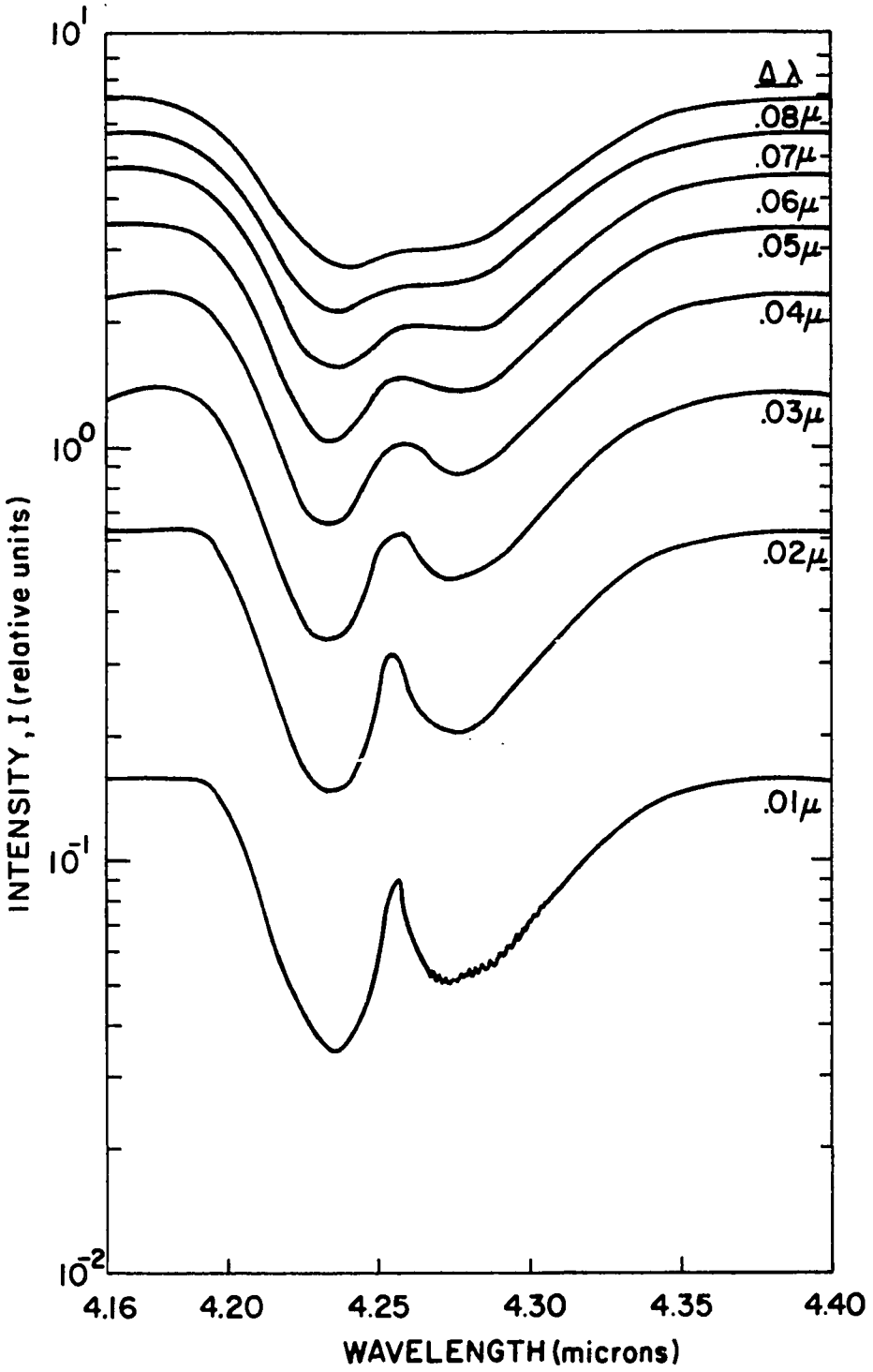

Figure 37 . Intensity,I, versus Wavelength with Bandpass as a Parameter.

lower limit for band model results. When the spectral resolution is near this limit, the corresponding CO_2 4.3 micron I spectrum requires a smaller sample interval than used in our experiments; this leads to a larger volume of data.

Figure 38 is a plot of the fluctuating intensity, δI, versus length with $\Delta\lambda$ as a parameter. A bandpass of less than .04 microns leads to a signal to noise level which is, on the average, too small to allow for accurate measurements with the LIA for these conditions. This does not represent a firm lower limit since increased integration times will allow for better measurements. Note the shift in the P and R branch peaks for changing $\Delta\lambda$ and the fact that the contribution in the wings gets smaller the better the resolution, as expected. The δP level is slightly larger here than that used in the δP = constant data. The intensity scales in Figure 37 and 38 are equal and therefore the intensity levels are comparable.

Figure 39 is a plot of the fluctuating absorption coefficient, δK versus wavelength with bandpass, $\Delta\lambda$ as a parameter. The dependence of δK on $\Delta\lambda$ is greatest in the area of the P and especially the R branch maxima. The dependence of δK on $\Delta\lambda$ is generally positive (an increase in $\Delta\lambda$ leads to an increase in δK) for this small wavelength interval range; however, there are two crossover regions for this bandpass variable, one at $\lambda = 4.20$ microns and another at $\lambda = 4.36$ microns. The δK- $\Delta\lambda$ dependence is slightly negative outside of these points. More important, δK is reasonably independent of $\Delta\lambda$ at these crossover points for the given small range of $\Delta\lambda$ and the given conditions. There is also a minimal, slightly negative dependence of δK on $\Delta\lambda$ @ the zero gap near 4.26 microns.

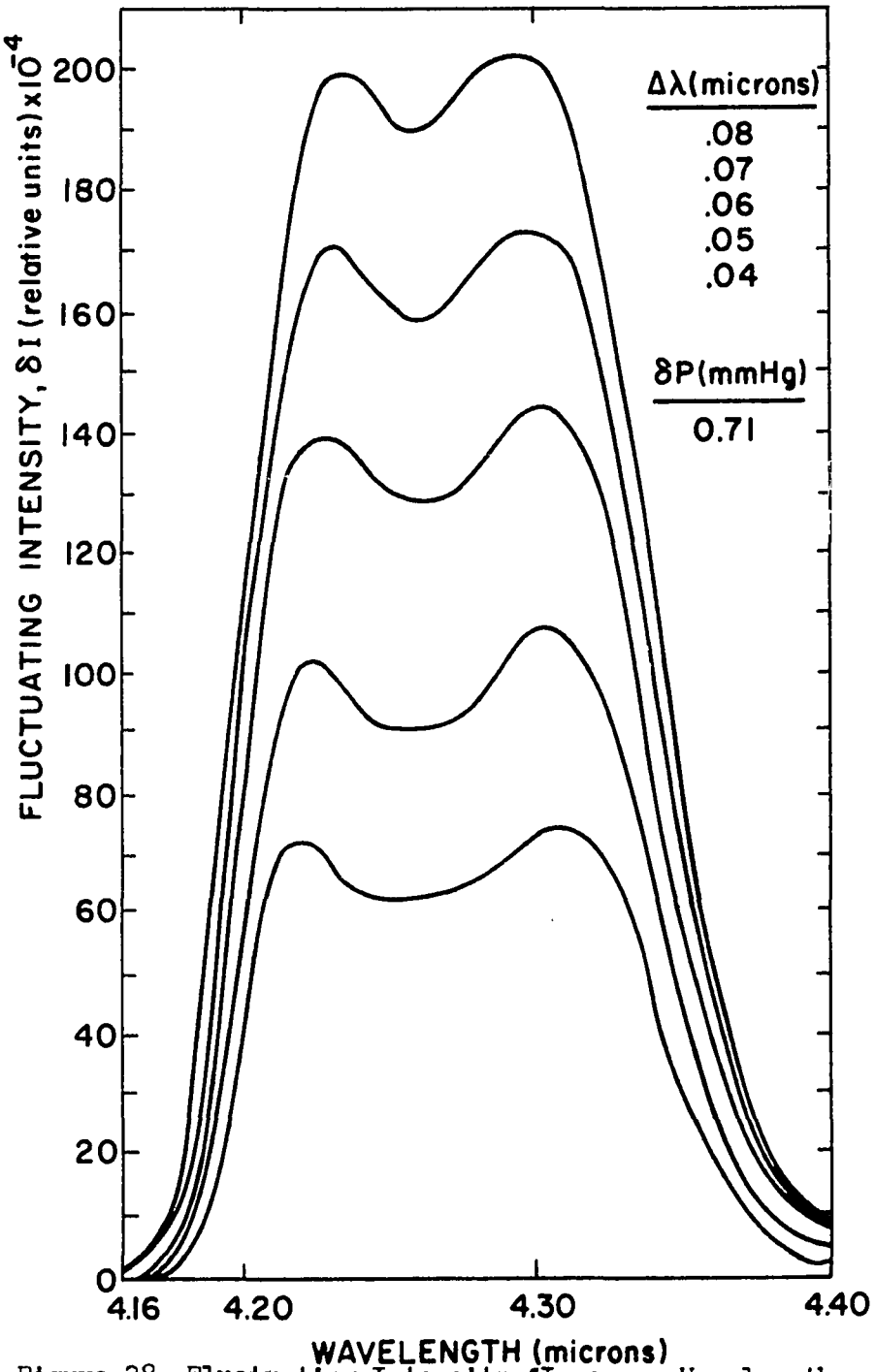

Figure 38 .Fluctuating Intensity, δI versus Wavelength with Bandpass as a Parameter.

Figure 39 . Fluctuating Absorption Coefficient, δK, versus Wavelength with Bandpass as a Parameter.

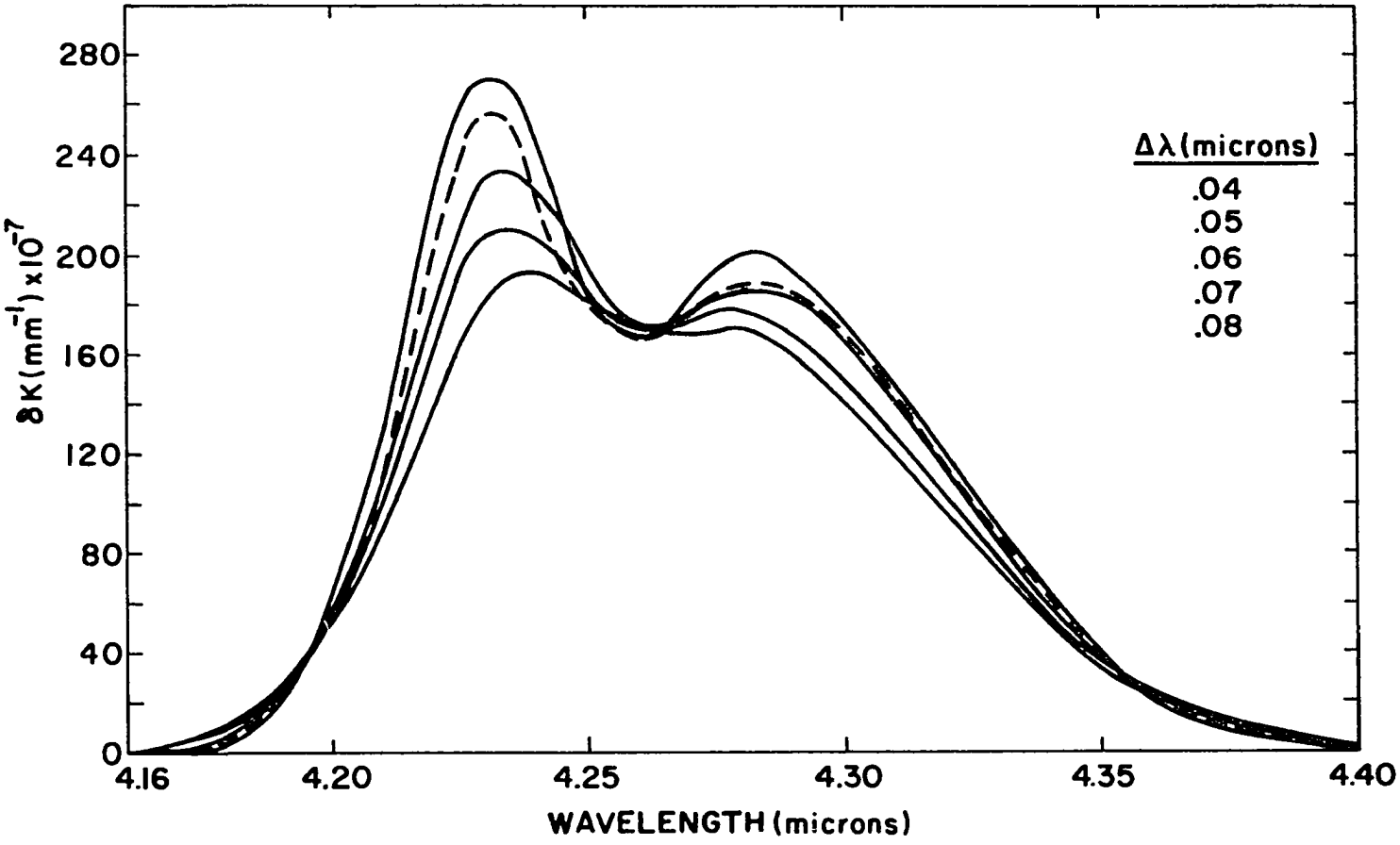

The thermodynamic conditions for figures 37, 38, and 39 are about one atmosphere total pressure, room temperature, and .121% CO_2.

F. Dependence on Amplitude of Fluctuation

According to equation (101), the fluctuating absorption coefficient should be a linear function of δP for frozen composition. If this is not true then one would be forced to include higher order terms in the Taylor series expansion. The validity of this assumption is best checked experimentally for typical conditions.

Figure 40 is a plot of the absorption coefficient fluctuation, δK versus λ with δP as a parameter. The range of δP includes the value used for the δP = constant data in this experiment. The conditions for this and the next figure are room temperature, one atmosphere, and .121% CO_2 with a .08 micron bandpass. Figure 40 shows a general positive δK-δP dependence over the entire band. To determine the actual δK-δP dependence we plotted δK versus δP for various wavelengths occurring throughout the band. This is shown in Figure 41. This figure shows a very good linear fit over the given range. Also an extrapolation of the curves beyond the low end of the range (dotted lines) shows that the δK intercept is at zero as expected. The results are a good indication that the linear approximation is valid.

G. Fluctuating Absorption Coefficient Spectrum

The results given in this section represent the most important results of the experiment; everything we have considered has led to the determination of these δK spectra. We shall now consider the general

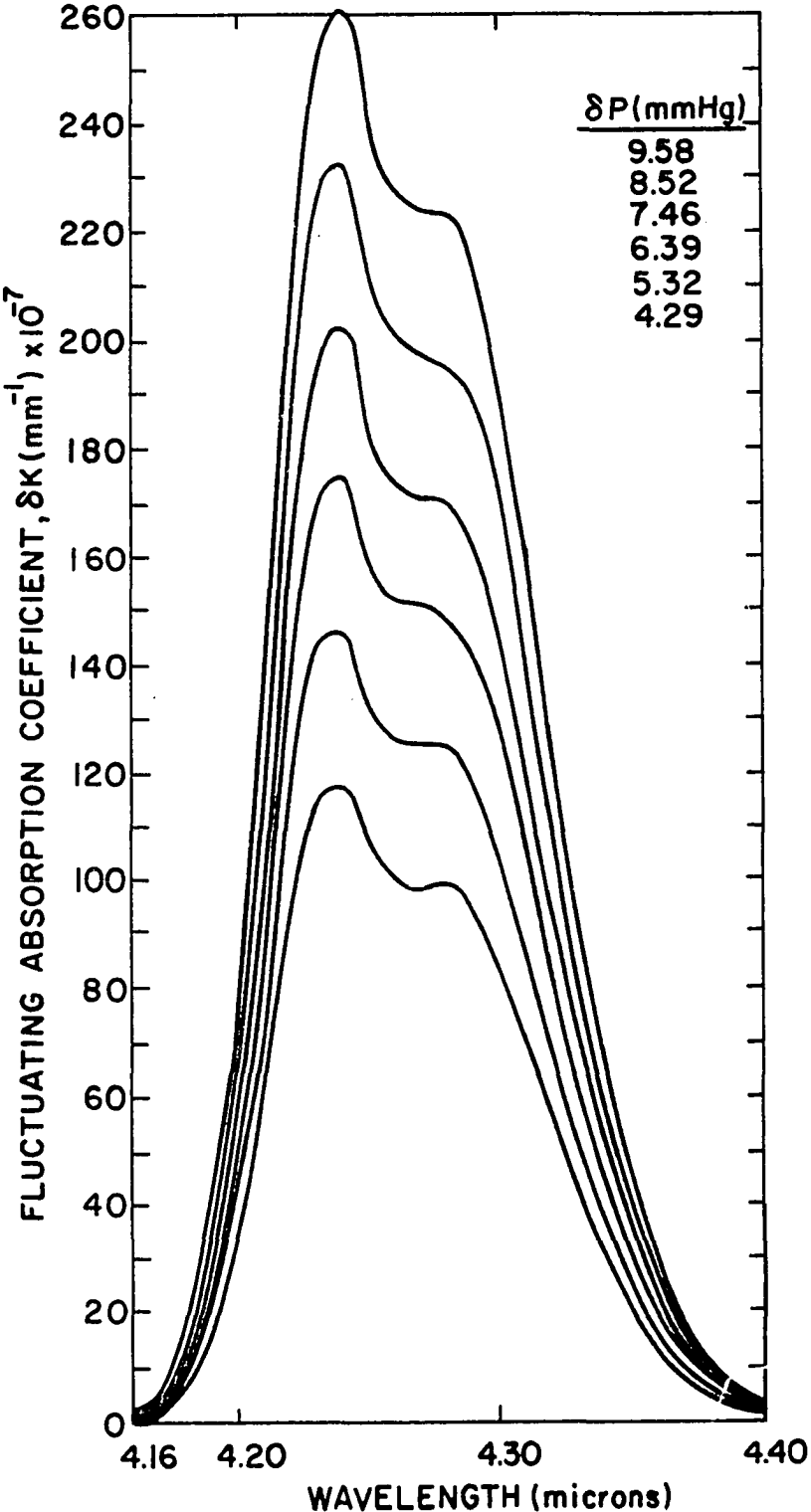

Figure 40 . Fluctuating Absorption Coefficient, δK, versus Wavelength with Fluctuating Pressure , δP, as a Parameter.

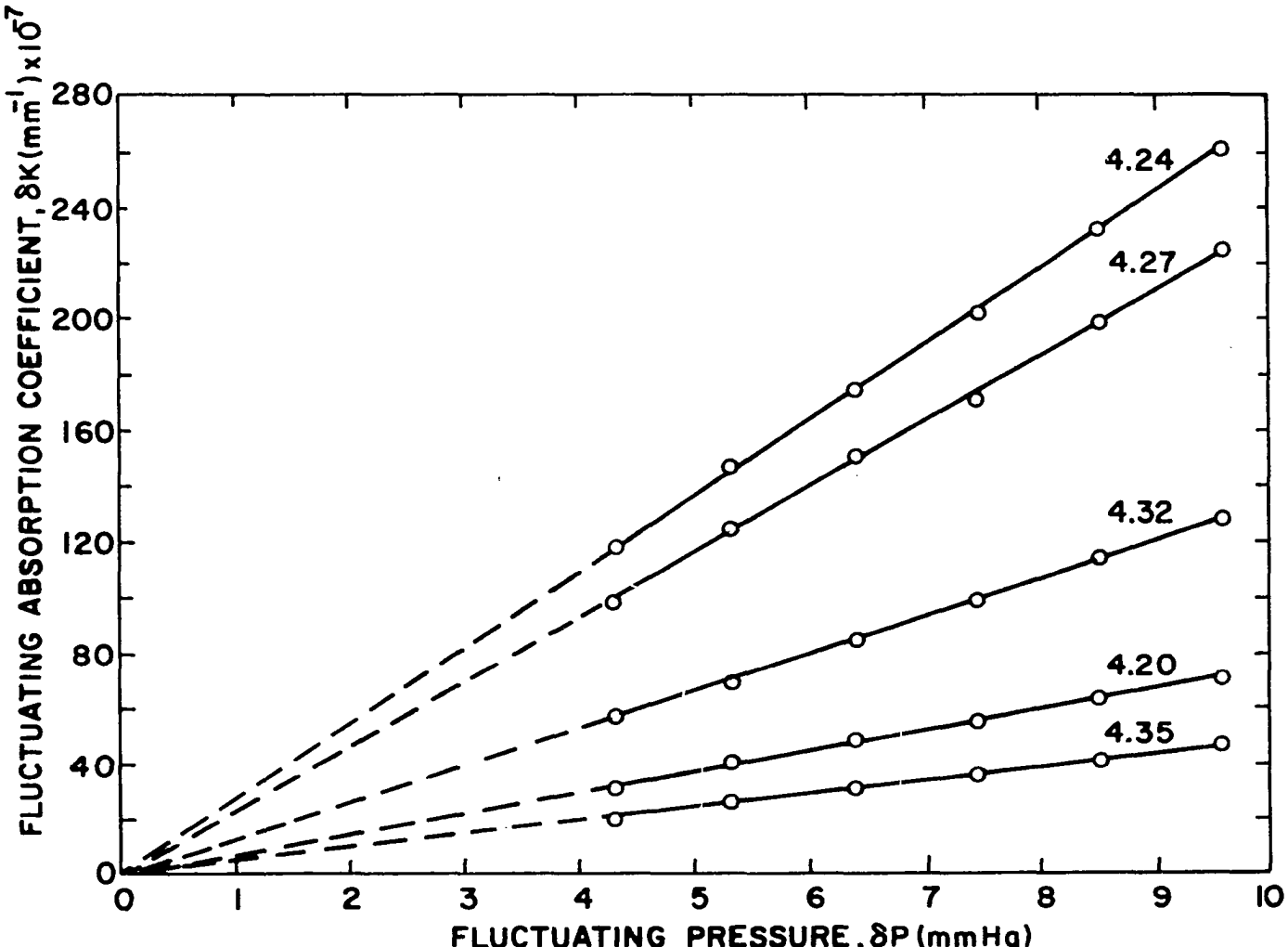

Figure 41 . Fluctuating Absorption Coefficient versus Fluctuating Pressure with Various Wavelengths in the Band as a Parameter.

properties of these spectra.

1. Constant δP Data. In this section we consider a general graphical analysis and the results of a general analysis of the data.

a. General Graphical Analysis. The constant δP data represents the main body of results. The fluctuating pressure was maintained at a constant value of 5.68 mmHg for all combinations of P,T,f,λ.

Let us first consider the pressure dependence of these spectra. We have predicted a minimal P(constant f) dependence with the possibility of the intermediate regions being independent of P.

Figure 42 is a plot of the fluctuating absorption coefficient δK versus wavelength with P(constant f,T) as a parameter. This represents a strong absorption case. The figure shows that there is a medium positive pressure dependence in the core regions, and a minimal and somewhat negligible P dependence in the intermediate and wing regions. Let us note that the points $\lambda = 4.20$ and $\lambda = 4.35$ are reasonably pressure independent. Figure 43 (compare with Figure 32) represents one of the lower signal to noise level conditions as evidenced by a slight increase in the scattering of the points as compared to those in Figure 42. These conditions yield a near weak line condition. There is again a positive δK-P dependence in the core and a negligible P dependence in the intermediate and wing regions. Figure 44 is a plot of δK versus λ with P(constant f) as a parameter. Again note the negligible P dependence as one goes into the wings. Also note that the Reversal Effect is not evidenced in the δK spectra.

Let us next consider the T dependence of the δK spectra. Figure 45

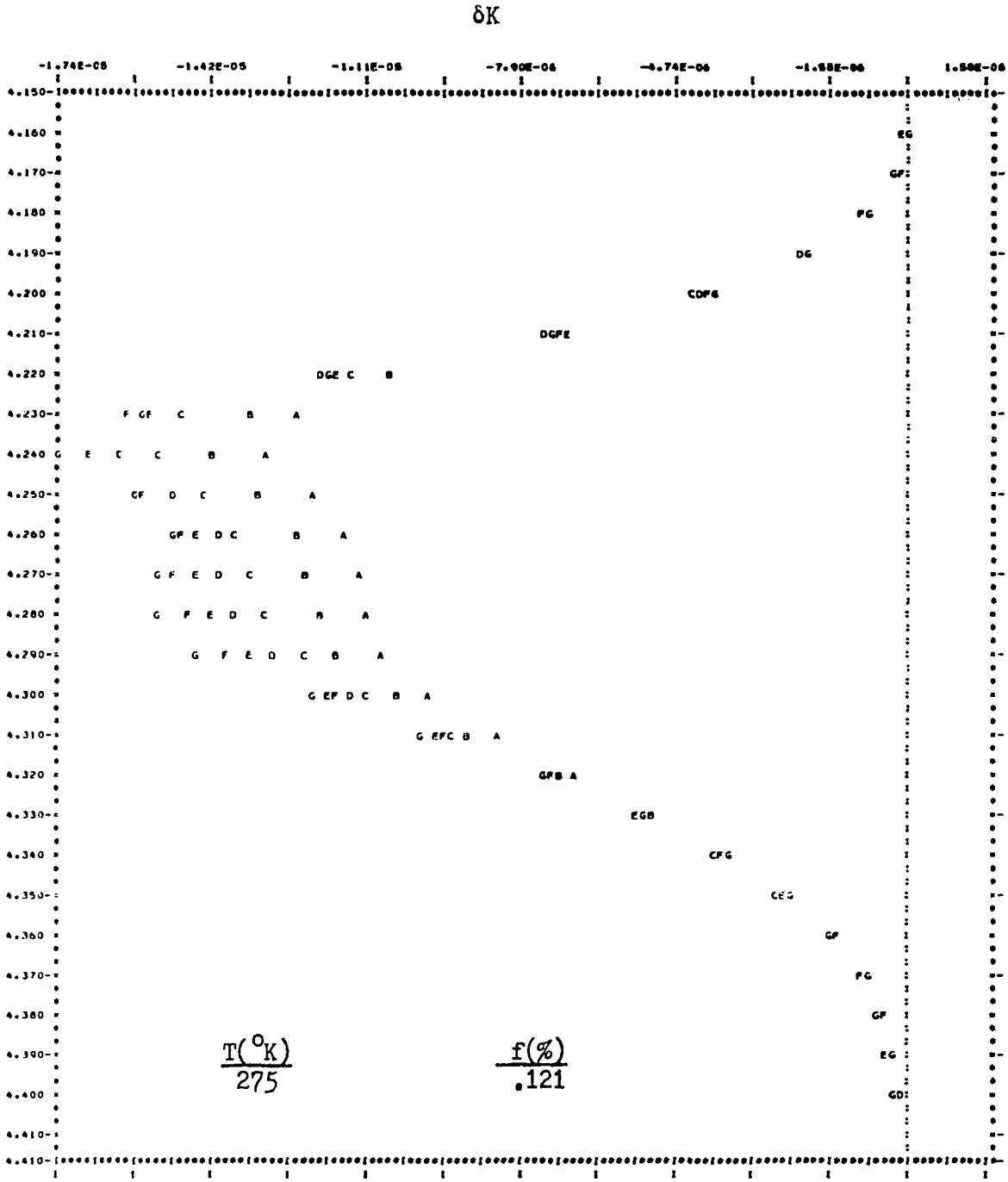

Figure 42. Computer Printed Plot of the Fluctuating Absorption Coefficient δK versus Wavelength with P as a Parameter. Plot Symbols Represent Pressure P from 422 mmHg to 1053 mmHg in Alphabetical Order.

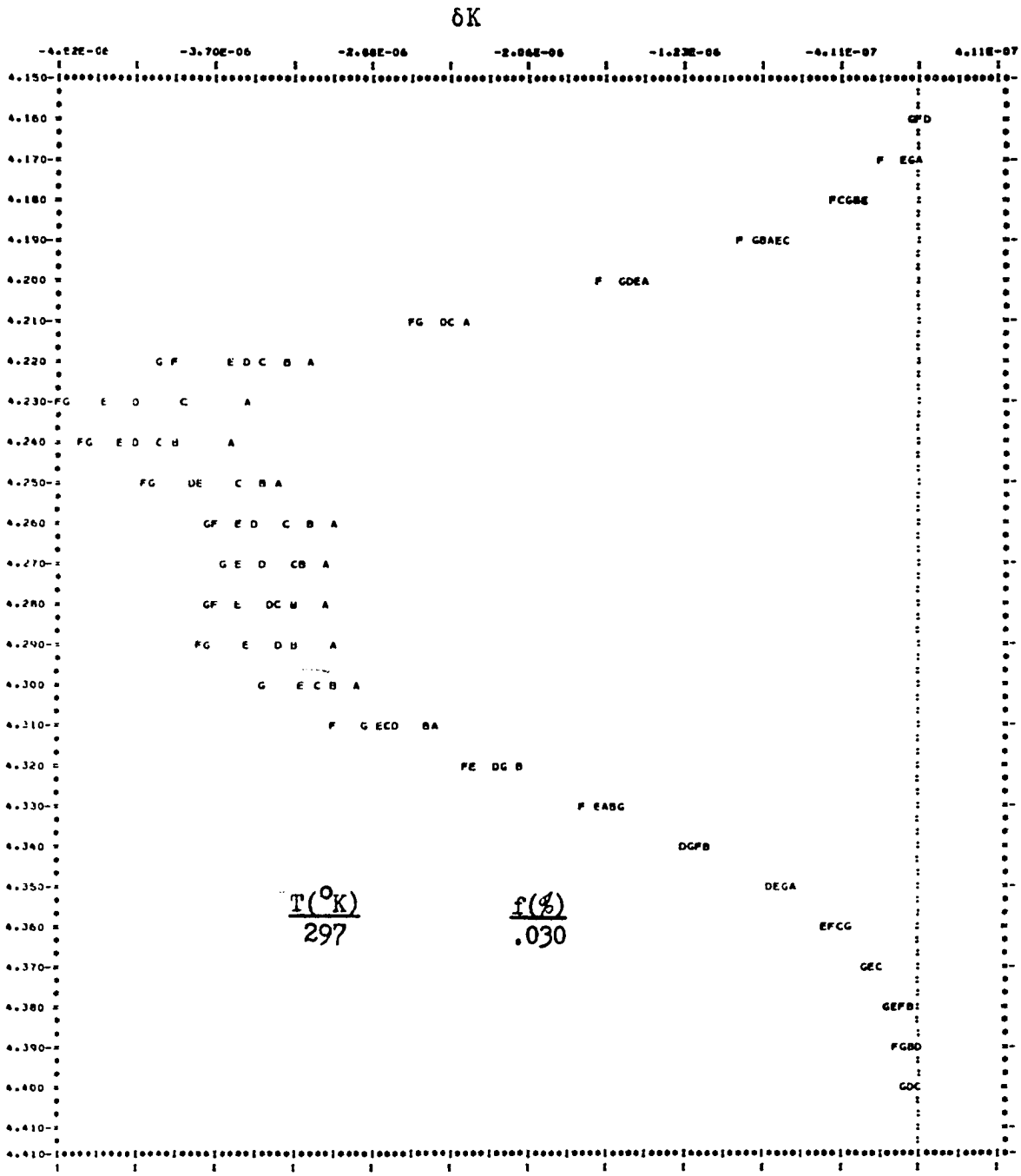

Figure 43 . Computer Printed Plot of the Fluctuating Absorption Coefficient δK versus Wavelength with P as a Parameter. Plot Symbols Represent Pressure P from 422 mmHg to 1053 mmHg in Alphabetical Order.

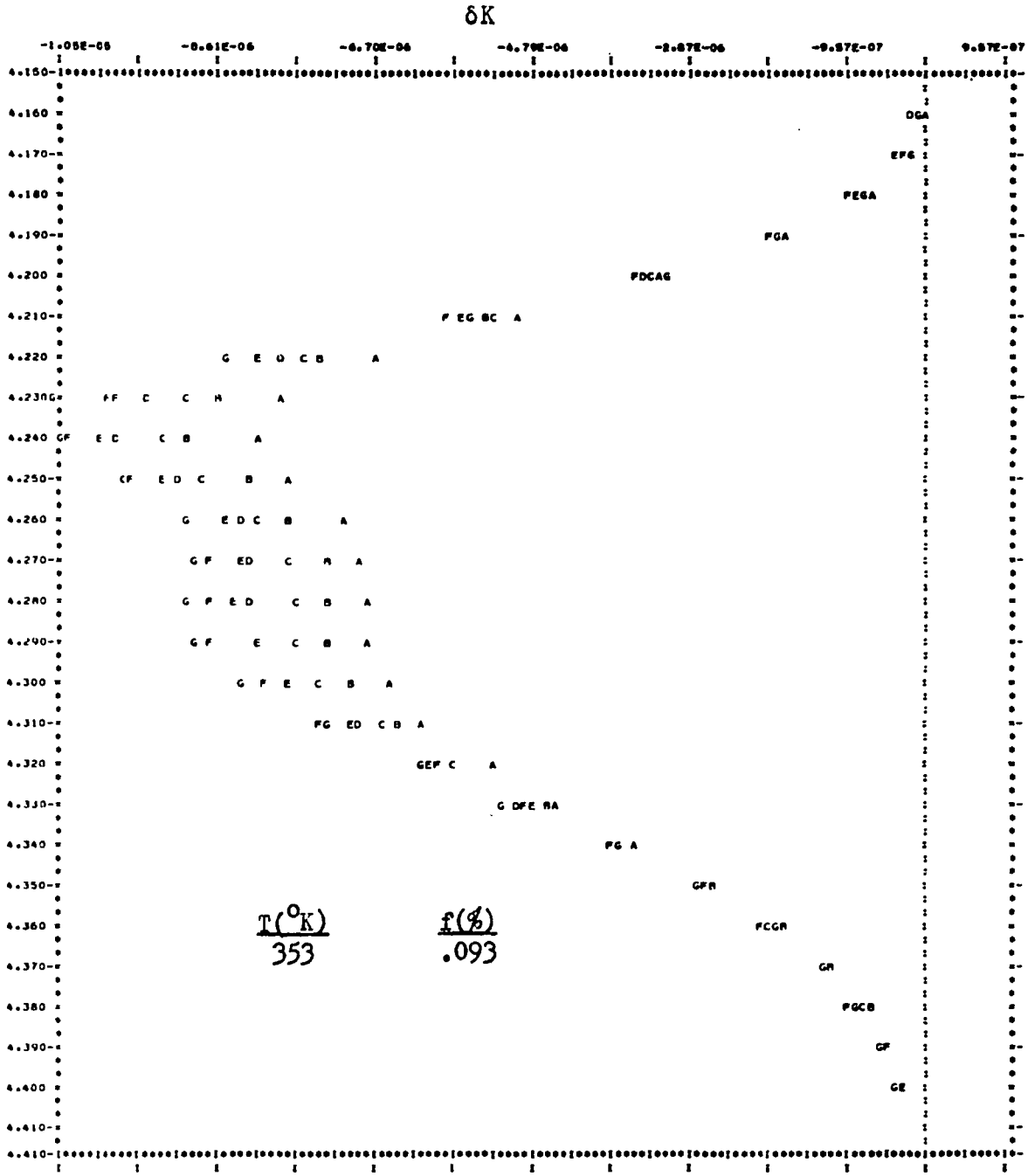

Figure 44 . Computer Printed Plot of the Fluctuating Absorption Coefficient δK versus Wavelength with P as a Parameter. Plot Symbols Represent Pressure P from 422 mmHg to 1053 mmHg in Alphabetical Order.

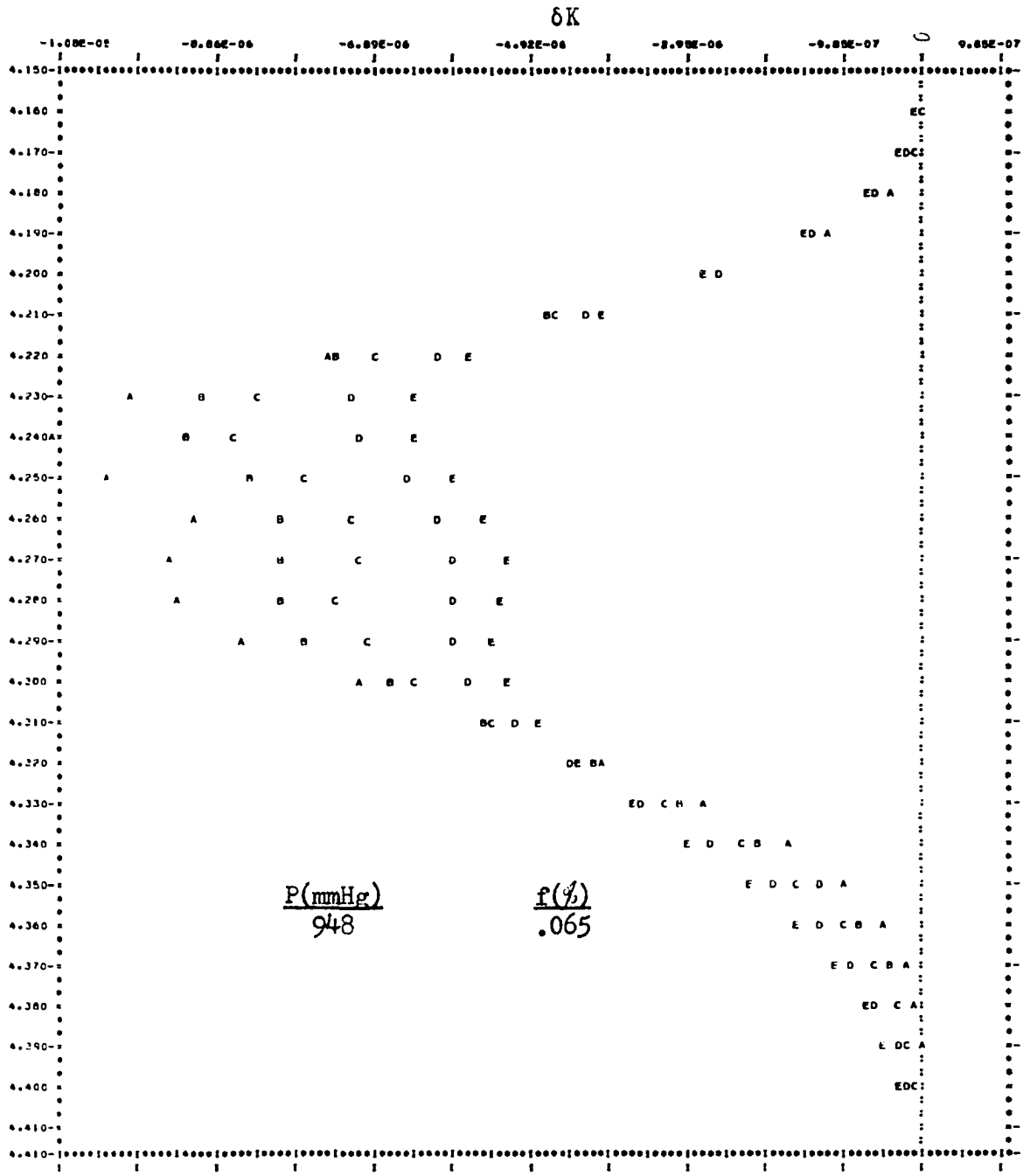

Figure 45 . Computer Printed Plot of the Fluctuating Absorption Coefficient δK versus Wavelength with T as a Parameter. Plot Symbols Represent Temperature T from 243 °K to 393 °K in Alphabetical Order.

(compare with Figure 33) is an example of the δK-T dependence for an intermediate case. Note the crossover points at λ = 4.32 and 4.20 microns. There is a strong negative T-δK dependence in the core and a strong positive T-δK dependence in the intermediate-wing regions, especially near λ = 4.35 microns. Figure 46 is another example of the δK-T dependence; it supports the findings in Figure 45. Figure 47 is a third example of a near strong line condition plot of δK versus λ with T as a parameter. Note the strong temperature dependence on the high wavelength side of the band as well as the crossover points at λ = 4.20 and approximately 4.32 microns.

The final dependence of δK is displayed in Figures 48 and 49. The δK-f dependence is the overall strongest thermodynamic variable dependence for δK. Figure 48 is a plot of δK versus λ with f as a parameter. This represents a weak line approximation condition. The δK-f dependence is positive and very strong throughout the band. There is no f independence or crossover points anywhere in the band. Figure 49 is a near strong line approximation plot of δK versus λ with f as a parameter. Although the overall width of the band has decreased from that δK spectrum represented in Figure 48, the δK-f dependence is still positive and strong over the complete band.

b. Results of General Analysis. The actual P,T,f dependence of δK can be determined by fitting the δK data at each wavelength to expected functions. The problem is that this dependence is quite complicated due to the fact that each of the three (or two) terms in the Taylor series expansion is dependent on the three variables.

To simplify matters let us note that there are points in the δK

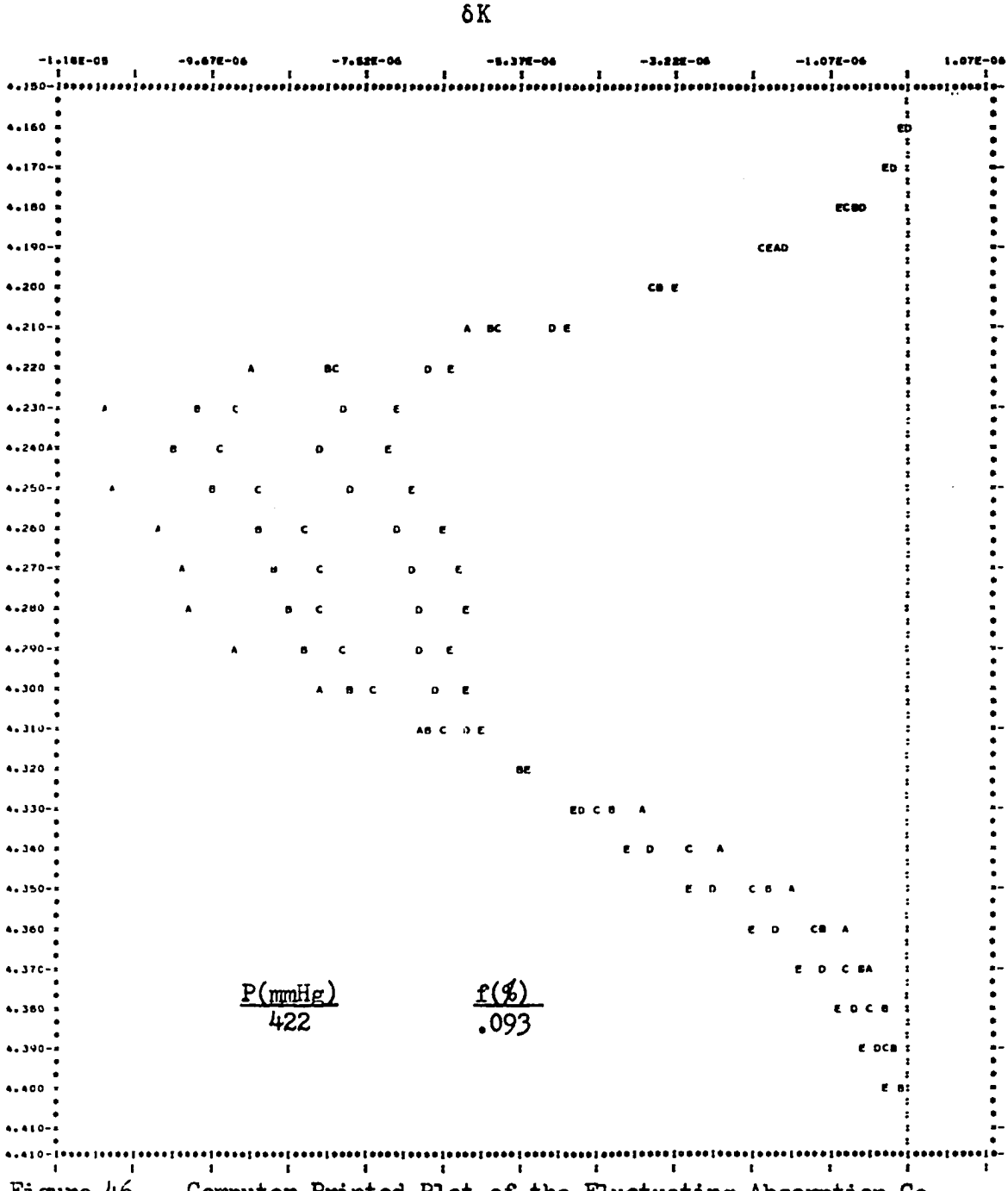

Figure 46. Computer Printed Plot of the Fluctuating Absorption Coefficient δK versus Wavelength with T as a Parameter. Plot Symbols Represent Temperature T from 243°K to 393°K in Alphabetical Order.

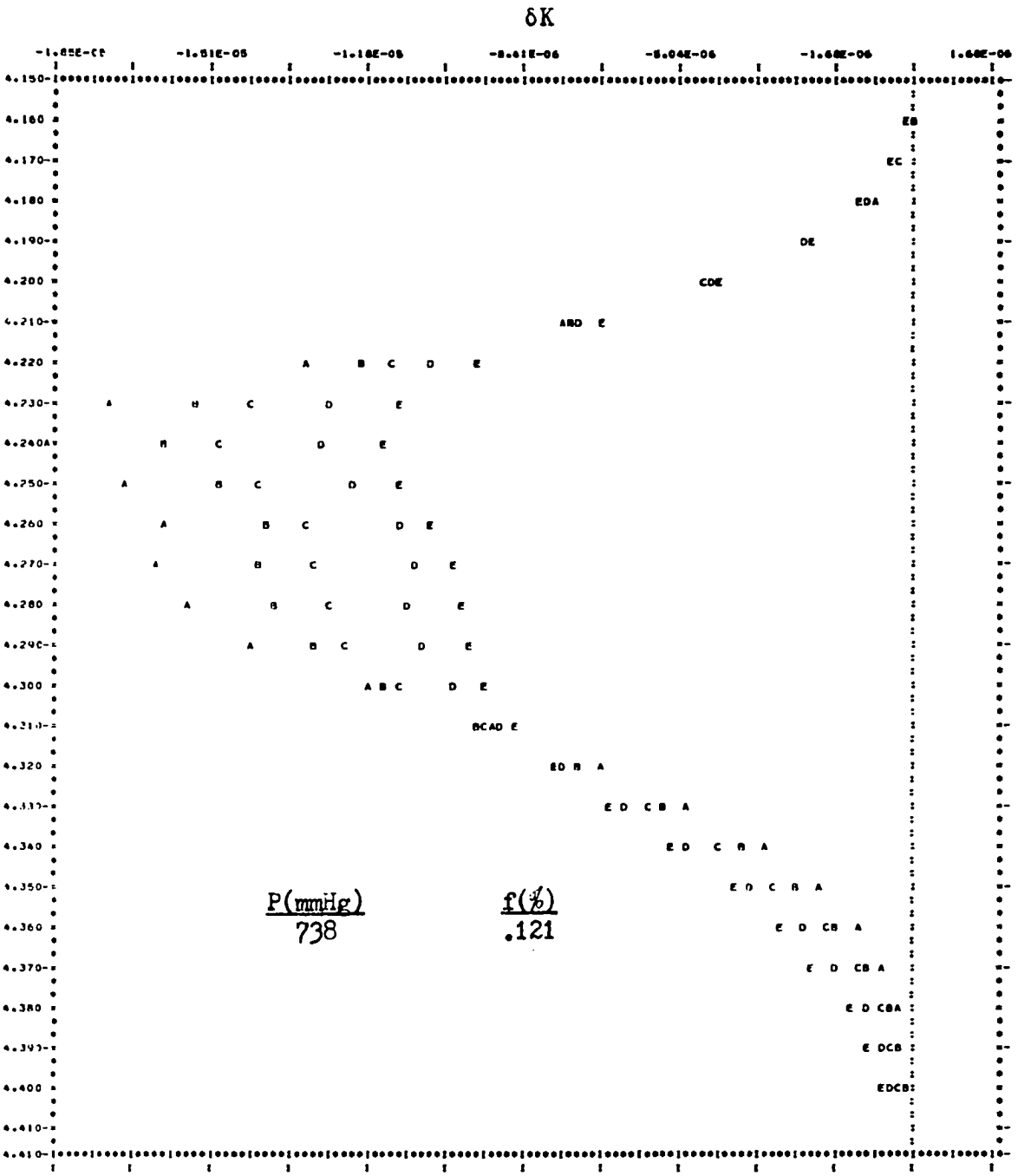

Figure 47 . Computer Printed Plot of the Fluctuating Absorption Coefficient δK versus Wavelength with T as a Parameter. Plot Symbols Represent Temperature T from 243°K to 393°K in Alphabetical Order.

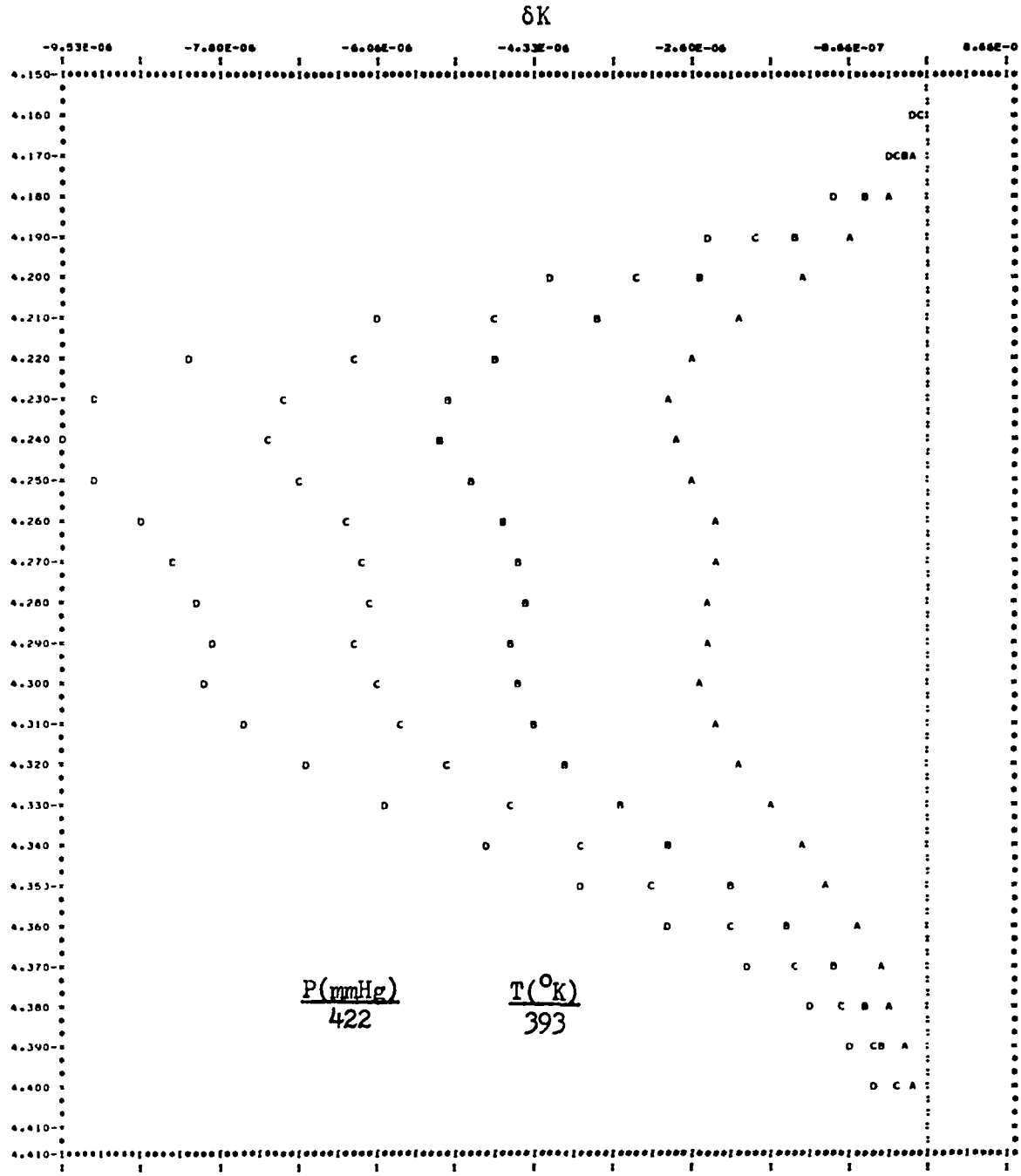

Figure 48 . Computer Printed Plot of the Fluctuating Absorption Coefficient δK versus Wavelength with f as a Parameter. Plot Symbols Represent CO_2 Concentration f from .030% to .121% in Alphabetical Order.

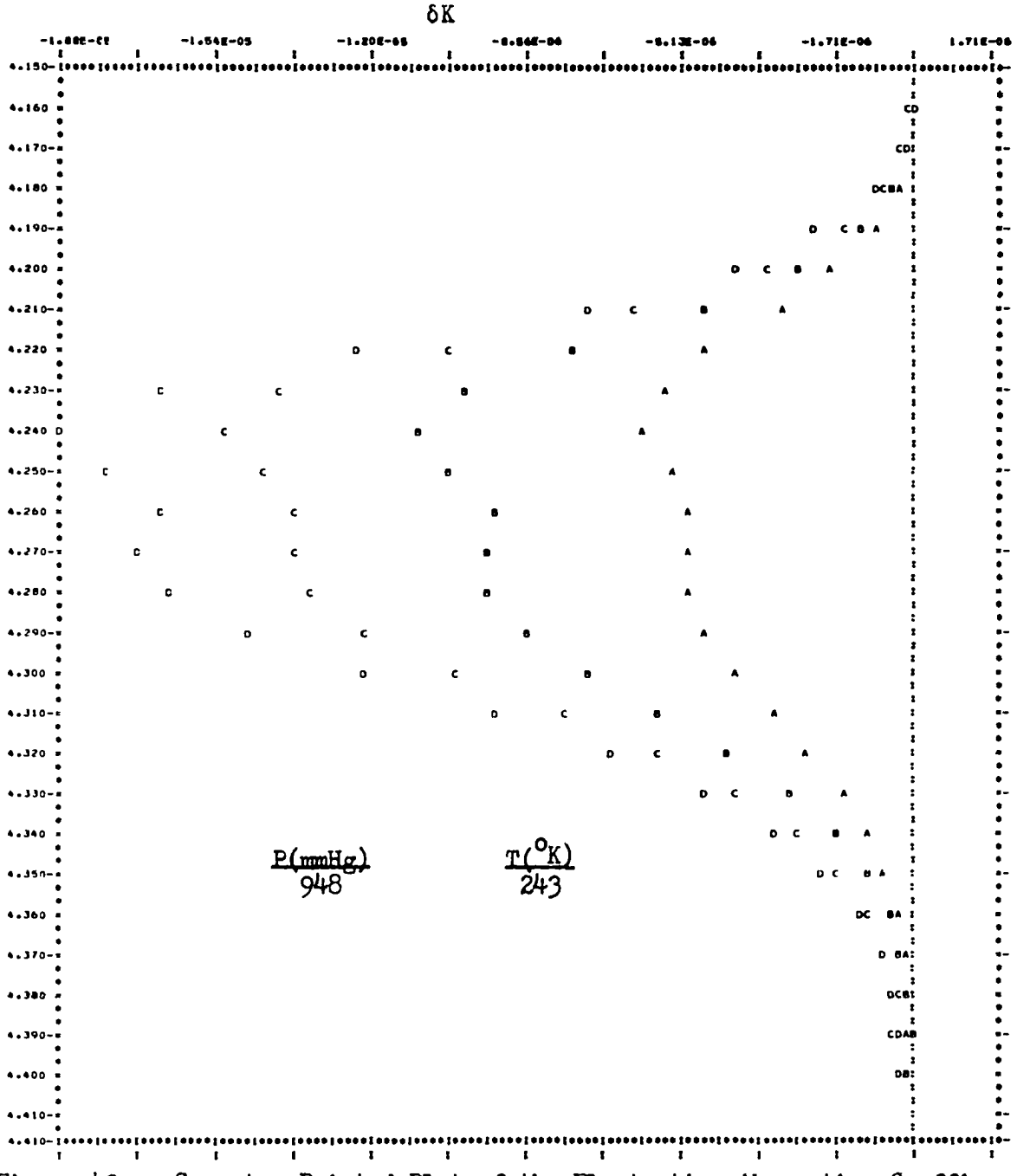

Figure 49 . Computer Printed Plot of the Fluctuating Absorption Coefficient δK versus Wavelength with f as a Parameter. Plot Symbols Represent CO_2 Concentration f from .030% to .121% in Alphabetical Order.

spectrum that have special significance. Perhaps the most important of these points is a $\lambda = 4.20$ microns. At this point the δK spectrum is reasonably independent of both T and P. This is an extremely important result; by going to the δK spectrum, we have been able to isolate the δK-f dependence for a particular region of the band. In other words, δK is a function of f only at this point, which means that δK is approximately constant for all values of P and T considered in this experiment. The f dependence is quite strong at this point.

It is now a simple matter to invert the δK spectrum to obtain a measurement of f from δK. It requires one measurement at $\lambda = 4.20$ microns. The δK-f dependence is roughly a power law dependence @ $\lambda = 4.20$ microns with an exponent which is approximately .76.

Now that we have measured f, we can go to another region of the band and make a second measurement to obtain the variable T. At $\lambda = 4.35$ microns, the δK spectrum is independent of P but strongly dependent on both T and f. But we have already measured f; therefore a second measurement at $\lambda = 4.35$ will yield the temperature. A very rough estimate of the strength of the T dependence @ this point can be obtained by plotting the data on Log-Log paper as K versus T. The resultant power law yields an exponent of approximately 1.5.

The P dependence is the most difficult to determine since this dependence was suppressed when forming the δK spectrum. Nonetheless a third measurement somewhere in the core of the band (say $\lambda = 4.24$ or $\lambda = 4.26$) will yield the P measurement; remember we have already determined T and f. It is also possible to go to $\lambda = 4.32$ since this position is a temperature crossover point. Two measurements only are necessary to

get P in this case. However, the P dependence is not very strong at $\lambda = 4.32$.

Thus we have shown that a spectral inversion can be made if one uses the 4.3 micron region δK spectrum of CO_2. Three measurements at three different wavelength positions are necessary to retrieve f, T and P and therefore T, P, p.

For completeness, we will now mention briefly that there is another possible solution to the inversion problem. It involves making measurements near $\lambda = 4.34$ and 4.35 for the temperature and using the second derivative information to determine the absorber concentration. Total pressure measurements can then also be made. Preliminary checks indicate, surprisingly, that the second derivative information is good; this method requires further study.

In order to get "deeper" into the δK spectrum we have resorted to an anlysis of the mean value derivatives of the K spectrum (or the mean absorption coefficient) which make up the δK spectrum (see equation 97 in Chapter IV). This is considered in section H.

Another possible means of further analyzing the δK spectrum is by controlling the variables of the recorded δK in such a way as to create a special dependence of δK on the variables. This is considered briefly in the next section.

2. $\delta P \propto P$ Data. The variables P,T,f and δP are independent; they can be controlled by the experimenter in any reasonable way when recording the δK spectrum. This allows for the possibility of creating artificial conditions which can be used as a tool to get further into the δK spectrum. For example, the relationship of the δK to the varia-

ble δT can be analyzed by varying δP proportional to P and keeping the temperature constant. This maintains δT constant, as can be seen by the adiabatic condition. The temperature derivative in the Taylor series expansion is now multiplied by a constant.

This data was recorded in this experiment for all room temperature measurements. Figure 50 is a plot of δK versus λ with $\delta P \propto P$ as a parameter. This was recorded at .121% CO_2 and room temperature. The power law dependence of δK on δP or P is described by a positive exponent of about 1.33 at λ = 4.24 and 4.27, 1.13 at λ = 4.32, .866 at λ = 4.20 and 1.03 at λ = 4.35 microns. The dependence of δK on P is stronger in the core in this case than in the δP = constant data.

H. Analysis of K Spectrum

1. General Trends. A review of the K spectrum computer generated graphs indicate the following general trends in the K data. The pressure dependence (constant f) is positive and very strong in the core and falls off to a very slight dependence in the near wing regions (see Figure 51). The temperature dependence is negative in the core and positive in the intermediate wing regions; the crossover points are at λ = 4.20 and 4.31 microns. The pressure dependence is stronger, overall, than the temperature dependence (see Figure 52). The f dependence is positive throughout and very strong in the core (see Figure 53). The reader should make a visual comparison between the figures representing the K spectrum and those representing the δK spectrum.

2. Weak Line and Strong Line Approximation Formats. We shall now plot the K spectrum in the weak line and the strong line approximation

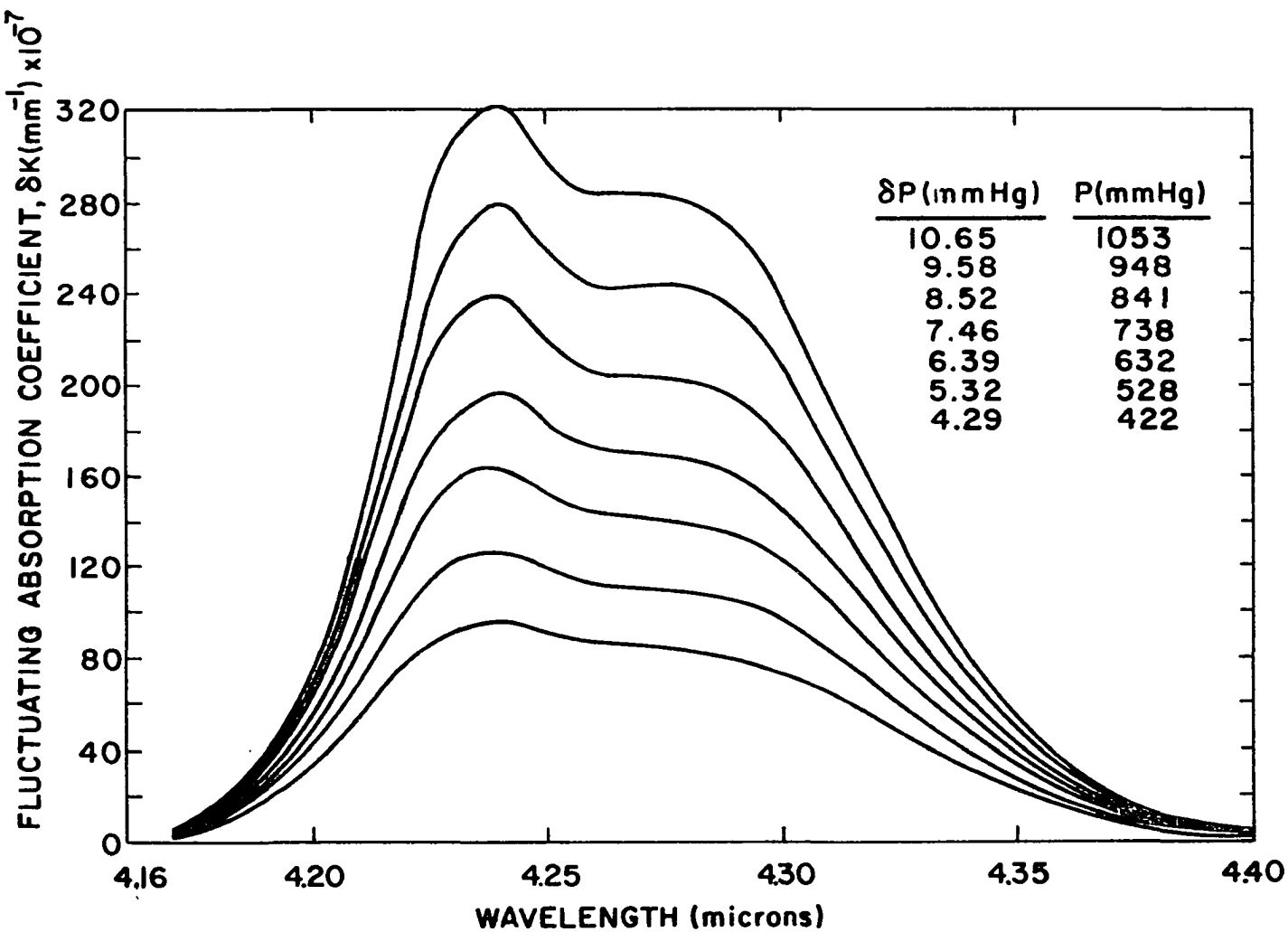

Figure 50 . Fluctuating Absorption Coefficient versus Wavelength with Fluctuating Pressure Set Proportional to P as a Parameter.

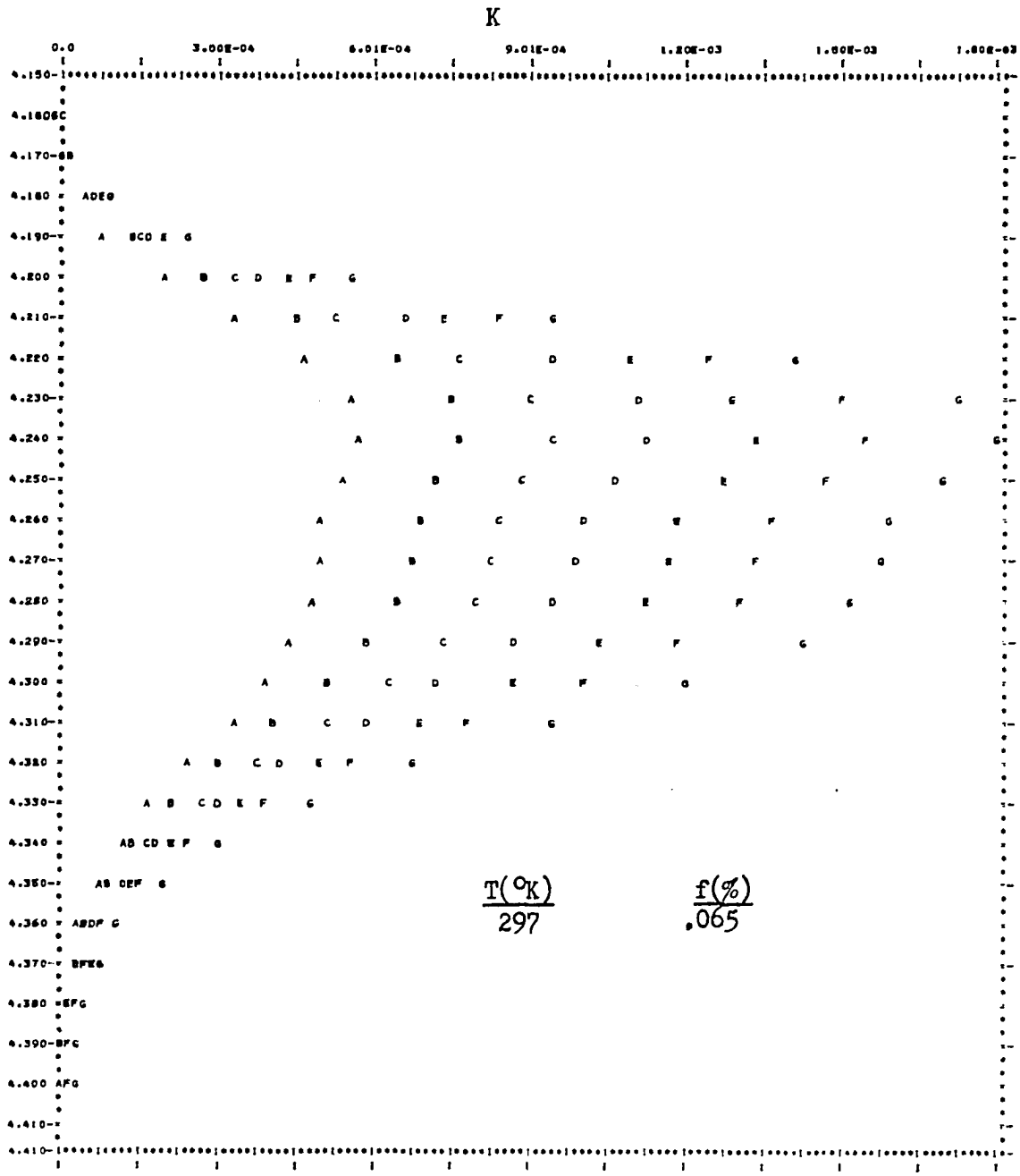

Figure 51. Computer Printed Plot of the Absorption Coefficient K versus Wavelength with P as a Parameter. Plot Symbols Represent Pressure P from 422 mmHg to 1053 mmHg in Alphabetical Order.

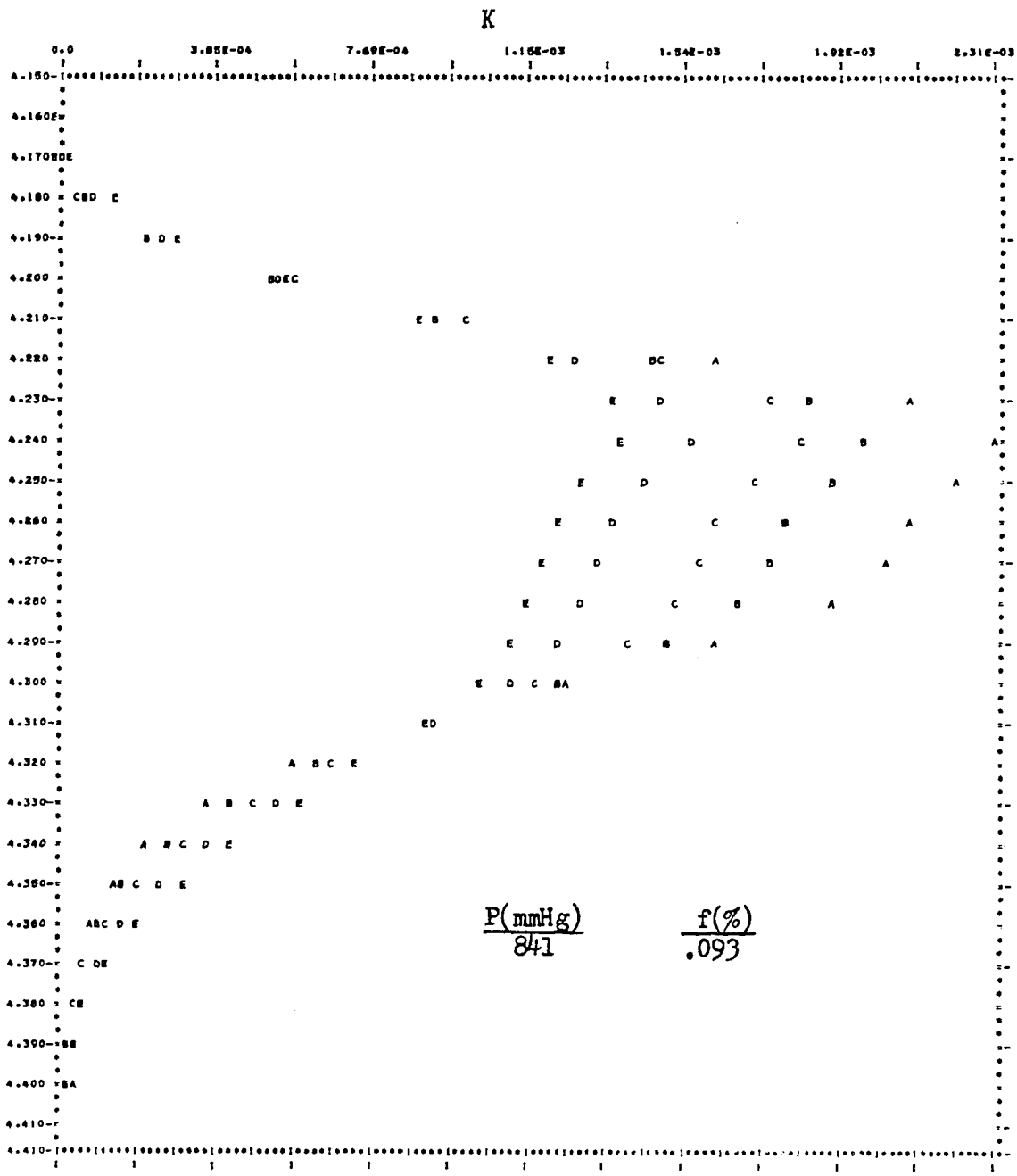

Figure 52. Computer Printed Plot of the Absorption Coefficient K versus Wavelength with T as a Parameter. Plot Symbols Represent Temperature T from 243°K to 393°K in Alphabetical Order.

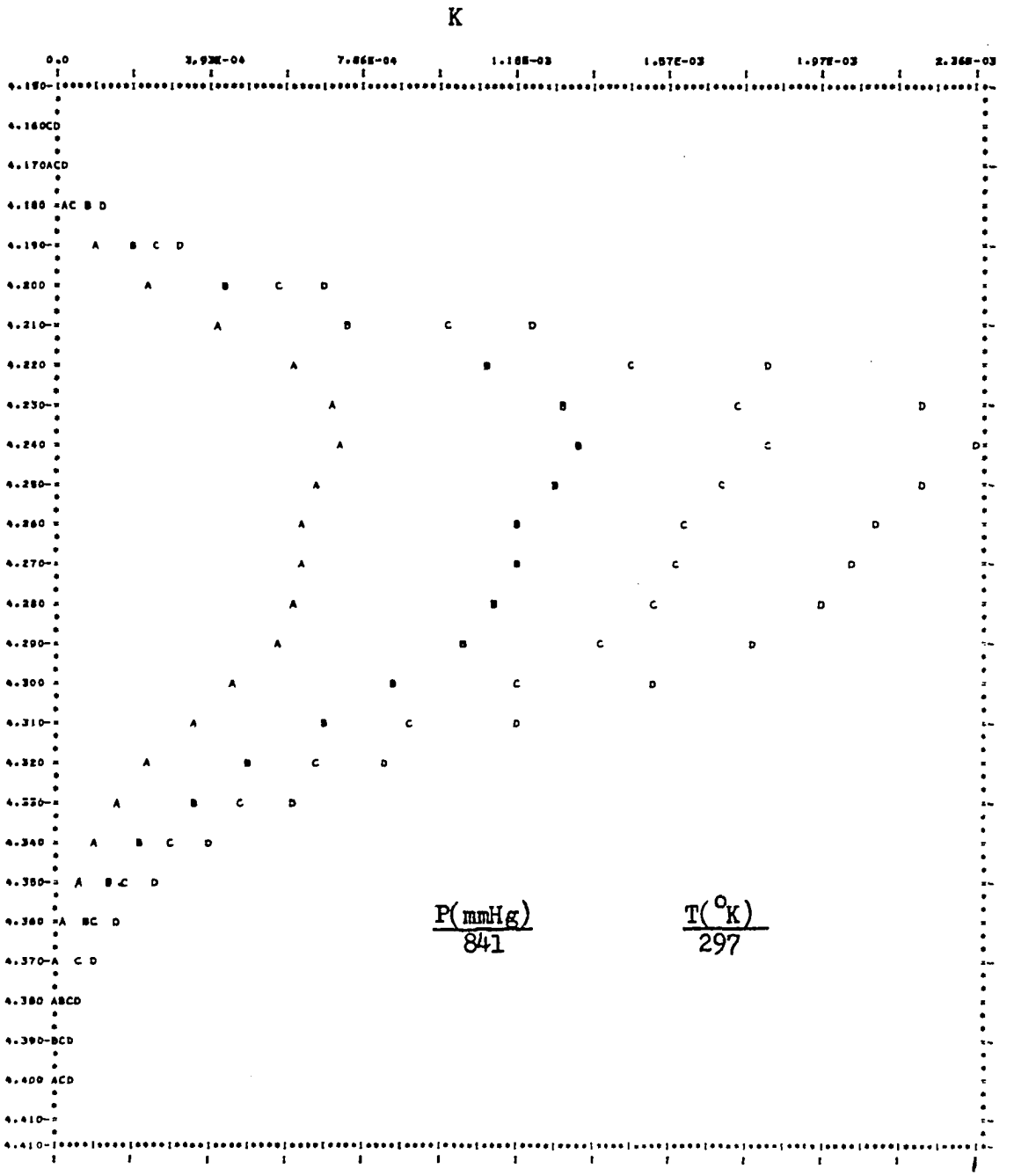

Figure 53. Computer Printed Plot of the Absorption Coefficient K versus Wavelength with f as a Parameter. Plot Symbols Represent CO_2 Concentration f from .030% to .121% in Alphabetical Order.

formats, and compare the results with the same data plotted as an absorption spectrum in the same formats. The absorption formulation is the usual method of analysis as reported in the literature.

Figure 54 is an example of the absorption coefficient, K, plotted in the strong line approximation format as K versus Pp (= P^2f). The data that was used to calculate the K^S in this plot is the same data that was used to calculate the A^S in Figure 23 in Chapter VI section C. Again $\lambda = 4.35$ tends to be furthest away from the strong line approximation format; the $\lambda = 4.24$ data is in a near strong line condition.

Figure 55 is an example of the same absorption coefficient K, plotted in the weak line approximation format as K versus p(=Pf). This figure again indicates that the $\lambda = 4.35$ data can be represented by the weak line approximation for these conditions. This figure should be compared with Figure 24.

The difference between the figures in both cases is that the K spectrum results include the effects of the exponential function exp-kl whereas the absorption spectrum results do not include its effects. One expects that the exponential decay function will play a considerable role in the formulation of the theory for the range of the data recorded in this experiment; this is especially true if the data that is used corresponds to the fact that the absorption approaches saturation. For data above the approximate linear region of the 1-exp-kl curve, the exponents obtained from the power law fit of K to P and f will therefore be larger than those corresponding to the power law fit of A to P and f.

The nominal values of the exponents obtained from the absorption coefficient curves are given by $m + 1 \approx 1.20$, $1 \approx .81$ for $\lambda = 4.24$; $m + 1 \approx$

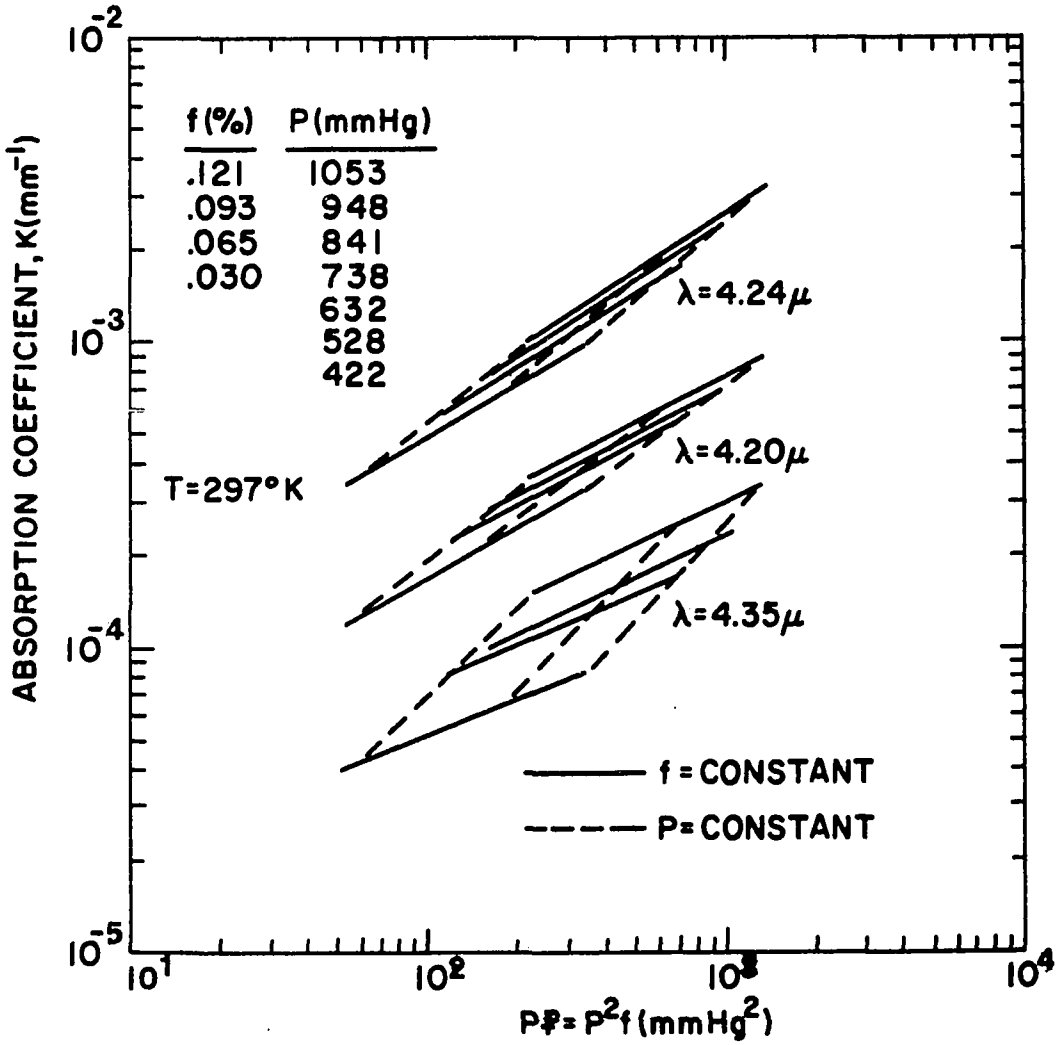

Figure 54 . Absorption Coefficient Plotted in the Strong Line Approximation Format.

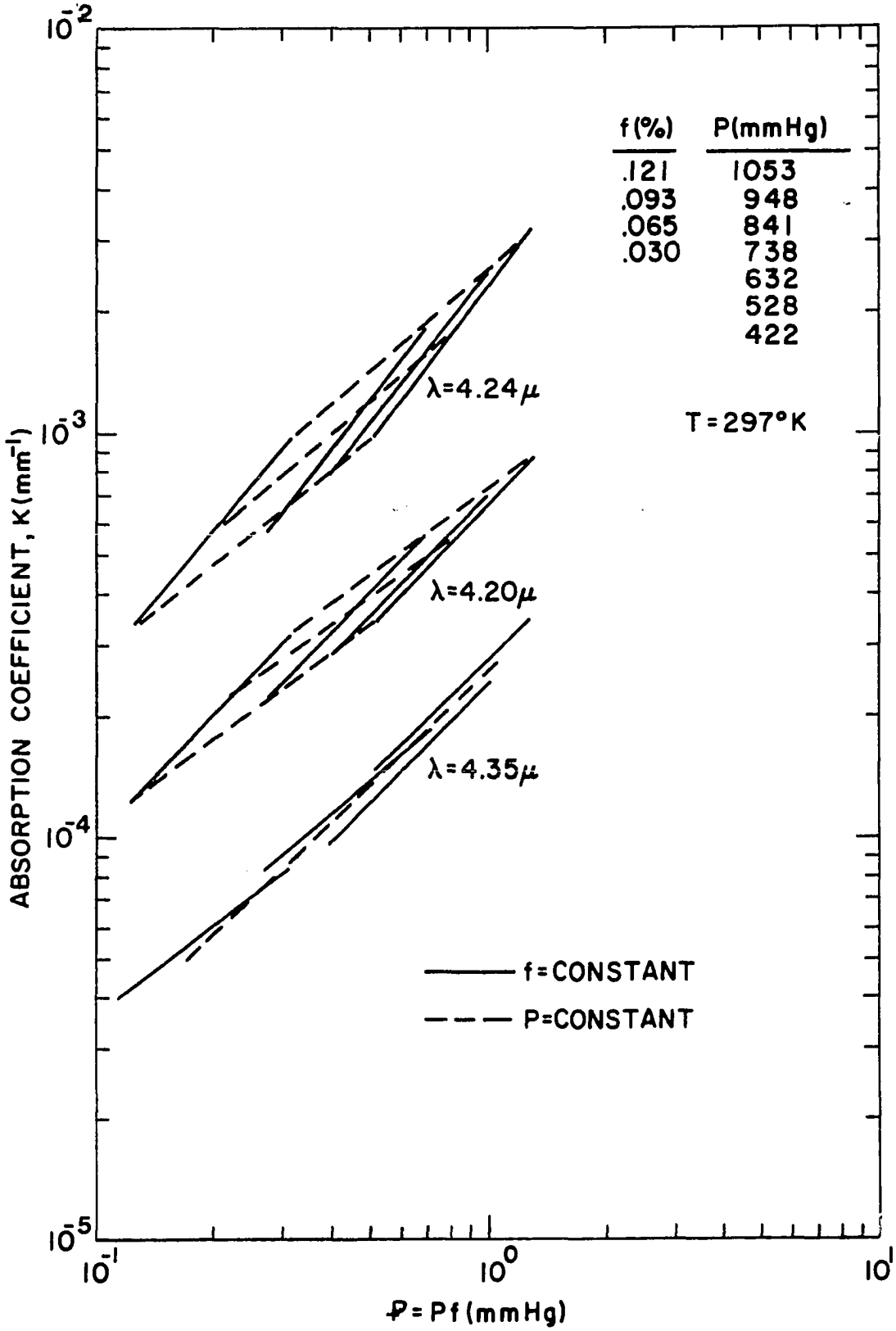

Figure 55 . Absorption Coefficient Plotted in the Weak line Approximation Format.

1.04, $l \approx .71$ for $\lambda = 4.20$; and $m + l \approx .98$, $l \approx .96$ for $\lambda = 4.35$ (compare these values with the primed values in Chapter VI section C). These values for the exponents are considered to be more accurate than the values of m' and l', especially in the strongly overlapping line region of validity. The absorption coefficient exponents are better related to the general band model results than are the absorption exponents. The exponents should be identical in the linear and square root nonoverlapping line regions of validity.

3. Mean Value K Derivatives. We shall now consider the δK formulation and evaluate the derivatives of the mean value absorption coefficients. The derivatives are calculated by first fitting the data to the predicted functions derived in the Theory section and given in the Basis For Analysis section. This results in a smoothing of the data; the derivatives are then calculated from the smoothed data.

a. Temperature. The temperature dependence of the strong line approximation absorption coefficient was determined to be a better overall fit to the existing data than the weak line approximation absorption coefficient. This dependence is given by equation (104) in Chapter IV. The best procedure would of course be to determine whether the weak or the strong line absorption coefficient was the better fit at each considered position in the band. This procedure allows for a more accurate analysis of the data than would be the case if one immediately calculates a total band function, since the weak line approximation may change to the strong line approximation with in a given band and usually does. This is one of the benefits of using spectral functions. However we did not feel that we had enough data to go this extra step.

Referring again to equation(104) let us redefine the coefficients as $A(1) \equiv Aa_{\lambda}$, , $A(2) \equiv Bb_{\lambda}$, . These coefficients were determined in the least square fitting procedures; they are a function of P,f and λ (or J). The temperature dependence of the strong line approximation absorption coefficient is easily shown to be

$$K_{S.L.}(T) = \frac{A(1)}{T^{3/4}} \exp - A(2)/T \qquad (109)$$

A good test for the validity of the temperature results is to determine the dependence of A(2) on P; it should be independent of this quantity since the exponential function arises from the Boltzman distribution function for the population of the states. Figure 56 is a plot of the temperature coefficient A(2) vs. λ with P as a parameter. One can see that the curves overlap quite satisfactorily indicating a general independence of P for A(2). This is true for all absorber concentrations. The dependence of A(2) on the absorber concentration f is very small, although a slight decrease in A(2) in the core regions with increasing f is seen. This figure also provides a basis for considering the T - J dependence as discussed in Section II.C.2.

Figure 57 is the corresponding plot of A(1) vs λ with P and f as a parameter. The minimum of "saddle" region of the family of curves falls near the band origin or zero gap. The P and f dependence is strongest near the P and R branch maximum regions. The P and f dependence is positive in both cases.

The temperature derivative is displayed in Figure 58; this gives the $\partial K / \partial T$ versus λ with T as a parameter for P = 760 mm Hg and f = .093%. Temperature crossover points are indicated at λ = 4.21 and

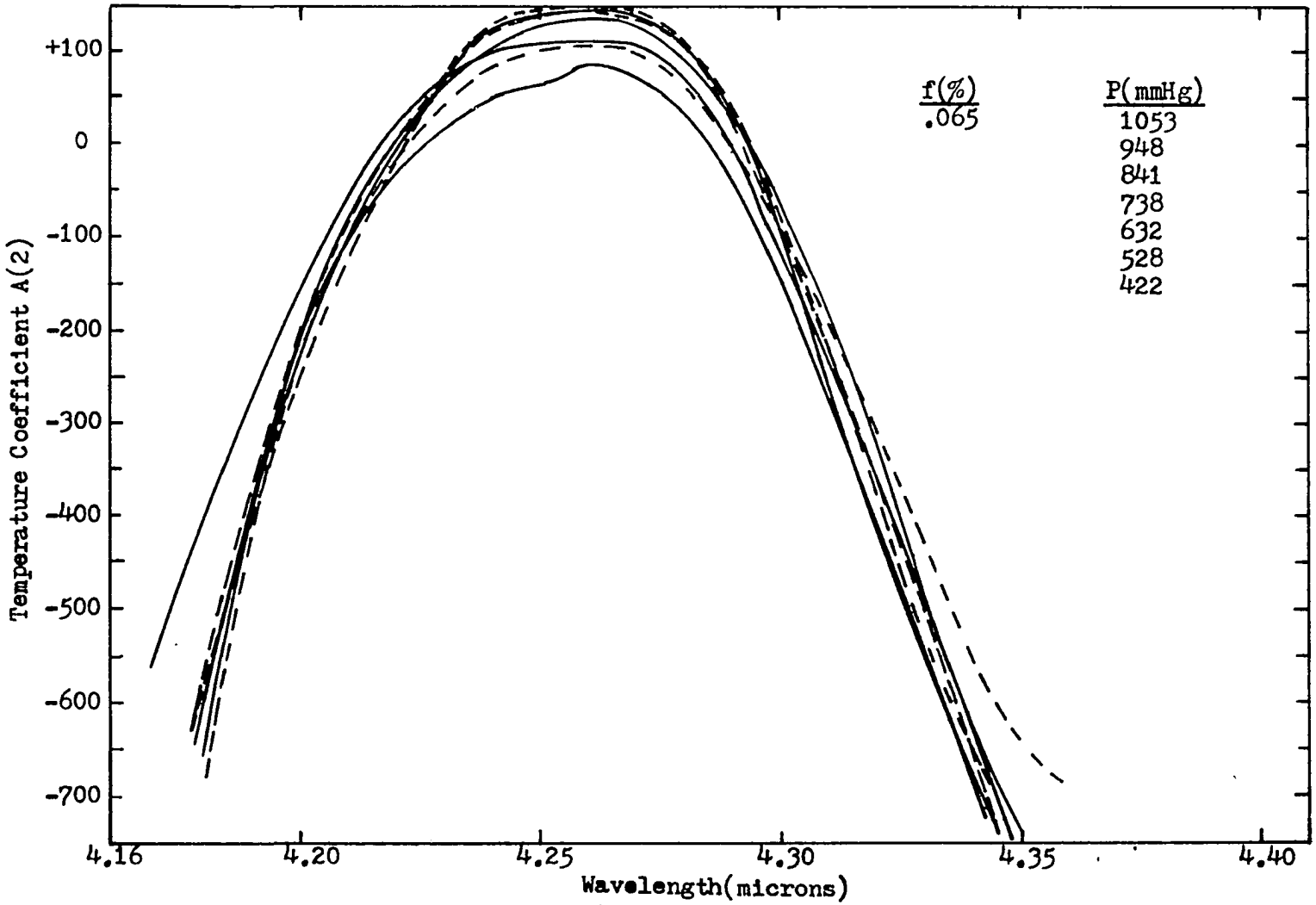

Figure 56 . Temperature Coefficient A(2) versus Wavelength with Pressure,P, as a Parameter Using $K = (A(1)/T^{3/4}) \exp A(2)/T$.

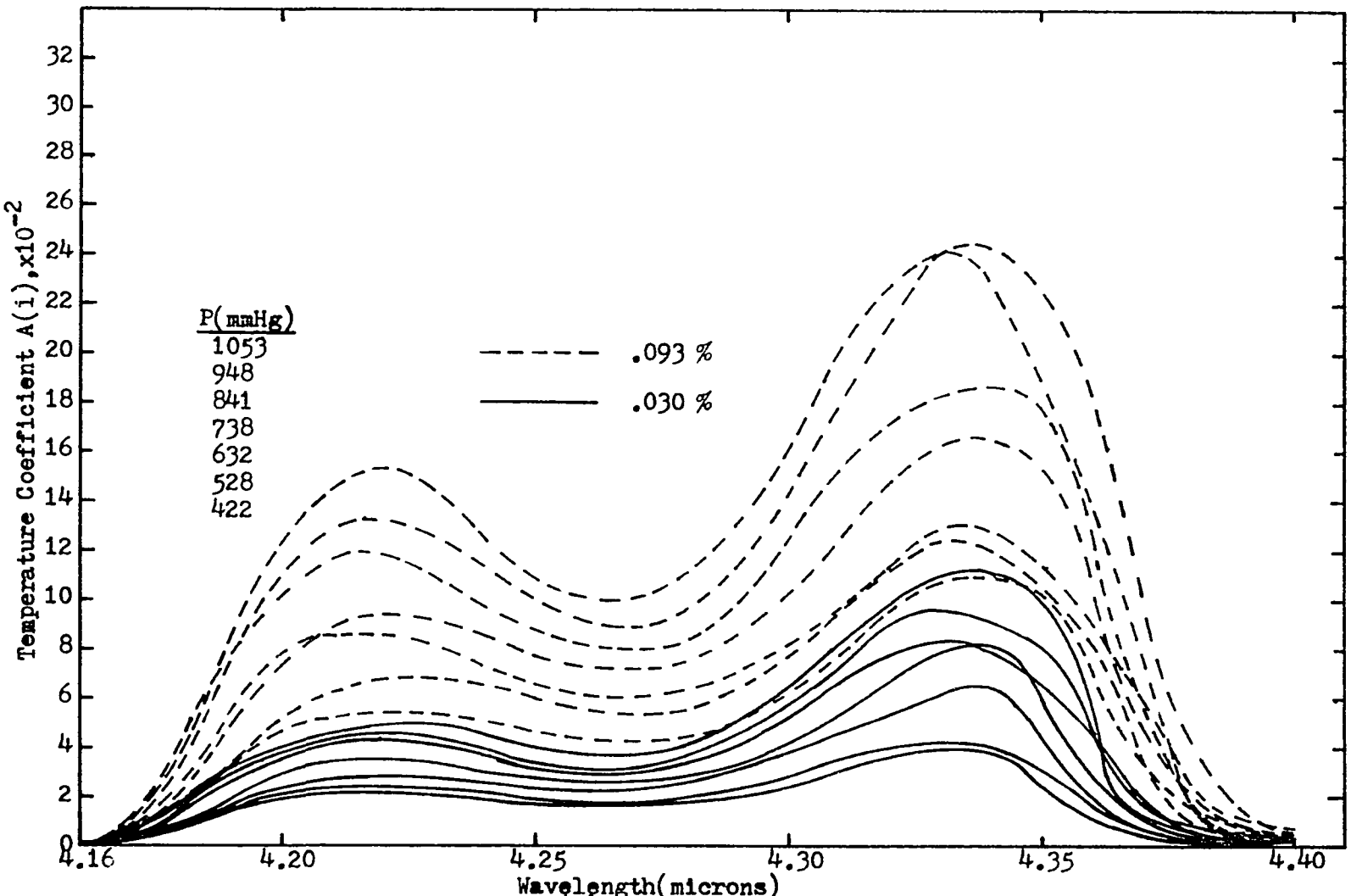

Figure 57 Temperature Coefficient A(1) versus Wavelength;P and f as Parameters Using $K = (A(1)/T^{3/4})\exp A(2)/T$.

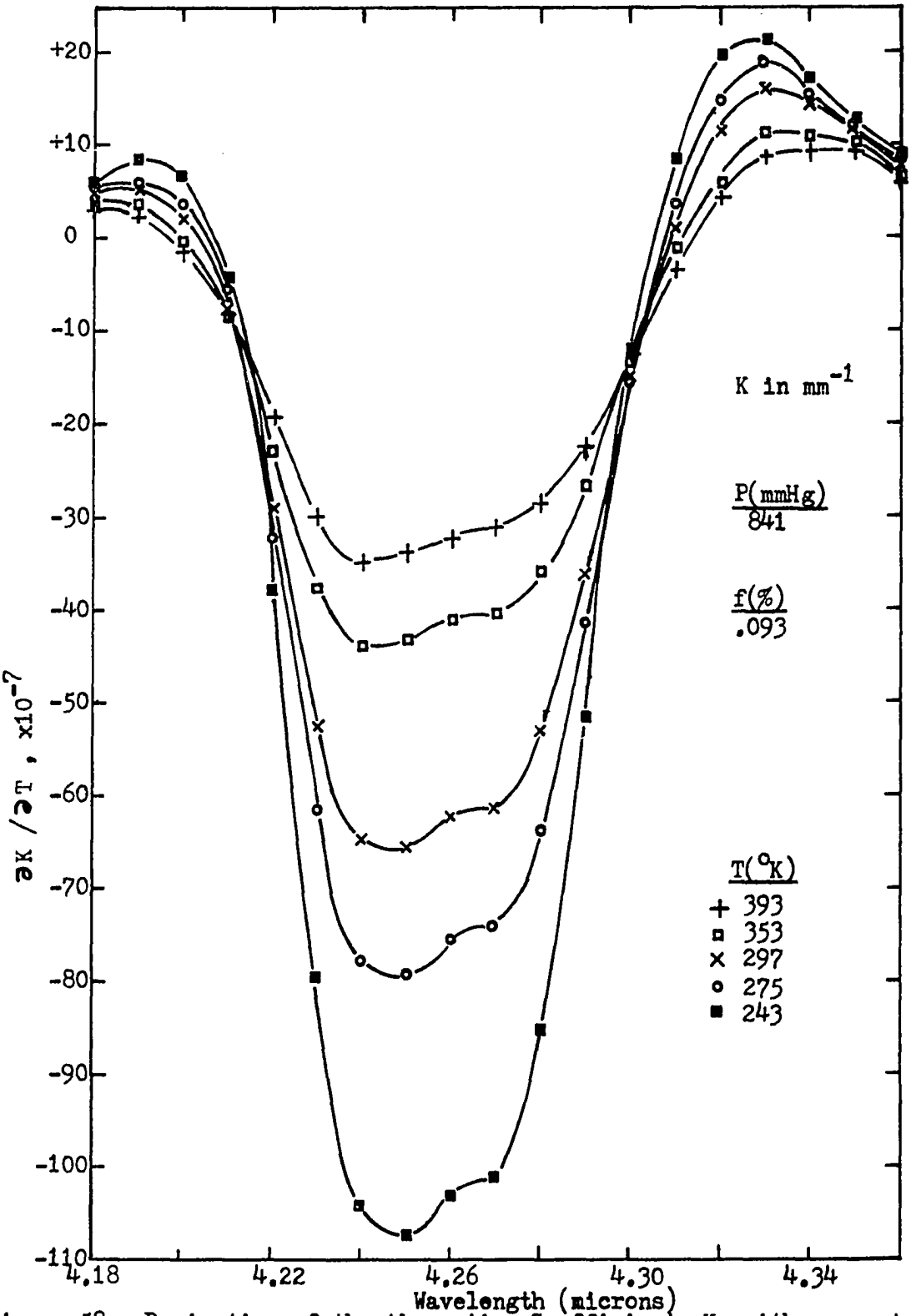

Figure 58 . Derivative of the Absorption Coefficient, K, with respect to Temperature versus Wavelength with Temperature as a Parameter.

$\lambda = 4.30$. The major portion of the curves is negative, although the intermediate-wing regions do go slightly positive. The quality of this derivative information is felt to be excellent considering the number of points used.

The temperature derivatives were calculated and fit using the expression given by

$$\frac{\partial K}{\partial T} = -\frac{K}{T}\left[3/4 + \frac{A(2)}{T}\right] \quad . \tag{110}$$

Figure 59 can be used to give second derivative information. The derivative of K with respect to T is plotted versus Pressure, P, for various wavelengths and the maximum and minimum concentrations. The derivatives is quite linear with pressure for all except one of the curves (which itself is quite close to zero) for these conditions.

b. CO_2 Concentration. These derivatives are perhaps the most difficult to calculate because there were only four concentration points. However, the f dependence of K is reasonably strong and simple; for example, one does not expect any reversals of the f dependence over the band.

The results are expected to follow the ill defined region absorption coefficient K_{IDR} defined in equation (106) in Section IV. Defining $1 \equiv A(2)$, the equation used to fit the mean value absorption coefficient was

$$K_{I.D.R.} = A(1)f^{A(2)} \quad . \tag{111}$$

P,T and λ were held constant for each least squares fit. A(2) is expected to vary in the vicinity of 0.5 and 1.0 being nearer to 1.0 in the

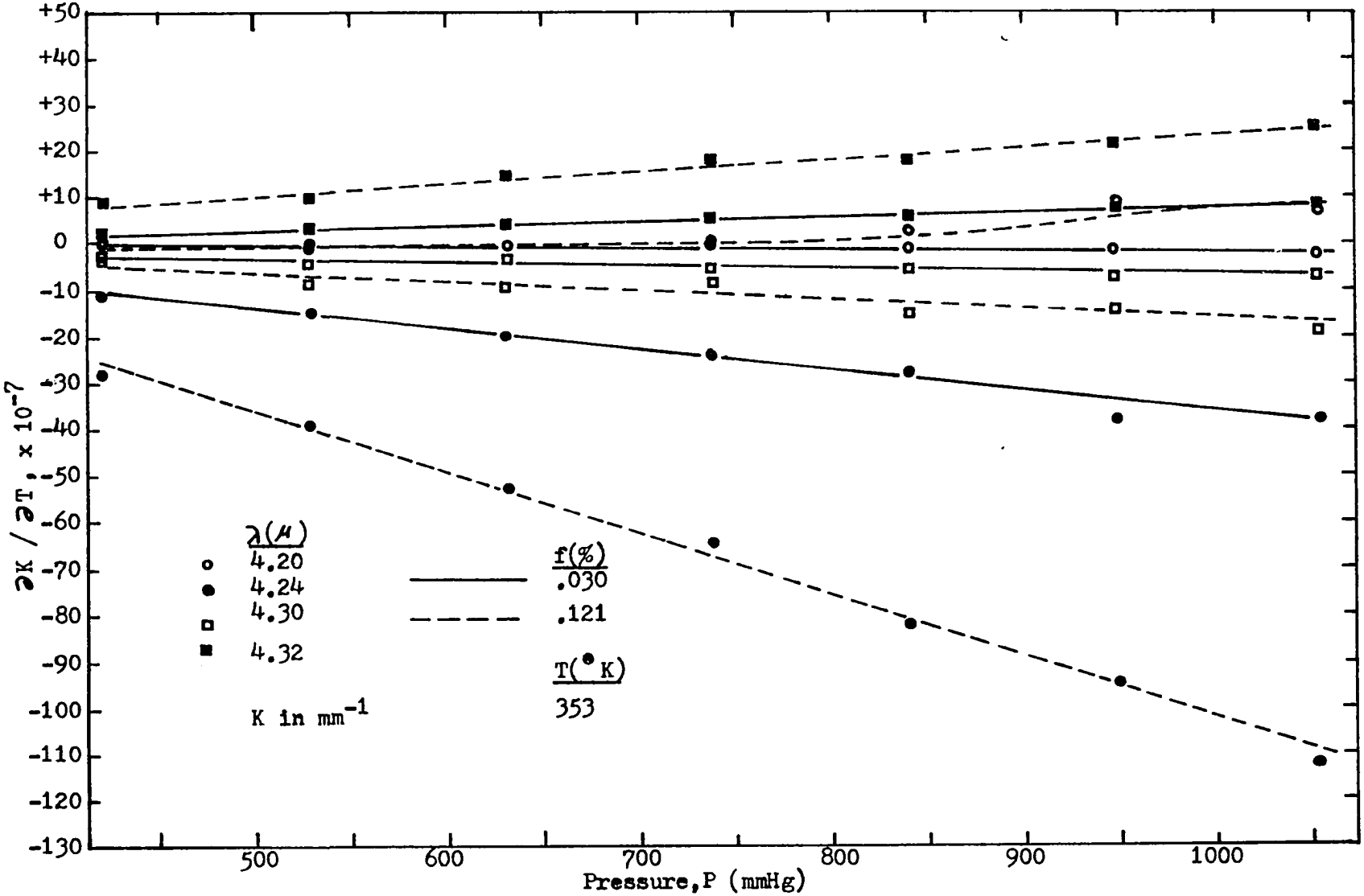

Figure 59 . Derivative of the Absorption Coefficient, K, with respect to Temperature versus Pressure with Wavelength and CO_2 Concentration as Parameters.

weak line approximation region of validity and near to 0.5 in the strong line approximation region of validity.

Figure 60 is a plot of the CO_2 concentration coefficient A(2) versus wavelength with P as a parameter. This shows a slight though not distinct increase in A(2) with P. This curve (when viewed with other similar plots) shows two separate minima as a function of λ near the maxima in the P and R branches; this indicates that these regions are closer to a near strong line condition than the surrounding points. The R branch minima is deeper than the P branch minima; this is as expected since the R branch lines are deeper than the P branch lines. There is a wide peak near the zero gap indicating that the data is slightly closer to the weak line approximation and the wing region coefficients are on the rise as one goes into the wings. This is also as predicted. The overall average value for A(2) or 1 is about 0.85; this is typical of the ill defined region.

The temperature dependence of this coefficient is displayed in Figure 61; again as in the P case, the dependence is not strong. However, a slight increase in the value of A(2) is indicated with increasing T. This is an indication that the lines are smoothing out and moving toward the weak line approximation with increasing T.

The P and T dependence lies primarily in A(1). The dependence of A(1) on P is positive and strong through the band especially in the core. The A(1) - T dependence shows the usual crossover points.

The derivatives are easily found; they are given by

$$\partial K / \partial f = A(1)\, A(2)\, f^{(A(2) - 1)}. \qquad (112)$$

Since A(2) is almost always less than unity, the coefficient of

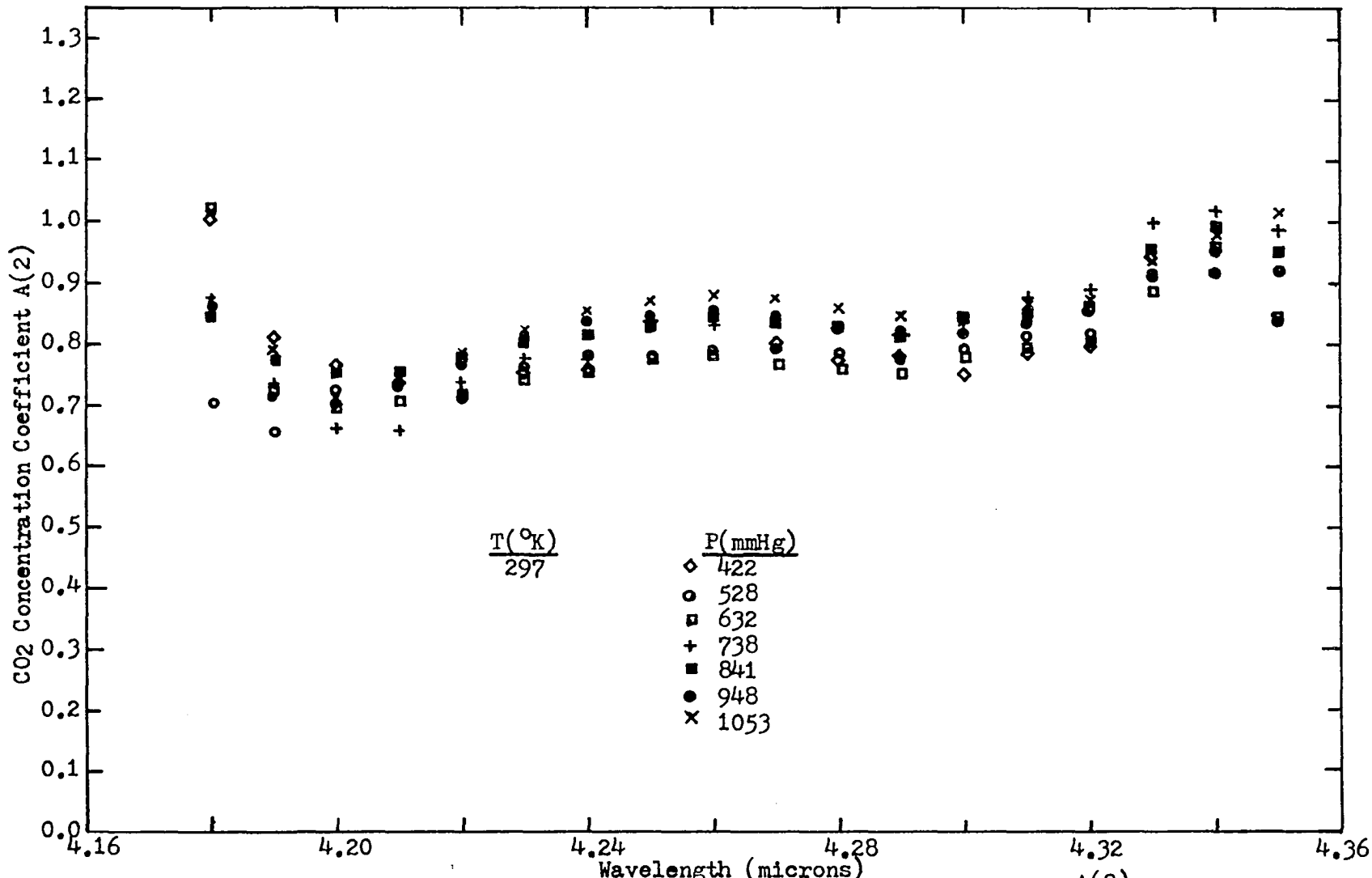

Figure 60 . CO_2 Concentration Coefficient A(2) versus Wavelength Using $K = A(1)f^{A(2)}$ with P as a Parameter.

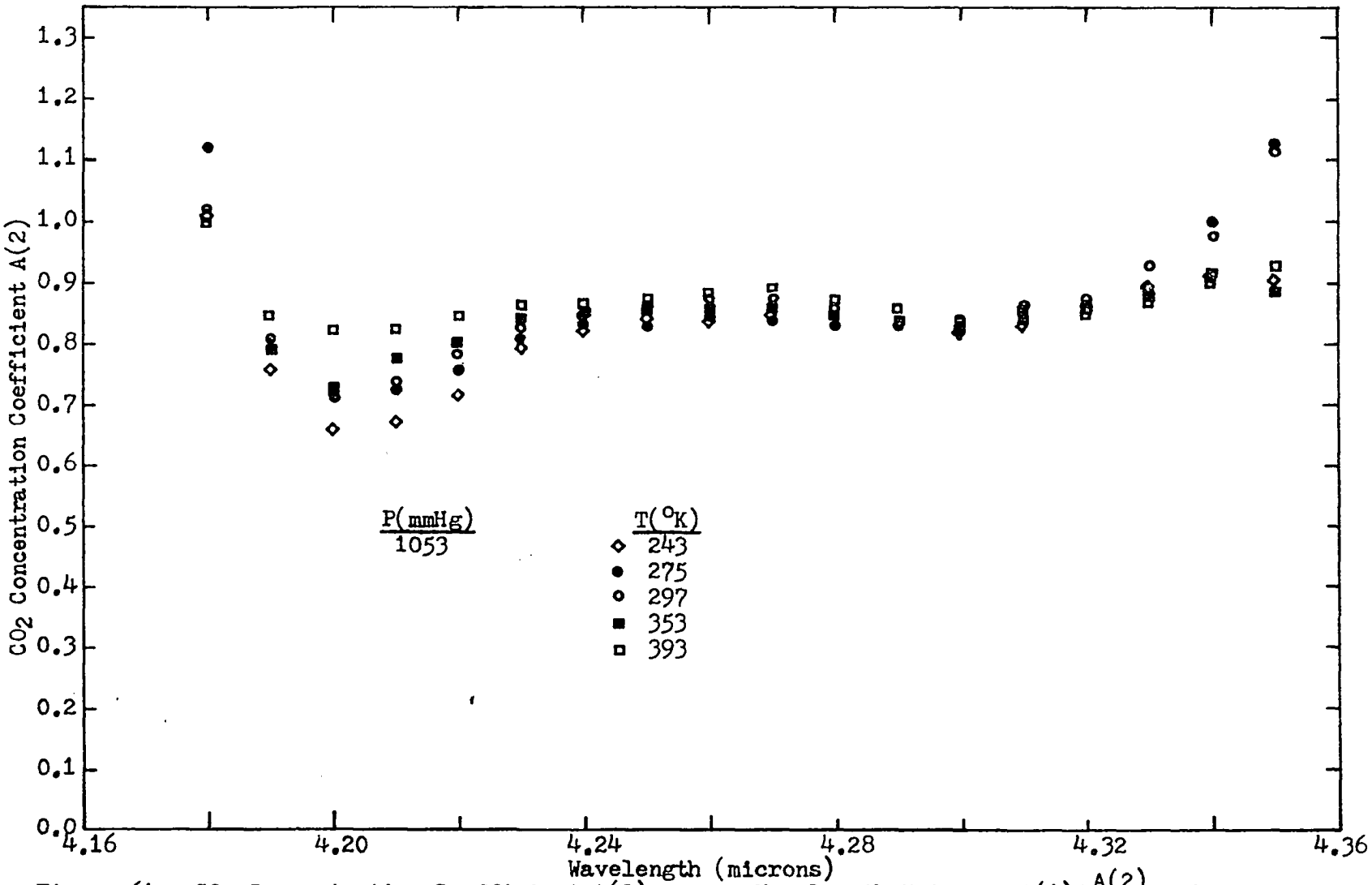

Figure 61 . CO_2 Concentration Coefficient A(2) versus Wavelength Using $K = A(1)f^{A(2)}$ with T as a Parameter.

f is negative but generally small. Figure 62 is an example of the derivative of K with respect to f with f as a parameter. The dependence on f is small and negative over the band. This derivative information is very good except in the far wings. The derivative of K with respect to f with P and T as parameter is shown in Figure 63 and 64. Note the existence of the crossover regions in Figure 64.

These derivatives are always positive. Also they are proportional to the derivative of K with respect to the partial pressure of the absorber, p.

c. Total Pressure. These derivatives are quite important since they contain the information concerning the change in the number of absorbers and the change in the pressure broadening; remember, the P derivative is evaluated at constant f not constant p.

The P dependence of the absorption coefficient is similar to the f dependence, although the P dependence is somewhat stronger than the f dependence.

The results are again expected to follow the ill defined region absorption coefficient K_{IDR} defined in Section IV. Using $1 + m = A(2)$, the equation used to fit the mean value absorption coefficient to P is given by

$$K_{IDR} = A(1)\ P^{A(2)} \qquad (113)$$

The absorption coefficient must equal zero when P equals zero as it must when f equals zero. The exponent A(2) is expected to vary within the range $\frac{1}{2}$ to 3/2 in a somewhat ill defined manner. The P (constant f) dependence of the strong line approximation absorption coefficient is

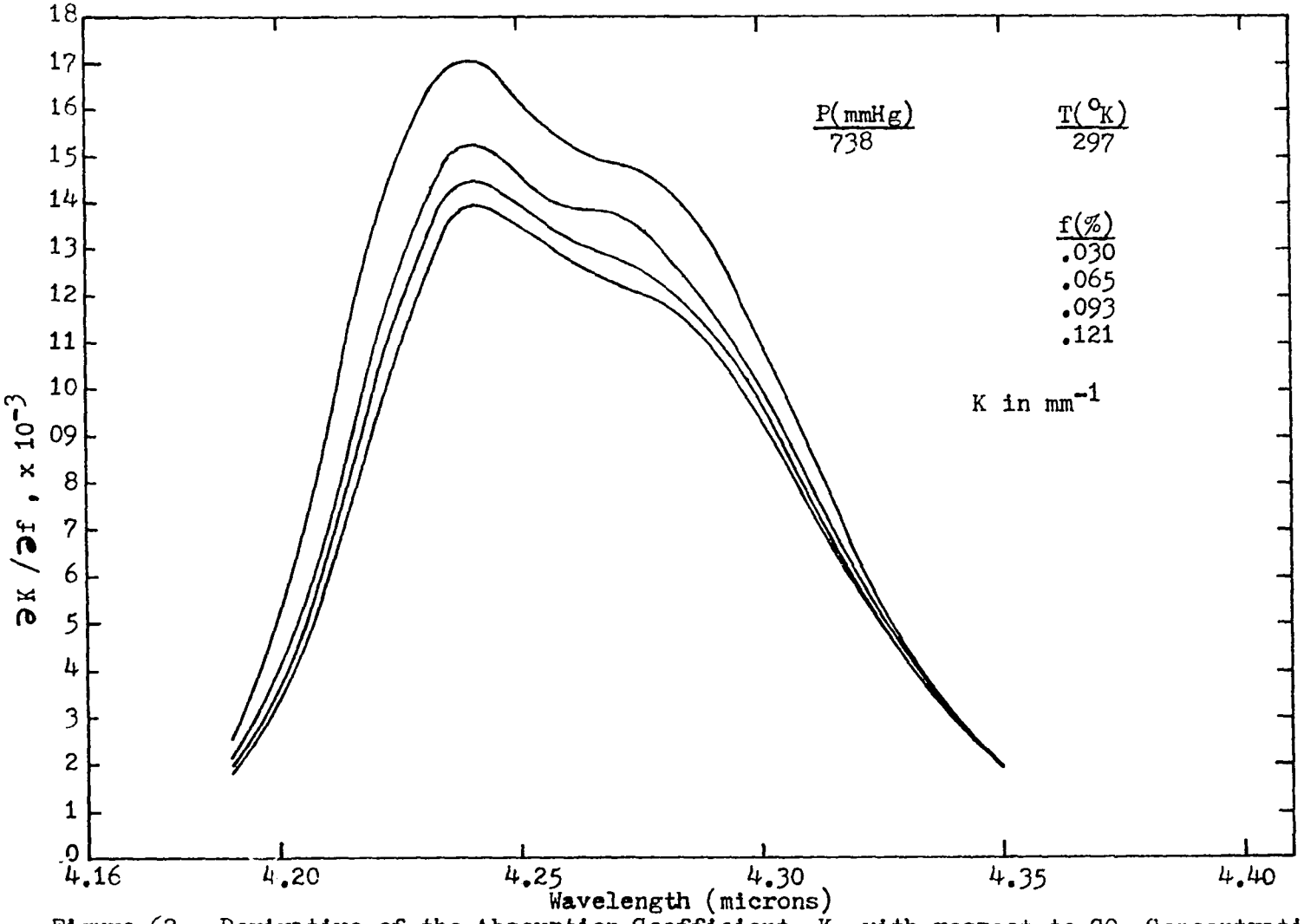

Figure 62 . Derivative of the Absorption Coefficient ,K, with respect to CO_2 Concentration, f, with f as a Parameter, versus Wavelength.

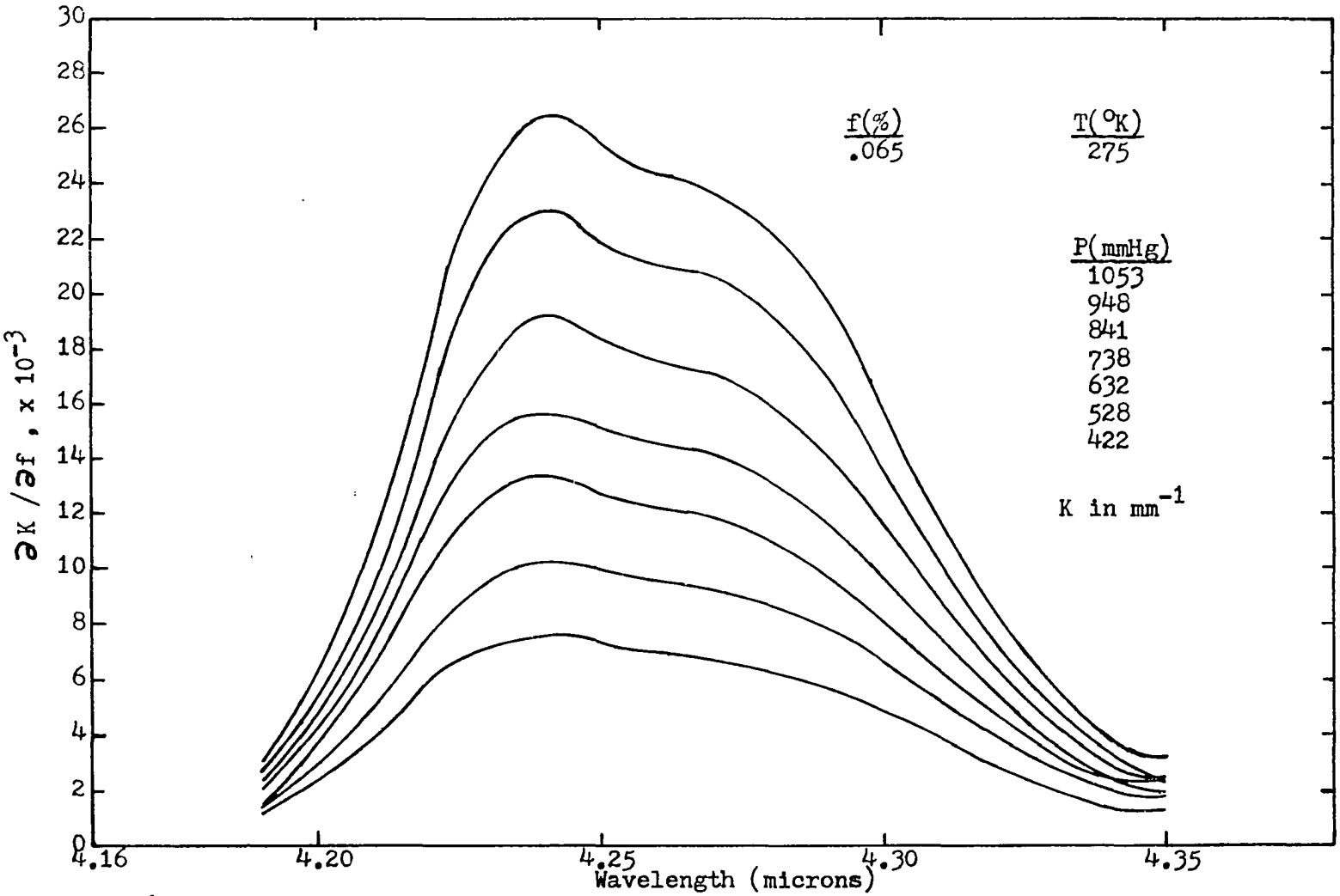

Figure 63 . Derivative of the Absorption Coefficient, K, with respect to f versus Wavelength with P as a Parameter.

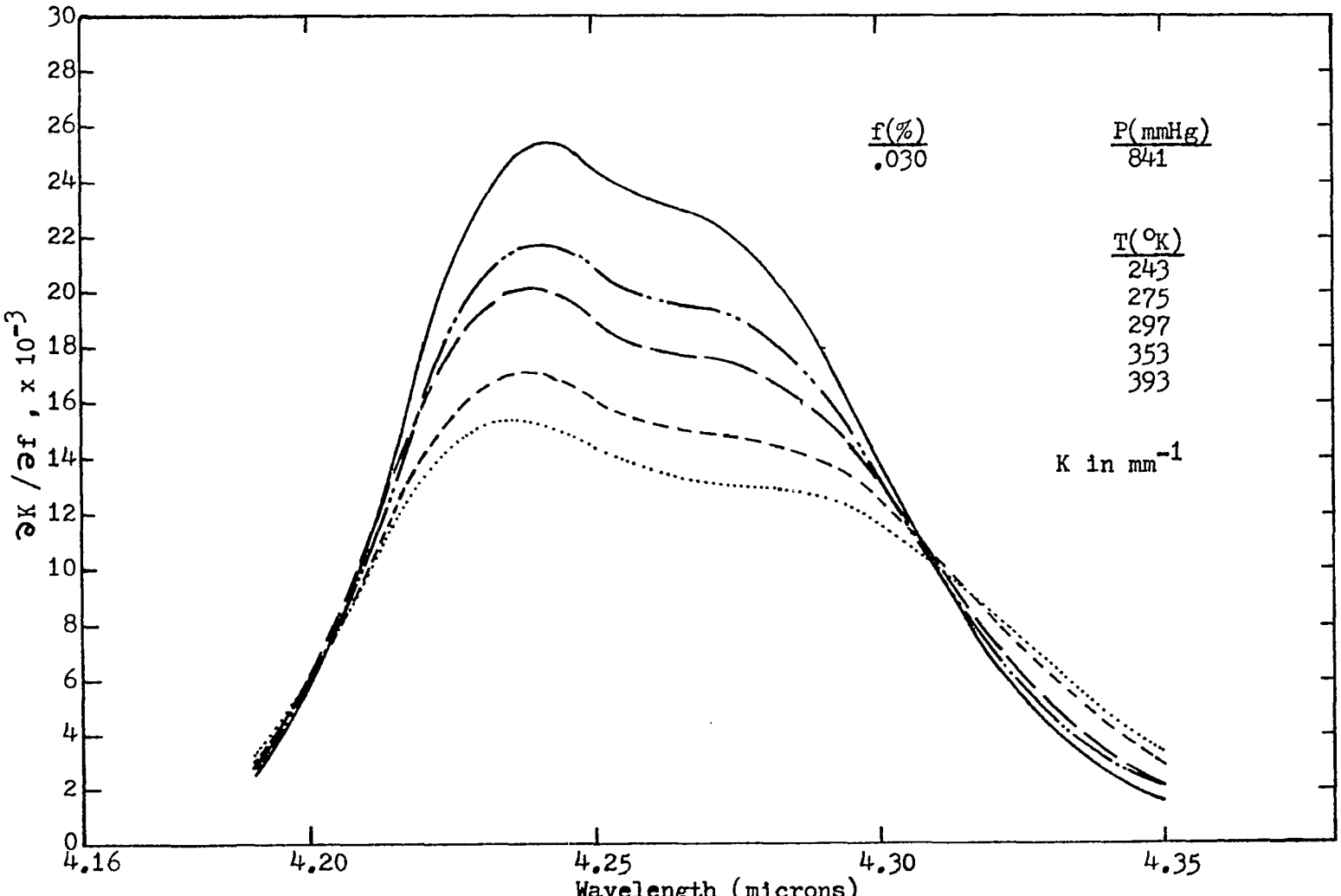

Figure 64 . Derivative of the Absorption Coefficient, K, with respect to CO_2 Concentration, f versus Wavelength with T as a Parameter.

expected to be the same as that of the weak line approximation absorption coefficient (see Basis for Analysis Section).

Figure 65 is a plot of the Total Pressure Coefficient A(2) versus λ with T as a parameter. This figure indicates that A(2) or (1 + m) is not constant over the 4.3 micron band. This may be an indication that neither the strong nor the weak line approximation is valid in this case; rather the ill defined region, within which l and m vary in an undefined way, is a better basis for analysis. A(2) reaches a minimum of about 1.0 in the low wavelength wing and a minimum of about .95 in the high wavelength side. The A(2) versus λ curve then rises on both sides to reach two "soft" maxima near the P and R branch maxima and then decreases just slightly to reach a minimum near the zero gap at 4.26 microns.

The T dependence is positive and quite noticeable in the core regions. There is a possible crossover point near λ = 4.31 visible in this figure. We estimate the average maximum value of A(2) to be on the order of 1.25 and the minimum to be about .90.

Figure 66 is a plot of the Total Pressure Coefficient A(2) versus λ with f as a parameter. There is no clear dependence of A(2) on f seen in this figure. The general dependence of A(2) on λ is as in Figure 65.

The dependence of A(l) on f and T is substantial. There are two major peaks in the A(l) versus λ curves near the P and R branch maxima; the R branch maximum is the strongest at low temperatures. There is a general increase in A(l) with f.

Figure 67 is a plot of the derivative of K with respect to P

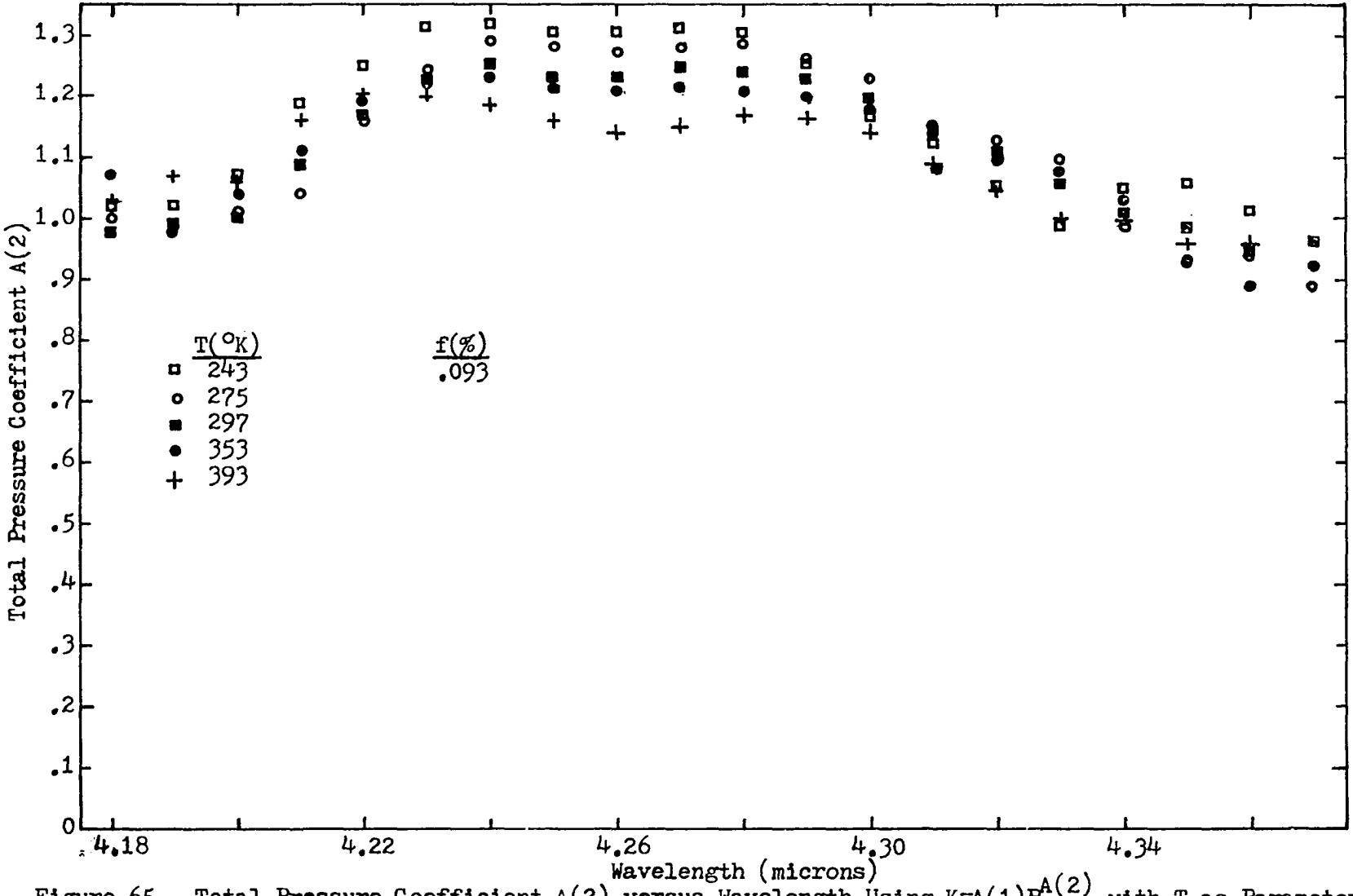

Figure 65 . Total Pressure Coefficient A(2) versus Wavelength Using $K=A(1)P^{A(2)}$, with T as Parameter.

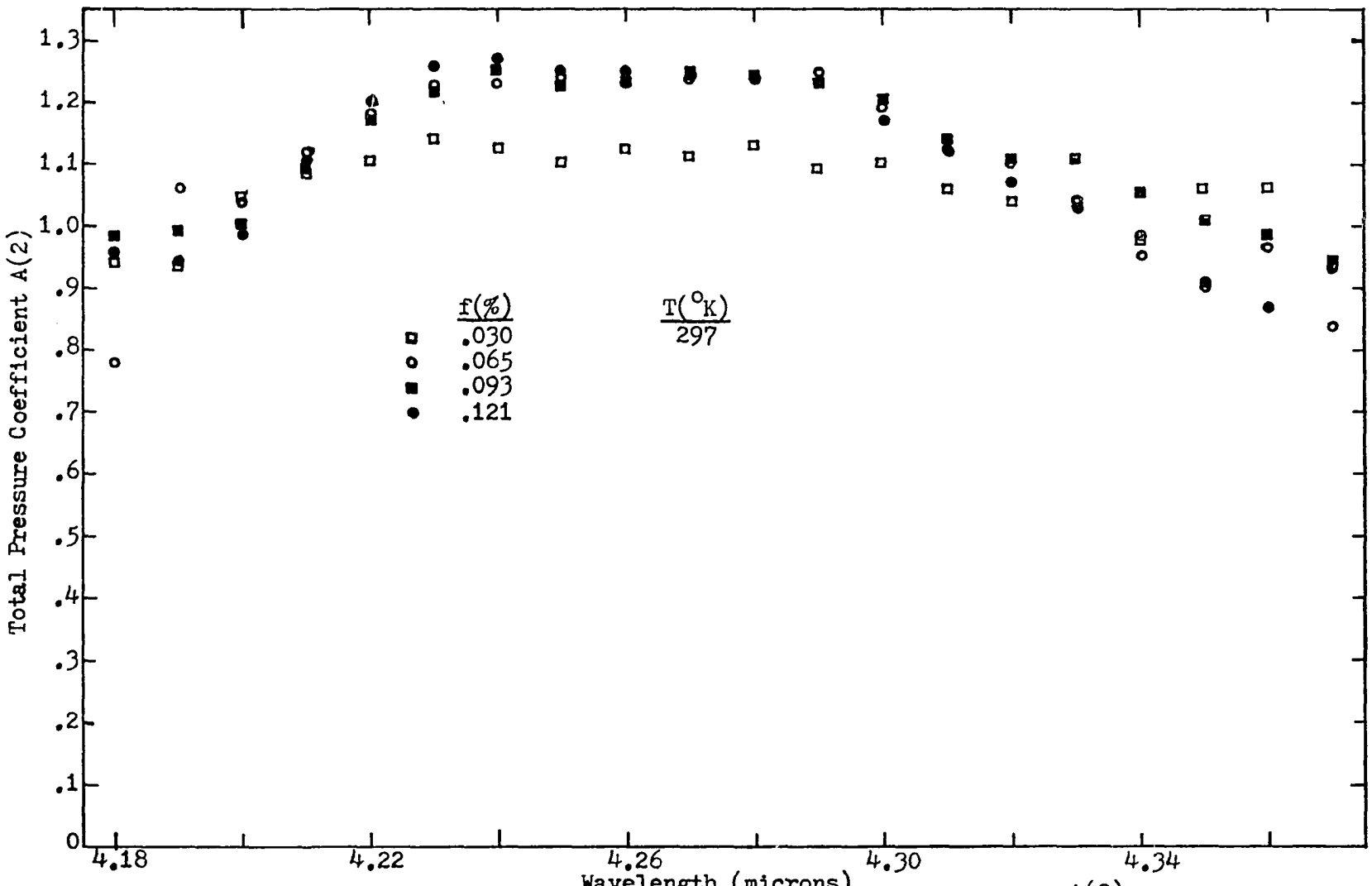

Figure 66 . Total Pressure Coefficient A(2) versus Wavelength Using $K=A(1)P^{A(2)}$, with f as Parameter.

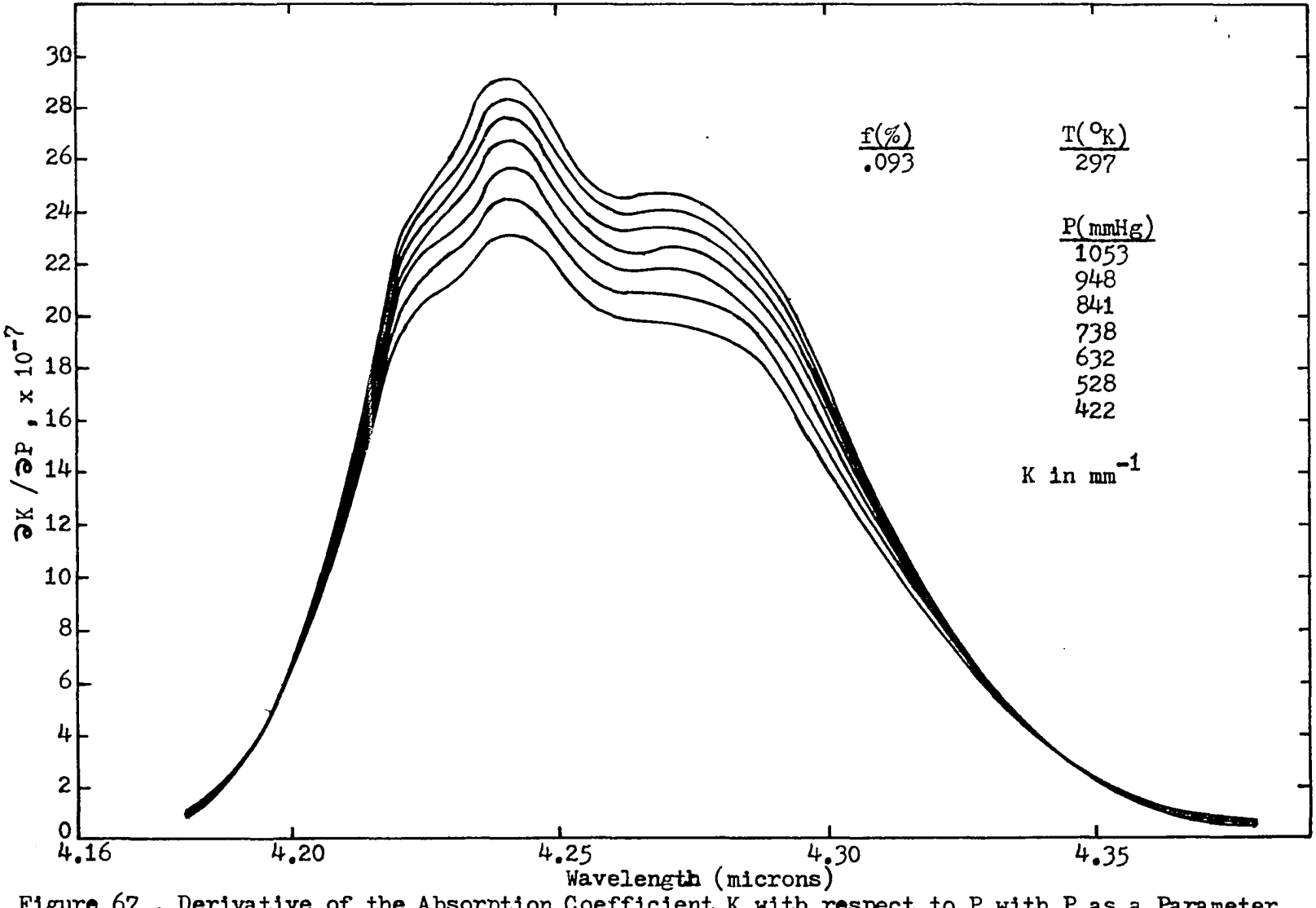

Figure 67 . Derivative of the Absorption Coefficient K with respect to P with P as a Parameter, versus Wavelength.

versus λ with P as a parameter. This figure shows a small positive dependence of the pressure derivative on P in the core and gives an indication of pressure crossover points at about 4.20 and 4.35 microns. The crossovers result from the fact that the exponents are slightly less than unity in the wing regions. The pressure dependence in the wings is very small.

Figures 68 and 69 are plots of the pressure derivative versus λ with T and f as parameters. The temperature crossover points are evident in Figure 68 at 4.20 and 4.315 microns. The dependence on f is strong and positive throughout the band.

The pressure derivative is positive for all combinations of the parameters. Figure 70 is a plot of the pressure derivative versus temperature for four different wavelengths. This type of plot will yield second derivative information. This figure should be compared with Figure 59 which contains a plot of the temperature derivative versus pressure.

J. Comparison of δK with δK_c as Calculated from the Mean Value Derivatives.

Referring back to the Basis for analysis Section, we see that δK has been characterized by the linear terms in a Taylor series expansion. In order to show that this is a valid representation for δK as measured in this experiment, we shall now calculate δK using the mean value absorption coefficient derivatives. We shall restrict the calculations to derivatives evaluated at $\bar{P}$, $\bar{T}$, and $\bar{f}$ (instead of $\bar{P}$, $\bar{T}$,$\bar{p}$); this allows us to use equation (101) in the Basis for Analysis Section given by

$$\delta K_c = \left[\frac{\partial K}{\partial P}\bigg|_{\bar{P},\bar{T},\bar{f}} + \frac{\partial K}{\partial T}\bigg|_{\bar{P},\bar{T},\bar{f}} \frac{\gamma-1}{\gamma} \frac{T}{P} \right] \delta P \quad . \tag{114}$$

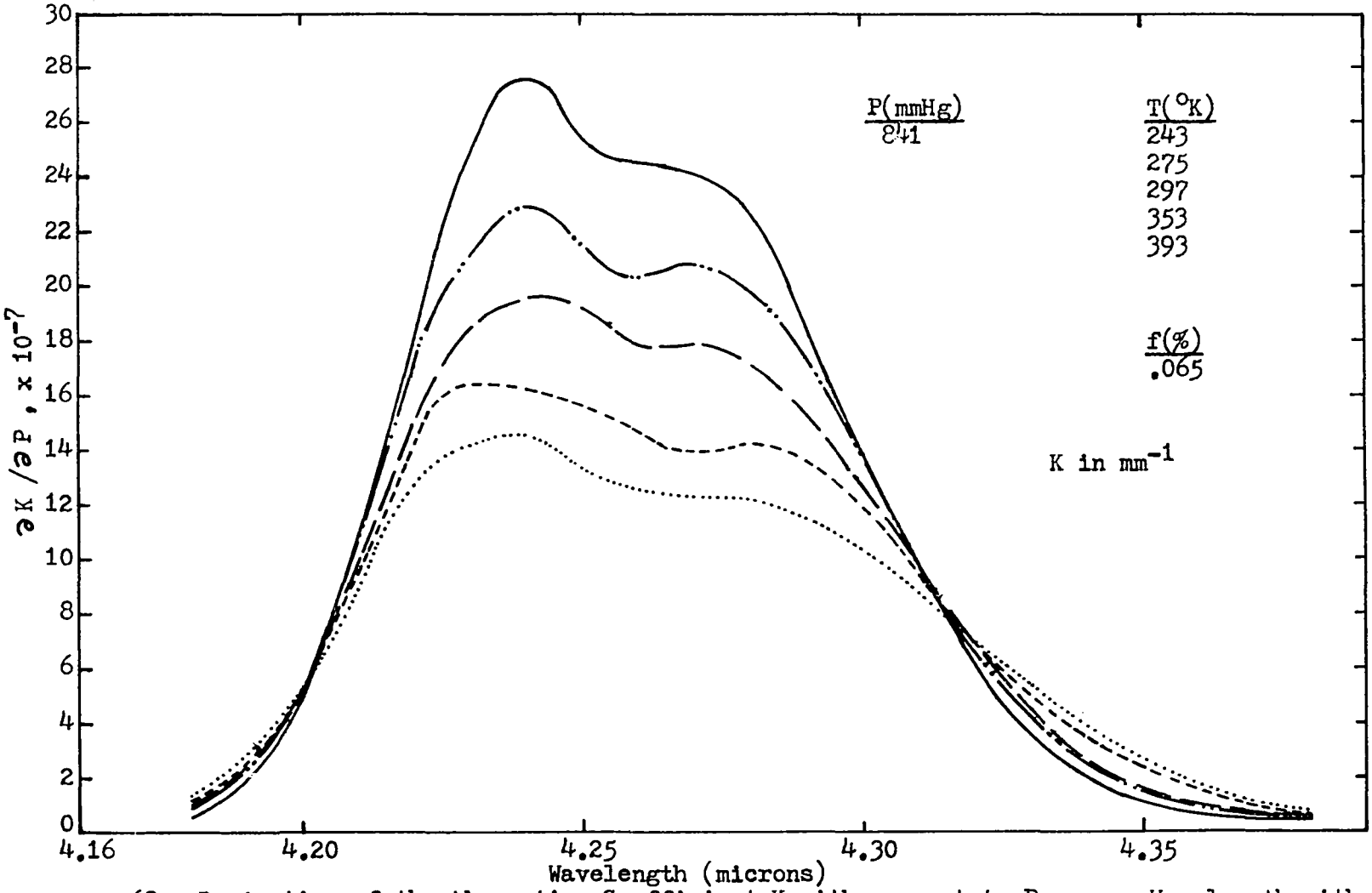

Figure 68 . Derivative of the Absorption Coefficient K with respect to P versus Wavelength with T as a Parameter.

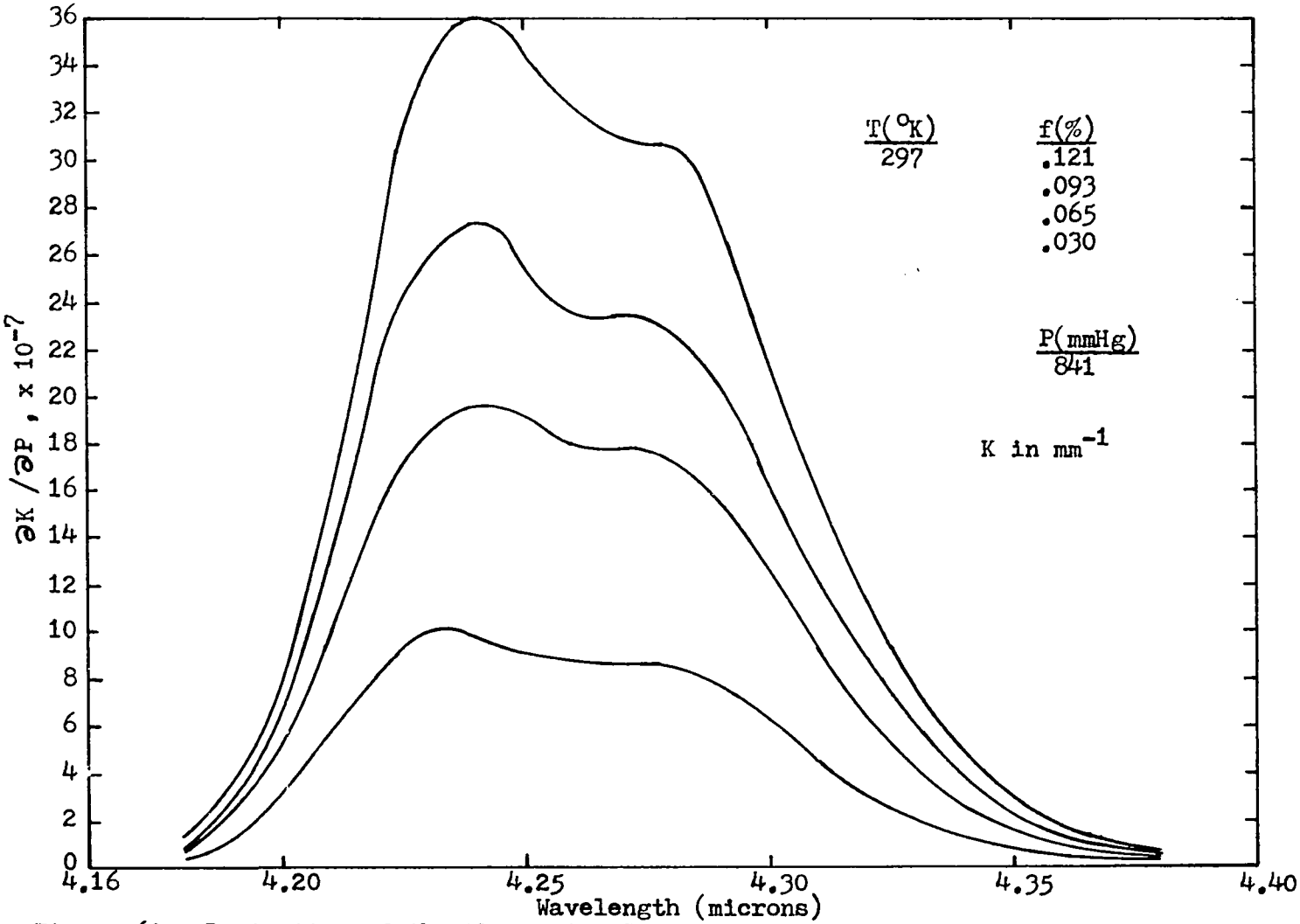

Figure 69 . Derivative of the Absorption Coefficient K with respect to P versus Wavelength with f as a parameter.

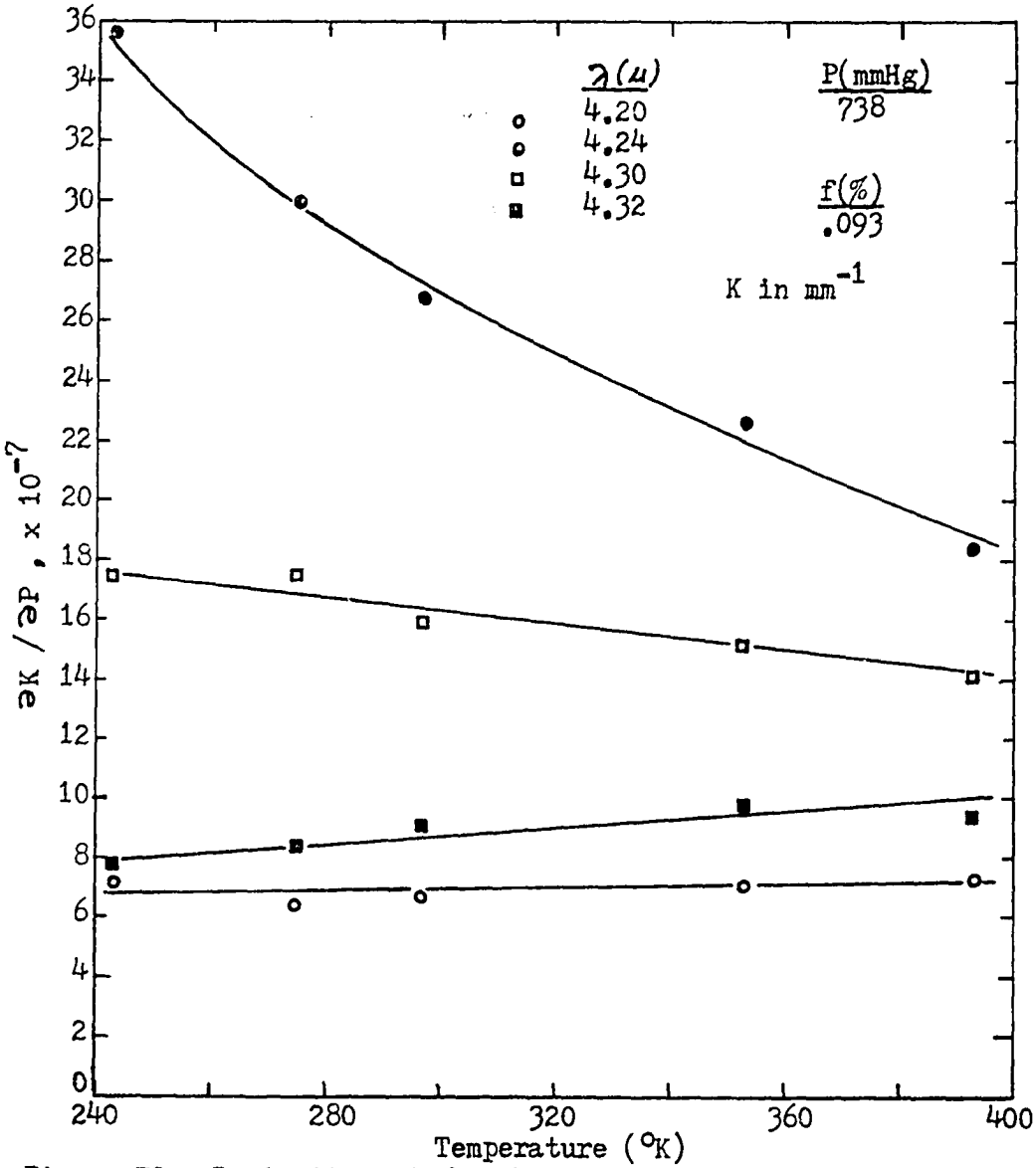

Figure 70 . Derivative of the Absorption Coefficient K with respect to P versus Temperature

The temperature derivative does go negative in the core regions of the band, however the factor $\frac{(\gamma - 1)}{\gamma} \frac{T}{P}$ maintains the temperature derivative term smaller than the pressure derivative term; therefore δK_c is always positive. More importantly, the function does not change sign.

An initial attempt was made to fit the absorption coefficient as a function of P to $K = A(1)' + A(2)' P$, where therefore the derivative was simply $A(2)$ independent of P. When this was used in the above equation δK_c was in error relative to δK (measured) in the core regions by approximately 25%; the higher P data having the largest error. This error was reduced considerably when the pressure data was fit to the correct nonlinear pressure function $K = A(1) P^{A(2)}$.

The correct pressure derivatives and the strong line approximation temperature derivatives (as calculated in Section VI.H.) were therefore substituted into the above equation for the given conditions of P, T, and f, for $\gamma = 4/3$ and the constant value of δP given by 5.68 mm Hg.

The agreement between δK_c and δK was very good, especially in the core regions.

An average relative error for the 0.30%, 841 mm Hg, 297° K data is approximately 5% over the band except at the endpoints near 4.16 and 4.40 microns where the least square fits had the largest variances.

An average relative error for all the 4.3 micron data is on the order of 5 to 10 percent. There were no substantial trends in the sign of the errors. We therefore conclude that the δK formulation given as

the linear terms in a Taylor series expansion, is valid for the conditions chosen in our experiment.

L. Magnetic Tape Data.

The magnetic tape data contains the recordings of the instantaneous intensity signals for α and β traces. Several typical runs were recorded on magnetic tape, digitized, and then processed, however we shall give the results of only one such series which we shall refer to as OU-188. An analysis and a comparison of these results with the LIA results is made and then we take a look at the fluctuation structure for the simple case of a near harmonic wave.

The OU-188 data was processed in a manner described in the Measurements Section and the Data Section. The OU-188 data was recorded continuously, at a slow scan rate, across the 4.3 micron region. The conditions were approximately room temperature and 1 atmosphere with .121% CO_2; δP was a constant nominal value.

1. Single Point Correlation Analysis. Figure 71 is a plot of the cross correlation of the fluctuating intensity δI and the fluctuating pressure δP normalized to the standard deviation of the pressure signal or the rms value of the fluctuating pressure signal. The factor .0370 is a gain factor which puts the recorded signal at the optical detector. Each of the points in the figure represents one piecewise correlation for a piecelength of 10 seconds. A single point in the correlation is used, namely that value at $\tau = +.064$ seconds where τ is the time lag. The .064 second point corresponds to one period of the 15.1 c / s information that we are interested in. The solid line represents the LIA results which was recorded simultaneously.

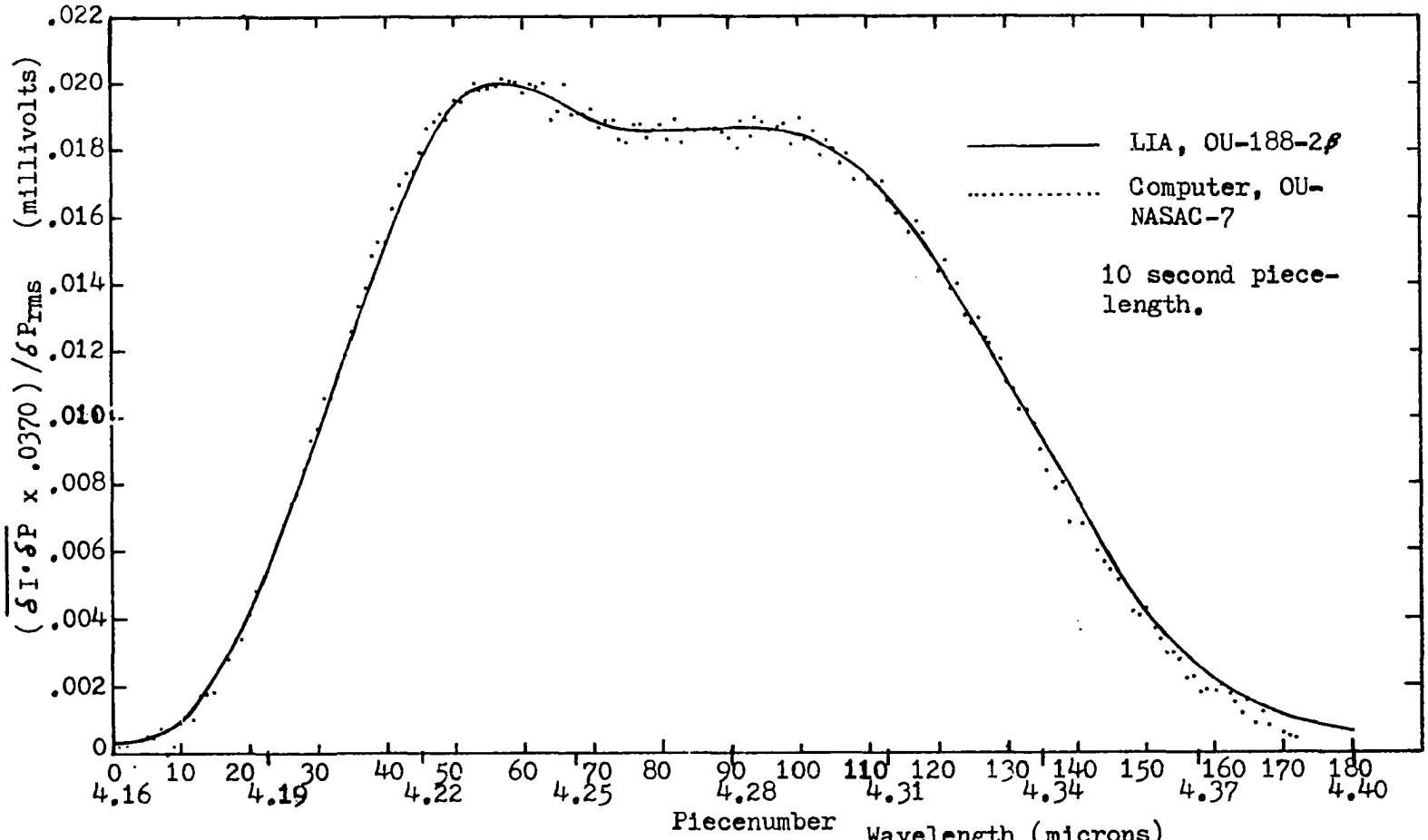

Figure 71 . Crosscorrelation at τ= +.064 seconds Normalized by δP_{rms} and Compared to LIA Result.

The abscissa contains the piece number which identifies the particular piecewise correlation and the actual wavelength position in the 4.3 micron CO_2 band. The normalization is necessary to compare these results with the LIA results (see Equation 91 in the Measurements Section).

The figure shows that the agreement between the two measurements is excellent. Therefore the LIA measurements are identical to a reduced form of the magnetic tape measurements. Still, one must remember that even though we have compared the magnetic tape results to the LIA results, the magnetic tape data contains more general information than does the LIA data.

The crosscorrelation result is of further interest because of its relationship to the turbulence factor, Q_p. The temporal crosscorrelation $\overline{\delta I \cdot \delta P}$ is proportional to the temporal crosscorrelation $\overline{\delta K \cdot \delta P}$ (through the relationship $\delta K = - \delta I / \gamma I$) which is the integrand of the spatial correlation in Q_p. In the special case where the integrand is independent of position along the path, the turbulence factor reduces to the temporal $\delta I - \delta P$ crosscorrelation times 1 divided by I. This condition occurs when the structure of the fluctuation (the wavelength of the acoustic excitation) in the single beam experiment is much greater than the length of the cell, therefore causing a uniform homogeneous path across the cell at any given instant of time. Of course the two paths are now equivalent. The shape of the $\overline{\delta K \cdot \delta P}$ correlation is the same as that shown in the previous δK figures; the magnitude is found from the separate magnitudes of δK and δP. The quantity δP_{rms} is approximately constant for all piecewise correlations and given by .334 for OU-188-2B.

We have considered of course only a single time lag value; a further analysis as a function of τ is in VI, L 2.

It is also of interest to consider the autocorrelation of the optical signal, δI. This result is very noisy especially at τ = zero since the two channels have identical signal plus noise. In the crossed beam experiment, the two channels would correspond to two different beams where a good deal of the noise is then expected to be statistically independent.

Although the autocorrelation $\overline{\delta I \cdot \delta I}$ at τ = zero results in a major portion of the signal being buried in the noise, the autocorrelation at τ = .064 (the first signal maximum) has a noise level which is reduced sufficiently to allow for a reasonable recording of the square root of the autocorrelation for δI.

Figure 72 is a plot of the square root of the autocorrelation (times the same gain factor that appears in the result shown in Figure 71) at the single point τ = + .064 versus wavelength or piece-number. Each point corresponds to a single piecewise correlation with a 10 second piecelength. The solid curve again represents the LIA result. This time the piecewise auto-correlations are slightly greater than the LIA result especially in the wing. This is due to the noise level. The increase is predictable by expanding the square root of the product of the sum of the signal and the noise, with itself. The negative points were included as such only to give an indication of the true scatter in the data points.

This result is of further interest because it represents a special case of the function we have referred to as $G(\vec{x}, \tau)$ in the theory

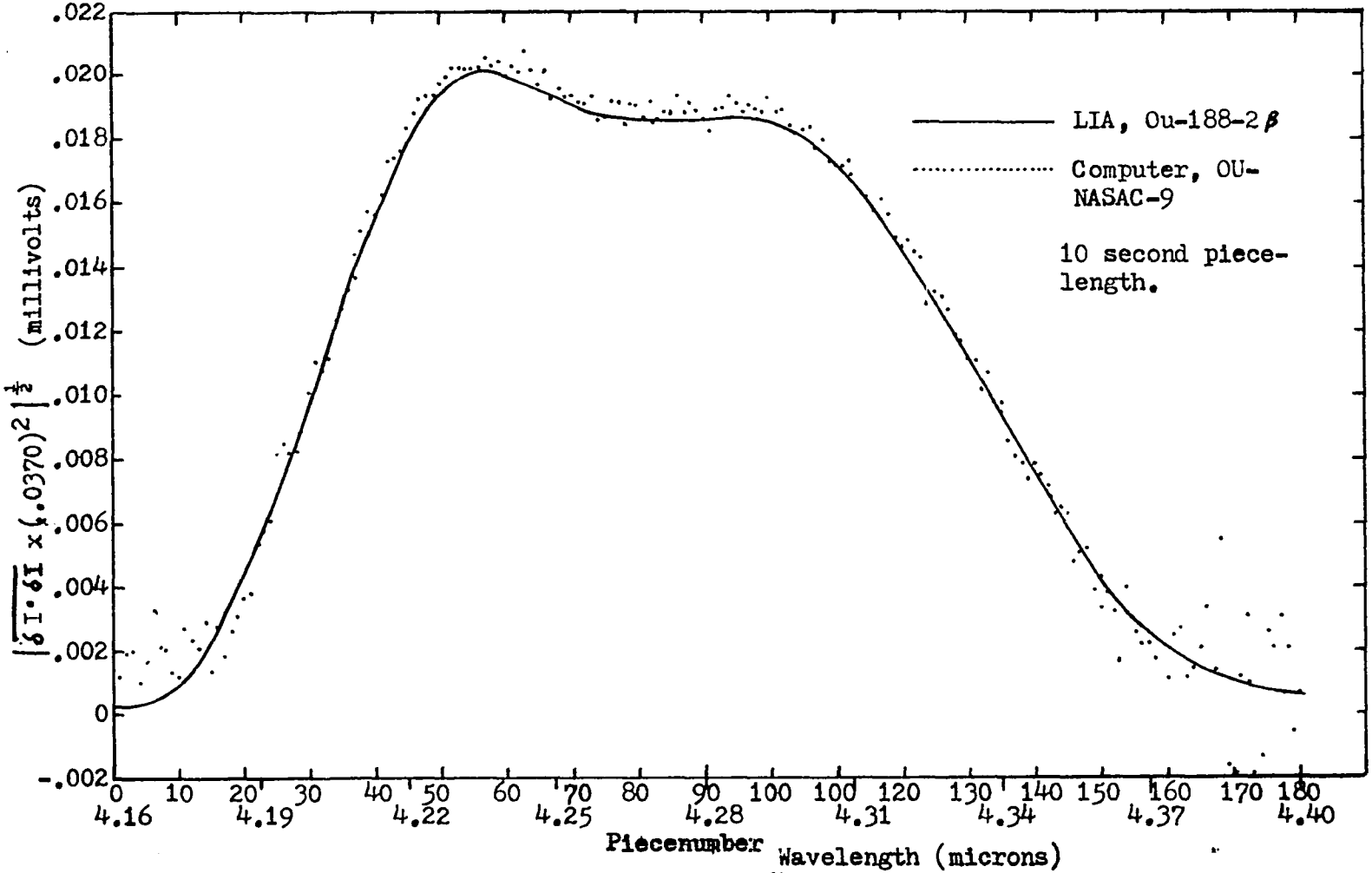

Figure 72 . Square Root of Autocorrelation at τ = .064 seconds Compared to LIA Result.

section. This function represents the temporal cross correlation between the fluctuating intensities of the two beams. In our case Beam #1 is identically equal to Beam #2, in which case there is no signal to noise enhancement. Also all the signal fluctuations in these two beams are now common; in other words, there are no uncorrelated portions which would ordinarily tend to average out. Therefore this special case represents a maximum value type of measurement relative to the crossed beam system. Nonetheless the result does give an indication of the general expected form of the related crossed beam measurements. A further analysis in terms of τ is given in the next subsection.

Figure 73 is a plot of the cross correlation of I and k normalized by the standard deviation of k. k represents the somewhat "artificial" chopped reference signal which is approximately constant in amplitude and synchronous with the I signal. The corresponding gain factor is not included in this plot. The single point $\tau = .00560$ corresponds approximately to the third signal maximum in the 340 c / s wave that we are interested in. Each point corresponds to a 3.5 second piecelength.

The correspoinding δK spectrum can easily be formed from the magnetic tape data. Actually the δK spectrum does not require recording the I and δI spectrum separately and then combining their results; it would be more practical to run the chopper and speaker simultaneously and record the resultant signal on one channel of the tape recorder only.

2. Fluctuation Structure. Since the signals that are recorded on magnetic tape are instantaneous signals in the form of a

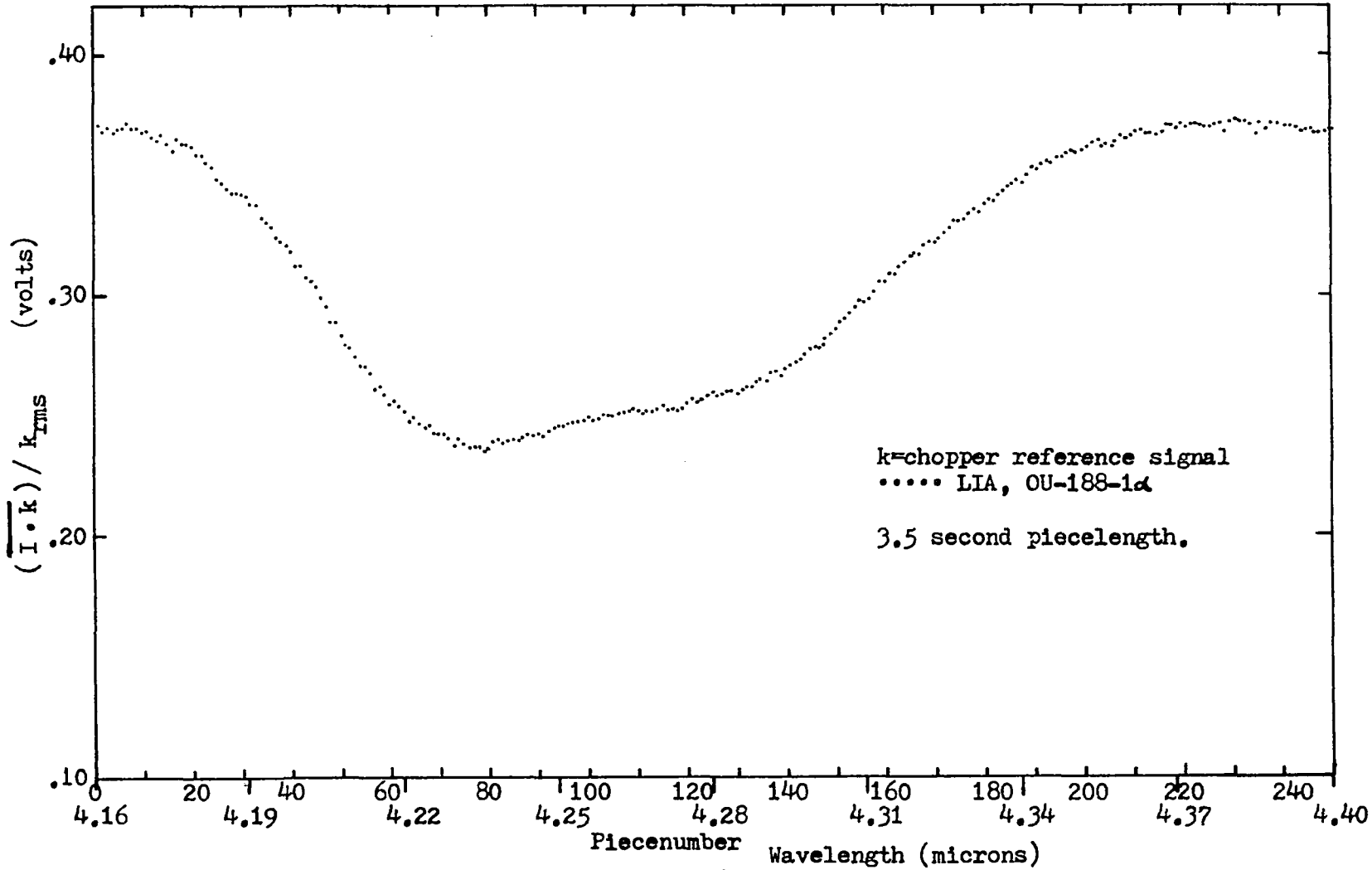

Figure 73 . Crosscorrelation of I and k at τ = -.00560 seconds Normalized by k_{rms}.

time series, it is possible to determine the structure of the fluctuations that exist in the cell. In our experiments the fluctuations used were nearly sinusoidal signals; this greatly simplified the analysis. It is correspondingly noteworthy that the crosscorrelation method is in general a very powerful tool for detecting periodic (for i.e. sinusoidal) signals imbedded in noise; this is our situation.

The fluctuation structure is analyzed in this case, by fourier transforming the auto-correlation of the fluctuating intensity signal; this yields the power spectral density function. The power spectral density function $\mathcal{P}(f)$ is given in its limiting form by

$$\mathcal{P}(f) = \int_{-\infty}^{+\infty} \varphi_{\delta I \delta I}(\tau) \exp -2\pi f \tau \, d\tau \ , \qquad (115)$$

where φ is the auto-correlation function. This function determines the frequency content of the fluctuating signal and can therefore be used to determine the fluctuation structure. For example, a delta function type of function indicates that the fluctuation is harmonic or sinusoidal.

Figure 74 is an example of an accumulative auto-correlation with its corresponding standard error for the total wavelength interval from 4.24 to 4.28 microns. It represents the cumulative effects of 30 ten second piecewise auto-correlations for the 300 second interval in the core of the 4.3 micron band. Since it is in the core region, the signal to noise is expected to be pretty good relative to the length of the pieces chosen. The basic waveform of the correlation function is sinusoidal in nature with a period of about .066 seconds. The larger peak at zero time delay corresponds to the effects of noise. We have

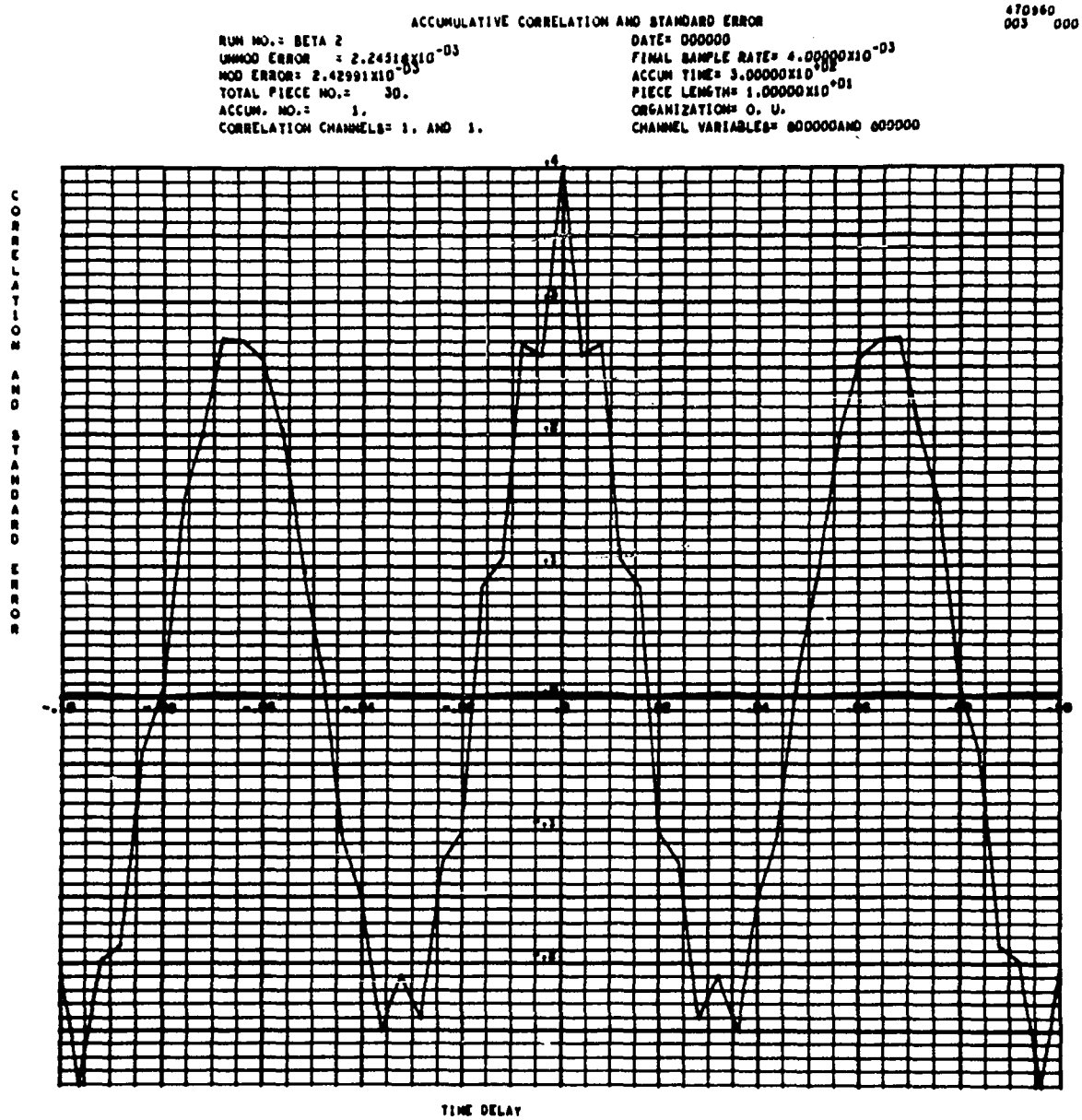

Figure 24 . Computer Printed Plot of the Accumulative Autocorrelation Function of δI.

included in this figure a time delay of only $\pm$ 0.10 seconds which is about one and one half times the period of the fundamental of interest.

Figure 75 shows the gain or power spectral density function for this correlation. One sees from the figure that there is a dominant impulse response type of function near 15 c/s; this corresponds to a reasonably pure sinusoidal fluctuation in the cell. There is also a smaller secondary peak at about 5 c/s; this low frequency signal has not been identified. There is another secondary peak at approximately 120 c/s; this is the position of the first harmonic of the 60 c/s power frequency. This peak is a result of electrical "pick up" and not the fluctuations in the cell. The remainder of the fluctuation spectrum is quite flat.

Thus we have determined that the fluctuation structure in the cell can be determined under these conditions and is reasonably sinusoidal with a fundamental frequency of about 15 c/s. The pureness of the periodic wave can be determined by measuring the width of the peak at its half power points and by determining its symmetry properties.

The auto-correlation and power spectral density functions were also determined in the wing regions of the 4.3 micron band. The relative strength of the 15.1 c/s signal decreased as expected although the shape of the fluctuation structure was predicted to be the same.

It must be realized that the single beam experiment measures the fluctuation structure along the line of sight; this represents a one dimensional measurement. The crossed beam technique measures the three dimensional fluctuation structure; the measurement in the direction perpendicular to the two crossed beams being of great interest.

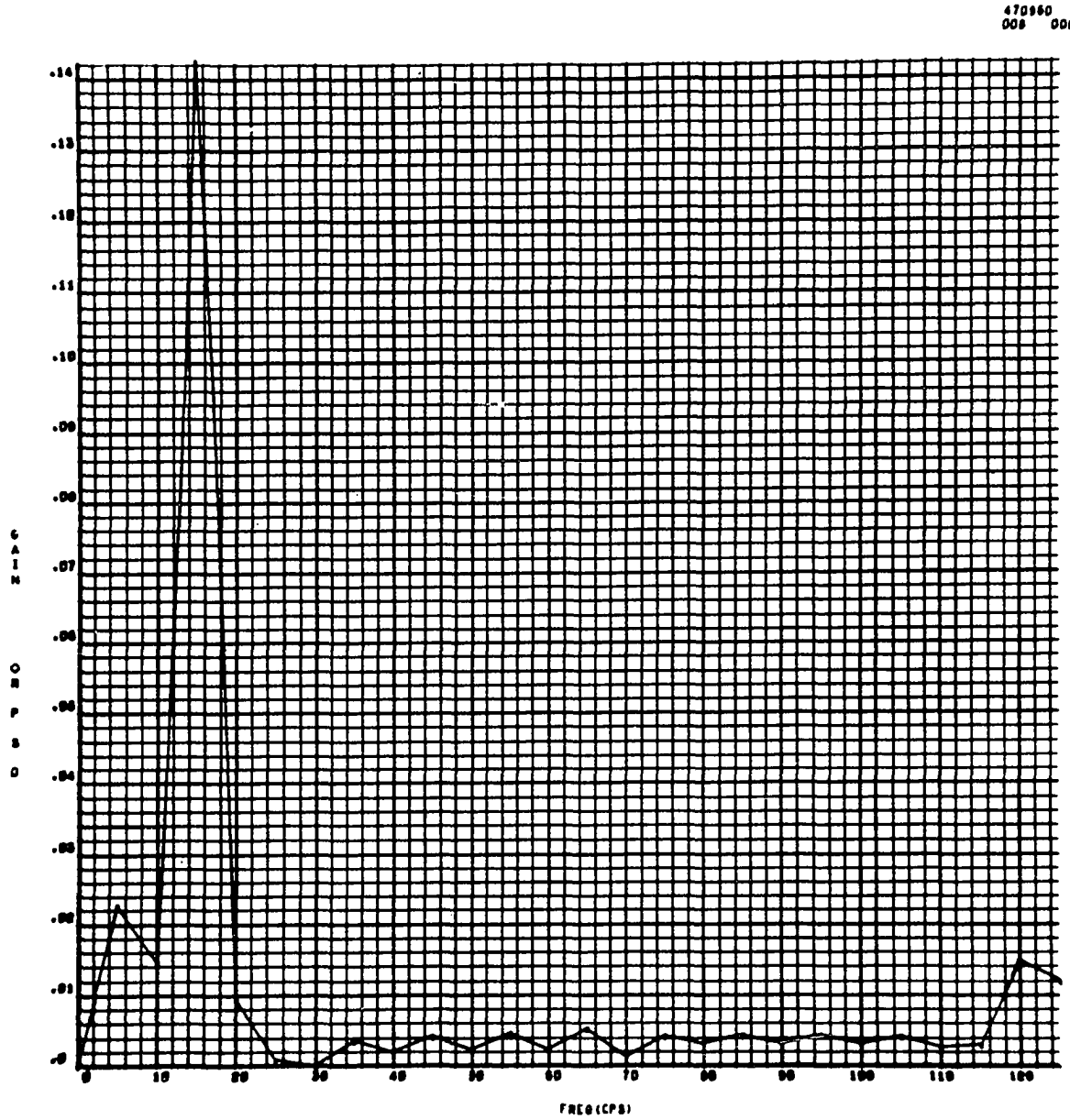

Figure 75. Computer Printed Plot of the Power Spectral Density Function for the Autocorrelation of δI.

Furthermore the "correlation length" is set apriori in the single beam experiment by the cell length; however a wide range of lengths can be used for any given fluctuation.

It is also of interest to record the cross correlation function for δI and δP for a given range of the time delay. δP can now be considered to represent a measure of the fluctuation intensity existing for a given gas in the cell. Figure 76 is a sample of this accumulative cross correlation function for a wavelength interval from about 4.33 microns to 4.37 microns which is the intermediate wing region on the high wavelength side of the band. Again 30 ten second piecewise correlations were calculated and accumulated. Since δP is a reasonably pure constant amplitude sinusoidal signal, one expects that the resultant correlation will be quite clean, and it is. The indicated period of the approximately periodic correlation function is about .065 seconds. The corresponding cross spectral density function is given in Figure 77. There is a slight 60 c/s contribution shown here with no first harmonic. The secondary peak at about 5 c/s is present but still relatively small.

It is of interest to note that this type of information cannot be otained from a static experiment.

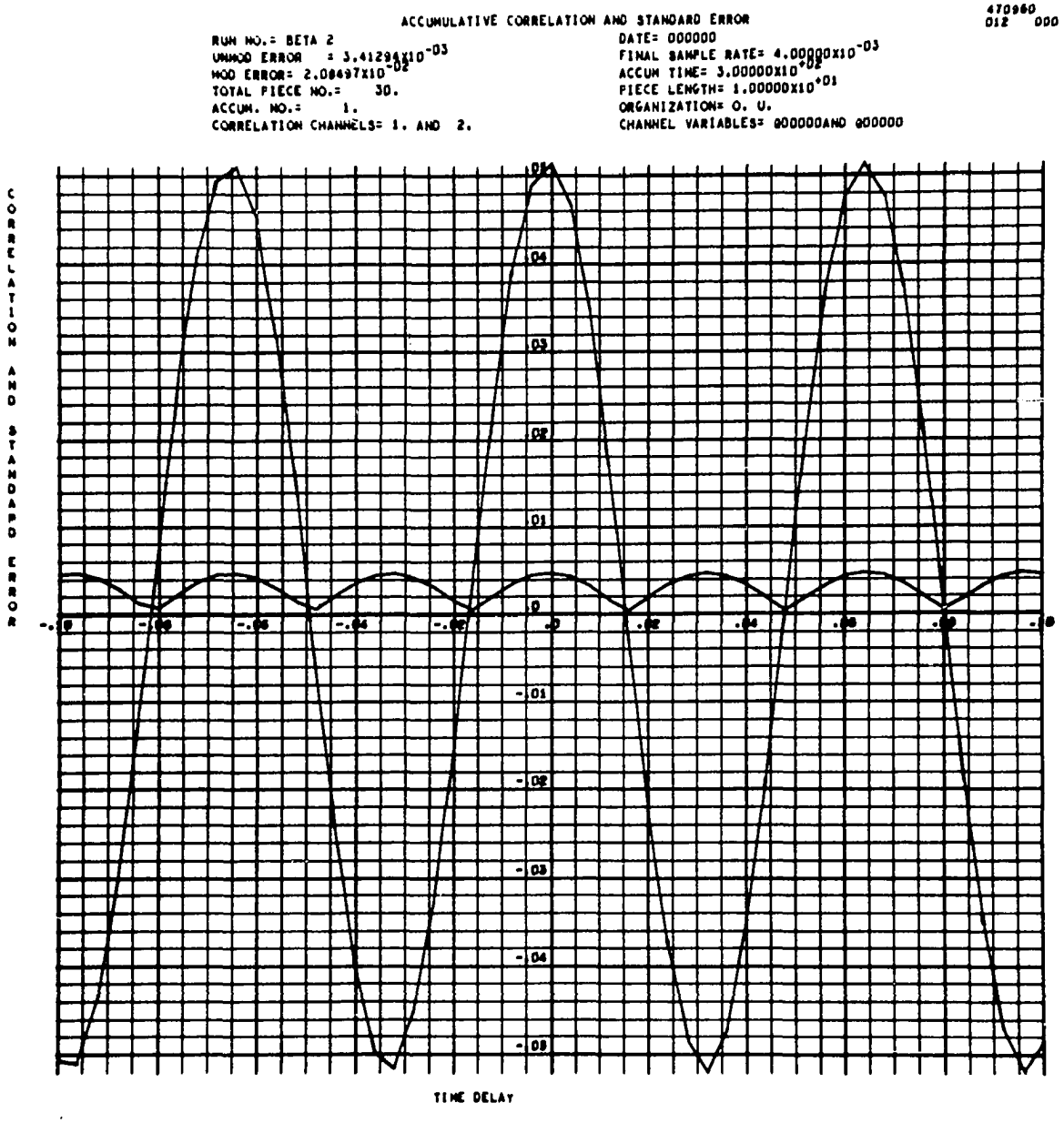

Figure 76. Computer Printed Plot of the Accumulative Crosscorrelation Function of δI and δP.

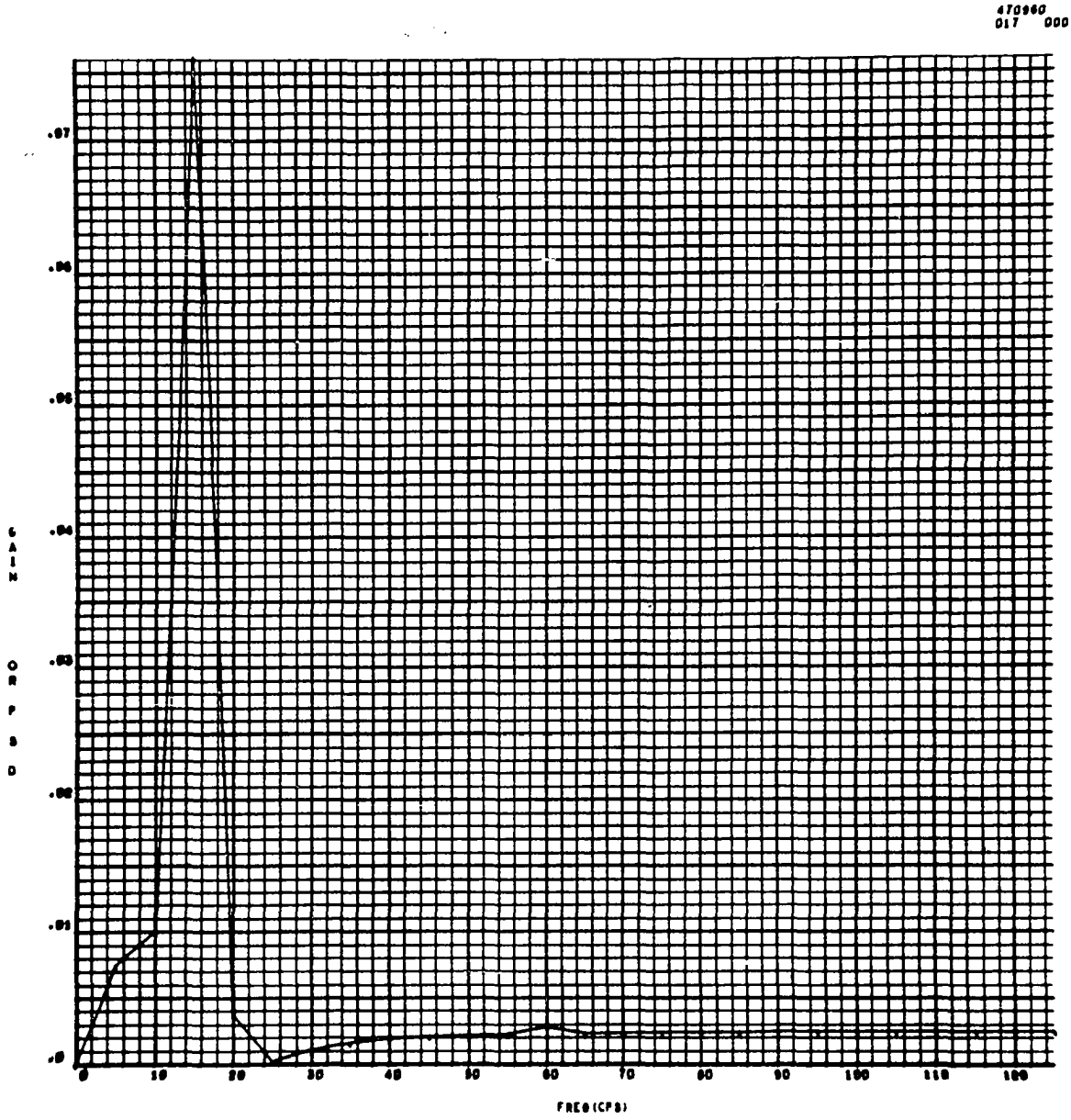

Figure 77. Computer Printed Plot of the Cross Spectral Density Function of δI and δP.

CHAPTER VII

CONCLUSIONS

The 4.3 micron bands of CO_2 were shown to be a suitable extinction process for an analysis of atmospheric conditions. It has been determined that the sensitivity of the optical fluctuations is sufficient to allow for accurate measurement of the nominal thermodynamic variable fluctuations.

A technique for performing a spectral inversion has been described and analyzed; this relies on the fluctuating absorption coefficient (δK) spectrum as a basis for such an inversion. The symbol δ represents the fluctuation operator; this denotes the change or fluctuation in the variables due to the acoustic excitation process. Going to the δK spectrum allowed us to suppress the pressure dependence which, when combined with the temperature "crossover points" led to the inversion. The inversion was made possible by using the fluctuation approach; the A (absorption) and K (absorption coefficient) spectra are not suitable for such an inversion.

The information related to the time series has yet to be explored fully. However, the fluctuation structure existing in the cell along the optical path was determined for the simple near-sinusoidal case, by utilizing the power spectral density function. The existing conditions are therefore suitable for analyzing the fluctuation structure of a gas-

eous medium.

The characteristics of the various possible spectra were discussed and related.

The results are being used to calibrate a crossed beam system for use in the atmosphere; they are also of use when disentangling the space time correlation functions discussed in the theory section in connection with crossed beam molecular spectroscopy.

In particular one of the important results of this experiment is that we have been able to isolate the dependence of the fluctuating absorption coefficient on the CO_2 concentration, at the point $\lambda = 4.20$ microns. Thus one measurement at $\lambda = 4.20$ microns can be used to find f. A second measurement at $\lambda = 4.35$ microns can be used to find T, and a third measurement anywhere in the core region (preferrably near 4.24 or 4.25 microns) can be used to find P. These wavelength points are applicable to the crossed beam local value measurements of P, T, and f.

The absorption coefficient derivatives were calculated and graphed for typical cases (extensive tables of these derivatives have been compiled). This was done because it is this derivative information that is of primary interest in the fluctuation absorption coefficient spectrum. The dependence of these derivatives on P, T and f has been shown, here, graphically. Furthermore, the mean value derivatives were used to calculate δK_c which was then compared with the measured adiabatic value. These results agreed within five to ten percent which was sufficient to show that the linear term in the Taylor series expansion is a valid representation for δK in this experiment. In support of this is the fact that δK was shown to be proportional to δP.

Some of the second derivative information for K is shown to be accurate; it is generally better than we expected it to be.

Some effort was spent in comparing the results of an absorption spectrum analysis with the results of an absorption coefficient spectrum analysis. The absorption coefficient method was found to yield more accurate information over a wider range of data. The weak line and strong line approximations themselves were felt to be of limited value in general. It is necessary and more pertinent to use the ill defined region formulation in most cases of interest. This formulation needs to be developed further than it has been to date.

One of the benefits of using spectral absorption coefficients is that the spectral functions are allowed to vary over the band. The absorption in an actual case will be closer to the weak line approximation in the wing and closer to the near strong line approximation in the core (for typical cases). This variation is generally not taken into account in band model approaches since the total band absorption is generally found first before any analysis is done. We have avoided this approximation by working directly with the spectral functions.

In addition, the temperature results of this experiment (both static and fluctuating) are important since such results have not previously been published; this is because of the fact that band models are generally used at a standard temperature and for Total Absorption.

We have subjected the basic data set to exhaustive analyses both theoretically and experimentally; it is our opinion that the basic data has withstood all the various tests relative to its consistency and accuracy. Considering the small number of data points in some instances,

the data has even exceeded our expectations. For example, the agreement between the calculated δK_c and the measured δK was better than we had hoped for.

REFERENCES

1. Andig, D. E. Band Model Methods for Computing Atmospheric Slant-Path Molecular Absorption. IRIA State of the Art Report, 7142-21-T. Ann Arbor: Willow Run Labs., University of Michigan, 1967.

2. Bevans, J. T., and R. V. Dunkle. "Radiation Interchange Within an Enclosure," Part 1, 2, 3, Journal Heat Transfer, Trans. ASME. Feb., 1960, pp. 1-19.

3. Breeze, J. C., and Ferriso, Ludwig, Malkmus, "Temperature Dependence of the Total Integrated Intensity of Vibrational Rotational Bands Systems," J. Chem. Phys., Vol. 42, No. 1 (1965), pp. 402-406.

4. Burch, D. E., and Gryunak, Patty, and Barthy. "Absorption of Infrared Radiant Energy by CO_2 and H_2O, IV, Shapes of Collision Broadened CO_2 Lines," JOSA, Vol. 59 (1969), pp. 267-280.

5. Burch, D. E., and Gryvnak, Williams. "Total Absorptance of Carbon Dioxide in the Infrared," Appl. Optics, Vol. 1, (1962), pp. 759-765.

6. Cann, M. J. "An Optical Absorption Cell with Variable Path Length and Temperature," Review of Sci. Instr. Vol. 40, No. 4 (1969), pp. 595-596.

7. Courtoy, C. P. Can. J. Phys., Vol. 35 (1957), pp. 609-648.

8. Dennison, D. M. "The Infrared Spectra of Polyatomic Molecules," Part II, Rev. Mod. Phys., Vol. 12, No. 3 (1940), pp. 175-214.

9. Fisher, M. J. and R. J. Damkevala. "Fundamental Considerations of the Crossed Beam Correlation Technique," NASA Contractor Report, CR-61252, Jan., 1969.

10. Fisher, M. J. and F. R. Krause. "The Crossed Beam Correlation Technique," J. Fluid Mechanics, Vol. 28, No. 4 (1967) pp. 705-717.

11. Foley, H. M. "The Pressure Broadening of Spectral Lines," Phys. Rev. Vol. 69 (1946), pp. 616-628.

12. Goody, R. M. "A Statistical Model for Water Vapor Absorption," Q.J.R.M.S., Vol. 78, (1952), pp. 165-169.

13. Goody, R. M. Atmospheric Radiation. I. Theoretical Basis. Oxford at Clarendon Press, 1964.

14. Gray, L. D. "Spectral Emissivity Calculations for the Parallel Bands of Carbon Dioxide at 4.3 Microns," J.Q.S.R.T., Vol. 5, 1965, pp. 569-583.

15. Howard, J. N. and Williams, Burch. "Infrared Transmission of Synthetic Atmospheres, II. Absorption by Carbon Dioxide," JOSA, Vol. 46, No. 4, 1956, pp. 237-241.

16. Jakob, M Heat Transfer, 1949, J. Wiley and Sons.

17. Kondratyev, K. Ya. Radiation in the Atmosphere, Acad. Press, 1969.

18. Krause, F. R. and W. Davies, M. J. Cann. "The Determination of Average Thermodynamic Properties with Optical Cross Correlation Methods," AIAA, 5th Aerospace Sciences Meeting, New York, 1967.

19. Krause, F. R. and J. B. Stephens. "Remote Detection of Local Temperatures and Local Partial Pressures with Crossed Beam Spectroscopy, Proc. of Spec. Conf.: Molecular Radiation and Its Application to Diagnostic Techniques," M.S.F.C., NASA, Huntsville, Ala., Oct. 1967.

20. Lindholm, E. "Pressure Broadening of Spectral Lines," Arkiv För Matematik Astronomi Och Fysik, Vol. 32A, No. 17, 1946, pp. 1-18.

21. Lorentz, H. A. Proc. Roy. Acad. (Amsterdam) Vol. 8, 1906, p. 591.

22. Malkmus, W. "Infrared Emissivity of Carbon Dioxide (4.3 micron Band), JOSA, Vol. 53, No. 8, 1963, pp. 951-961.

23. Margenau, H. "Statistical Theory of Pressure Broadening," Phys. Rev., Vol. 82, 1951, pp. 156-158.

24. Oppenheim, V. P and Ben-Aryeh, Y. "Statistical Model Applied to the Region of the ν_2 Fundamental of CO_2 at 1200°K, JOSA, Vol. 53, No. 2, 1963, pp. 344-350.

25. Penner, S. S. Quantitative Molecular Spectroscopy and Hot Gas Emissivities (1959), Addison-Wesley Publ.

26. Plass, G. N. "Models for Spectral Band Absorption," JOSA, Vol. 48, No. 10 (1958), pp. 690-703. "Useful Representations for Measurements of Spectral Band Absorptions," JOSA, Vol. 50, No. 9 (1960), pp. 866-875.

27. Plass, G. N. "The Influences of the 15 Micron Carbon Dioxide Bands on the Atmospheric Cooling Rate," Q.J.R.M.S., Vol. 82, 1956, pp. 310-324.

28. Plass, G. N. "Regions of Validity of Various Absorption Coefficient Approximations," J. Mete., Vol. II, No. 1, April, 1954, pp. 163-165.

29. Santeler, D. J. and D. H. Holkeboer and Jones, Pagano. Vacuum Techology and Space Simulation, 1967, NASA, SP-105.

30. Stull, V. R., Wyatt, Plass. "The Infrared Transmittance of CO_2" Appl. Optics, Vol. 3, 1964, pp. 243-254.

31. Stull, V. R. Wyatt, Plass, "Vibrational Energies of the CO_2 Molecule," J. Chem. Physics, Vol. 37, No. 7, 1962, pp. 1442-1445.

32. Tourin, R. H. "Measurements of Infrared Emissivities of Hot Carbon Dioxide in the 4.3 Micron Region," JOSA, Vol. 51, No. 2, 1961, pp. 175-183.

33. Wachowski, A., and M. R. Phillips. "Computer Program for Crossed Beam Studies of Clear Air Turbulence Program Description (MLTCOR), NASA Contractor Report, 61313, 1969, MSFC, Huntsville, Alabama.

34. Weisskopf, V. F. Z. Physik, Vol. 77, 1932, p. 398.

35. Winters, B. H., Silverman, Benedict. "Line Shape in the Wing Beyond the Band Head of the 4.3 Micron Bands of CO_2," J.Q.S.R.T., Vol. 4, 1969, pp. 527-537.